NEWCASTLE UNIVERSITY

SCHOOL OF MECHANICAL AND SYSTEMS ENGINEERING

A Thermo-economic Model and a Simulation Analysis of a Solar Hydrogen System Using IPSEpro

By

Abdulhamid Abdulsalam El-sharif

B.Sc, M.Sc.

A thesis submitted to the School of Mechanical and Systems Engineering for the degree of

Doctor of Philosophy

In Mechanical Engineering

Supervised by

Professor Brian Agnew

May 2013

IN THE NAME OF ALLAH

THE MOST GRACIOUS AND THE MOST MERCIFUL

Abstract

The high growth of world population and modern lifestyle are increasing the world's energy consumption and fossil fuel depletion, as well as increasing environmental and economic adverse impacts. This concern is encouraging scientists and governments to create more reliable, long-lasting and environmentally benign energy sources. Renewable energy sources, particularly solar energy, are nowadays suggested as being one of the main alternative and future sources of energy to traditional fossil fuel sources. Nevertheless, the main challenge in utilizing solar energy is its high utilization cost and variability, when a storage or backup system is required. To overcome this problem, many researchers have introduced hydrogen because it is the cleanest, most abundant and safest fuel that can be used as an energy carrier or a backup system in place of batteries and fossil fuel generators. Solar hydrogen system (SHS) technologies are still immature and a few experimental projects have been installed around the world, inspiring more studies to improve these technologies towards a hydrogen-economy objective. Very little software is commercially available to use for simulation and optimization of a solar hydrogen system and no effective software has been developed for thermo-economic analysis. However, in this study a thermo-economic model library component for solar hydrogen system units such as photovoltaic (PV), photovoltaic thermal (PV/T), fuel cell and electrolyzer have been developed and validated using the commercially available software package IPSEpro. The developed models, along with the existing IPSEpro model libraries have been used to; design, optimize and simulate the entire system to meet the energy demands of a small community in three different sites. The sites considered were Sabha and Misurata in Libya, a hot region as well as Newcastle in United Kingdom in a cold region, using yearly average and a typical summer and winter actual weather data for each site. A parametric study was carried out to investigate the effects of the environmental, main operation and economic parameters on the performance and outputs of each component and the entire system. A thermo-economic analysis of the SHS showed that the PV unit has the highest factors for; (exergy destruction (exdf), destruction cost (CD), investment and destruction summation (ZTCD), and the lowest exergoeconomic (fk), followed by the fuel cell and the electrolyzer. However, the low (fk) factor of the PV and the fuel cell units indicated that a high level of attention has to be focused on increasing the unit's exergy efficiency. Moreover, the high (fk) factor of the electrolyzer indicates that the reduction of the unit investment cost (ZT) has the priority for unit performance improvement and production cost reduction. It has also been established that, for a SHS at base condition,

the system's exergy efficiency was 5.07% with a daily average output electricity cost of 0.23$/kWh. However, for Sabha and Newcastle, the yearly average electricity cost was 0.40$/kWh and 0.77 $/kWh respectively. This is still uncompetitive compared with (+-0.15 $/kWh) typical current electricity market prices. In addition, the study clarified that SHS will be economically reasonable if the costs of the CO_2 emission and fossil fuels consumed are considered in the analysis, particularly in Sabha and Misurata regions. Nevertheless, in these regions the photovoltaic electricity is competitive to the traditional power plant current prices. The analysis also shows that the variation in the environmental, economic and operation parameters have a significant effect on the system and its units' performance and output costs. The parametric study mainly considered the variation of; ambient temperature (Ta), solar intensity (Sirr), module surface temperature (PV/Tc), interest rate (ir), capacity factor (CF), capital cost (CFC), lifetime (ny), price of output hot water (cwh), cell voltage (Vc), stoichiometric ratio (StH2), hot water temperature and mass flow rate. The parametric study results revealed that the optimum SHS operation conditions will achieve at the smallest ambient temperature and the highest solar intensity. It is also found that recycling the output streams, particularly the hydrogen and utilizing the output hot water of the unit's cooling system will significantly enhance its performance and reduce the production costs. The study proves that increasing the output hot water of the PV/T system to utilize it in a low thermal energy system using an electric heater is unfeasible. More investigation is recommended to build an integrated IPSEpro thermo-economic model to utilize the SHS output hot water in a low thermal energy system using a solar collector.

Acknowledgment

At first I thank God Almighty for the blessing and that gave me the strength and patience to complete this research work.

I am deeply appreciative to Professor Brian Agnew for his supervision, advice and guides throughout this work, and I ask Allah to give him healing.

This work has not come to its end without the help and patience of my family; my wife and my sons.

I would also like to thank the Ministry of higher education and scientific research in Libya and the cultural affairs section of the Libyan Embassy in Britain for their assistance and the opportunity to accomplish this work.

Lastly, but not least, my thanks to all who helped and encouraged me from my colleagues and the staff of the school of mechanical and systems engineering in Newcastle University.

إِهْداء

أُهْدِي هَذا العمل إِلى رُوحِ أُمِّي الغَالِيَةِ الَّتِي ارْتَفَعَتْ إِلَى بارِئِها أَثْناءَ إِنْجازِي لِهذا العَمَل...

كما أُهْدِيهِ إِلى عائِلَتي... زَوْجَتي وَ أَبْنائِي الَّذِين تَحَمَّلوا وَصَبَروا مَعي طِيلَة فَتْرَةِ هذا العَمَل.

إِلى أَرْواحِ الأَبْطالِ الَّذِين ضَحُّوا بِأَرْواحِهِم لِتَحْريرِ بَلَدِي وَ تَحْكِيم شَرْعِ اللهِ فيهِ....داعِياً اللهَ العَلِيِّ القَدِيرِ أَنْ يَتَقَبَّلَهُم عِنْدَهُ مِنْ الشُّهَداءِ..

وَ أَنْ يَحْفَظَ بَلَدي وَ يَرْعاها .

Table of Contents

Chapter Six

Methodology

Chapter Seven

IPSEpro Models configurations and validation

Chapter Eight

Energy, exergy and thermo-economic study of SHS and its components

List of Figures

Chapter One

Chapter Three

Chapter Four

Chapter Five

Chapter Six

Chapter Seven

Chapter Eight

List of Tables

Chapter Two

Chapter Three

Chapter Four

Chapter Eight

Abbreviations

act	Actual
CO	Carbon monoxide
CO_2	Carbon dioxide
comp	Compressor
conv	Conversion
exp	Experimental
EGM	Entropy generation minimization
ESDU	Engineering Science Data Unit
EL	Electrolyzer
FC	Fuel cell
he	Heater
HC	Hydrocarbons
HEX	Heat exchanger
H2	Hydrogen
IPSEpro	Power Plant Design/ Analysis Software
Loss/L	Loss
MPPT	Maximum power tracker
MDK	IPSEpro Model development kit
NOCT	Normal operation temperature, at (800 W/m^2, 20 ˚C)
N/No./n	Number
O2	Oxygen
PSE	IPSEpro Process simulation environment
PSEconomy	IPSEpro Process simulation economy
PSExcel	IPSEpro Process simulation MS Excel
PSLink	IPSEpro Process simulation Link
PV	Photovoltaic
PV/T	Photovoltaic thermal
PM	Particular matter
SimTech	Simulation Technology
sim	Simulation
STC/sta	Standard test condition at (1 kW/m^2, 25 ˚C)

Nomenclature

A	Surface area (m^2)
ASOC	Resources annual saving cost ($)
ACC	Annual capital cost ($/kW yr)
ALFATAO/ $\alpha\tau$	Lumped transparency and emissivity factor
TAOG/ αG	Glass or cover emissivity factor
ALFAC/ αC	Cell emissivity factor
C_R	Heat exchanger capacity ratio
C_P	Specific heat capacity (KJ/kg K)
C/C_w	Exergy or thermo-economic cost ($/GJ)
$\dot{C}$	Exergy cost rate ($/unit time)
CO2-COST	Carbon emission damage cost ($/ton)
CO2-PF	Carbon emission value per power produced (ton/MWh)
CO2-SAVA	Annual saving from avoidable carbon emission ($)
COM	Annual operation and maintenance cost factor (%)
CF	Capacity factor (%)
CFC	Capital cost ($/kW)
CRF	Capital recovery cost (1/yr)
el	Electricity (kW)
ex/x	Specific exergy (KJ/kg)
$\dot{E}_X$	Exergy rate (kW)
en	Specific energy (kJ/kg)
FF	Fill factor
fk	Exergoeconomic factor (%)
h	Specific enthalpy (KJ/kg)
h_{ca}	Convection and radiation heat transfer coefficient (W/m^2 k)
ir	Interest rate (%)
I	Current (A)
I/Irev	Irreversibility (kW)
Im	Maximum current (A)
LMTD	Log means temperature difference (˚C)
$\dot{m}$	Mass flow rate (kg/s)
NTU	Number of transfer units
ny	Life time (Year)
PVEL	Photovoltaic electricity cost ($/kWh)
P_{cell}	Cell pressure (bar)
P_{el}	Electric power (kW)
Q/q	Heat (kJ/kg)
$\dot{Q}$	Heat rate (kW)
rk	Relative cost difference (%)
S_{gen}	Entropy generation (kW/K)
S	Entropy (kJ/kg.K)
S_t	Stoichiometric ratio (kg/kg)
S_{irr}	Solar radiation (kW/m^2)
T_R	Reference temperature at NOCT (˚C)
T_o	Reference temperature (˚C)
T_{sun}	Sun temperature (5526 ˚C)
T_a	Ambient temperature (˚C)
T_c	Cell temperature (˚C)
T_r	Temperature at STA conditions (˚C)
T_b	Module back surface temperature (˚C)

TIMED	Time interval (hours)
TSOC	Total (unit lifetime) resources annual saving cost ($)
Vm	Maximum voltage (V)
V	Voltage (V)
$\dot{V}$	Volume rate (m^3/s)
v/v	Wind velocity (m/s)
v_s	Specific volume (m^3/kg)
$\dot{W}$/W	Work transfer rate (kW)
Y_D	Exergy destruction factor (%)
UA	Overall heat transfer coefficient area (kW/K)
$\dot{Z}/ZT$	Annualized investment cost (total) ($/unit time)
ZCI	Annualized capital cost ($/unit time)
ZOM	Annualized operation and maintenance cost ($/unit time)
Z	Elevation (m)
N	Normal condition at(0 ˚C, 1 Atmosphere)

Subscripts

acc	Accessory or auxiliary
c	Cell
ch	Chemical
D	Destruction
F/f	Fuel
in	Inlet/input
kn	Kinetic
max	maximum
m	Module
oc	Open circuit
out	Outlet/Output
o	Reference state
phy	Physical
pt	Potential
p	Product
st	Stream
sc	Short circuit
tot/t	Total
th	Thermal
tot-equiv	Total equivalent
wt	Water

Greek Symbols

η/eta	Efficiency
Δ_t	Temperature difference
β	Cells to module area factor
Ɛ	Effectiveness
μ	Temperature coefficient (1/˚C)

CHAPTER ONE

Chapter One

Introduction

1.1 Background

Energy is the core of the requirements of modern life and today no one can imagine life without electricity, transportation and communication. As reported by United Nations (UN) the world population increased to 7 billion in 2011 and is rising by 1.5% yearly, which represents a rapidly increasing high-energy demand. Moreover, British Petroleum (BP) reports on world energy for 2010 and international energy statistical centres reports indicated that the global energy consumption in 2010 had been the largest since 1973 and the yearly demand enormously increased as presented in Figure 1.1[1, 2]. The world's main energy sources are currently fossil fuels such as petroleum, natural gas, coal and nuclear energy, which will become depleted in a foreseeable future, as shown in Figure1.2 [3]. However, the renewable energy forms accounted only for 1.8% of global consumption in 2010, up from 0.6% in 2000 while the comparable figures are 29.6% for coal, 10% for nuclear and hydro. Furthermore, the world's proven reserves of oil, natural gas and coal were estimated to be sufficient to meet 46.2, 58.6 and 118 years of global production respectively [1]. In addition, the safety restrictions related to using nuclear energy and the global pollution problems caused by fossil fuel combustion products has encouraged research for sustainable and environmental benign energy alternatives. Consequently, finding alternative to fossils fuel is more urgent today than ever before, due to the effect of the use of these fuels on our environment and ultimately on life on our planet as well as the significantly increases in fossil fuel prices, Figure 1.3[1].

Renewable energy sources (e.g. solar, wind, biomass, hydrogen and geothermal) are the main alternative forms of future energy for our currently used sources. However, the utilization of renewable energy is restricted by its influence by time, season and climate causing problems for power-on-demand requirements.

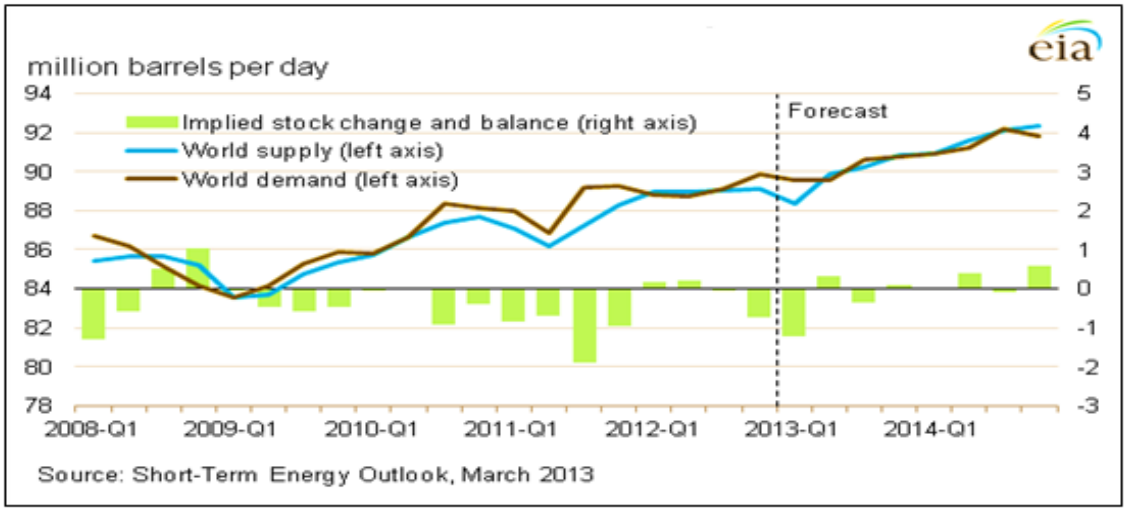

Figure 1.1 World liquid fuels supply and demand [1]

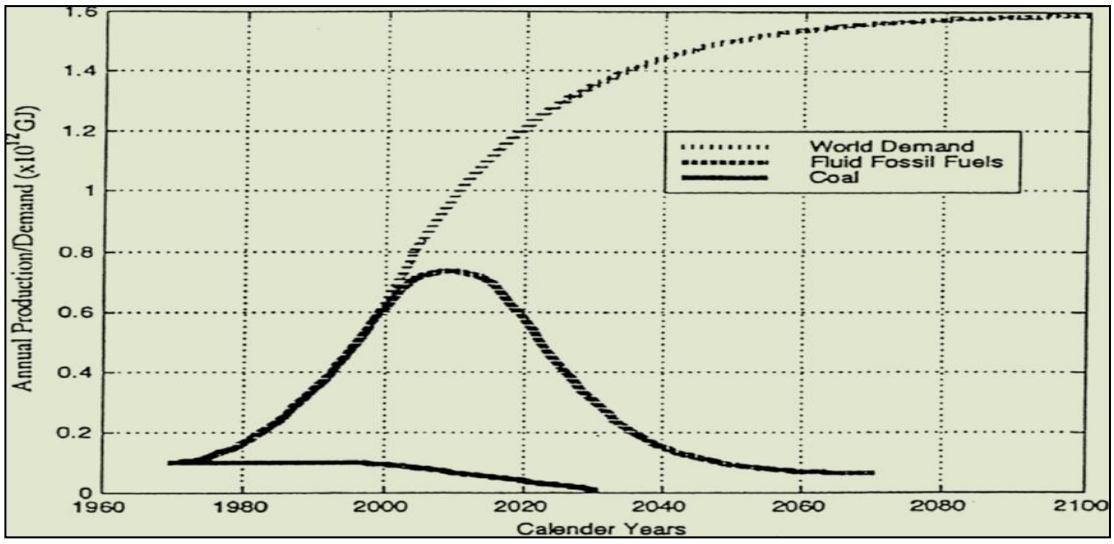

Figure 1.2 Estimates of world fossil fuel production [3]

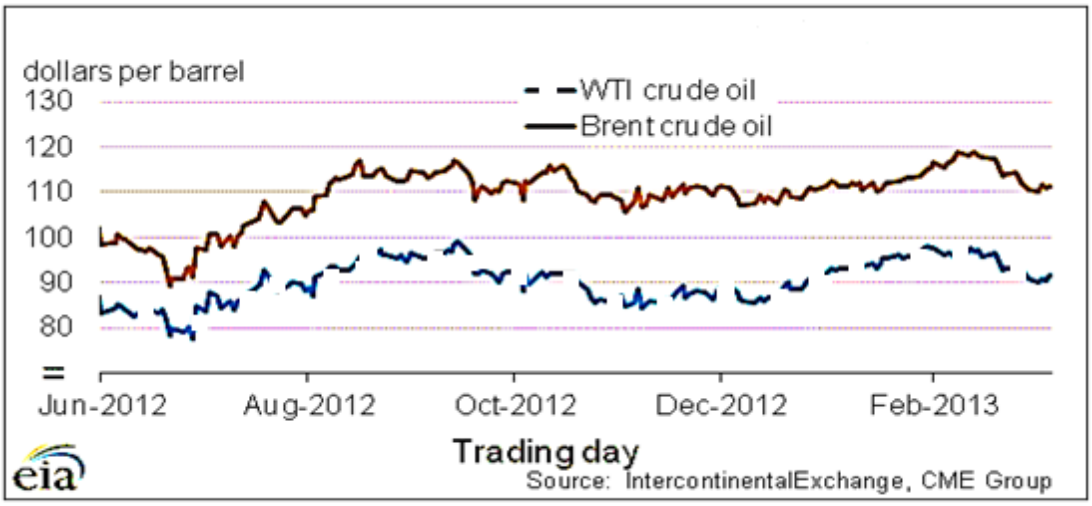

Figure 1.3 Historical and current crude oil prices [1]

To overcome renewable energy storage problem, a backup system such as one involving batteries and generators is necessary. However, battery system viability, widely used today as a storage system, is limited by it's; volume, weight, efficiency, usage and cost particularly for stationary and large systems. Moreover, the use of diesel generators may also be restricted by its noise and pollution. Therefore, many scientists suggest hydrogen as future alternative energy source and energy storage medium.

According to Robert Hefner's analysis, as presented in Figure 1.4, the world has been slowly shifting from one form of energy to another since the mid-nineteenth century and a complete change over from fossil fuels to hydrogen energy needs to occur by the end of this century [4]. Achieving this will involve dealing with many challenges towards the hydrogen economy such as hydrogen storage, infrastructure, production efficiency and cost.

Hydrogen is one of the most abundant elements in the universe and it can be extracted from many materials such as water and natural gas. Furthermore, it has found to be the best fuel and energy carrier medium due to its advantages as a convenient fuel for transportation. It has high utilization efficiency and is safe, versatile and environmentally benign. Furthermore, hydrogen can be stored in a gaseous, liquid or as a solid state. The choice of the storage method is depends on its efficiency and cost. Because hydrogen has very low density, hydrogen storage techniques are now a major research concern.

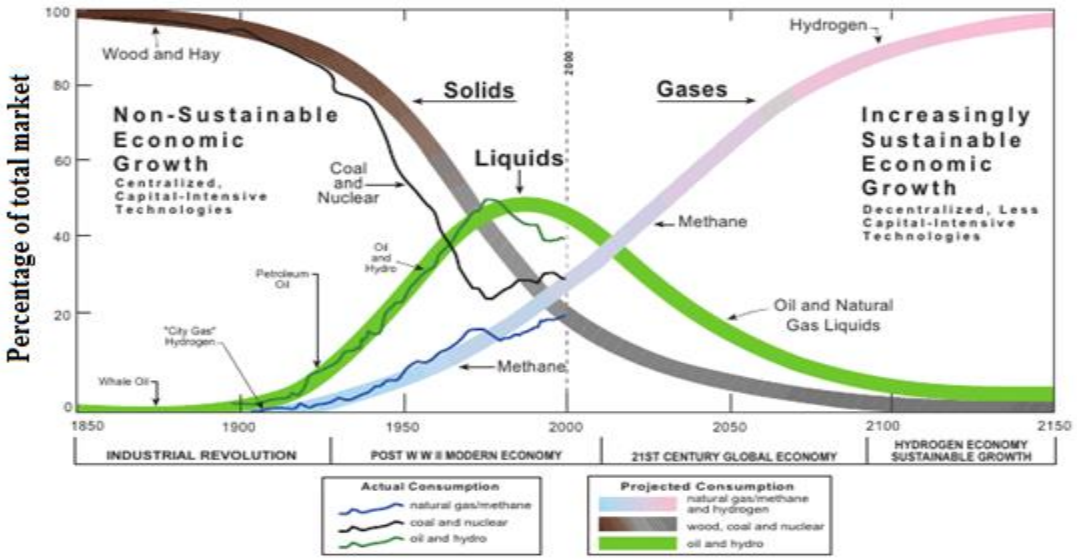

Figure 1.4 Global energy system transitions [3]

Hydrogen production methods depends on primary resources such as fossil fuels, nuclear, biomass and other renewable forms of energy such as wind, solar, geothermal and hydro-electric power. Nowadays, most of the hydrogen produced is done by fracturing fossil fuels, where cost and environmental consideration are the two main challenges to hydrogen production by this method. However, hydrogen production methods can be classified in to three main processes: thermal, electrolytic and photolytic processes. The electrolyzer processes produce hydrogen without any environmental impact when renewable electric source are involved such as solar energy [5, 6]. This process requires more attention in the current scientific research plans in order to reduce costs and increase efficiency. For this reason, the solar hydrogen system is the main topic for investigation, evaluation and performance improvement in this research study.

1.2 Objective of the study

As mentioned in the previous sections, hydrogen can be produced or captured in several ways. Preferring one to another depends on the availability of feedstock or resources, the quantity of hydrogen required, its cost and purity and its environmental impact. Environmental pollution exists when hydrogen is produced from fossil fuels. Therefore, renewable energy sources, particularly solar hydrogen systems were using water electrolyzers and photovoltaic to produce emission free hydrogen is the key factor in overcoming the pollution and continuity of primary sources. This system usually consists of Photovoltaic (PV) panels, water electrolyzers, and storage system. Hydrogen can be utilized in fuel cells to produce electricity in a highly efficient way with only water and heat as by products, as shown in Figure 1.5. Current hydrogen production prices are still high, based on these production methods, varying from 2 US$/ kg H_2 for coal gasification to 7 US$/kg H_2 for a solar hydrogen system. However, the system is still under development and there are challenges to overcome before the solar hydrogen systems can become competitive and realized [7, 8]. Research and development efforts regarding Solar Hydrogen System (SHS) technologies are in progress in order to improve their efficiency, establish techniques for accurately predicting their output, reduce costs, reduce or eliminate the empirical nature of the system's models, and reliably integrate them with other conventional generation sources.

The design and operation of the SHS could change noticeably, depending mainly on, the type of components, management and control strategy, size, as well as availability of primary source. Furthermore, in order to predict system performance, its individual

components have to be modelled and investigated first and then their mix can be evaluated to meet the demand requirements [9].

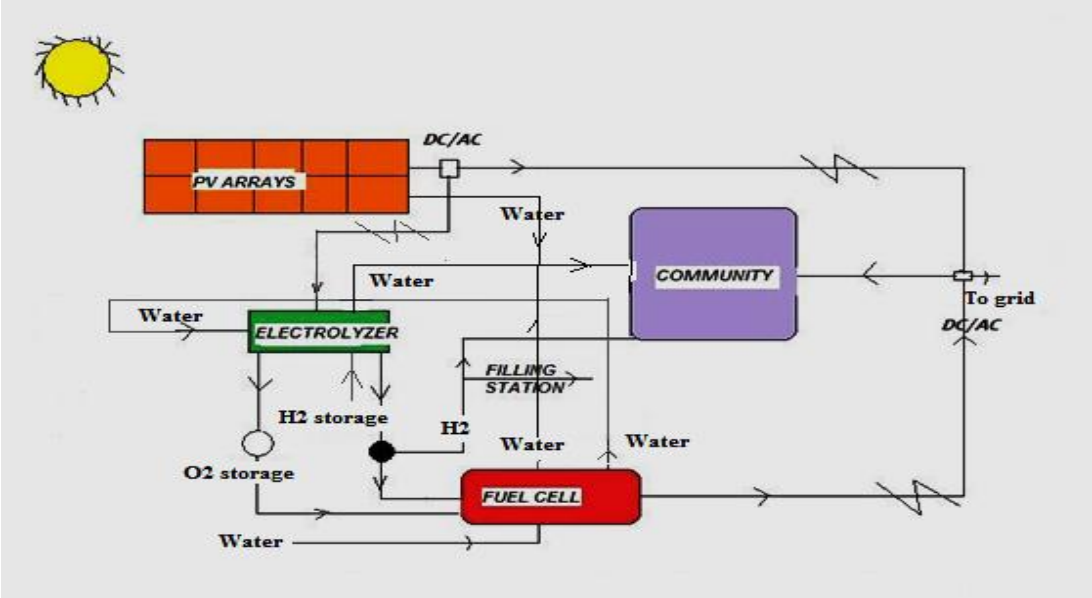

Figure 1.5 Solar hydrogen system (SHS)

A huge effort in the recent past have been performed to model and study the various components of SHS, based either on individual components or collectively for the overall system. Most of these studies, models and the software focused on energy, electro chemical and economic analysis of particularly small standalone systems. Recently exergy (defined as the available or useful energy or work) analysis and thermo-economic analysis, rather than energy and economic analysis have been prominent in the research activity. This technique has not been widely used for SHS analysis and to date there is no known commercially available software code based on this method. Furthermore, there is no established form of detailed simulation and parametric thermo-economic analysis for high production capacity SHS. Additionally, none of the previous studies of such systems included a comprehensive parametric and sensitivity thermo-economic analysis, the environmental impact, and the resources consumed as well as examine it in hot regions like Libya. This subject is the main goal of this study, which is described in brief in the five following objectives:

First, to develop a new simple and general model library for SHS based on energy, exergy and thermo-economic analysis, using the commercially available energy analysis IPSEpro (open source and friendly interface software). The library includes the key system subroutines for photovoltaic, photovoltaic thermal, water electrolyzer, compressor, heat exchanger and fuel cell integrated with the existing IPSEpro libraries.

Data from commercially available components manufacturers' data sheets, and previous simulation and experimental results have to be used for unit and system validation and evaluation.

Second, to investigate the effect of varying; weather condition, the main operation and economic parameters, on the performance and the output of the entire system and its components. **Third**, the SHS system and its components have to be optimized individually and evaluated thermo-economically to ensure optimum performance and outputs.

Fourth, to design and simulate the SHS to meet the environment conditions and energy and electricity demands of a small community in three different hot and cold cities (Misurata at the Libyan coast side, Sabha at the southern Sahara of Libya and Newcastle Upon Tyne at the north of England) for which the necessary data has been obtained.

Fifth, to develop a photovoltaic thermal system (PV/T) IPSEpro model, that used to cool the PV surface, and utilize the production of hot water in domestic use or a low energy thermal system, as well as to enhance its performance and lifetime. In addition, to perform a trade-off and evaluation study between the system output electricity and hot water according to the demands, weather condition and the unit's main function.

1.3 Structure of the thesis

The thesis is organized in 9 chapters, references and appendixes. In the **current chapter,** the introduction includes a general view of the state of energy in the world and concerns regarding looking for sustainable and environmental friendly energy source are presented. In addition, the motivations and the main objectives of the study are explained.

Chapter 2 includes a description of hydrogen characteristics, production and storage methods as a fuel and an energy carrier medium used to overcome the influence of the renewable energy sources. The existing SHS projects and previous research studies are concluded and discussed.

Chapter 3 illustrates the technical aspects and general over view of the solar energy source. Furthermore, this chapter includes an explanation of the technology, aspects of the market, working principles and the most important research works of the solar hydrogen system's main components (photovoltaic, photovoltaic thermal, fuel cell, and electrolyzer).

Chapter 4 presents a general view of the energy analysis tools and their applications and advantages. A description of the software package (IPSEpro) used to develop a thermo-economic model for SHS simulation and evaluation is presented. The principles of the key modules (PSE) process simulation model and (MDK) model development kit and the software main libraries are also clarified.

Chapter 5 illustrates and analysed a national energy overview and the climate and solar data collected for the case study sites.

The mathematical models for solar hydrogen system components as well as the methodology used based on energy, exergy and thermo-economic methods are described in **Chapter 6**.

Chapter 7 presents and explained the developed IPSEpro models' configurations and validation processes.

Chapter 8 includes an energy, exergy and thermo-economic analysis of the system and its units. Furthermore, a parametric study to investigate the effect of the environmental conditions and the main operation and economic parameters on the SHS and its unit's performance and outputs is presented. The study considers the daily and yearly average weather data of three different sites (Misurata on the Libyan coast, Sabha in the south of Libya and Newcastle upon Tyne in the north of England). The IPSEpro developed model for a photovoltaic thermal water system is also illustrated. The chapter also presents a trade-off analysis between electricity and hot water production of a PV/T system. A parametric study to investigate the system's performance and optimum output utilization in low thermal energy systems is also conducted. The IPSEpro energy model developed for optimizing and study an electric water heater used for increasing the water temperature produced by the PV/T system is also clarified and presented in this chapter. **Lastly Chapter 9** concludes the research by discussing the results obtained and recommendations for future work.

CHAPTER TWO

Chapter Two

Hydrogen as an energy carrier for the solar system

2.1 Introduction

The search for reliable, clean and long-lasting sources of energy has been an ever-challenging task for humanity. However, the most important renewable, sustainable and clean form of energy is solar energy. The solar energy received by our planet in one hour is enough to cover the world's energy demands for one year. The restriction is its influence during the day, seasonally and its utilization in an economic way. Therefore, hydrogen as an energy carrier and a fuel has been suggested to be a solution to overcome these problems through a SHS. This system consisted mainly of photovoltaic arrays, inverters, electrolyzers, compressors, storage system, heat exchangers and fuel cells. This chapter describes the characteristics of hydrogen, its production and storage methods as a fuel and an energy carrier medium used to overcome the influence of the renewable energy sources. The chapter also includes a discussion of the most important previous research works on studying SHS, as well as its existing projects.

2.2 Hydrogen Properties

Hydrogen represents one of the most abundant elements in the universe. It can be extracted from many materials such as water and natural gas. Furthermore, it is considered as the best fuel and energy carrier medium due to its advantages as a convenient fuel for transportation, its high level of efficiency, safety, versatility and its being environmentally benign (Tables 2.1, 2.2, 2.3, 2.4 and 2.5 represent the characteristics of the hydrogen compared to other fuels) [3]. A brief description of each characteristic will be presented in the following sections.

2.2.1 Safety

Many people view the using of hydrogen as a very dangerous. This is mainly due to some historical accidents related to the using of hydrogen. However, hydrogen has been routinely used for many years in the industrial sector with a safety code and standards for its handling and use without any major concerns about its safety compared with other fuels. This is clear when comparing its properties with other fuels with regard to their toxicity and their potential for fire hazards as presented in tables 2.1 and 2.2. Due to hydrogen's lightness, its flame disperses quickly upwards and it releases less energy in a given volume compared to other fuels. Fires in which it is involved generally go

out in a short time. Nevertheless, there are some disadvantages of hydrogen, which are mainly its wider ignition limit, low ignition temperature, flammability, pressurized, and the fact that it is clear and odourless. It is necessary to choose suitable equipment design and apply appropriate safety standards and operating parameters in order to overcome these problems.

Characteristic	Fuel ranking[a]		
	Gasoline	Methane	Hydrogen
Toxicity of fuel	3	2	1
Toxicity of combustion (CO, SOx, NOx, HC, PM)	3	2	1
Density	3	2	1
Diffusion coefficient	3	2	1
Specific heat	3	2	1
Ignition limit	1	2	3
Ignition energy	2	1	3
Ignition temperature	3	2	1
Flame temperature	3	1	2
Explosion energy	3	2	1
Flame emissivity	3	2	1
Totals	30	20	16
Safety factor	0.53	0.80	1.00

1, safest; 2, less safe; 3, least safe.

Table 2.1 Safety ranking of fuels

Property	**Gasoline**	**Methane**	**Hydrogen**
Density[a] (kg/m^3)	4.40	0.65	0.084
Diffusion coefficient in air[a] (cm^2/s)	0.05	0.16	0.610
Specific heat at constant pressure[a](J/g K)	1.20	2.22	14.89
Ignition limits in air (vol%)	1.0–7.6	5.3-15	4.0-75.0
Ignition energy in air (millijoules)*	0.24	0.29	0.02
Ignition temperature (^oC)	228–471	540	585
Flame temperature in air (^oC)	2197	1875	2045
Explosion energy (g TNT/kJ)	0.25	0.19	0.17
Flame emissivity (%)	34–43	25-33	17-25

a: At normal temperature and pressure.

*: Minimum energy for spark ignition at atmospheric pressure.

Table 2.2 Characteristics related to fire hazard of fuels

2.2.2 Versatility

Table 2.3 describes the possibilities of converting hydrogen into other forms of energy. It is clear that hydrogen can be converted to other forms of energy (flame combustion, steam, heat through chemical reactions, electricity) [5].

Conversion process	Hydrogen	Fossil fuels
Flame combustion	Yes	Yes
Direct steam production	Yes	No
Catalytic combustion	Yes	No
Chemical conversion	Yes	No

Table 2.3 Versatility (convertibility) of fossil fuels

2.2.3 Utilization efficiency

The utilization efficiency factor (η_F/η_H) presented in table 2.4 is defined as the fossil fuels utilization efficiency divided by the hydrogen utilization efficiency, for different applications. Hydrogen can be converted to many other forms of energy in a more efficient way than fossil fuels.

Application	Utilization efficiency factor $= \eta_F/\eta_H$
Thermal energy	
Flame combustion	1.00
Catalytic combustion	0.80
Steam generation	0.80
Electric power, fuel cells	0.54
Surface transportation	
Internal combustion engines	0.82
Fuel cells/electric motor	0.40
Subsonic jet transportation	0.84
Supersonic jet transportation	0.72
Weighted average	0.72
Hydrogen utilization efficiency factor	1.00
Fossil fuel utilization efficiency factor	0.72

Table 2.4 Utilization efficiency comparisons of fossil fuels and hydrogen

2.2.4 Pollution

The pollutants of the hydrogen production from solar energy compared to coal/synthetic fossil and fossil fuel systems are listed in table 2.5. The solar hydrogen system will not produce any pollutant substances except some NOx. However, this small amount of NOx will not evolve if the hydrogen is utilized through fuel cells.

Pollutant	Fossil fuel system (kg/GJ)	Coal/synthetic fossil system (kg/GJ)	Solar-hydrogen system (kg/GJ)
CO_2	72.40	100	0
CO	0.8	0.65	0
SO_2	0.38	0.5	0
NOx	0.34	0.32	0.1
HC	0.2	0.12	0
PM[a]	0.09	0.14	0

a: Particular matter.

Table 2.5 Pollutants produced by three energy systems

2.3 Hydrogen storage

The very low density of hydrogen compared with other fuels (For instance, it is around 50 times lighter than gasoline) creates a technological challenge for its storage and transporting. Hydrogen can be stored as a gas, liquid or in a solid state. Preferring one method to another depends on its efficiency and cost. However, hydrogen storage techniques are now a major research concept. Compressed hydrogen tanks are the most common system currently used; it is compressed to a high pressure up to 800 bar (1 bar=10^5 Pascal) to increase its volumetric energy density. The compression process consumes a high level of energy, around 20% of the hydrogen's energy content, increasing the process cost and safety concerns. Vessels produced from a high strength and thin wall thickness composite materials are developed for a high and low cost storage system. Hydrogen liquefaction method at 20K and atmospheric pressure is one of the promising hydrogen storage methods currently used [6]. However, the energy needed for hydrogen liquefaction and compression is still too high. Caverns and depleted fuel wells are also used for hydrogen storage under high pressure without any leakage. Unfortunately, the high cost and energy consumption for the pumping system used in this process is significant. Solid hydrogen storage in metal hydrides or other chemicals is used as an alternative method with a high volumetric energy density, particularly for stationary storage systems. This method is under development to overcome the high weight, cost and energy needed to release hydrogen from metals. Many other techniques for hydrogen storage are in an early stage of development, including carbon absorption, glass microspheres and poly-hydride complexes [6,7].

2.4 Hydrogen energy production

Hydrogen can be produced in various ways, depending on primary resources such as fossil fuels, nuclear, biomass and other renewable energy such as wind, solar, geothermal and hydro-electric power. However, most of the hydrogen produced today uses fossil fuels. The challenge is how to produce it economically and in an environmentally benign way. Hydrogen production can be classified into three main methods: thermal, electrolytic and photolytic processes. In the following paragraphs, a brief description of each method will be presented [6,7].

2.4.1 Thermal processes

Thermal and thermo-chemical processes use heat sources or heat with chemical reaction to produce hydrogen from different resources such as ethane, methane, coal and biomass by different ways;

- **Industries hydrogen off- gas**

Colleting and purifying of hydrogen off-gas evolving in the production process of many industrial plants becomes one of the most common sources of hydrogen at present. These off-gases are often used on-site by the industries that produce them.

- **Steam reforming**

Hydrocarbon fuels such as methane, ethane, propane and gasoline can be used to produce hydrogen via steam reforming processes. Natural gas is commonly used today to produce hydrogen in the industrial sector with a competitive cost to the traditional fuel. The processes involve using a high-temperature steam (700-1000 ^{O}C) and 3-25 bar pressure in the presence of catalyst in an endothermic reaction to convert methane to hydrogen and carbon dioxide.

- **Coal gasification**

Hydrogen can be produced by reacting coal with oxygen and steam under high pressure and temperature to form a synthesis gas, a mixture of carbon monoxide and hydrogen. The monoxide reacts with the steam to create more hydrogen and carbon dioxide.

- **Biomass gasification**

Biomass, including agricultural residues and waste is converted to hydrogen and carbon dioxide using heat under pressure in the presence of steam and controlled oxygen amount or the absence of oxygen as in pyrolysis processes. Biomass resources can also be converted to a bio liquid fuel through fermenting the sugar in the source to produce ethanol.

- **Partial oxidation**

This is a gasification of hydrocarbons through an exothermic reaction with a limited amount of oxygen to form hydrogen and carbon dioxide.

- **High-Temperature water splitting**

Direct thermal chemical conversion processes at a high temperature (500-2000 ^{O}C) is used to split water to oxygen and hydrogen. This process is in the early stages of development.

2.4.2 Photolytic process

Direct sunlight is used to produce hydrogen by splitting water in various ways. The main two methods using this technique include photo-biological and photo chemical systems. The process offers a sustainable and environmentally benign hydrogen production method, but it is in a very early stage of development.

- **Photo-biological water splitting**

In this processes, hydrogen is produced from water using sunlight and certain microorganisms, such as green algae and cyanobacteria. Similar to the photosynthesis process of plants, the microorganisms consume water to produce hydrogen in their natural metabolic processes.

- **Photo chemical water splitting**

A photo electrochemical (PEC) semiconductors system produces electric voltage when it is exposed to light and can be used to split water into hydrogen and oxygen.

2.4.3 Electrolytic processes

Electrolysis of water means its dissolves into hydrogen and oxygen when electric current passes through it. Various kinds of electrolyzers are widely used today such as

alkaline, polymer electrolyte membranes and solid oxide electrolysers. Hydrogen can be produced using electrolyzers without any environmental impact when a renewable electric source such as solar is used. This process now takes more attention in the current scientist's research plans in order to reduce its cost and increase its efficiency.

2.5 Solar hydrogen system (SHS)

The solar hydrogen system presented in the previous chapter in Figure 1.5 is used to cover the energy demands of a community or a remote village as stand-alone system connected or completely separated from the grid. The electricity produced from the photovoltaic arrays is used to cover the community demands and to produce hydrogen from the electrolyzers. A fuel cell is used as a complementary and backup system to cover the energy demands in the absence of solar intensity at night and during cloudy days. Compressed hydrogen and oxygen tanks are used to store the fuel for the fuel cell. Hot water produced from the units' cooling systems and the fuel cell can be used in the system and to meet the energy needs of the community for domestic use and cooling or heating purposes. Hydrogen produced in the system can be used as a direct fuel for cooking, powering cars and for domestic needs. Several SHS have been installed in many countries since the 1980s. Table 2.6 summarises the technical characteristics of the systems installed worldwide up to 2009. These were mainly small systems used for research and development purposes [8, 9]. Many countries have allowance for a considerable budget for fuel cell and hydrogen research programmes for achieving hydrogen energy economy. The European-Union supports a frame work programme which includes hydrogen and fuel cell related research with a budget which increased from €8 million in (1982-1990) to €486 million in EP7 (2006-2013). China spent $3.08 million from 2003-2008 on SHS research. The US government currently spends about $400 million annually on hydrogen and fuel cells related programmes. Japan has planned to spend about $11 billion for a period of 28 years ending in 2020 to develop the basic technologies of hydrogen systems. Governments and industry in Canada, Italy, UK, Germany, Spain and Asia are also investing in hydrogen and solar research programmes [7].

Project name time and state	Source		Electrolyzer		Battery		Hydrogen storage			Fuel cell	
	Type	Installed power (kWp)	Type	Power (kW)	Type	Energy capacity (kW h)	Type	Volume capacity (Nm^3 H_2)	Energy capacity (kW h)	Type	Power (kW)
FIRST (2000–2004) Spain	PV	1.4	PEM	1	Lead acid	20	Metal hydrides, 30 bar	70	248	PEM	0.42
HARI (2002–) UK	PV–wind–micro-hydro	13–50–3.2	Alkaline	36	Lead acid	120	Pressurized tanks, 137 bar	2856	10,127	PEM	7
HRI (2001–) Canada	PV–wind	1–10	Alkaline	5	Lead acid	42	Pressurized tanks, 10 bar	40	142	PEM	5
INTA (1989–1997) Spain	PV	8.5	Alkaline	5	–	–	Metal hydrides – pressurized tanks, 200 bar	24–9	85–32	PAFC–PEM	10–7.5
PHOEBUS (1993–2003)Germany	PV	43	Alkaline	26	Lead acid	304	Pressurized tanks, 120 bar	3000	10,638	PEM	5.6
SAPHYS (1994–1997)Italy	PV	5.6	Alkaline	5	Lead acid	51	Pressurized tanks, 200 bar	120	426	PEM	3
SCHATZ (1989–1996)USA	PV	9.2	Alkaline	6	Lead acid	5.28	Pressurized tanks, 8 bar	60	213	PEM	1.5
Solar house (1992–1995)Germany	PV	4.2	PEM	2	Lead acid	20	Pressurized tanks, 28 bar	400	1418	PEM	3.5
Solar hydrogen pilot plant (1990–1992)Finland	PV	1.3	Alkaline	0.8	Lead acid	12	Pressurized tanks, 25 bar	200	709	PAFC	0.5
SWB (1989–1996)Germany	PV	370	Alkaline	100	–	–	Pressurized tanks, 30 bar	5000	17,730	PAFC	80
CEC(2007–Turkey	PV	5	PEM	3.35	Lead acid	28	Metal hydrides, 14 bar	5.4	19	PEM	2.4

PV: photovoltaic; PAFC: phosphoric acid fuel cell; PEM: proton exchange membrane fuel cell.

Table 2.6 Worldwide photovoltaic-hydrogen/fuel cell systems for stationary power production and their specifications

As mentioned in previous sections, solar energy can be involved in the hydrogen production using different methods. One of these methods is the water electrolyzers use

electricity produced from photovoltaic arrays at a low temperature. This promises to be the most efficient and environmentally friendly method of producing hydrogen, whereas other methods are still in the early stages of development. Hydrogen produced by using water electrolyzers still far away from being competitive in the energy market, but more researchers are involved in experimenting with it. Many researchers have developed and studied SHS, either experimentally or by using simulation tools and software. These studies have been performed in order to improve system performance, create new simulations, analysis and evaluating tools as well as reducing components and operation costs. In the following section, a general revision and discussion of the most important research works related to the current study which have been carried out to investigate SHS is presented and discussed.

Joshi, *et al*. [10] presented a theoretical exergy analysis study to compare hydrogen production using an electric source from a water electrolyzer and photovoltaic or solar thermal source as concentrating collectors. They concluded that a solar thermal hydrogen production system has a higher sustainable index than a PV hydrogen system, due to its higher exergy efficiency. Furthermore, a PV system is better because it does not involve any moving parts. The exergy analysis in this study neglected the heat transfer losses from the units. The results also have not been validated. A thermo-economic study is required to produce accurate results.

Negrue, *et al*. [11] studied the technical and economic effects of the combination of a solar chimney power plant and hydrogen as a storage and energy carrier medium. Tmanarasset, a city with high solar intensity in the southern area of Algeria, has been used as a case study. The authors suggested the use of a tower of $2.06*10^9$ m^3 to produce 9 MW in order to provide an alkaline water electrolyzer to produce $3.5*10^6$ kg H2/year. General economic analysis has shown that at a capacity of $8*10^6$ kg H2/year with a hydrogen cost of 3.25€/kg H2 will be achieved.

E. Belgan, [12] developed a theoretical mathematical model in order to optimize the thermal and economic performance of large-scale photovoltaic-electrolyzer systems. He was using a five-point method to solve five nonlinear equations by using a numerical technique to create the (I-V) characteristics curve of the PV system. The (I-V) characteristics of the electrolyzer system were expressed as a polynomial equation, using the least square method with empirical data to solve it. The results obtained showed that the hydrogen cost is correlated to the yearly solar intensity received by the PV surface. Furthermore, a minimum hydrogen cost of 44 $/GJ can be achieved with a

PV system cost of 1$/Wp in high solar intensity places such as Saudi Arabia. The overall thermal efficiency of the system has been calculated as 10.33% for fixed panels and 10.85% for sun tracking panels.

Tani, *et al*. [13] designed and constructed an experimental system based on a small capacity PV module coupled directly to a PEM hydrogen electrolyzer. The system's characteristics were measured and analysed. They developed a method to design the most cost effective hydrogen generation system according to the unit costs and the weather conditions. The results showed that the system characteristics and the hydrogen cost were affected by the variations of the climate conditions. Moreover, the evaluation index for the optimal solar hydrogen system with hydrogen production cost per unit volume was presented. The analysis showed that at a cost ratio of 0.75 (PV installation cost to the installation cost of the electrolyzer), the optimal design point of solar intensity is 0.5 $kW/m^{2,}$ the system efficiency is 4.47% and the hydrogen production cost per unit volume (utilization factor) in this case is 22% cheaper than the hydrogen production cost at standard conditions. No details have been given for the simulation tool used in this study.

C. Wang and M. Nehrir [14] designed an overall power management strategy for a hybrid (wind/PV/fuel cell) energy system, in order to coordinate the power flows from a different energy sources. A simulation analysis using MATLAB/Simulink model based on control, electric and empirical relation of the units has been carried out. The effect of the climate condition on the power output in winter and summer as well as the effectiveness of the overall power management strategy of the system was investigated.

Yilanci, *et al*. [8] presented a general review of solar hydrogen projects worldwide until 2009 as well as their production method and specifications. The SHS installed at Denizli Turkey was used as a case study for an energy and exergy analysis study. The analysis used data for the PV monthly power production estimated from PVGIS software, developed by the European Commission. The power output of the PV unit was increased by 10% as an assumption that mounted the PV on a fitted tilt of 45^{o}, while 10% for the PV losses were estimated as being due to cables, dirt, snow and cells mismatching. The results showed that the overall efficiency values of the system varied between 0.88% and 9.7% while the minimum and maximum overall exergy efficiency values of the system were 0.77 and 9.3% respectively. Three different demand paths of energy systems were considered for investigation; a PV with inverter, a PV with two inverters and a SHS with two inverters. The SHS path has the least efficiency with

minimum and maximum energy and exergy efficiencies of 0.88, 1.79 and 0.77, 1.66 respectively. The study suggested some improvement to encourage system performance, particularly the PV unit, such as using one inverter instead of two and a PLC control devices in order to control the power and hydrogen production. The effects of the ambient condition on the heat transfer coefficient, PV surface temperature, hydrogen production, power, and many other parameters are not analysed in this study. The study has been recommended to be continued to conduct a detailed cost and thermo-economic analysis for the system. The analysis also used an assumed constant PV cell temperature, while it is not constant and varied according to daily ambient conditions, which will affect the accuracy of the results obtained.

Calderon, *et al*. [15] performed an exergy analysis study of SHS based on experimental data used with a simple model. The results indicated that the exergy efficiency of the PV, electrolyzer and the fuel cell can be calculated as 8.39%, 68.7% and 35.9% respectively. The analysis shows that the PV efficiency is more likely to be affected by the solar irradiance and power output rather than by the ambient temperature. The fuel cell and the electrolyzer efficiency are more sensitive to the hydrogen/power produced and supplied. The electrolyzer used in the experiment operated at a fixed power operating point, so that it is not affected by the solar irradiance variation. The model ignored the exergy losses of the water and oxygen streams in the system.

Bahman Shabani and John Andrew, [16] investigated the performance of a 0.5 kW combined heat and power (CHP) PEM Fuel cell and compared the results with a simulation analysis carried out for the same unit's specification and data worked in a solar hydrogen system. The energy efficiency of the unit, as measured experimentally, was found to be 72% on average, while its efficiency in power only mode was only 35-50%. However, the unit efficiency in a SHS, using a similar analysis, is predicted to be less than 70% and in a power mode only 46% on average. The study showed that the poor performance of the fuel cell (40%) at a lower operating temperature can be partly overcome by increasing the air flow rate ratio to 4. That is encourages evaporation of the water produced and the purging of the accumulated water in the fuel cell membrane. An economic analysis shows that 10% reduction in the net cost of the total SHS will achieved when the fuel cell cooling load is utilized during the project time period. It has been found that the energy efficiency of the Electrolyzer-Storage-Fuel cell system rose from about 34% in a power only application to about 50% in a combined heat and power (CHP) mode. The simulation analysis assumed that the heat transfer coefficient is

zero (fully insulated unit) and a hydrogen utilization factor (90-98%). The energy efficiency was reduced to 63% instead of 70% when a hydrogen utilization factor was assumed as (85%) in the model.

G. Zini, *et al*. [17] studied SHS system with activated carbon storage. They implemented a system dynamic theoretical model based on experimental and empirical data, using Matlab Simulink software. A case study related to a single load profile in San Diego California, USA was chosen to simulate this system on a yearly base. The behavior and thermal working cycle of the storage tanks using nitrogen as cooling medium (pre charging – charging – pre discharging – discharging) are investigated thermally. However, the study indicated that activated carbons are not the ideal material for hydrogen storage since they require operating at very low temperatures (77k), while other materials such as (Bi CH_4) have shown high adsorption capabilities at temperatures as high as (115k). This study also mentioned that activated carbon storage can be considered a potentially feasible way of providing a stationary application of solar hydrogen systems in the future. The real economic viability of this storage process is not examined in this study, a thermo-economic study is necessary to investigate this.

K. Hacatoglu, *et al*. [18] used the energy analysis method to investigate the solar hydrogen system with activated carbon storage proposed by G. Zini [17]. The analysis shows that the exergy efficiency of the system can be improved from 4% to 11% through utilizing the hot energy streams from PV/T and fuel cell units. Also cold thermal streams and excess nitrogen can be recovered from the adsorption process of hydrogen to activated carbon. The PV unit is the least efficient component with energy efficiency at the base case 14% and 18% for the PV/T unit, which encouraged more efficiency improvement. The analysis of the PV unit is based on a way of calculating the heat transfer coefficient and it is not clear how it is calculated. The surface temperature of the PV is assumed to be constant, although during the day it is affected by solar intensity and ambient conditions variations. The analysis uses the average intensity of solar insulation during the summer day instead of hourly data, which gives more accurate results. The study did not mention how the sizing method of the system components was performed to meet the load requirements all the day.

Yilanci, *et al*. [19] investigated experimentally the exergy efficiency of a SHS built in Denizili, Turkey. The analysis is based on a real data during a week of system operations. The heat transfer coefficient of the PV unit was based on a general empirical relation. Furthermore, the analysis ignored the thermal losses from the fuel cell and the

electrolyzer. The result showed that the exergy destruction of the PV units is 93.3%, the electrolyzer 4.76% and the inverter 1.29% and for the batteries was 1.94%. The average overall exergy efficiency of the system during the experiment week was about 3.18%. The exergy efficiency of the fuel cell was not considered in this study. The study mentioned that the amount of hydrogen produced during the experiment was 4.43kg, which represented a saving in CO_2 emissions of more than 6.8 times compared with the steam performing process of natural gas for the same amount of hydrogen production. The study did not show whether the heat transfer coefficient was considered from one side or both sides of the unit.

A power control system for hydrogen system consisting of a PV unit (250 kW_p), an electrolyzer and a battery was designed and investigated to reduce losses by Contreras, *et al*. [20]. The simulation tools Simulink, Lab View and Pspice were used in the analysis. The study showed that the designed control system working for the electrical transformer between the PV generator and the electrolyzer had an efficiency level of about 94%. This was due to the reduction in loss, as well as the controller switching the power elements in the system. In general this did not create a significant change to the control systems and transformers available on the market.

Paola, *et al*. [21] developed a simulation program called RenHydrogen based on Lab View in order to simulate a PV generator connected to an electrolyzer. Hydrogen production was studied under different system working conditions and the production costs were analyzed. The program was used to predict the PV output and solar radiation at specific latitude, connected directly or indirectly to an electrolyzer. The study did not present a sensitivity analysis for the PV and electrolyzer operation parameters. The models are based on empirical mathematical relations with an input data for references components presented in the literature. In spite of this, the PV model was based on a specific theory which is valid only for latitudes lower than 65˚ and the analysis in the study included a case of 90˚ tilt angle. The study shows that the PV-electrolyzer direct connection is more efficient. The lowest hydrogen cost was obtained for a 60˚ tilt angle in Rome as a case study, in direct connection, in which 1.61 €/Nm^3.

A single and four stages high pressurized hydrogen gas compression and storage subsystem was investigated through an exergy analysis and parametric study by Ozsaban, *et al*. [22]. The study shows that multistage process at constant inlet and storage pressure and high compression stage number is more effective and less costly than one compression stage process. For a constant hydrogen gas storage pressure,

increasing the inlet pressure of hydrogen gas increases the exergy efficiency of the system. The results could not be realistic without a more detailed thermo-economic analysis.

Akyuz, *et al*. [23] developed a novel computational tool in Matlab-Simulink for analyzing the probability distribution of the hydrogen production for a PV assisted PEM electrolysis system. Experimental data taken from a real system installed in Balikesir University in Turkey was used in the analysis. The amount of hydrogen production as a parameter of the intensity of solar radiation is investigated hourly and yearly. The study presents a correlation by calculating the hydrogen amount and cost as a time-function with solar intensity variation. The results showed that the highest amount of hydrogen production occurred at 650 W/m^2 for a selected year for Balikesir region, Turkey. The average energy efficiency of the selected PEM electrolysis was 60.5% with current density of 0.48 A/cm^2. The cost of hydrogen calculated in yearly average was 4.8 $/kg for this region. The study was based on an energy analysis and the study did not present detailed equations of the model and the used technique. The analysis mentioned without proof that the PV efficiency was dependent on the PV area which was not proven in any other study.

M. Santarelli and S. Macagno [24] developed a simulation model based on the Matlab-Simulink software in order to compare and investigate the performance and the behavior of two different stand-alone energy systems. The system consisted of a photovoltaic unit, an electrolyzer, a compressed gas storage system, a battery and a PEM fuel cell (SHES) and another integrated system of a micro-hydro power with a PV unit (SμHHES). The system was designed to meet the electricity needs of a residential area in a remote area (a valley in the Alps in Italy) during a complete year of operation. The systems used three electrolyzers with 1 kWe, PEMFC of 3 kWe and 47 m^2 PV surface area. The SμHHES used a micro-hydro turbine of 1.4 kWe with a 15 m^2 PV surface area. The analysis showed that, in a complete year of operation, 50% of the electrical demand was covered by the PEMFC in the case of SμHHES, while the figure was 67% in the case of SHES. The PEMFC produced 38% of the input electric energy sent to the elctrolyzer. The internal heat flow was positive for SHES and negative for SμHHES. During the year, the SHES produced 450 Nm^3 of hydrogen, whereas the SμHHES produced 630 Nm^3. Based on the authors previous economic study of the same case study, the electricity cost of SHES was in the order of 45 C$ at 1:00 pm and 200 C$ at 8:00 pm, while in the case of SμHHES it was 30 C$ at 1:00 pm and 130 C$ at 8:00 pm.

The study showed that the prices would be competitive only if a value of a carbon tax is considered as 155 $/tons CO_2 in the case of SμHHES. The study did not include any details about the mathematical model and the computer codes used in the study. The model is based on an experimental data which could be used only for a specific type of equipment instead of general use. The same authors studied the system thermo-economically [25] in order to investigate its performance based on exergy analysis. They used the fundamental structure method which is an evaluation of the costs of each exergy flow in the plant in monetary terms according to the function of each unit based on the cost of the fuel entered and product leaving the unit. The analysis shows that the unit thermo-economic cost (UTC) of the electricity is very high, even if the solar irradiance is free. Three scenarios were studied according to different unit costs. The optimum one, which is based on 775 $/kW for PV unit cost, 1000 $/kW for the fuel cell and 3000 $/KW for the electrolyzer, for this scenario the kWh is in the order of 15 C$ at 1:00pm and in the order of 100 C$ at 8:00pm where the fuel cell only is worked. The results showed that the cost was not competitive with the actual energy market (2004), but that if the external cost due to pollution was internalized the competitiveness of this system would be increased. No details have been given about the software used in the calculation. The exergy efficiency and exergy destruction at each unit were not considered in the analysis, neither its effect on the thermo-economic factors and unit parameters were taken in consideration.

Lagbise *et al*. [26] analyzed the electricity production cost of three different configurations of a solar hydrogen systems consisted of:1- PV+FC+Battery, 2- PV+EL+H_2 tanks+FC and 3- PV+EL+H_2 tanks+Battery+FC. The systems were optimized and sized analytically by a simulation model based on Matlab-Simulink which used an empirical valuation mathematical model. The analysis was applied to a small load for a one year operation. The result showed that the configuration costs over 20 years working in the three systems were 0.519, 4.943 and 0.645(€/kWh) respectively. The global configuration efficiency which allows for an estimation of the waste of energy between the production and the consumption was calculated to be 50%, 22.4%, and 50% respectively for the three configurations. The analysis consider a high unit cost (€/W) for the system components PV, EL and FC as (5, 15 and 8) which is too high compared with the unit's current prices, along with the hydrogen cost of 0.39 €/Nm^3. This means that the electricity cost produced from the three configurations was high in comparison with the traditional energy production cost, particularly for the second configuration.

Joshi, *et al*. [27] studied various methods of hydrogen production. The study shows that water electrolyzer using photovoltaic is the most mature method for producing hydrogen. Meantime, more research had to be carried out in order to improve the exergy efficiency of the PV unit in order to enhance the overall efficiency cycle of the solar hydrogen system.

Kolb, *et al*. [28] proposed using a large-scale solar thermo-chemical hydrogen plant at lower cost. This system consists of a solar power tower with a sulfuric acid cycle to produce hydrogen instead of a solar-electrolyzer plant. The study showed that for a large scale power plant (100MW) the hydrogen production cost is 2.8 $/kg via a thermo-chemical process compared with (5.1 $/kg) if it is produced from a solar-electrolyzer plant.

El. Shatter, *et al*. [29] designed a 2.24kW SHS system. Electrical models for each system components are introduced based on empirical parameters. The system was simulated using Simulink-Matlab software. The analysis showed only the PV output variation from season to another during the year, the hydrogen production amount and the fuel cell output.

A comparison of three different energy production methods according to its electricity production cost and CO_2 emission reduction was carried out by L. Harvey [30]. The systems are a centralized fossil fuel electricity generation, hybrid photovoltaic-fossil fuel electricity and solar hydrogen system. The study shows that the electricity production from the solar-hydrogen system was 0.2-5.4 cents kW/h greater than from a natural gas power plant for the cost and performance assumptions adopted in the study. The carbon tax required to create a solar hydrogen system which could be competitive with fossil fuels ranged from $70-660 per ton. The estimated component cost of the study was around 6 times less than the current component's prices. Also, the current natural gas prices were much higher than the estimated one used in this study. The study was general study without any details of the economic analysis procedure.

Park, *et al*. [31] used PSCAD/EMTDC, a simulation tool for the transient analysis of an electric power system, to simulate a photovoltaic solid polymer electrolyte system. The analysis and model components were developed based on its I-V characteristics. The solar irradiance, cell surface temperature and electrolyzer input water temperature were controlled for specific purposes in an actual system and its experimental results were compared with the simulation results. The system showed good operational characteristics. The simulation results are agreed with the results from the actual system.

G. Eljrushi, and T.Veziroglu, [32] developed a mathematical model for a solar hydrogen energy system for Libya by obtaining relationships for and between the main energy and energy related parameters. The following variables were chosen to construct the model: population, energy-demand, energy production, energy price, gross national product, air pollution and quality of life. The same analysis was applied to Egypt by M. Abdullah, *et al*. [33] and for Saudi Arabia by S. Almogren and T. Veziroglu [34]. Also a similar study was been carried out in Spain by Contreras, *et al*. [35]. The results indicate that the fossil fuels resources in both countries are being vastly depleted. So, adopting the solar hydrogen system would extend the availability of fossil fuel resources, reduce pollution and establish a permanent energy system. However, these countries could become exporters of hydrogen. The fossil fuels and hydrogen prices, as well as the fuel reservoirs predicted by these studies are very different from the current prices and amounts expected today.

Shabani, *et al*. [36] developed a computer simulation model for solar-hydrogen system (CHP) using visual Pascal-Delphi software, based on I-V characteristic mathematical relations. The analysis used a household (5kWh load) located in south east Australia as a case study to investigate the influence of the key parameters on the system's economy and the potential of waste heat and hydrogen recovery from a fuel cell. The analysis showed that this system is not competitive at the moment, but that it could be a serious competitor against a diesel/petrol generator if the assessment period was 20 years or more. The study showed that, for a 30 year assessment, the system could supply half yearly demand for hot water to a house hold by means of the heat and hydrogen recovery with an average cost of 90 C/$kWh. Moreover, this study suggested that increasing the fuel cell size would improve its average efficiency to a certain extent and reduce the electricity production unit cost. The study also shows that constraining the size of the hydrogen tank would not improve the system from a cost point of view, since it leads to a large PV and electrolyzer. The analysis considered only the energy equation for calculating the heat generated from the fuel cell. Additionally, the life cycle time of the proposed units was small compared with larger units produced today for a lifetime of over 20 years.

Ganguly, *et al*. [37] developed a solar hydrogen system model integrated with a floriculture greenhouse using C+ language program based on electric I-V characteristics. The study predicted the performance of the individual components and the integrated system for a different climate condition and year seasons for Kolkata

India. The analysis shows that the system under a standalone manager provides a viable option for its power demand.

Lopez, *et al*. [38] described the main criteria which have to be considered in designing a hydrogen storage system. The exergy analysis method was used to investigate three different methods to store hydrogen: low-pressure tanks, high-pressure tanks and metal hydride. Real data from a solar hydrogen storage facility was used in the analysis. The study shows that, from exergetic point of view, direct use of hydrogen from low pressure storage is most efficient and simple option, while high pressure hydrogen storage is the most inefficient option. The detailed equations required to calculate the exergy destruction for each system were not presented in this study. The study used real data from a small scale system. A thermo-economic study was necessary to produce more accurate results, particularly for large scale systems.

O. Ulleberg, and R. Glöckner, [39] developed a solar-wind hydrogen library model using FORTRAN software called HYDROGEMS. The library included components subroutines for PV arrays, wind systems, diesel engines, batteries, electrolyzers, fuel cells, compressor, power conditions equipment, storage tanks and logical control functions. The components models are written as FORTRAN subroutines and are primarily designed to run with the transient simulation program (TRANSYS) and the non-linear equation solving program (EES). The models have been designed to be as generic as possible. They are designed so that specific components characteristics obtained from the manufacturers, or from experiments, can readily be added to a data base. The models have been tested, verified and have been successfully used as the basis for modelling in several simulation case studies. However, the models' subroutines are mainly based on an empirical experimental data which restricted the general use of these models. The model also is based on an energy analysis without exergy and thermo-economic codes which is a powerful tool of a power system's analysis and investigations. More research is necessary to develop more general, simple and friendly interface software based on exergy, environment effects and thermo-economic codes which could be used with more power and thermal systems.

A simulation analysis based on a TRANSYS-HYDROGEMS library was developed by Briguglio, *et al*. [40] in order to design a wind-supplied hydrogen filling station for a fuel cell mini-bus fleet in Messina. Economic subroutines were developed to calculate the cost of the hydrogen. The analysis showed that the hydrogen vessel cost have an important effect on final hydrogen costs. The hydrogen costs were strongly linked to the

boundary conditions, such as the specific wind source available, the hydrogen demand and the basic electrolyzer management. The mathematical equations are not presented in this study.

Santarelli, *et al*. [41] examined three different stand-alone energy systems to supply the electricity needs of a small residential mountain area in Italy, during a complete year. Three different sources have been considered; PV/ wind/ micro-hydro turbine along with electrolyzer, fuel cell, battery, hydrogen storage. A code has been developed to estimate the I-V characteristic of the main units, depending on the empirical parameters obtained from measurement producers and the experimental data from literature or manufacturers. The study shows that at the specific location the micro-hydro source is the best plant option, while the wind source is not convenient to use due to varied weather conditions, requiring a higher hydrogen seasonal storage and over size equipment. The analysis considered a one hour time step as a successful steady state situation. There were, however, no details of the I-V characteristic components code written for the system simulation, design and behavior. Classical methodology was used for an analysis of component sizing according to specific operation conditions instead of using a computer program.

Hwang, *et al*. [42] used dynamic simulation software SIMPLORER to model a solar hydrogen system. These models are mainly based on electrical and electro chemical relations and several empirical relationships. The model was successfully applied for assess the daily power consumption of a typical family. The analysis neglected the parasitic loads such as water pumps, compressor. Furthermore, the system analysis tools provided by this work did not specify in depth how they could be used to improving a component's efficiency, costs and time saving in the design of such systems. There is no clarification on how the software mathematical solution works or any assessment of its advantages.

A. Zahedi [43] presented general technical aspects of design, size optimization, and performance prediction for SHS in supplying electricity to a remote community. The results of the optimum sizing of the system components and their efficiency are presented in this paper without any details or information about the use of the software or how it's applied.

Pedrazzi, *et al*. [44] used Matlab-Simulink software to develop and implement an electrochemical model for a solar hydrogen system and applied these to real data on a

typical residential user over a year long period. Results show that the system could be working alone and achieve complete grid independence with a system efficiency of 7%.

Andrew Mills and, Said Al-Hallaj, [45] used Hybrid2, a form of modeling software, to predict the long-term performance of hybrid systems. They used site-specific resource data to simulate a solar wind-hydrogen system. The system was designed and simulated using real data available in Chicago, in order to meet a varying load with a mean of 1kW. The results show oversized estimation system components. The model consists of a new model library for the electrolyzer and the compressor, whereas the existing models in the Hybrid2 are used for the other components. The compressor power is estimated from similar conditions and it is not calculated in the analysis. The analysis indicates only the power produced and consumed. The software component models are based on actual performance and data of specific components commercially available from manufacturers, rather than the behavior of a theoretical process. Also it is based on a quasi-steady state model. The analysis did not include optimum system sizing and economic analysis.

An experimental measurement and study of a solar hydrogen system consists of a 5 kW PV and 2.4 kW_p fuel cell, at Denizli, Turkey by Cetin, *et al*. [46]. In this study an electrical energy analysis was performed in order to evaluate the power quality of the hybrid energy system and it is electrical characteristics. The results show that to prevent the decrease in voltage, electricity supply cables should be selected correctly along with suitable capacitor groups.

G. E. Ahmed, and E.T.EL Shenawy, [47] performed an experimental study of small PV power systems to produce hydrogen using photovoltaic modules connected to the electrolyzer with and without a maximum (MPPT) power tracker. The results show that connecting the PV with (MPPT) will increase system efficiency and the hydrogen production flow rates.

M Alam, and D. Gao, [48] used the HOMER software 'Hybrid Optimization Model for Electric Renewables', which was used mainly for electric power analysis and cost benefits for a hybrid system, to simulate cost analysis and investigate a small solar-wind-hydrogen system. Moreover, annual performance, electric produced/ consumed, and annual emissions were simulated. The sizing of the component or operation parameters sensitivity analysis was not considered in the analysis. The software did not include an open source code and then it is not flexible to be used for any application. Furthermore, no thermodynamic and thermo-economic code was included.

E. Bilgen, [49] implemented a simulation study on a solar hydrogen system using a simplified model for a PV and electrolyzer unit, in order to determine and optimize the system thermally and economically. The study derived correlations for the system thermal performance using annual total solar radiation on a horizontal surface. The economic feasibility of the system was also correlated as a function of the PV and electrolyzer price and the annual solar radiation on a horizontal surface. Data from twelve different climate locations in the United State has been considered for hydrogen production analysis cost and quantity as a function of solar intensity. The analysis shows that, varying the PV cost from 1 to 6 $/W_P$ and the EL cost from 1 $/W_P$ to 11 $/W_P$ for a solar radiation decreasing from 7.8 to 4.3 GJ/m^2 will vary the cost of hydrogen production from 3.5 $/kg to 38 $/kg and 25.3 to 268 ($/GJ H2) and its quantity from 26 to 42 (kg H2/ kW$_p$/year) for fixed PV unit. Similarly, for a tracking panels it varies from 2.5 to 28 $/kg and 17.7 to 199 ($/GJ H2) and hydrogen quantity from 36 to 62 (kg H2/ kW$_p$/year). The study indicated that the hydrogen price could be competitive with the present day automotive fuels if the unit price (2004) was reduced several times, and / or the price of fossil fuels became several times higher and / or the solar intensity was higher than 6 GJ/m^2/year. The overall thermal performance of the system varied between 8.64% and 9.34%, depending on the solar intensity. The energy analysis is not included in this study and the calculation tool is not specified. The equation used to calculate the efficiency of the PV unit assumed the reference temperature of the unit surface temperature to be zero, while most of the references and researchers take it to be 20℃. The analysis used a general correlation equation to calculate the PV power output and to predict the PV surface temperature using the general balance method based on more than one predicted factor. The study indicated that power produced from tracking panels is higher than a fixed one by about 50%.

K. Christopher and R. Dimitrios [50] compared the exergy efficiency of hydrogen production with and without liquefaction processes, using 4 different renewable energy sources (wind, solar, hydro, and biomass). The analysis shows that the liquid hydrogen production using solar had the lowest exergy efficiency at 1% while highest exergy efficiency was for the hydro power method at 5.6%. It was also found that the liquefaction processes was very energy intensive, consuming a lot of exergy. The study considered the PV exergy efficiency at STC to be 12.5% and the electrolyzer's nominal exergy efficiency to be 67.5%. The authors mention that it is recommended to include the environmental impact and the exergy cost structure of the process in such analysis.

An economic analysis has been performed by A. Raj and P. Ghosh [51] to compare a photovoltaic standalone system using a diesel generator and a solar hydrogen system. It has been found that, in addition to the advantage of the SHS as being environmentally benign and low noise, it is also cost-effective particularly when a high pressure electrolyzer as well as metal hydrate and high pressure tanks are being used. The study also indicated that these results are more reliable as the fuel price increases and the platinum used in the fuel cell can be recovered at the end of its life time.

The previous works and studies on SHS presented in this section indicated that these technology are still immature and have a high costs. It is also showed that several models and software are developed and applied to analysis these systems based on energy analysis using empirical and experimental factors rather than thermo-economic analysis, explicit and general models.

2.6 Summary and conclusions

The hydrogen production methods; thermally, photolysis, reforming, and electrolysis one, as well as hydrogen characteristics, are described in this chapter. Producing hydrogen using electrolysis of water is suggested to be the cleanest and most attractive method currently used. Due to hydrogen's very low density, storage and transportation technologies are a key research and development challenge. Low and high pressure tanks and hydrogen liquefaction are the most promising storage systems used nowadays. However, many other techniques are under development such as the metal hydrate method. From the literature survey it is clear that the currently production cost of SHS is still too high compared with the traditional power plants using fossil fuels or nuclear energy. These systems will be more competitive when the environment damage and resources consumed by the traditional system have been taken into consideration. Research and development efforts in SHS technologies are required in order to; improve its efficiency, establishing techniques for accurately predicting their output, reducing costs. These resarch activities are also nesasary to reduce or generally eliminate the empirical nature of the current models as well as creating new simulation tools and reliably integrating them with other conventional generation sources. Most of the previous research studies, models and the developed software are focused on energy, electro chemical, management and control system, storage technology and economic analysis of particularly small standalone systems. However, recently exergy analysis and thermo-economic analysis rather than energy and economic analysis have used up a considerable amount of effort in the research activity. This technique has not been

widely used for SHS analysis and to date, there is no commercially available software code developed based on this method. Furthermore, there is no fully simulation and parametric and thermo-economic analysis for a high production capacity system taking the environmental impacts and resources consumed into consideration, and apply it to hot regions such as North Africa.

CHAPTER THREE

Chapter Three

Solar hydrogen system components;

(Description and literature review)

In this chapter a general view of the working principles, technology and market concepts of the main components of the SHS; photovoltaic, photovoltaic thermal, fuel cell and electrolyzer are presented. The most important previous research works mainly related to the objectives of this research on studying SHS components are also discussed and evaluated.

3.1 Solar energy

Solar energy, as the most abundant, inexhaustible and clean form of energy, is the source of all direct or indirect energy supplies, such as wind, waves, geothermal and hydro, apart from nuclear energy. The solar energy received by the earth in one hour could cover all human energy needs for one year [52]. The radiations beyond the atmosphere are called extra-terrestrial with a density of around 1367 W/m^2 and the one below the atmosphere is known as terrestrial. The terrestrial radiations passing through the atmosphere can be divided into direct radiations coming directly from the sun, diffuse radiations which absorbed, scattered and reflected by atmosphere, snow, ice and ground reflected radiations (albedo). The total or global radiations are defined as the summation of direct, diffuse and albedo radiations. The global radiation power density is approximately 1 kW/m^2 on sunny days, and will be less in cloudy days. Solar radiation intensity fluctuates with time and seasonally according to the rotation of the earth on its axis and around the sun. It increases in the equatorial regions and in areas such as the North Africa desert.

Solar energy can be classified in terms of its frequency: high (<0.38 μm/ Ultra-violet), Visible (0.38-0.78/ Light), and low (>0.78/ Infra-red). It is measurement uses a Pyrheliometer device to measure direct radiation and a Pyranometer to measure total radiation [53]. However, solar energy can be utilized thermally through; direct collectors, solar towers, graduated temperature in a salted lake, or concentrated parabolic systems to heat fluid or salts. This thermal energy can be used either directly in industrial and domestic applications or indirectly by converting it to steam to produce electricity in turbines or mechanical work. Photovoltaic panels are used to convert solar radiations directly to electric energy.

3.2 Photovoltaic

Photovoltaic is the process of converting light to electricity when it is falls on a semiconductor material. The first person to who discover the photo galvanic effect was Becquerel in 1839 and then the process was improved and taken as the basis for producing the first solar cell that had an efficiency of 6% by Chapin et al in 1954 [52, 53]. A brief description of the working principles of the photovoltaic processes will be presented in the following section.

3.2.1 Working principle

The photovoltaic cells are usually produced from silicon. Pure silicon is an isolated material with a very low electrical conductivity. Silicon atoms consist of four electrons with their valence involved in covalent bonds with neighbouring without moving. To change the electric state of pure silicon to a semiconductor material, a doping process is necessary. The doping process can be achieved by adding some impurities such as phosphorus atoms with five electrons combined with the silicon atom to create an n-type structure, on the top surface that faces the light. In the n-type an extra electron is created after the doping process while adding a boron atom with three electrons on its outer orbit to the silicon atom to create a p-type with a hole. When the two types n and p are put on each other the falling light, with specific wavelength and band-gap, on the n-type will cause a fast moving exchange between the electrons from the n-type to the holes in the p-type and vice versa. This movement will continue until barrier junction (+ and – charges) on each side creates a diode, which prevents the moving of the electrons through the barrier. The charges are forced to travel on an outer circle to the other side and an electric current will be produced when a wire is connected between the two types as presented in Figure 3.1. Several junctions of n and p types will form a solar cell that is connected together in different configurations to form a module. The minimum band-gap energy of 1.1 eV is required for the above-mentioned electron–hole excitement. However, the minimum threshold of photon energy required to excite an electron–hole pair dictates the cell's efficiency. Moreover, equivalent to a third of the integrated energy within the spectrum cannot be used to excite electrons, while only the energy contained within the (300–1100 nm) band can contribute to the cell voltage. The excess energy is lost in photon transitions that contribute to thermal losses [52, 53, 54, 55].

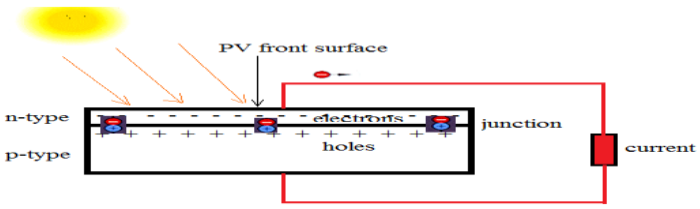

Figure 3.1 Photovoltaic working principles

3.2.2 PV Global market

The PV global market has grown by 139% Y/Y (2009/2010) and reached its 18.2 GW installed capacity in 2010. It generated $82 billion in 2010 which rose from $40 billion in 2009. Meanwhile, solar cell production capacity increased to 20.5 GW in 2010 from 9.86 GW in 2009. European markets, mainly in Germany, Italy, the Czech Republic, France and Spain account for 81% of global demand. However, crystalline silicon cells are still governing the market with 87% of the total production. The heavy activity and development in the PV technologies and mass production pushed the module price index towards decline every month as presented in Figure 3.2. The module price decreased from around $5.5 /Wp in December 2001 to around $2.5/Wp as an average in February 2012 [56].

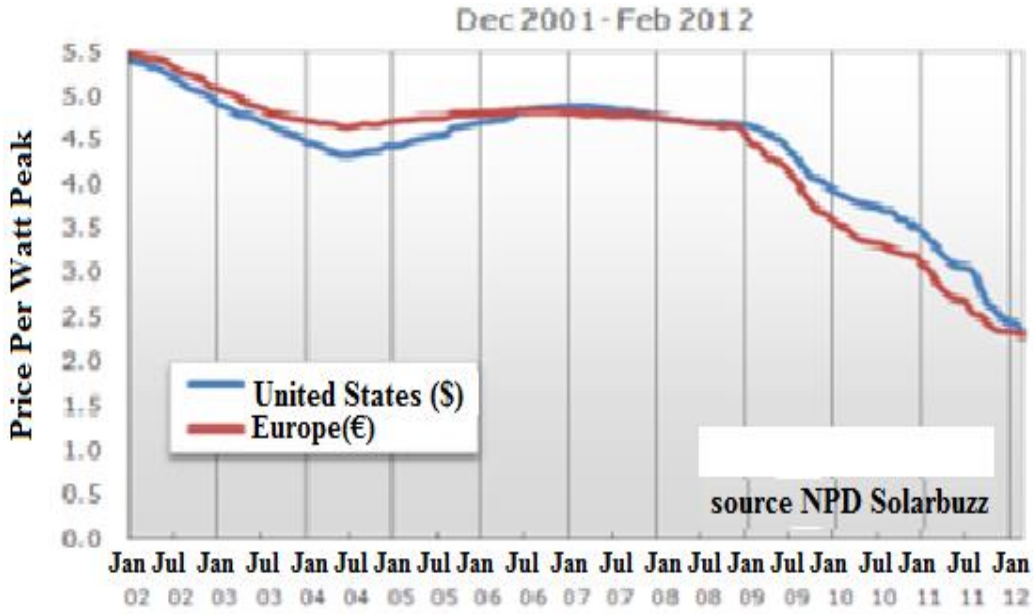

Figure 3.2 Module price index [56]

3.2.3 Photovoltaic types

Different materials and technologies are used to produce several types of photovoltaic. However, choosing of proper material, encapsulation and application of UV-filter will enhance the cell efficiency, stability and decrease its degradation. Cells are mainly

produced from silicon and can be classified as crystalline silicon, thin-film, multi junction and emerging technologies. Some of the most important types and cell technologies are summarized in the following table [52].

Cell Type	**Material**	**Efficiency % com-lab**	**Remarks**
Monocrystalline	Pure mono-crystalline silicon	16-25	-Cheap
Silicon ribbon	Poly or single crystal silicon melt	10	-Cheap
Polycrystalline	Grains of mono-crystalline silicon wafers	14-20	-Cheap -Simple
Polycrystalline thin film	Thin layer of silicon(20µ)/ ceramic	15-30	
Gallium arsenide	Pure gallium arsenide /germanium (Ga As)	-20	-High cost
Thin film	1µ amorphous silicon(a-Si) or Copper indium(CIS) or Cadmium telluride (Cd Te)	-12 4-7	-degradation -expensive -cadmium/ toxic gases
Multi junction	Number of thin film junctions on each other	-43	-High efficiency
Concentrating cells	Mirror or lenses used to concentrate the radiations		-Reduce cells -Need a track

Table 3.1 Types of photovoltaic

In this study, a polycrystalline cell module produced by a2-peak Company with a rated power of (240/W_p) glass to tedlar type was chosen for the analysis, while detailed specifications for this module are described in the company data sheet presented in Appendix A. An estimated price for the PV unit of (3000 $/kW) and (3500 $/kW) for PV/T is considered according to the average national prices index and the prices given by the module manufacturer representative in hydrogen and fuel cell exhibition in Hannover April 2009, for industrial installations over 1 MW.

3.2.4 PV Research and development

The research and development work on the photovoltaic and its systems was focused on reducing its cost and enhancing its performance. One of the practical drawbacks of the PV viability is its low efficiency, as around 80% of the falling solar radiation on the cells were dissipated and absorbed as heat losses. The optimal electrical or conversion

efficiency of PV cells (η_{ref}) is defined as the percentage of incident solar irradiance that is converted into electricity at standard conditions (T_{ref}=25 ^{0}C) and solar intensity of 1 kW/m^2. The PV efficiency is mainly dependent on the characteristics of the semiconductor and it decreases as the PV surface temperature increases. On the other hand, the cell efficiency and its production technology improve steadily over time. This improvement is clear from the data collected and recorded from solar companies, universities and national laboratories for various types of cells up to February 2012. This is presented in Figure 3.3 [55].

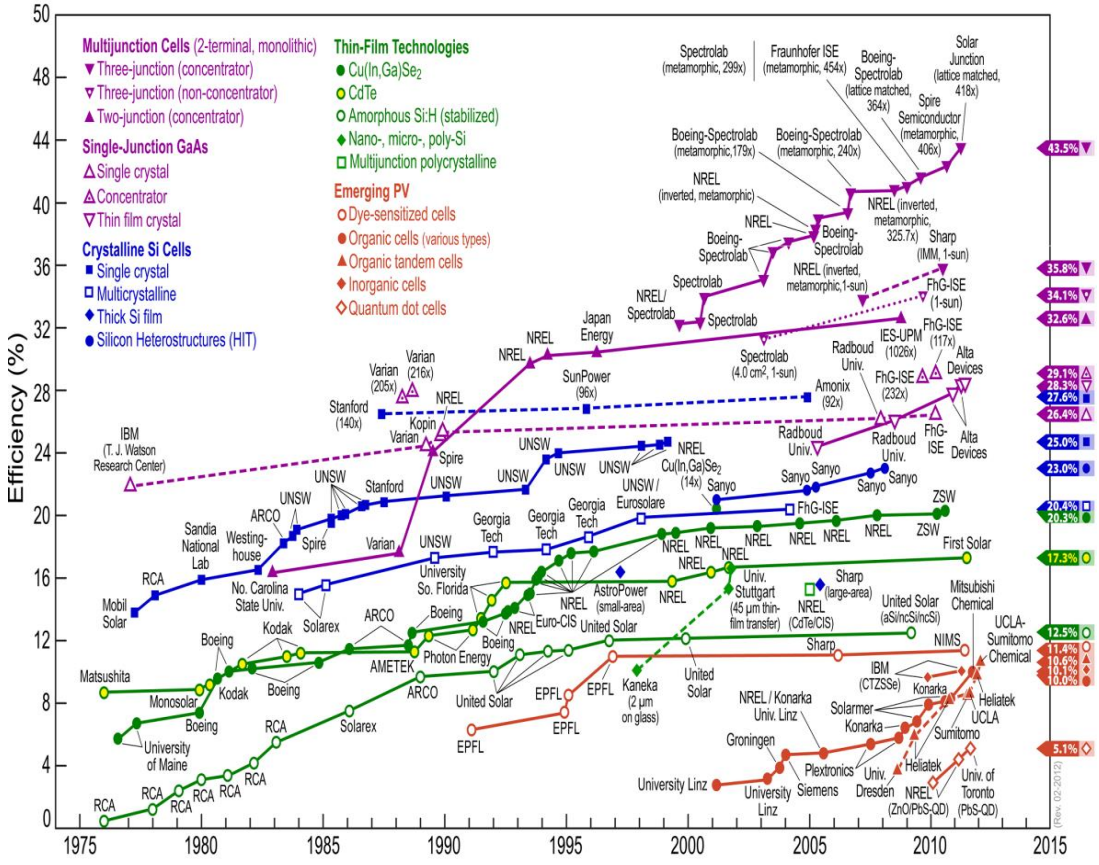

Figure 3.3 Best research-cell efficiency [55]

3.2.5 PV Previous research

As mentioned in the previous sections, the efficiency, technologies and prices of the PV systems improved steadily over time. This is mainly a result of the intensive research works undertaken in that field. This activity focuses particularly on developing novel semiconductor materials, new modelling and simulation tools to predict and evaluate the system performance, and management and control techniques for the operation processes. The following paragraphs present a general review and description of the previous research work being carried out in this field.

A general cost benefits and economical study of a 5 MW grid-connected solar PV power plant has been carried out by E. Hruyshat, [57]. The study performed used data recorded (1994-2003) at a different location in Jordan. The results shows that such plants installed in Jordan, especially ones in the Karak or Tafila areas are economically feasible. The greenhouse gas (GHG) emissions were avoided as a result of utilizing this plant at Karak and Tafila are expected to be 9338.19 and 9327.11 tons/year respectively with an annual electricity generation of 11.919 and 11.094 GWh/year at Karak and Tafila respectively. Also the study pointed out that it is crucial for Jordan to develop an abundant solar energy source for electricity generation. The study was carried out based on 2007 prices. However the current equipment prices were reduced and the fuel prices increased, which affected the accuracy of the results. In the analysis the effect of dust, sand (soiling factor), wire connection losses and cell mismatching on the cell efficiency were not considered.

E. Harder, and J. Gibson, [58] examined a 10 MW PV plant using a recorded data of the climate in Abu Dhabi city, using RET screen modeling software to estimate the power output, benefits and GHG emissions cost reductions. The results show that the expected energy cost price is 0.16 $/kWh and the plant can avoid 10,732 tons of CO_2 emission annually. The authors concluded that due to the high initial cost of the low electricity tariff price in Abu Dhabi, these kinds of plants will not be economically viable. However, this conclusion would be different if environmental damages were taken in to account. The estimated PV unit cost at 9.2 $/W is far away from the current prices of around 3 $/W, which means that this study over estimated them.

A cost benefit analysis has been carried out by M. Ramadan and A. Nasseb [59] in order to determine the feasibility of implementing a 1 MW PV solar energy plant in the state of Kuwait. The analysis takes into account the value of saved energy resources used in producing traditional electricity, and the cost of CO_2 emissions. The analysis showed that the plant feasibility will be achieved under the estimated system price of 5 $/W, with a production energy cost of 0.2 $/KWh, only when the oil prices are as high as 100 $ a barrel. However when the value of CO_2 emissions are accounted, the true electricity produced cost from the system will decrease to 0.09 $/kWh which is feasible compared to the current cost of traditional electricity. The calculation in this study has been running manually in this individual case. The study indicated that the main factors

which will reduce costs are technology and operation improvement and mass production.

A. Hamid Marafia [60] carried out a basic economic evaluation of a 100 MW_p PV plant using the weather data for Qatar, according to a system cost of (5 $/W_p$) and (10% PV electricity efficiency). The analysis showed that the plant electricity cost price 0.12 $/kWh is not far from being economically feasible. The study did not take into consideration the cost of the environmental damage or energy resources saved.

M. EL-Shimy [61] used RETscreen software to investigate the viability analysis of 10 MW PV power plants in Egypt using data collected from different locations. The analysis shows that the mean electricity cost production is 0.2 $/kWh, the maximum value of GHG reduction is 14538 tons of CO_2 in the Wahat Karga area and its minimum value is 11930 tons of CO_2, at the Safaga area. The result shows the considerable profitability of the PV power plant for all the sites in Egypt with maximum energy production of 29.49 GWh/year at the Wahat Kharga area.

Fuents, *et al*. [62] validated five theoretical and experimental simple algebraic methods used to predict the performance of a mono-crystalline and a polycrystalline silicon PV module in the Mediterranean climate. The results shows that the constant fill factor (FFK) or Osterwalds' methods produce accurate results. This method involved the use of simple equations based on the effect of incidence of global irradiance and cell temperature variation on PV performance.

The methods used to calculate the Nominal Operation Temperature (NOCT) based on international standards has been investigated by Garcia, M. and Balenzategui, L. [63]. The standards were applied to the crystalline and thin-film PV modules. The result showed inaccuracies of about ± 3 ˚C in NOCT value during the day. These inaccuracies were not excessive errors (about ± 1.5%) on yearly performance estimations, as temperature has a second order influence on module energy output. To obtain more accurate cell temperature and the performance prediction of the PV, the module encapsulations, structures and location should be taken into consideration.

Mattei, *et al*. [64] studied the effect of the meteorological parameters, solar irradiance, ambient temperature and wind on the PV performance. Two simple models to calculate the cell temperature and electric efficiencies were validated theoretically and

experimentally. The energy balance method neglected the radiation effect and NOCT methods were used. The results showed that such simple models gave satisfying results. Furthermore, several correlations were available to estimate the heat transfer coefficient of the PV versus the wind speed with a wide discrepancy in its value. More investigations are needed to choose a particular and accurate correlation for the PV overall heat transfer coefficient. The effect of the radiation on the energy balance is significant and it must be considered in the analysis.

Hand calculations for sizing and average performance prediction of a long-term PV system based on energy balance method has been described by T. Hove [65]. The system consisted of photovoltaic array, power conditioning equipment, a storage battery and an auxiliary power utility. The study shows that greater computational speed can be achieved using computer application.

Kurnik *et al*. [66] examined experimentally the effect of PV mounting conditions with varying the operating and environment conditions on its performance. The results demonstrated that the differences in cell temperatures and ambient temperatures increase when the module mounting changed from open rack to roof integrated. This increase was more noticeable as the irradiance increased. The temperature difference decreased when changing the module operating conditions from open-circuit to MPP (Maximum Power Point tracking) mode. This decrease was more noticeable as the wind increased. This study used an energy balancing method when a large number of input parameters needed to be determined. Most of these parameters had been extracted by using measured data such as the heat transfer coefficients, while others such as the emissivity were taken from the literature with considerable uncertainty about the reported values. This involved dealing in inaccurate results and restrictions in using this model as a general method for all modules.

A dynamic thermal model of a photovoltaic unit based on an energy balance method is presented by A.D. Jones and C.P. Underwood, [67]. Using measuring data for the cell temperature at different wind speeds, they predict a value of the heat transfer forced convention coefficient. It is predicted to be 2 W/m^2 K for 2-4 m/s wind speed and 4 W/m^2 K at +4 m/s wind speed. These values are less than the one predicted in many other studies in the literature.

S. Armstrong and W.G. Hurley [68] used experimental results to verify the thermal behavior of a photovoltaic panel for low and strong winds. The total heat transfer coefficient factors are calculated through a mathematical thermal model using measured data. The values at the time constant of the PV panel at different wind speeds were predicted and the results agreed with the literature. The analysis did not specifically describe how the measurements or the calculations of the time constant and the heat transfer coefficients were carried out.

Quesda, *et al*. [69] conducted a dynamic model for a 7.2 kW_p photovoltaic system installed in Spain using TRNSYS software. The model and the simulation results were validated experimentally and theoretically. The study mentioned that several uncertainties must be taken into account, such as the choice of the meteorological database, which led to 4% difference in the PV output and the radiations and cell temperature models, especially on a daily basis. The result shows that the models should include the ohmic, mismatch and tracking of the maximum power point losses, which is in the range of 8.3%. The authors pointed out that simple algebraic model can be as accurate as detailed dynamic models for the predication of the long-term PV output.

Joshi, *et al*. [70] developed a method for energy and exergy analysis for a PV and PV/T system. Experimental data from an actual system at New Delhi was used to investigate the performance of the system in a typical day. The results showed that the energy efficiency varies from a minimum of 33% to a maximum of 45% respectively, while the exergy efficiency of the PV/T system varies from a minimum of 11.3% to a maximum of 16% and the exergy efficiency of the PV varies from a minimum 7.8% to a maximum of 13.8% respectively. The result also shows that the higher the fill factor the better would be the exergy efficiency. These studies assume that the total heat loss from PV system becomes a heat gain for a PV/T system. These assumptions lead to inaccurate results because some of the heat generated will not be utilized at the PV/T system and would go out as heat loss mainly at the top of the PV surface.

G. Eljrushi and J. Zubia, [71] performed a comparison study, technically and economically, between 100MW gas turbine generation and a PV power plant of the same capacity, to be built in the Southern region of Libya/Sabha. The result shows that over a period of about 20 years, the PV power plant is found to be more economical in the region. The study did not take in consideration the environmental effect, and the PV system cost priced as 3.5 $\$/W_p$.

An experimental outdoor performance of a 2.32 kW_p standalone PV system in New Delhi for four weather conditions was carried out by Arvind Chel and G.N. Tiwari [72]. The life cycle cost analysis for the system was performed for two types of models at 25 years and 8 years respectively. The electricity unit cost for these systems was 0.82 €/kWh. These costs were too high compared to the current PV electricity unit cost due mainly to the system's over estimated cost at 7000 $/$kW_p$, low module efficiency and high degradation rate.

Sarhadi, *et al*. [73] conducted a simulation analysis for PV array, based on the exergy method. The five parameter method was used to investigate the performance and PV parameters such as surface temperature, open voltage and current. The effect of wind speed, ambient temperature, solar intensity, cell temperature and array area on the energy, electrical and exergy efficiency of the PV array was investigated. The parametric study showed that the exergy efficiency of the PV was decreasing as the surface temperature increased. While the exergy, energy and electrical efficiency increased along with the wind velocity due to the cooling of the PV's surface. The results were in full agreement with the previous experimental result. However no details were given about the software used in the analysis. The same analysis of the PV unit was carried out by the same authors [74], taking a detailed equations for the exergy destruction in the unit into consideration.

The most important implicit and explicit correlations formed in the literature to predict the operating temperature of PV module have been reviewed by E. Ekoplaki and J. A. Playvos [75]. The authors indicated that it is important to use these correlations according to each particular form of application and system configuration.

Cherigui, *et al*. [76] presented an overview study of the opportunities and possibilities of utilizing the solar energy available in the great Sahara desert in North Africa, using hydrogen as a solar energy carrier. The study proposed a connection between North Africa and Europe as energy consumer countries. The authors mentioned that North Africa countries are well-positioned to play a greater role in the European clean energy equation and that there is good chance of starting such cooperation.

Using RETscreen software, a 5 MW installed capacity PV system has been investigated by S. Rehman, M. Bader and S. AL-Moallem [77]. The study was performed in 41 different locations in Saudi Arabia. The power output, environmental impact and

economical evaluation has been carried out and compared for each site. The study used a monthly average daily global solar radiation and sunshine duration data over Saudi Arabia. The result shows that the yearly production output from the plant varied between 8,196 MWh at Tabouk and 12,360 MWh at the Bishah area. While the mean value of the internal rate of return was found to be 13.53%, the plant would reduce 8182 ton of greenhouse gas from emissions into the environment every year. The economic study was carried out according to the system cost at 2007 prices. The study assumed a fitted system at an inclined angle to the latitude at each site, instead of the optimum inclined angle which gives the maximum output during the year.

A generic mathematical model for a mono-and polycrystalline silicon PV modules was investigated by Huld, *et al*. [78]. The usefulness of the power output as a function of irradiation and module temperature was investigated. The empirical coefficients used in this model are determined through an indoor measurement procedure and the model has been validated using outdoor measurements. The result shows that the model gives a prediction within 1% of the actual energy output over a wide range of irradiation above 200 W/m^2, while below this range the model predictions were lower by 5-10% than the actual energy output. Furthermore, the results show that mono-and poly crystalline modules exhibit similar behavior.

The research and current development activities on the PV systems presented in this section can be concluded on the following:

-Polycrystalline panels are the most PV units currently used, however its efficiency is less than 20% due to the unit heat losses, which reached 80% of the total inclined heat.

-Algebraic and energy balance method using explicit heat transfer coefficient relations and data from the manufacturer could be used to develop an accurate general and simple model to predict the unit performance and outputs.

- It is recommended to develop a thermo-economic model and a comprehensive parametric study taking in considerations the unit; exergy, operation, economic and design parameters as well as the saving from the environment impact and fossil fuel resources consumed.

3.3 Photovoltaic thermal systems (PV/T)

It is well known that the PV electric efficiency and its lifetime are deeply affected by increasing the cells temperature. The cells are heated by the out range wavelength

photons hitting the surface which were not transferred to electricity and then absorbed by the cells as heat. To overcome this problem and enhance the performance of the cells, they could be cooled from the back, front or both using different fluids such as water, air, mixture and organic fluids to form a PV/T system. The PV/T system can be produced in different configurations consisting of tubes, channels or plate frames inserted in the back of the cells and insulated as illustrated in Figure 3.4.

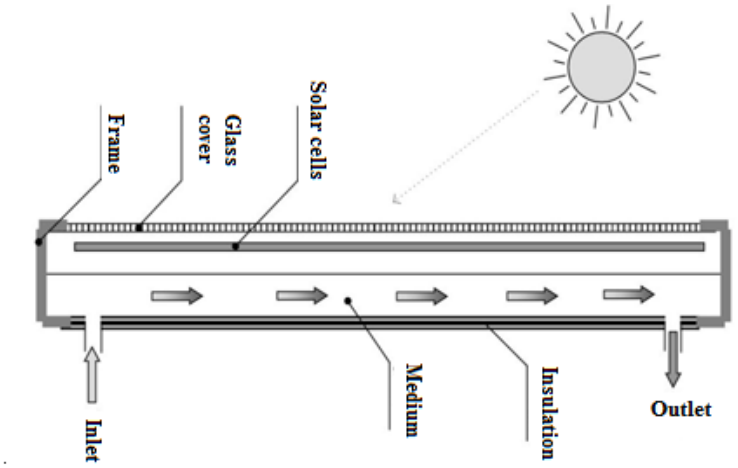

Figure 3.4 Construction of PV/T system

The cells also could be submerged in water or water could be sprayed on its surface to cool it. The PV/T systems could be substituted the traditional evaporator in many energy systems such as absorption chillier and heat pumps. The cells in these systems supply the necessary electricity as well as the heating to change the state of the working fluids in the system cycle while it is being cooled.

Many studies have been carried out related to PV/T system analysis, modelling, control, and performance enhancement over the last decade, some of these research works are described in the following paragraphs.

A. Tiwari and M. Sodha [79] developed a quasi-steady state thermal model based on the energy balance method of PV/T integrated system (Glass-tedlar-water). The model has been validated using previous experimental parameters and the data of a similar system. The results showed that the overall daily thermal efficiency at the PV/T integrated system is 58%, which was in complete agreement with the calculation of the experimental value. This study also showed that the mass flow rate of water in the range between 0.005 and 0.075 kg/s had only a small effect on the hourly variation of water

temperature. The results also showed that the hourly water temperature was close to the cell surface temperature by less than 4˚C. The calculations were carried out manually.

Cristofori, *et al*. [80] used the finite difference and energy balance method to investigate the performance of the PV/T system with a polycarbonate absorber at low flow rate conditions, compared with a metallic one. It was found that the average efficiencies were equal to 55.5% for the thermal one, 12.7% for PV only, whereas the figures for system efficiency and energy saving efficiency were 68.2 and 88.2% respectively. The study showed that a copolymer PV/T design would reduce the system weight, making manufacturing more easily and decrease the production cost, compared with the copper systems. In the analysis the power consumed to recirculate the water was neglected, which affected the result's accuracy, particularly for large systems and high flow rates.

Huang, *et al*. [81] performed an experimental study to investigate the performance of a PV/T system with a polycarbonate absorber and conventional solar water heaters. The study introduced the concept of primary-energy saving efficiency, which exceeded 0.6 for this system. This was higher than for a pure solar hot water heater or an individual PV system. The results show that the temperature of the PV module was very close to that of the water temperature during the day, with only a 4˚C difference. The results indicate that the performance of a PV/T collector can be improved as the direct thermal contact of the collecting plate and the PV cells is increase. A better design of a PV/T system can be implemented to improve its thermal performance and reduce production cost. The study showed that the system was economically feasible. It recommended an economical simulation and optimization analysis based on the total primary-energy gain per unit investment.

S. Kalogirou [82] conducted a simulation model for a PV/T system in a house using TRNSYS software and meteorological data for Cyprus. The system output and life cycle was compared to the standard PV system. The system consisted of a PV/T collector with a copper heat exchanger, battery, converter, water storage tank, a pump and a differential thermostat. The thermal and design parameters used as inputs in the analysis were obtained from previous works. The daily and monthly performance of the system was investigated. The results show that the optimum value of water flow rate of that system was 25 l/h. The mean annual efficiency of the standard PV system was 2.8% which increased to 7.7% for the PV/T system at the optimum low rate. The total system efficiency increased to 31.7% when the thermal output was considered. The payback

time was found to be equal to 4-6 years. The optimization procedure used in these studies was traditional and complicated.

S. Dubey, and G. Tawari [83] developed an analytical expression based on energy and exergy equations of PV/T flat plate water collectors connected in parallel and in series. The performance of the system has been investigated by varying the number of collectors, the mass flow rate, partially or fully covered by the PV module. The collection of $2m^2$ has been investigated according to previous meteorological data and system parameters for four weather conditions in five different cities in India. The cost analysis and carbon credit earned by the system annually has been calculated. The same authors in a previous study [84] showed that the flat plate collector experimentally covered partially with a PV module gives better thermal and average cell efficiency compared to a fully covered PV/T system. The study observed that the benefit of such a system is dependent on the user's primary energy requirement as electricity or hot water and also the weather conditions. The exergy and the electrical costs as well as the calculation tools in this study were not described in detail. It is recommended to develop software and an optimization tool for the energy saving related to the investment in such systems, which was necessary to investigate its performance.

A. Tiwari and M. Sodha [85] presented an energy balance analysis and numerical computations to investigate the thermal performance of a PV/T water/air heating system. Four configurations, namely: a) unglazed with tedlar, b) glazed with tedlar, c) unglazed without tedlar, d) glazed without tedlar were considered. The results showed that the water system performed was better than the air system. The overall thermal efficiency obtained for the summer and winter in New Delhi was about 65% and 77%, respectively.

The performance of an unglazed glass to glass and glass to tedlar PV/T air collector system was carried out by Joshi, *et al*. [86]. A parametric study was carried out to investigate the effect of the duration velocity and length of the collector. An energy balance method was used to predict the outlet air temperature, the cell temperature, the back surface temperature and the performance parameters. The result was validated with an experimental data according to Indian climate conditions. The results showed that the glass to glass type gave a better performance than the tedlar one with a daily energy overall thermal efficiency of 45% for glass to glass and 43% for the glass to tedlar one. The efficiency of the system decreased with the increase in the duct length and the

increasing air velocity. Thermo-economic analyses are recommended in order to achieve accurate results.

A. Joshi and A Tiwari [87] investigated the efficiency of a hybrid PV/T air system using energy and exergy analysis. The analysis was performed in cold climate conditions in India. It was found that the energy and exergy efficiency of the system during the day varied between 55-65% and 12-15 %. The exergy analysis was based on an empirical relation and a constant heat transfer coefficients parameter taken from a previous study. The study indicates that the energy and exergy efficiencies increase with increasing air flow rate. Furthermore, a significant decrease in exergy is noticeable due to more heat losses from the system. There are no details about the equations used or evidence related to this statement.

Hartmann, *et al*. [88] studied solar thermal and solar electric cooling for a small office building according to two different climates in Spain and Germany using a conventional compression chiller as a reference. The simulation tools used a SACE tool for calculating hourly solar gains and TRNSYS for calculating the hourly cooling and heating loads of the building. The results showed that the grid PV systems lead to lower costs of primary energy savings than the solar thermal system. The study indicates that the high cost of the absorption chiller and backup heater unit have the most adverse impact on the system viability. There are no details on the economic analysis procedure or the software used in this study.

A. Abdulzadeh and M. Ameri [89] proved experimentally that PV water pumping system optical performance can be improved by 1.8% by spraying water over the front of the PV surface through reducing the temperature of the cells.

Tiwari, *et al*. [90] used energy and exergy analysis methods to investigate the performance of a PV/T water heater system, under a constant flow rate and constant collection temperature modes. Numerical computations were carried out based on a design and climate parameters of a previous study of a small system. The analysis shows that the daily overall thermal efficiency of the system increased with the increase of constant collection temperature. Moreover, the exergy and the thermal overall efficiency were at a maximum, as the optimum flow rate of these systems was 0.006 kg/s. In addition the study showed that the difference between the cell temperature and the water temperature was in the range of 4 to 5 ˚C during the day. However, the exergy destruction, environmental and economic impact factors were not included in this study.

Sarhaddi, *et al*. [91] developed a simulation program to investigate the performance of a PV/T building integrated air collector, based on a detailed energy and exergy analysis. The heat transfer coefficient has been calculated as convection, conduction and radiation losses. Five parameter PV models were used to calculate the model parameters in any climatic and operation conditions. The results were validated with experimental findings. There was no description or details of the software used or developed. The five parameter model and the detailed equation analysis needed several input parameters.

B. Agrewal, and G.Tiwari, [92] presented a simple energy and exergy analysis in order to select an appropriate (building integrated system (BIPVT) suitable for the cold climate conditions of India. The study shows that for a constant mass flow rate of air, the system connected in series was more suitable for systems on rooftops. It was found that the system with covered (65 m^2) and (7.2 kW_p), will produce annual electrical and thermal exergy at 16.209 MWh and 1531 kWh with an average overall thermal efficiency of 53.7%. There was no optimization analysis or parametric study to optimize the heat gain with the electricity produced in the system.

G. Xu, *et al*. [93] carried out a simulation and comparison study for a modified PV/T heat pump system consisting of a multi-port flat extruded aluminum tubes instead of a round copper tube for a conventional system. A numerical study based on an energy analysis to investigate the performance of the system according to the meteorological data in China is presented. The result shows that a better performance can be achieved by using the modified system. There is no information given about the simulation tool or the type of refrigerant fluid used in the study.

Chow, *et al*. [94] used a numerical energy analysis of a dynamic simulation model to investigate the performance of PV/T heat pump system in Hong Kong, the result shows that the proposed system with R-134a is able to achieve a yearly average COP of 5.93 and PV output efficiency of 12.1%, which is better than the conventional system and PV performance at standard conditions individually.

A. Ucar and M. Inalli [95] developed an exergy economic model for the analysis and optimization of a solar heating system for residential building in Turkey. The optimum collector area and seasonal storage type and volume are obtained by using MATLAB optimization toolbox. The results showed that the exergy loss and total cost increased

with the increase of collector area per house. Moreover, the exergy loss at the cylindrical tank was 19.8%, while for the trapeze tank it was 8.3%. It was found that the total cost of the cylindrical tank systems was higher than that of the trapeze tank system. No other exergy economic parameters were considered in this study.

An experimental study was conducted by Fang et al. [96] to investigate the performance of PV/T heat pump air-condition system. The performance parameters such as the evaporation and condensation pressure, the system coefficient of performance (COP), the water temperature, the PV surface temperature and efficiency were investigated based on energy analysis. The result showed that the average PV efficiency could improve by 23.8% in comparison to the conventional PV model. The average COP of the system could attain 2.88 and the water temperature inside the water-heater can increase to 42 ˚C.

E. Radziemska [97] achieved energy and exergy analysis to investigate the performance of a water-cooled Solarwaat PV/T module. The analysis indicated that a kind of trade-off would be necessary to optimize the system for the maximum electric and thermal efficiency. The study showed that the most important parameters were the water flow rate and the inlet temperature. The solar cell efficiencies were in the range of 13-15% for standard conditions, which increased by 10-30% after cooling.

R. Mishra and G. Tiwari [98] using exergy analysis methodology to study PV/T water panels system connected in series in a totally or partially PV cells covered mode. The study was considered a constant hot water temperature at 40 ^{o}C and the weather condition of Delhi in India. The results revels that the totally cell covered system was more active for electricity production, whereas the partially covered system is preferable for hot water production. The study also observed that the annual overall thermal energy gain for the partially covered system is increased by 9.48% compared with the fully cell covered system values. While, in terms of overall annual exergy gains the values performed for the fully covered configurations is increased by 39.11 % above the values for the partially covered system.

C. Rajoria, S. Agrawal and G. Tiwari [99] performed an environmental cost analysis in terms of thermal and exergy gains for an air cooled PV/T system installed in four different sites in India. The analyses consider 18 PV/T modules connected in series and in parallel configure. The CO_2 emission equivalent value consider a coal power thermal plant in India is estimated at 2 kg CO_2/kWh with a cost estimated as 14.5 \$/ton CO_2. The study shows that the series connected PV/T modules compare with the parallel

modules have lower surface temperature (19.1%), higher electric efficiency (6.5%), and higher outlet air temperature (18.1%). The analysis also indicated that, in terms of overall thermal energy gains, the series connection system will avoid a CO_2 emission cost (1447.2 $/annum) compared to (1317 $/annum) for the parallel connection modules. While, in terms of overall exergy gains it is (658 $/annum) for the series modules and (602 $/annum) for the parallel configuration.

The main conclusion from the PV/T system previous studies indicated that its recommended to developed a thermo-economic and comprehensive parametric study. An optimization study for the system maximum thermal and electrical energy according to the weather conditions is also recommended using simple and general thermal model. The previous experimental studies shows that a steady stat and general energy balance model can be applied. The suggested model can consider a fixed and estimated output water temperature as 4 ^{o}C above the cell temperature.

3.4 Fuel cell

A fuel cell is an electrochemical energy converter that converts the chemical energy of a fuel and an oxidant to an electrical current (DC) without combustion. The main fuel was hydrogen which reacted with pure oxygen extracted from the air or other substances such as water. In the case of a $H_2 – O_2$ fuel cell H_2 was the fuel and O_2 is the oxidant. The only product was pure water and heat. The fuel cell was more efficient than conventional engines, involving easy maintenance, high availability, a wide range of applications, a silent operator, high power density and clean energy production [100].

3.4.1 Fuel cell history

The first person to discover how to reverse the process of water dissociating to produce electricity was Sir William Robert Grove (1811-1896). He concluded that combining oxygen and hydrogen could be done to produce electricity. From this hypothesis, Grove developed a device to produce electricity without combustion, which was later known as a fuel cell. The fuel cell technology research and development was continued until the work of F. Bacon (1958) was licensed and used to develop the first alkali fuel cell. The first polymer electrode fuel cell, used in spacecraft, was developed by the General Electric Company in the 1950s. In the early 1990s in the Los Alamos National Laboratory (USA), they developed a thin, low cost platinum and more active electrode for PEMFC [101].

3.4.2 Fuel cell types

Fuel cells can be classified into different categories according to its electrolyte type and use. The following fuel cells could be defined according to its electrolyte type as; polymer membrane (PEMFC), alkaline (AFC), phosphoric acid (PAFC), molten carbonate (MCFC), and solid oxide (SOFC). Other parameters such as working temperature and the type of chemical reaction produced can be used in fuel cell classification. In addition, the PEMFC, AFC and the PAFC, working at low and medium temperatures, show variations in efficiency of between 30-45%. However, the MCFC and SOFC types working at high temperatures need more expensive and corrosive resistance materials and have a high efficiency up to 60%. A comparison of the most well-known fuel cells technology is presented in table 3.2.

Fuel cell energy efficiency could be enhanced when a cooling system, in utilizing the excess heat generated, is used in heat and power systems (CHP). However, PEMFC operates at low temperature and allows them to start quickly. They need only hydrogen and oxygen to operate and do not need corrosive fluid. This type of fuel cell was widely used in last decade in a capacity range up to 250 kW at a reasonable cost, particularly in marine ships.

Recently, the Ballard company in Canada (who were rated number one in terms of public companies with the most global gross revenues in the fuel cell business activity, with over $65 million in 2010) developed a 1 MW combined heat and power PEMFC [102]. The main advantage of this unit in addition to its high capacity is its life operation time over 20 years. This unit has scalable nature that consisted of separate units which could be operated individually or together to operate the units on its rated capacity, reduce operation costs, increase unit life time and cover load in demand variation. According to this, the 1 MW Ballard unit recently installed in 2009 was suitable for stationary systems at a reasonable cost (3000 $/kW), and has been chosen for more investigation in this study. More technical details from the company manufacturing data sheet are provided in appendix B.

	PEMFC	AFC	PAFC	MCFC	SOFC
Electrolyte	Hydrated Polymeric Ion Exchange Membranes	Potassium Hydroxide in asbestos matrix	Immobilized Liquid Phosphoric Acid in SiC	Immobilized Liquid Molten Carbonate in LiAlO2	Ceramics
Electrodes	Carbon	Transition Metals	Carbon	Nickel and Nickel Oxide	perovskite /metal
Catalyst	Platinum	Platinum	Platinum	Electrode Material	Electrode Material
Interconnect	Carbon or metal	Meta	Graphite	Stainless steel or Nickel	Ceramic/ Steel/ Nickel
Operating Temperature	40 – 80 °C	65 – 220°C	205°C	650°C	600-1000 °C
Charge Carrier	H+	OH-	H+	CO3=	O=
External Reformer	Yes	Yes	Yes	No, for some Fuels	No, for some fuels cell designs
External shift conversion of CO to hydrogen	Yes, plus Purification to remove trace CO	Yes, plus purification to remove CO and CO2	Yes	No	No
Prime Cell Components	Carbon-based	Carbon-based	Graphite-based	Stainless based	Ceramic Product
Water Management	Evaporative	Evaporative	Evaporative	Gaseous Product	Gaseous Product
Product Heat Management Process	Gas + Liquid Cooling Medium Process	Gas + Electrolyte Circulation Process	Gas + Liquid cooling Or steam generation	Internal Reforming + Process Gas	Internal Reforming + Process Gas

Table 3.2 Summary of major differences of the Fuel cell types [101]

3.4.3 Fuel cell structure and working principles

The PEMFC consisted of bipolar plates, channels, gas diffusion layers (GDL), cathodes, anodes, catalysts and membrane commonly produced from Nafion materials. The membrane was used to conduct protons and forced electrons to travel away. A thinner catalyst layer was used to enhance the electrochemical reaction rates at the anode and cathode. A gas diffusion electrode (GDE) provides electric contact between electrodes and bipolar plates. GDE consisted of a gas diffusion backing layer and porous material such as carbon cloths or carbon fiber paper, which was assembled together with the membrane and the catalyst to form the membrane-electrode-assembly (MEA). A fuel cells stack was separated by bipolar plates, which included the cooling system channels [101, 103]. The basic operating principle and construction is illustrated in Figure 3.5. Hydrogen fuel was fed to the cell through the gas supply chamber at the anode, whereas the oxygen entered the cell at the cathode side. The membrane, with the help of the catalyst, allowed the hydrogen to split into hydrogen ions and electrons so that the ions could penetrate through, while preventing the electrons passing and forcing them to travel in an external circuit, creating a useful current. In the cathode the hydrogen ions and electrons combined with the oxygen to form water and heat as byproducts [104, 105].

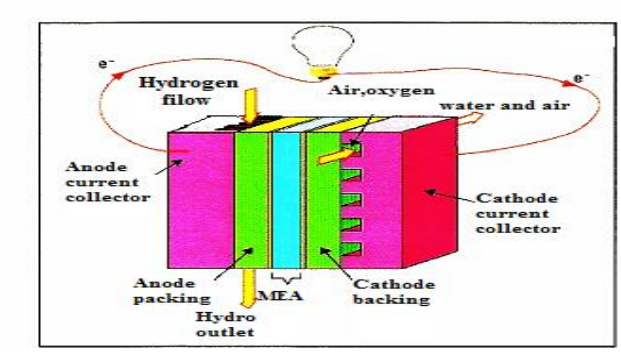

Figure 3.5 Operating principles and construction of BEMFC

3.4.4 Fuel cell potential

The theoretical electromagnetic voltage (EMF) or reversible open circuit voltage ^{o}E of the fuel cell at 80 ^{o}C cell temperature was around 1.18V, with an efficiency limit of 80%. This voltage would drop down to around 0.6 V due to the increased voltage losses. The cell performance would be enhanced through a proper water and heat management system, an adjustment of the stoichiometric gas ratio defined as the

theoretical to the depleted gas fed to the cell, as well as reducing the over voltage losses. The over voltage losses in fuel cell were divided to [106]:

- The activation losses occurred at low current densities in low temperature fuel cells and this was due to the delay in chemical processes and the losses caused by forcing the reaction to complete.
- The internal current loss was related to the electrons and fuels not reacting and leaking through the electrode.
- Ohmic loss occurs due to the resistance to the flow of electrons in; interconnect, the anode and the cathode. This loss is directly proportional to current density and it was the major source of loss in fuel cells, particularly at high current densities.
- Concentration loss occurs as a result of the effect of losing a high concentration and using fuel and oxygen faster than could be supplied at the anode and cathode.

Figure 3.6 illustrates the over voltage losses in a low temperature fuel cell. These over voltage concepts will not be considered in this study, whereas the analysis is based on a thermal model at a steady state at specific temperature, pressure and voltage. However, for the PV unit, an electro-thermal model based on I-V characteristics along with a thermo economic model was considered. This was due to the nature of thermal transformer to electricity in the photo energy process. While for other SHS components, mainly a PEMFC and an electrolyzer, a thermo-economic model was considered. A brief description of the electrochemical mathematical equations for these units is given in chapter 6.

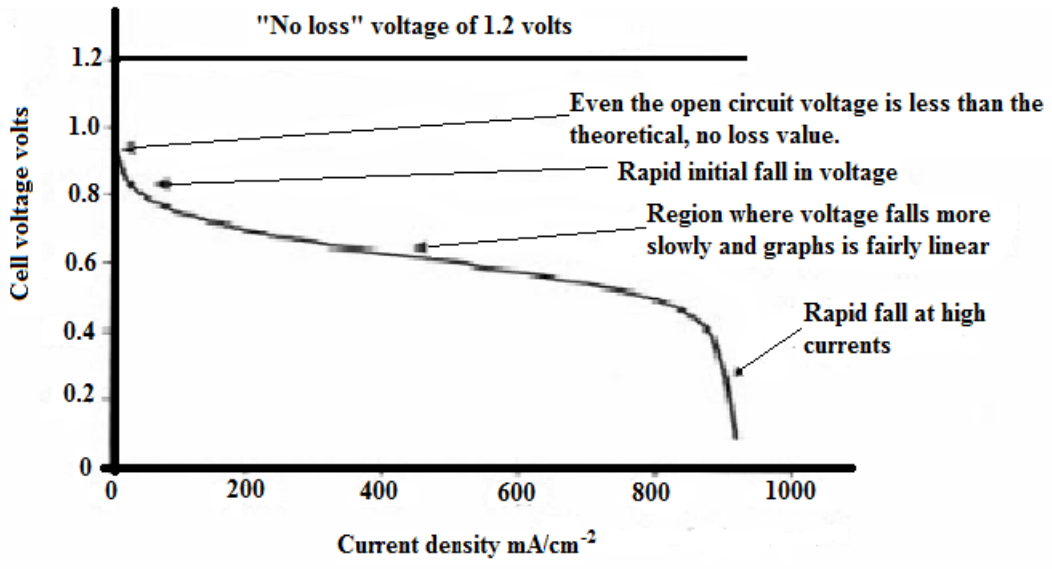

Figure 3.6 The over voltage loss in a low temperature fuel cell [106]

3.4.5 Fuel cell global market

Many countries around the world have invested heavily in fuel cells and hydrogen technology activities and research, in the period 2000-2010, when total global investments in this field exceeded $1.7 billion. U.S. investors made the greatest cumulative investment during that period with $774 million, followed by U.K. investors at $297.3 million. However, cost and durability were the major challenges to make fuel cells competitive. The fuel cells cost for stationary systems must be reduced to about 1000 $/kW from around 3000 $/kW. The life span of the cells was still far from reasonable durability. For stationary applications it had to be increased to be accepted in the current market [102].

3.4.6 Fuel cell research and development

To improve and design effective fuel cells, intensive research and development work has been carried out. The key challenges of fuel cell improvement were to reduce its cost and improve its performance. Durability, reliability, size, weight, materials used, control systems and water and heat management systems are the most important barriers to the commeralization of fuel cell technology. The main area of fuel cell modifications and development can be summarized as follows [107]:

- Developing membranes and electrolytes to meet all the targets with improved conductivity, stability, and durability with a thinner and low cost material.
- Developing a recycled membrane assemblies (MEA) with high performance, effectively integrated, to meet all operation parameter ranges.
- Developing low cost, durable, effective gas diffusion layers (GDL), bipolar plates, seals, catalysts and physical and chemical sensors.

The cell performance could also be improved by modifying the operation conditions, such as pressure, temperature, lowering gas impurities, avoiding hydration, auxiliary work and humidification of gases. Furthermore, creating new tools for the testing, simulating and evaluating of fuel cell systems could help improve its performance. In the following section, a brief description of the system is given and there is a discussion of the most important research work in this field.

F. Barbir, and T. Gomez, [100] presented a general economic study of a 10 kW PEM fuel cell. The relationship between the optimum nominal efficiency of the unit and its economics has been considered. The efficiency and economics of the fuel cell was

analysed in terms of various load profiles, taking into considerations the unit cost, the capacity factor and the hydrogen cost. The results showed that in the best-case scenario as the hydrogen cost at 10 $/GJ and unit cost 100 $/kW was operating at 50% efficiency, the electricity would be generated at less than 0.08 $/kWh. The study neglecting the M&O cost, the environmental cost and the cost of utilizing the heat generated in the unit.

Cownden, M, Nahon, and M. Rosen [108] used the exergy balance methodology to investigate the performance of a PEM fuel system. A previous model for the fuel cell stack and other system components was used. The model was based on an empirical data supplied by a specific company, for a particular unit used for transportation applications. This analysis considered the parasitic loads for the auxiliary components and the voltage loss separately from the mass transport loss in the unit. The results indicated that the most exergy destruction occurred within the fuel cell stack, followed by the hydrogen ejector, the air compressor and the heat rejected from the radiator. Moreover, the exergy efficiency of the system was similar to the energy efficiency. However, this study did not explain the influence of exergy destruction with the other operation parameters.

K. Haraldsson, and K. Wipke, [109] presented a general review and evaluation study describing the model selection criteria for choosing a PEM fuel cell model. The study indicated that the criteria for choosing the models included the area of interest, the state of the model (dynamic-steady…etc.), the level of complexity and dimensions. Also, the software speed, accuracy, flexibility, source code, time step, graphical representation, library of thermodynamic properties, system components, documentation and validation were considered. Heat transfer equations and mass and energy balances are important for providing an appropriate picture of all processes in such a system. Most of the commercial available fuel cell software models such as Emmeskay, GCtool, Easy5, FEMLAB, VT, and KTH are theoretically based and complex. The models are normally focused on one aspect or region of the fuel cell only. Some models are semi-empirical models based on a general voltage-current relationship. However, these models can only use one particular fuel cell with specific coefficients. Moreover, very few models are developed based on exergy or thermo-economic methodology in consideration of their environment impact**.** Ayoub Kazem [110] presented an exergy analysis study of a 10 kW PEM fuel cell. The chemical and physical exergy of each stream in the unit was calculated. In addition, the exergetic efficiency of the unit and the exergy of each stream

was conducted at variable operating temperature, pressures, cell voltages and air stoichiometry ratios. The results illustrated the significance of the higher operating temperature, pressure and cell voltage. However, the study recommended operating the unit at an air stoichiometric ratio of between 2 to 4 in order to maintain the relative humidity level in the air and to avoid drying the membrane at high temperature. The study did not consider the utilization of the heat generated or recycling the excess streams. In addition, the exergy destruction within the cell as well as the auxiliary components was not included. The author continued the study to an exergoeconomic study to investigate the effect of the operation parameters on the unit exergy cost [111]. The analysis showed that the cell temperature variation had no significant impact on the unit exergy cost. However, increasing the operating pressure, the inlet air stoichiometry or the cell voltage would improve the unit exergy cost. The study did not consider the exergy destruction cost and the other thermo-economic evaluation factors.

C. Frangopoulos, and L. Nakos, [112] developed a model for the thermo-economic design and optimization of a PEM fuel cell system. The study was part of a general economic study indicating the effect of the current density on hydrogen consumption, cell and system efficiency, the heat rejected, the cell temperature, the unit cost, the platinum cost and the hydrogen price. The effects of the hydrogen and unit costs on the electricity unit cost were also investigated. The methodology used in this study did not take into account the thermo-economic parameters such as streams exergy costs, exergoeconomic factor and the exergy destruction and its costs in the system components. No details were given about the calculation and optimization tools used.

Saidi, *et al*. [113] investigated a 5 kW PEM fuel cell for heat and power generation using exergy analysis. The unit was optimized for maximum efficiency and minimum entropy generation based on the main operation parameters. The results showed that, within the range of application, the fuel cell should be operated at a high temperature and voltage set at a low pressure and a stoichiometric air to fuel ratio. The heat losses were not considered in the entropy generation equation. Furthermore, the heat accumulated by the cooling system was considered as an energy quantity rather than as an exergy, which can be misleading in terms of results.

Hussain, *et al*. [114] carried out thermodynamic modelling based on energy and exergy analysis of a PEM fuel cell system for a specific light-duty vehicle. The effect of the operating parameters (temperature, pressure and air stoichiometry) on the system

performance was examined. The study showed that increasing the external load would increase the difference between the gross stack and the net system power because of an increase in the parasitic loads. It also found that the system efficiency increases with increasing the operation temperature and pressure. However, there was no significant increase in the system efficiency because of an increasing air stoichiometric ratio, due to the parasitic load of the air compressor. The largest amount of irreversibility took place in the fuel cell stack. The recirculating hydrogen stream in the system boundary condition was considered as input stream in the exergy balance and efficiency equations that can lead to imprecise results. The parametric analysis not considered many operation parameters in this study such as the hydrogen stoichiometric ratio.

Akkaya, *et al*. [115] introduced a new exergitec criteria called the exergetic performance coefficient (EPC), which was defined as the ratio of power to the loss rate of availability. The performance of a solid oxide fuel cell (SOFC) was analysed based on (EPC) with different operating conditions. However, better system performance can be achieved with a high (EPC) factor.

Mert, *et al*. [116] developed an exergoeconomic model for a vehicular PEM fuel cell system. A parametric study to investigate the effect of the operation parameters and the cost behaviour on the system performance was carried out. The results showed that by increasing the operation temperature and pressure, the system's efficiency increased and the production cost decreased. The system efficiency and the network output decreased as the membrane thickness increased. It was also found that increased cathode stoichiometry led to a small decrease in the system's efficiency, while increasing the anode stoichiometry would greatly decrease the system's efficiency. The fuel cell stack had the highest irreversibility and production cost affected factors in the system. However, the compression cost was not considered in the analysis. In addition, the exergy destruction cost, the hydrogen cost, the components cost and many others thermo-economic factors were not considered in this study.

Leo, *et al*. [117] carried out an exergy analysis study in order to compare the two types of PEM fuel cells used in surface ships and submarines. Direct methanol (DMFC) and methanol reforming (PEMFC) systems were considered. The results showed that the exergy efficiency for both systems was quite similar. However, exergy losses and destruction were greater in the DMFC system than in the PEMFC system. The study recommended that a further thermo-economic study would be necessary to compare the

visibility of each system and the unit cost of electricity produced by both systems. The heat generated was not considered in the analysis.

The previous studies and current development activities on the fuel cell presented in section 3.4 indicated that the activity has to be continued in order to improve the unit efficiency and the technology costs. It is recommended to develop a thermo-economic model and a comprehensive parametric study using friendly interface software. The model suggested considering the environment impact and fossil fuel resources consumed as well as the cooling and recycling systems.

3.5 Electrolyzer

As described in the previous chapter, hydrogen can be produced by many methods and many factors govern its production such as source availability, cost, hydrogen quality and purity. It can be produced using traditional energy and fuel sources, as well as renewable sources, such as solar. Several technologies can be used, including chemical and thermo-chemical, such as natural gas steam reforming, photolytic, biological, and electrolytic. Much research into and development of these technologies is carried out to produce hydrogen in an economically and environmentally safe way. Water electrolysis is one of the most important benign technologies and has been used for many years to produce hydrogen. The first persons to discover how to use the water electrolysis phenomena were Nicholson and Carlisle in 1800. This technology has since been greatly improved and by 1902 more than 400 industrial water electrolyzer units existed. The first water alkaline electrolyzer was produced in 1948 by Zdansky and in 1978 the first advanced alkaline system was produced [118]. Because of its advantages and convenience for solar PV systems, the use of a water electrolyzer was proposed for this research study.

3.5.1 Water electrolyzer

Hydrogen is produced by the decomposition of water into hydrogen and oxygen by passing an electric current between two electrodes separated by an aqueous electrolyte. Alkaline electrolyzers and proton exchange membranes (PEMs) are the two main types of electrolyzers, which are well developed. An alkaline electrolyzer with a capacity of 60 Nm^3 was adopted here. The specifications and technical details of this unit are presented in appendix C. The electrolyte used in conventional alkaline water electrolyzers has traditionally been aqueous potassium hydroxide (KOH), mostly in

conjunction with solution of 20-30 wt %, because of its convenient conductivity and the remarkable corrosion resistance of stainless steel in this concentration range [118]. The typical operating temperature and pressure of these electrolyzers is <100 ^{o}C and 1-30 bar, respectively. An electrolyzer consists of several cells linked together. Two distinct cell designs of electrolyzers are on the market, monopolar and bipolar [119]. In an alkaline solution the electrodes must be resistant to corrosion, and must have good electric conductivity, as well as good structural integrity, while the diaphragm should have low electrical resistance, Figure 3.7 shows the working principle of an alkaline electrolyzer [120]. Hydrogen and oxygen gases are separated from each other and impurities are removed. For safety and operations purposes hydrogen must be at least 99% pure before it is stored in a tank or used in a fuel cell.

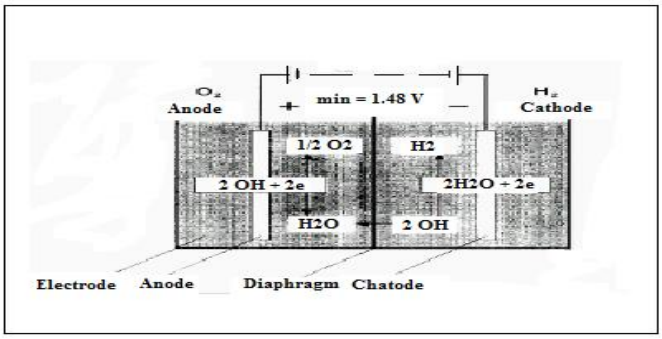

Figure 3.7 Working principle of alkaline electrolyzer [120]

The advantage of the bipolar electrolyzers is that they are more compact than those with monopolar design and have shorter current paths in the electrical wires and electrodes. This reduces the losses due to the internal ohmic resistance of the electrolyte, and therefore increases the efficiency of the electrolyzer. Bipolar electrolyzers can operate at high pressure, reducing the compression work needed to store the hydrogen. However, it has some disadvantages, such as the fact that their parasitic currents can cause corrosive problems. Furthermore, compactness and high pressure require a relatively sophisticated and complex system design and an increase in manufacturing costs. However, most alkaline electrolysers manufactured today are of the bipolar cell design. The operational cell voltage has been reduced and the current density of the new advanced alkaline electrolyzers has increased. This reduces the unit cost. Increasing the current will increase the ohms resistance and over potentials at the anodes and cathodes due to increasing gas bubbling. Basic electrolyzer cell improvements can be focused on; 1- new cell configurations, 2- higher processing

temperatures, in order to reduce the cell resistance and increase the electric conductivity at the electrolyte and 3- new electro-catalyzers to reduce anodic and cathodic over potentials 4- developing more active and viable PEM electrolyzer. Some of the research works implemented in electrolyzer technology, particularly those related to this study subject, will be concluded in the following section in brief and discussed:

M. Rosen [121] conducted an energy and exergy analysis to investigate a water electrolyzer system. Three cases are considered in which the principle driving inputs energy are; electricity, the high temperature and the hypothetical heat source. The analysis showed that the losses are mainly due to the irreversibility associated with converting a heat source to heat transfer in the context of a large difference in temperature. The exergy efficiency of the three cases, the H_2 from electricity and the heat or hypothetical heat source are 67%, 46%, and 26% respectively. The energy and exergy equations used in the analysis have not been described. The study presents the oxygen as a by-product while all the oxygen and water streams' exergy are not considered in the analysis. However, most of advanced electrolyzer systems can self-supply their electricity needs by means of solar cells or wind turbines with negligible heat involved. The effects of the design and operation parameters on system efficiency have not been considered in the analysis.

A dynamic mathematical model to optimize control strategies for an advanced alkaline electrolyzer has been developed by O. Ulleberg [122]. The model is based on a combination of fundamental thermodynamics, heat transfer (energy analysis) and empirical electrochemical relationships. It is used to predict cell voltage, hydrogen production, efficiencies and operating temperatures. Furthermore, the model has been made compatible with a transient system simulation program (TRNSYS). Real data from a reference solar hydrogen plant in Germany (PHOEBUS) is used for model validation. A detailed techno-economic study has been suggested as a future project.

Kazem [123] conducted an exergy analysis for 12900 kW PEM electrolyzer at various operation temperatures and pressures. The total exergy of each stream based on its specific mass flow rate and the exergy efficiency of the system has been calculated. The exergy efficiency increased by 26% as the operating temperature increased from 298 to 417 K at a constant pressure of 10 atm, while it increases by 2.5% if the operating pressure increases from 1 to 10 atm at a constant temperature of 298 K. The heat losses,

exergy destruction, cooling system and the economic concept have not been considered in the analysis.

M. Karim, and M. Iqbal [124] presented a dynamic model and simulation of a 30 Nm^3/h HYSTAT, 200kW alkaline electrolyzer. The model incorporates both the electrochemical and thermal behaviour of the unit. The cell voltage, energy efficiency, hydrogen production, heat losses and auxiliary cooling demands are studied. The MATLAB/Simulink software has been used to form a generalized model without any details being given. The study explains that the amount of hydrogen produced rises by increasing the current flows through the electrolyzer. In order to generalize the model, some input parameters have been chosen in such a way that the output parameters match with the practical model.

M. Ni, *et al*. [125] carried out energy and exergy analysis to investigate the thermodynamic-electrochemical characteristics of a PEM electrolyzer plant. Their analysis indicated that as the thermal energy needed to produce the electricity or input to the system is negligible, the exergy efficiency is almost the same as the energy efficiency. The PEM electrolyzer normally operates in an exothermic mode as the heat production exceeds the thermal energy demand. The parametric study suggests a high operating temperature, a thin PEM electrolyte and an electrode with high catalytic activity to enhance the system's performance. Developing a model to study the thermodynamic performance of a solar hydrogen system is recommended.

Dieguez, *et al*. [126] conducted a thermal performance analysis of a commercial water electrolyzer (HySTAT) designed for a rated hydrogen production of 1 Nm^3/h. The thermal behaviour of the system has been investigated under different operating conditions with an IR camera and several thermocouples. The results show that replacing the commercial electric power supply by providing the electrolyzer with an electronic convertor will reduce the power dissipated as heat by 50-67%. Using ANSYS V10.0 software, a mathematical thermal model can be implemented with a lumped capacitance and an overall heat transfer coefficient, mainly natural estimated as 4.3 $Wm^{-2}/{}^{\circ}C$. It was found that the internal heat generated could be optimized to reduce the cell overvoltage and enhance the energy efficiency.

A. Balablel, and M. Zaky [127], performed an experimental study to investigate the performance of an alkaline water electrolyzer coupled with PV generator in the

environment conditions of Egypt. The results showed that best performance and more hydrogen capacity were achieved as the gap between the electrodes were reduced and high voltage within the range considered was applied.

From section 3.5 it is appeared that water alkaline electrolyzers are fully developed and used for many years. The research activities have to be continued for improving the unit efficiency and reducing the technology cost. It is recommended to develop a general thermo-economic model including the cooling and recycling system. It is also suggested a comprehensive parametric study taking in considerations the unit; operation, design and economical parameters as well as the environment impact and fossil fuel consumed.

3.6 Summary and conclusions

Solar energy and its technology and uses are discussed in this chapter. Moreover, the working principles, market, and research and development works of SHS' main components are illustrated. The technology is still immature, while the costs and performance need to be periodically revised. However, crystalline solar cells and PEMFC and Alkaline electrolyzers are the most fully developed and the appropriate technologies for SHS components used for many years can be adopted for this research study.

A road map of the hydrogen economy is focused on heavy investment and extensive research and development work. The research work was focused on developing simulations and test tools, control and operation management systems and developing new materials. Furthermore, most of the simulation studies were based on energy, electro chemical, and economic analysis, leading to recommendations for developing a general and simple simulation and evaluation tool for SHS and its components, based on an exergy and thermo-economic models. The costs of environmental damage and the traditional resources consumed in traditional systems need to be taken in consecration in these models. Also it is recommended to apply and investigate a standalone SHS and its components at high rated capacities and investigate them in hot and arid zones regions such as North Africa, in order to utilize the high solar irradiance and heat recycling potential of such locations.

CHAPTER FOUR

Chapter Four

Case study

4.1 Introduction

One of the main objectives of this study is to design and investigate a standalone solar hydrogen system based on different weather conditions. For this reason, the energy demands of a small community in three different climate conditions have been considered here. Misurata, a coastal city and Sabha in the southern hot region of Libya, as well as Newcastle, a city in the cold climate of England, have been adopted for the case study. The main parametric weather factors affecting the system performance are ambient temperatures, global solar intensity at an optimal angle, sunshine duration, wind speed and other relevant meteorological parameters. These have been collected and analysed in this chapter. However, due to the shortages, uncertainty and limited years of measured data from the limited ground weather station available in Libya, particularly with regard to hourly and monthly global solar intensity at an optimum angle and the ambient temperatures, some other data sources has been used [128]. These data sources for meteorological and solar information at any location on the earth are based on a satellite image, radar and ground stations, and on using regression equations and software analysis to use the data appropriately for each site. The data collected from different sources for the three cities considered in this study, according to the availability for each parameter in either source, have been validated and compared to the data recorded in some available stations at or near these sites and also to each other.

4.2 Data sources

Three main data sources have been used for meteorological and solar radiation information. Firstly, data recorded (measured) from local ground climate stations has been collected, particularly for Libya [129, 130]. The second source was the data collected from the Atmospheric Science Data Centre (ASDC) at NASA Langley Research Centre [61,131]. This centre is responsible for the processing and distribution of NASA earth science and meteorological data. The renewable energy data source website which includes over 200 satellite-derived meteorology and solar energy parameters, averaged on a monthly basis over 22 years of observations and global solar data from 1195 ground sites. The third source was the Photovoltaic Geographical Information System (PVGIS) which provided web-based data from the European

Commission Joint Research Centre [132]. This centre provides a map-based inventory of solar energy resources and estimation of the electricity produced from any solar system at any particular location in Europe, Africa and South-West Asia. The PVGIS-CMSAF data base has been calculated based on the climate monitoring satellite images observed during the period 1998-2010. However, due to weather and geometrical conditions such as snow, cloud and mountains, some data uncertainties have occurred. A validation calculation using 18 stations in Europe has shown that the standard deviation of the local error in the yearly solar irradiance is about 5%. Some meteorological data, such as hourly, monthly average and yearly average ambient temperatures are taken from the Weather Underground web site, whose data originates from radar and weather stations [133].

4.3 The state of energy in Libya

Libya lies between 20^{o} and 32^{o} $55^{"}$ N. latitude and between 10^{o} and 25^{o} E. longitude, in the middle of the North Africa with a population of around 6.3 million in 2006. Its area is about 1.75 million km^2, mostly consisting of desert or semi desert land. It has a 1900 km long coastline facing the European continent, as illustrated in the map in Figure 4.1. The main source of energy and income in Libya are the oil and natural gas that are expected to be depleted within 40 years as the total reservoirs estimated at 47.1 billion gallons for oil and 52.8 trillion cubic meters (TCf) for natural gas. Figure 4.2 shows the trends in oil production, consumption and export for Libya. However, the CO_2 emission from fossil fuels production in Libya was 50 million metric tons (2012), whereas the installed electric capacity was 6.77 GWe (2010) [1]. As it is mostly desert, Libya has no hydro, biomass, or geothermal energy production facilities, which are alternatives to oil and gas energy sources. In addition, wind energy is very limited, with an average wind speed in the country of about 5 m/s. However, Libya is considered one of the highest solar insolation sites in the world with an average solar insolation estimated at 2200 kWh/m^2 annually average and average sunshine duration of more than 3400 hr/year. Solar energy is expected to be a viable alternative source of energy and could even become one of the main sources of income for this country, although it has not been commercially utilized yet due to the subsidised tariffs and cheap traditional energy now in use [32].

Figure 4.1 Map of Libya [1]

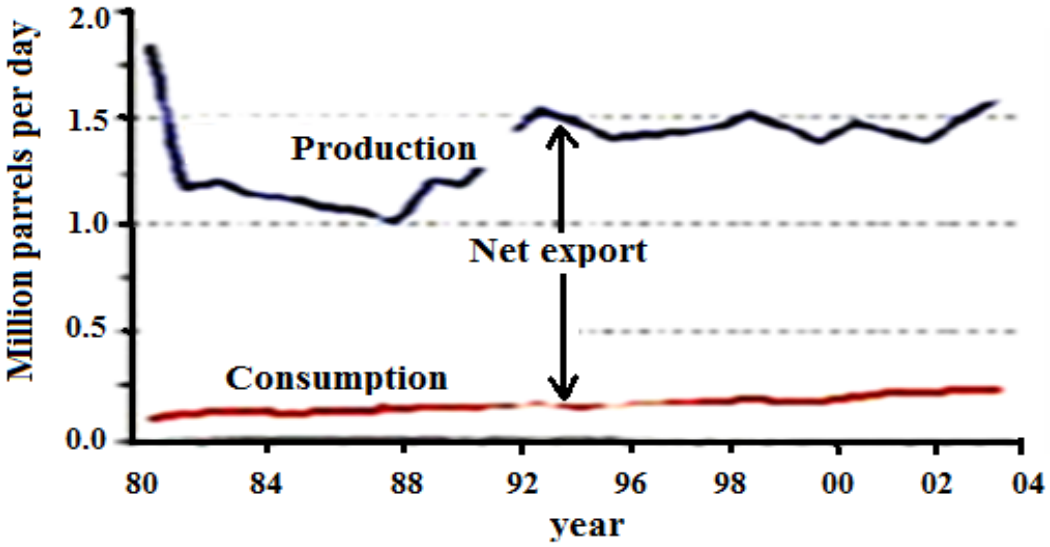

Figure 4.2 Fossil fuel state of Libya

4.4 Misurata site

The measured meteorological and solar radiation data (global, direct and diffuse) for Libya is very limited and because of very close latitude of Misurata to Tripoli, it has almost an identical climate. The solar energy centre in Libya has a monitoring station in Tripoli rather than Misurata, so some data obtained for Tripoli can be applied to Misurata. The measured global radiation in Tripoli varies from 2.744 kWh/m^2 in December, to 7.484 kWh/m^2 in July, on a horizontal surface. Diffused radiation is 0.967 kWh/m^2 in January, and 2.481 kWh/m^2 in May. Global radiation, received on a surface tilted at 32^o, ranges from 4.313 kWh/m^2 in November to 6.486 kWh/m^2 in August [32,130].

4.4.1 Misurata solar data

The maximum amount of solar radiation is always received on the surfaces in a way that corresponds to its direction. However, the amount of solar energy in a photovoltaic system is influenced by its orientation and tilt angle. The best way to maximize the amount of solar energy received by the system is to use tracking systems, which utilise a mechanical or an automatic mechanism to follow the direction of the sun in the sky. The cost and the maintenance of these systems are still too high now, even with performance enhancement and increasing productivity. Thus, a traditional fixed system on an optimal tilt angle that is fixed monthly, seasonally or yearly is often used today. It has been found that the drop in the amount of collected energy when using the yearly average fixed angle is around 8%, compared with the monthly optimum angle [134]. In order to design a solar PV system it is necessary to collect some information about the solar radiation being intercepted by the tilted surface and the site's meteorological data. The analysis in this study has been carried out based on the solar intensity for a fixed system with regard to the average annual tilt angle at each site. The monthly average optimum angle (OPTANG) during the year for Misurata has been calculated and presented in table 4.1 and Figure 4.3 using different sources with a mean value estimated as 30^{o}.

Month	OPTANG/PVGIS	OPTANG/NASA	OPTANG/EXP
Jan	58.0	55.0	61
Feb	50.0	48.0	51
Mar	37.0	34.0	36
Apr	20.0	19.0	16
May	6.00	4.00	1.0
Jun	-2.00	0.00	1.0
Jul	2.00	1.00	1.0
Aug	14.0	12.0	11
Sep	31.0	29.0	31
Oct	45.0	44.0	46
Nov	56.0	53.0	56
Dec	60.0	58.0	61
Year	30.0	29.6	31

Table 4.1 Monthly average tilt angle for Misurata from different sources

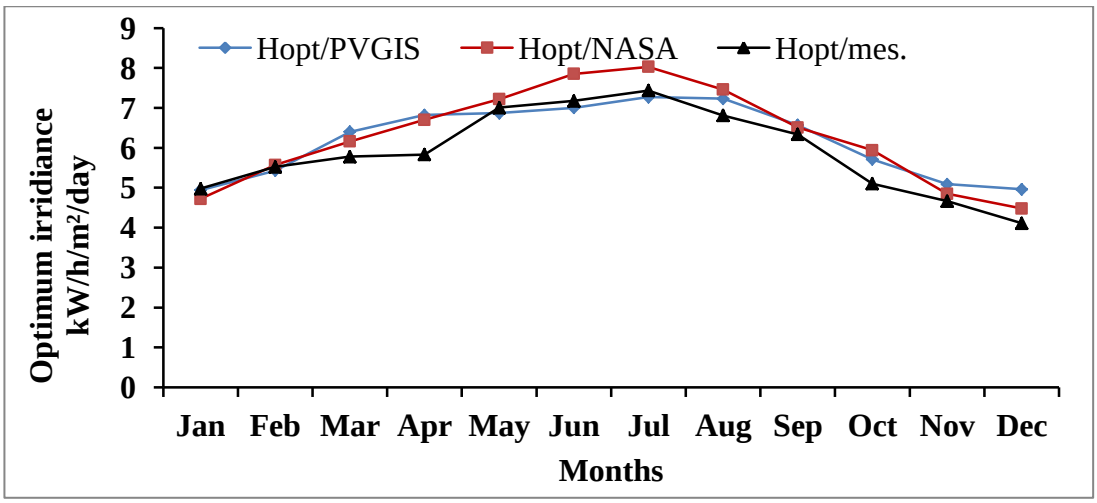

Figure 4.3 Misurata optimum global irradiance from different sources

Data for the optimum (Hopt) and horizontal (Hh) real sky solar intensity (Sirr) in kW/h/m^2/day was collected for Misurata measured by Solar Energy Center in Libya [130] (EXP) and compared with data from NASA and PVGIS and is presented in table 4.2 and Figure 4.4. It is clear that the maximum (Sirr) received by a system will be in the summer months of July and August and the least in the winter months of January and December, with the yearly hourly average estimated at 0.71 kW/h/m^2 from NASA and PVGIS and 0.67 from the measured data.

Month	Hh /PVGIS	Hopt/ PVGIS	Hh/ NASA	Hopt/ NASA	Hh/ EXP	Hopt/ EXP
Jan	3.26	4.940	3.07	4.720	2.848	4.976
Feb	4.01	5.430	4.09	5.570	3.802	5.523
Mar	5.43	6.400	5.36	6.160	4.940	5.781
Apr	6.58	6.820	6.57	6.700	5.660	5.833
May	7.31	6.870	7.24	7.220	7.005	7.005
Jun	7.83	7.000	7.90	7.850	7.176	7.176
Jul	7.98	7.270	8.07	8.030	7.436	7.436
Aug	7.27	7.230	7.37	7.460	6.715	6.810
Sep	5.86	6.570	5.96	6.510	5.654	6.338
Oct	4.49	5.710	4.59	5.940	4.424	5.100
Nov	3.48	5.090	3.31	4.850	2.972	4.663
Dec	3.23	4.960	2.77	4.480	2.783	4.113
Month-av	5.57	6.200	5.53	6.290	5.118	5.896
Day-av		0.704		0.714		0.670

Table 4.2 Solar intensity for Misurata from different sources

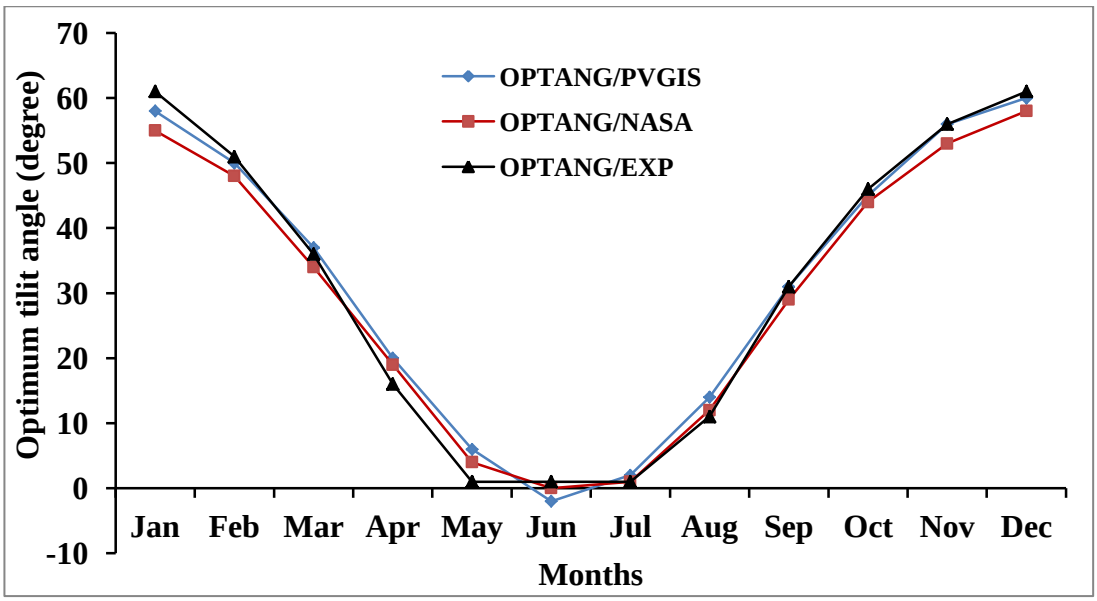

Figure 4.4 Misurata optimum tilt angle from different sources

4.4.2 Misurata weather data

The main meteorological parameter collected for Misurata, which is needed to design a solar system, is presented in Figures 4.5 to 4.8. The mean monthly sunshine duration measured for Misurata in 2004 had an estimated average of 8.8 hours per day and a maximum value of 12 h in July and least one of 6.5 h in December, as presented in Figure 4.5. The daily rainfall measured and data collected by NASA are presented in Figure 4.6 and table 4.3 with an average daily amount of 0.7 mm.

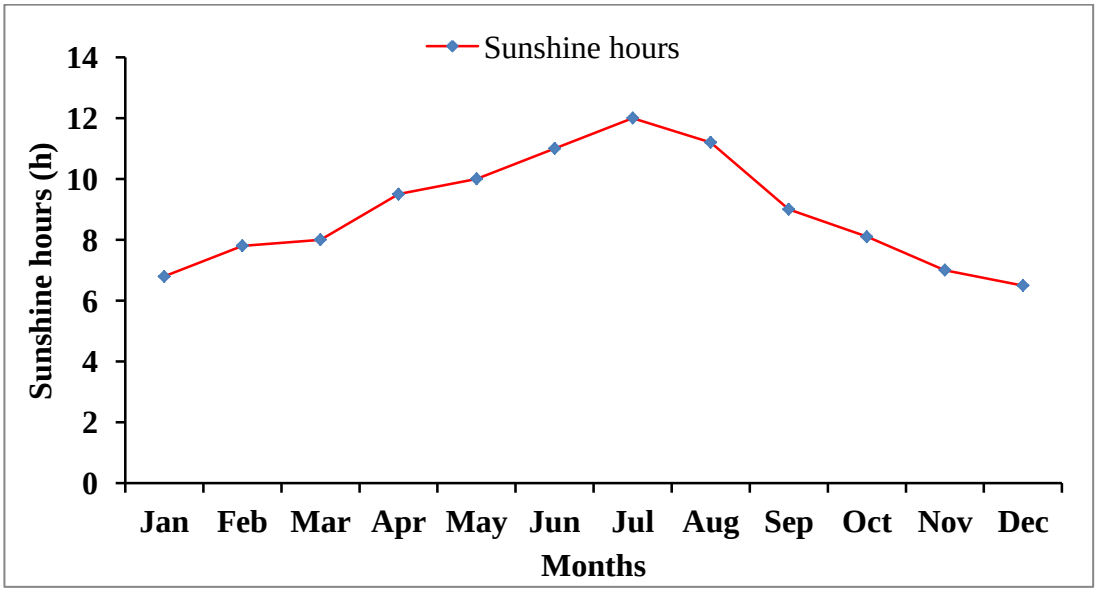

Figure 4.5 Average monthly sunshine hours in Misurata (2004)

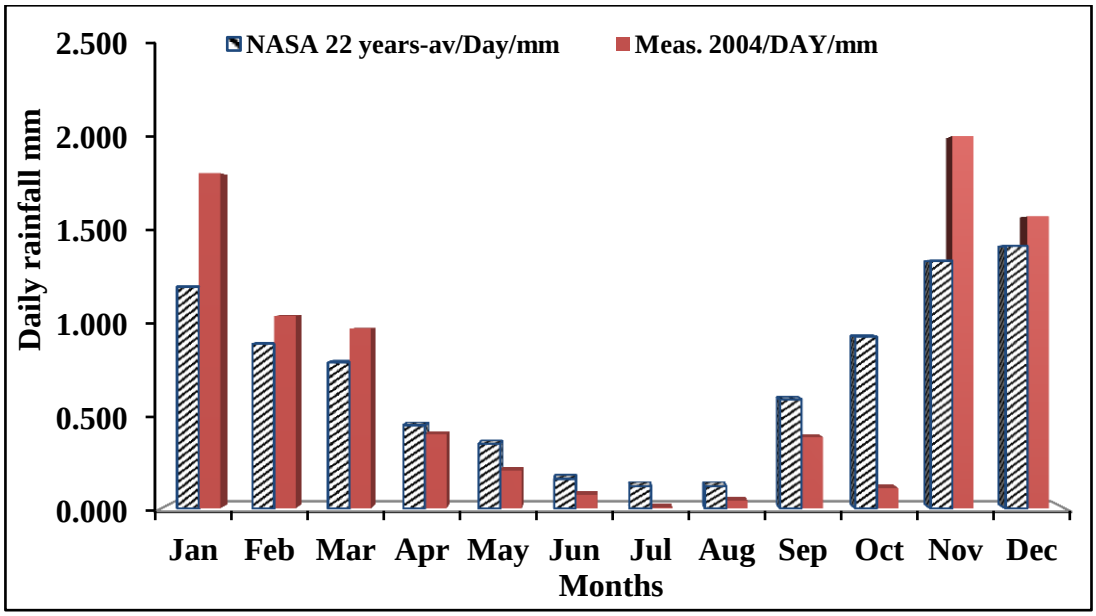

Figure 4.6 Misurata daily average rainfalls

Month	Measured 2004/Month/mm	NASA 22 years-Av./Day/mm	Measured 2004/DAY/mm
Jan	54.43	1.200	1.814
Feb	31.25	0.890	1.042
Mar	29.15	0.790	0.972
Apr	12.03	0.450	0.401
May	6.160	0.350	0.205
Jun	2.170	0.160	0.072
Jul	0.110	0.120	0.004
Aug	1.240	0.120	0.041
Sep	11.55	0.590	0.385
Oct	3.280	0.930	0.109
Nov	60.47	1.340	2.016
Dec	47.42	1.420	1.581
Average	21.60	0.690	0.720

Table 4.3 Misurata measured and NASA average rainfall

The yearly average wind speed is an important parameter that affects the solar system's performance. It was measured by two sources and presented in Figure 4.7 with an average of around 5 m/s. However, the average yearly clouds amount was calculated as 45% as illustrated in Figure 4.8 [129, 130, 133].

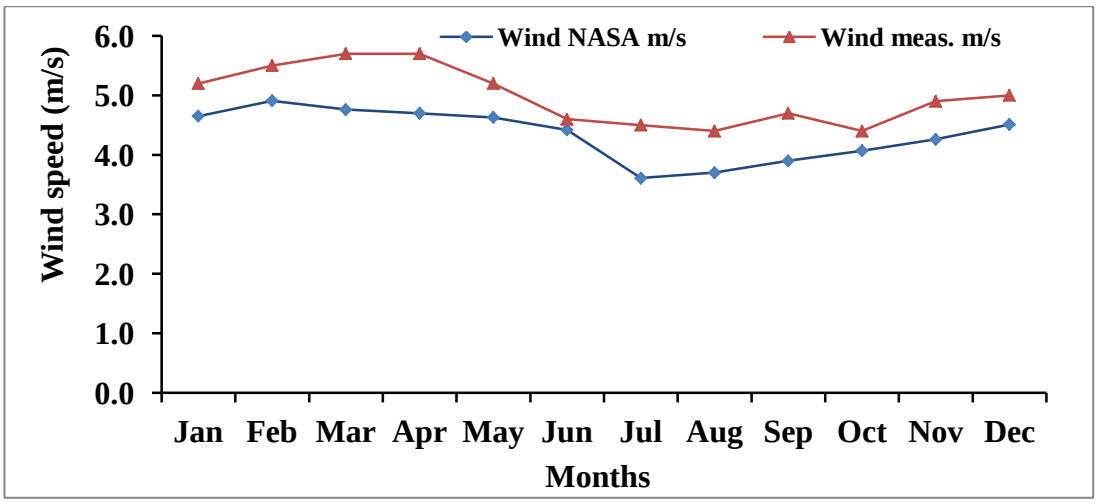

Figure 4.7 Average monthly wind speed in Misurata

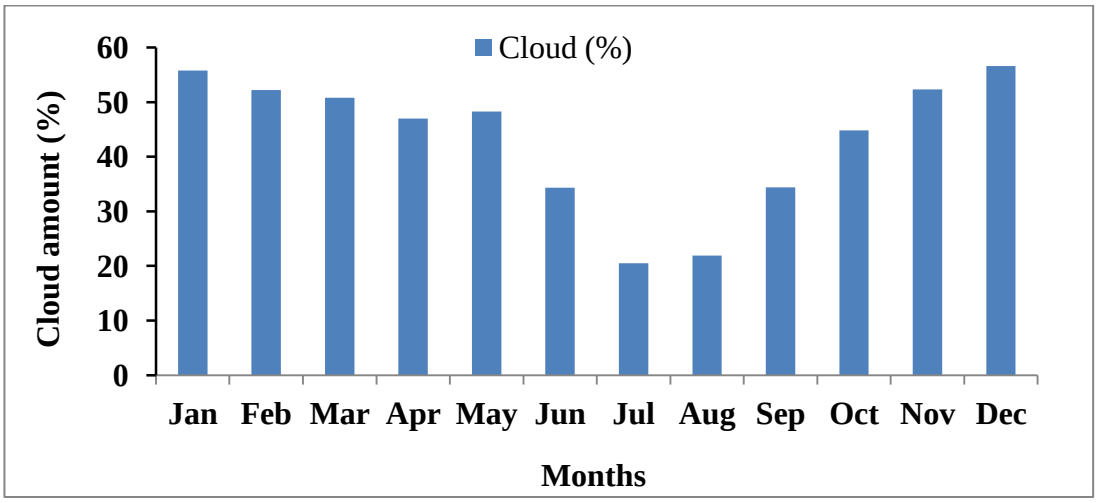

Figure 4.8 Monthly average cloud percentages in Misurata

4.5 Ambient temperature

Ambient temperature is one of the major climate parameter affecting the PV system's performance. However, as it is increases, the system efficiency will be reduced. In order to evaluate the system performance clearly during the year; daily, monthly and yearly average temperature data has to be collected. The average hourly minimum and maximum temperatures collected for Misurata from local weather stations during the period (1994-2004) (meas.) as well as from 22 years of observations by NASA are presented in Figures 4.9, 4.10 and table 4.4. It can be clearly seen from the figures that the temperature difference (ΔT) between the monthly mean maximum and mean minimum temperatures for Misurata is almost constant during the year in the range of 8 °C. The average day time (DT) temperatures calculated as the mean of the average 24 hours minimum and average maximum temperatures during the day are tabulated in

table 4.5 for the three sites [133]. The data collected indicate that the yearly average daytime temperature during the year for Newcastle, Misurata and Sabha can be considered as (10, 23 and 28.5 ^{o}C) respectively.

Month	Min T (°C)/ NASA (83-05)	Max T (°C)/NASA (83-05)
Jan	14.40	19.30
Feb	13.90	19.90
Mar	14.70	21.50
Apr	16.00	23.90
May	18.60	26.90
Jun	21.80	30.40
Jul	24.50	33.20
Aug	25.90	34.20
Sep	25.30	32.10
Oct	22.80	28.70
Nov	19.50	24.80
Dec	16.20	21.00
Average	19.47	26.33
Year-day-av/ NASA(83-05)	22.90	
Min T (°C)/ Meas.(94-04)	16.72	
Max T (°C)/Meas.(94-04)		25.43
Year-day-av/Meas.(94-04)	21.075	

Table 4.4: Misurata yearly mean day temperature

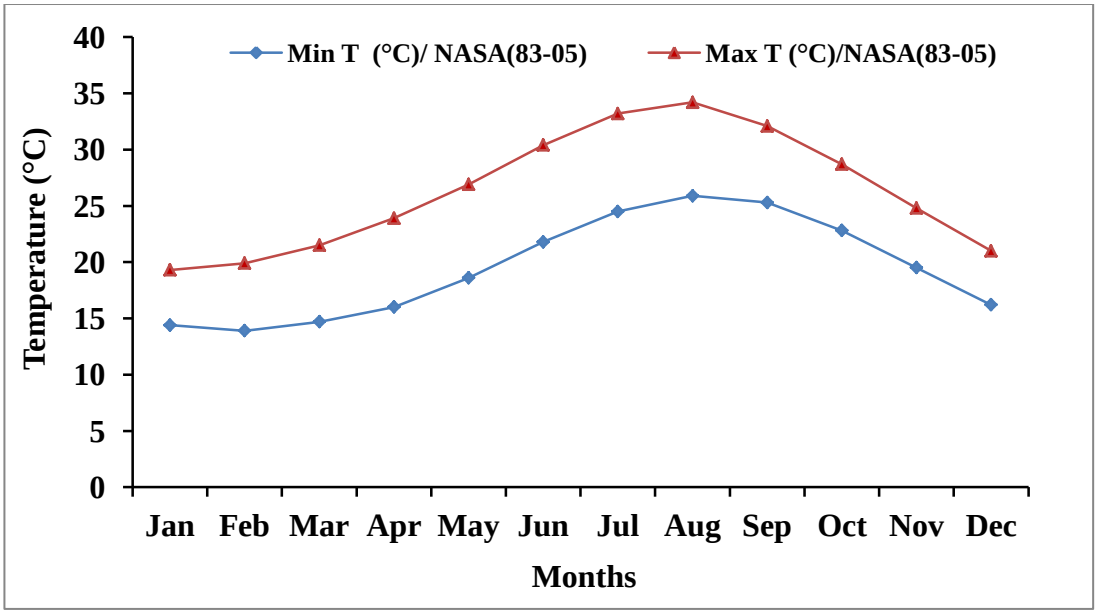

Figure 4.9 Misurata monthly average minimum and maximum temperature (NASA)

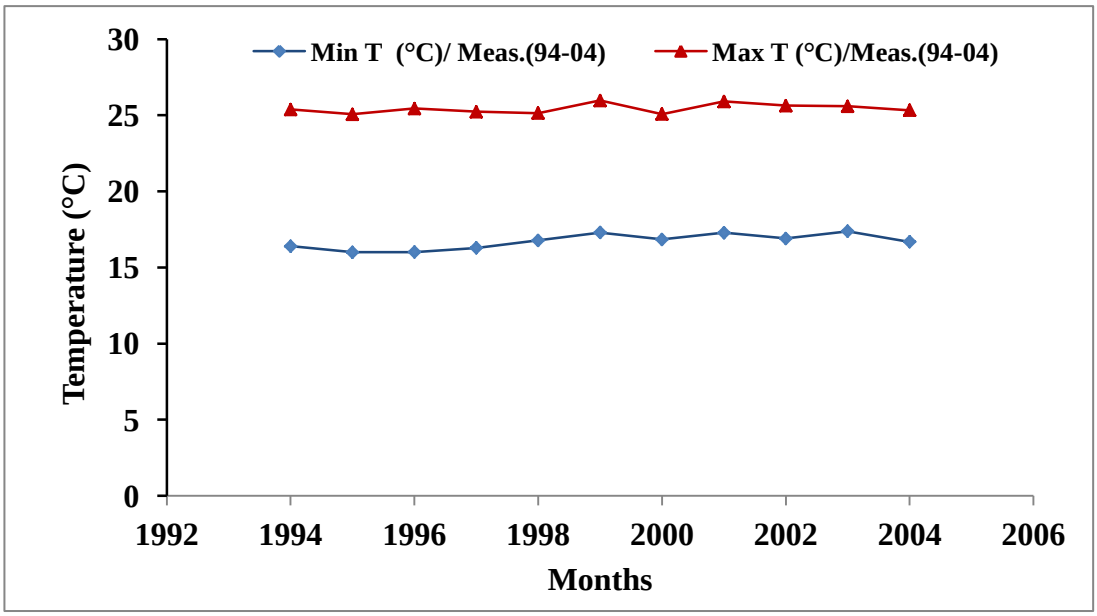

Figure 4.10 Misurata measured monthly average minimum and maximum temperatures

Month	Misurata day temp. T (^{O}C)		Sabha day temp. T (^{O}C)		Newcastle day temp. T (^{O}C)	
	meand	max	meand	max	meand	max
Jan	15.0	19.0	15.0	22.0	1.00	3.00
Feb	18.0	23.0	20.0	27.0	1.00	4.00
Mar	18.0	23.0	22.0	29.0	5.00	9.00
Apr	20.0	23.0	26.0	33.0	8.00	13.0
May	23.0	27.0	29.0	36.0	9.00	14.0
Jun	25.0	29.0	35.0	39.0	14.0	19.0
Jul	26.0	30.0	32.0	38.0	16.0	20.0
Aug	27.0	31.0	31.0	38.0	14.0	19.0
Sep	26.0	29.0	30.0	37.0	13.0	17.0
Oct	24.0	28.0	26.0	32.0	9.00	12.0
Nov	21.0	25.0	21.0	28.0	4.00	7.00
Dec	17.0	21.0	15.0	22.0	-1.00	2.00
Year-av	21.6	25.6	25.1	31.7	7.75	11.6
Year-DT-av	23.6		28.4		9.67	

Table 4.5 Yearly average daytime hourly temperatures [133]

The electricity and heat produced from any PV system is influenced on a daily and monthly basis by the solar intensity and climate conditions. So, in order to investigate the system, daily and monthly data for a typical day in cold and hot months during the year have been adopted for the analysis. Tables 4.6, 4.7 and 4.8 show the hourly-recorded ambient temperatures and the corresponding optimal solar intensity on 15th January 2011 and 15th August 2010 for Misurata, Sabha and Newcastle respectively [133]. The data shows that for Newcastle the average daily temperature on 15th of January 2011 is 10.7 ^{o}C, which is more than the average temperature for this month of 3.0 ^{o}C, while the average wind speed was recorded as 8.15 m/s. The average daily temperature recorded in August 2010 for Newcastle was 14 ^{o}C and the maximum was 23 ^{o}C, whereas the average increased to 15.8 ^{o}C in the middle of the month with a wind speed average on that day of 1.99 m/s.

	Newcastle Temp. 15 Jan 2011		Newcastle Temp. 15August 2010		Newcastle-Jan.		Newcastle-August	
Time	T (°C)	wind m/s	T (°C)	wind m/s	Hopt-av Kwh/m^2	Hopt-clear sky	Hopt-av kWh/m^2	Hopt-clear sky
7	10	8.333	12.0	1.556	0.000	0.000	158.0	215.0
8	11	10.27	12.0	2.056	0.000	0.000	258.0	419.0
9	10	8.278	13.0	1.556	94.00	248.0	349.0	621.0
10	10	9.111	15.0	2.056	172.0	477.0	422.0	788.0
11	10.5	9.250	14.5	2.056	218.0	618.0	469.0	899.0
12	11	9.250	16.0	1.556	237.0	674.0	488.0	944.0
13	11	9.250	16.0	1.556	226.0	640.0	477.0	917.0
14	11	9.778	18.0	2.056	186.0	520.0	437.0	821.0
15	11	7.194	21.0	2.056	119.0	320.0	370.0	667.0
16	11	7.194	19.0	2.056	0.000	0.000	282.0	471.0
17	11	7.194	18.0	2.583	0.000	0.000	183.0	264.0
18	11	6.694	17.0	2.583	0.000	0.000	89.00	88.00
19	11	6.694	17.0	2.583	0.000	0.000	31.00	25.00
20	11	5.667	13.0	1.556	0.000	0.000	0.000	0.000
Av.	10.7	8.150	15.8	1.990	89.29	249.7	286.6	509.9

Table 4.6 Newcastle temperatures, wind speed and optimum solar radiation in January and August

The average temperatures recorded at Misurata in January and August was 15 ^{o}C and 27 ^{o}C respectively with a maximum temperature recorded as 37 ^{o}C in August. The average wind speed and temperature in the middle of January and August was 5.51 and 5.54 m/s and 17 ^{o}C and 31.4 ^{o}C respectively [133].

	Misurata Temp. 15 Jan 2011		Misurata Temp. 15August 2010		Misurata Jan.		Misurata August	
Time	T (°C)	wind m/s	T (°C)	wind m/s	Hopt-av kWh/m^2	Hopt-clear sky	Hopt-av kWh/m^2	Hopt-clear sky
7	16	5.833	26.0	4.167	129.00	150.0	280.0	256.0
8	17	7.722	26.0	5.139	302.00	372.0	518.0	497.0
9	16	6.667	28.0	5.139	490.00	627.0	730.0.0	719.0
10	16.5	5.556	30.0	5.139	629.00	822.0	891.0	889.0
11	15	4.639	32.0	5.139	711.00	940.0	988.0	993.0
12	16.5	5.278	33.0	5.694	733.00	973.0	1010.0	1020
13	17	6.111	34.0	5.833	696.00	918.0	970.0	974.0
14	18	6.694	35.0	6.167	599.00	780.0	857.0	852.0
15	18	6.111	34.0	6.167	447.00	568.0	681.0	667.0
16	18	5.000	33.5	6.167	249.00	301.0	459.0	437.0
17	18	4.111	33.0	6.167	75.000	83.00	222.0	198.0
18	17.7	4.361	32.5	5.833	0.0000	0.000	48.00	33.00
19	17.4	4.444	32.0	5.667	0.0000	0.000	0.000	0.000
20	17	4.639	31.0	5.139	0.0000	0.000	0.000	0.000
Av.	17	5.510	31.4	5.540	361.40	466.7	546.7	538.2

Table 4.7 Misurata temperatures, wind speed and optimum solar radiation, in January and August

In Sabha the maximum temperature recorded in August 2010 was 43 ^{o}C with an average temperature of 31 ^{o}C. In January 2011 the average was 14 ^{o}C. However, the average wind speed and temperatures recorded in the middle of January and August were 3.43 and 4.2 m/s and 12.1 ^{o}C and 36.5 ^{o}C respectively, as illustrated in table 4.8.

The average optimum hourly solar intensity (kWh/m^2) in a real sky (Hopt-av) and clear sky (Hopt-clear) recorded for Newcastle during the chosen months indicated that it was lower than the highest one recorded in Sabha and Misurata in August, as presented in tables 4.6 to 4.8 [132].

	Sabha Temp. 15 Jan 2011		Sabha Temp. 15August 2010		Sabha Jan.		Sabha August	
Time	T (°C)	wind m/s	T (°C)	wind m/s	Hopt-av kWh/m^2	Hopt-clearsky	Hopt-av kWh/m^2	Hopt-clearsky
7	3	2.778	27.0	1.111	107.00	111.0	258.00	252.00
8	4	3.333	28.0	0.278	355.00	397.0	488.00	497.00
9	6	3.611	32.0	3.889	564.00	650.0	694.00	722.00
10	10	2.778	34.0	6.694	720.00	843.0	849.00	894.00
11	11	3.333	35.0	5.139	812.00	960.0	942.00	999.00
12	13	3.056	38.0	2.583	838.00	992.0	968.00	1030.0
13	14	3.083	39.0	2.056	795.00	938.0	925.00	980.00
14	15	5.139	40.0	2.583	687.00	801.0	816.00	857.00
15	16	5.000	40.0	5.278	517.00	592.0	646.00	670.00
16	16	4.639	40.0	7.722	297.00	328.0	432.00	436.00
17	16	2.583	40.0	5.139	26.000	17.00	202.00	193.00
18	16	4.111	41.0	6.167	0.0000	0.000	38.000	29.000
19	15	2.056	39.0	5.139	0.0000	0.000	0.0000	0.0000
20	14	2.583	38.0	5.139	0.0000	0.000	0.0000	0.0000
Av.	12.1	3.430	36.5	4.200	408.29	473.5	518.43	539.93

Table 4.8 Sabha temperatures, wind speed and optimum solar radiation (January and August)

4.6 Sabha solar data

The monthly average optimum angle (OPTANG) during the year for Sabha has been calculated and presented in table 4.9 and Figure 4.11 using different sources with a mean value estimated as 26˚. Data for the optimum (Hopt) and horizontal (Hh) real sky solar intensity in kW/h/m^2/day collected for Sabha from NASA and compared with data from PVGIS are presented in table 4.9 and Figure 4.12. It is clear that the maximum solar intensity received by a system in Sabha will be in the summer months of July and August and the lowest in the winter months of January and December ,with a yearly hourly average estimated as 0.67 kW/h/m^2.

Month	Hh/ PVGIS	Hopt/ PVGIS	OPTANG/ PVGIS	Hh/ NASA	Hopt/ NASA	OPTANG/ NASA
Jan	4.10	5.69	54.0	3.56	4.91	50.0
Feb	4.95	6.32	46.0	4.68	5.96	43.0
Mar	6.04	6.79	31.0	5.86	6.47	30.0
Apr	6.76	6.81	14.0	6.66	6.67	14.0
May	7.24	6.74	0.00	6.79	6.76	0.00
Jun	7.75	6.90	-7.00	7.62	7.58	0.00
Jul	7.95	7.19	-4.00	7.78	7.75	0.00
Aug	7.49	7.29	9.00	7.12	7.12	7.00
Sep	6.47	6.98	25.0	6.12	6.45	23.0
Oct	5.23	6.29	40.0	5.20	6.34	39.0
Nov	4.36	5.88	51.0	3.81	5.07	48.0
Dec	4.23	5.95	56.0	3.17	4.51	52.0
Month-av	6.05	6.57	26.0	5.70	6.30	25.4
Day-av		0.68			0.66	

Table 4.9 Sabha solar intensity from different sources

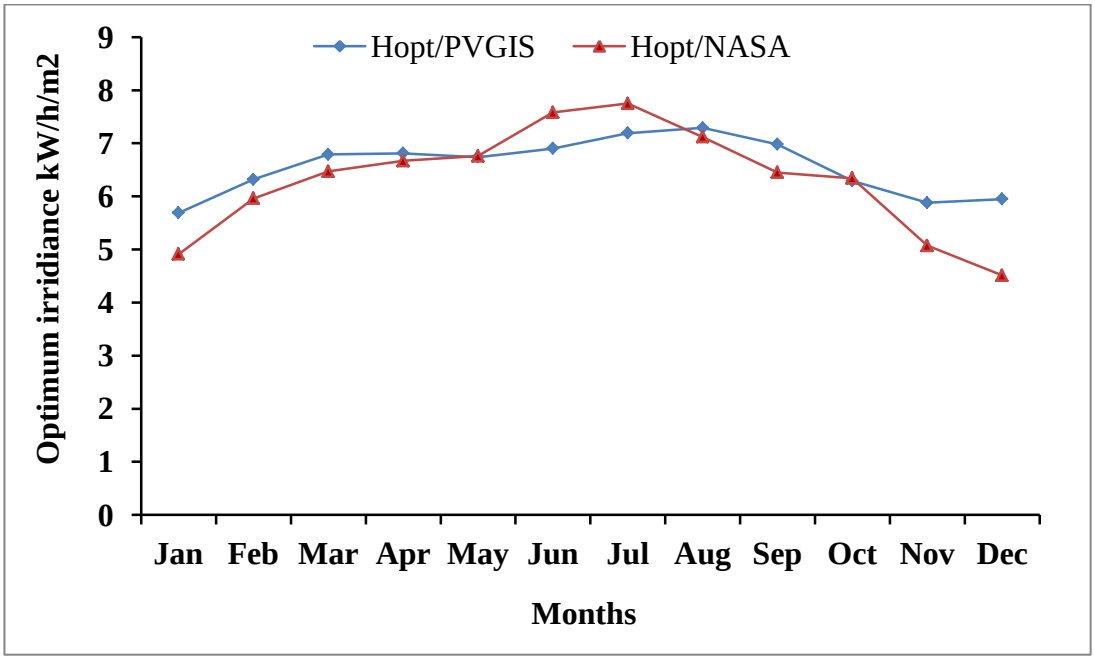

Figure 4.11 Sabha monthly average solar intensity

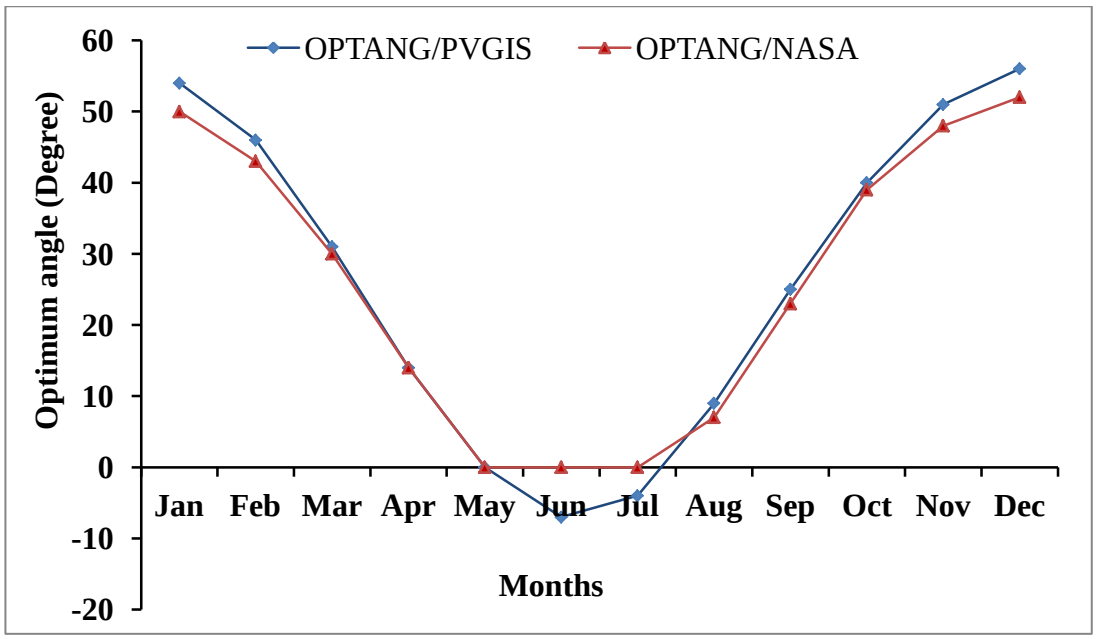

Figure 4.12 Sabha monthly average optimum angle

4.6.1 Sabha weather data

The main meteorological parameters collected for Sabha are presented in Figures 4.13 to 4.16. The mean monthly sunshine duration for Sabha is shown in Figure 4.13 with an average daily sunshine duration estimated at 9.8 hours and a maximum value (12 h) recorded in July with the lowest (6.5 h) in December. The daily rainfall measured and data collected by NASA are presented in Figure 4.14, indicating that it is almost dry throughout the year, with an average amount of around 0.05 mm/day.

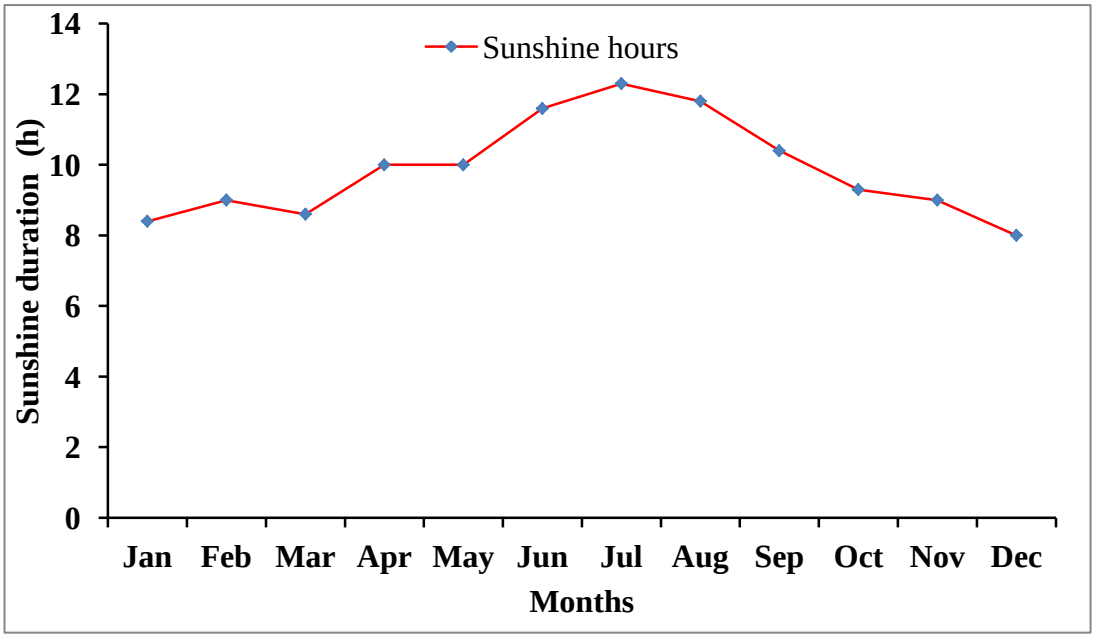

Figure 4.13 Sabha average monthly sunshine duration

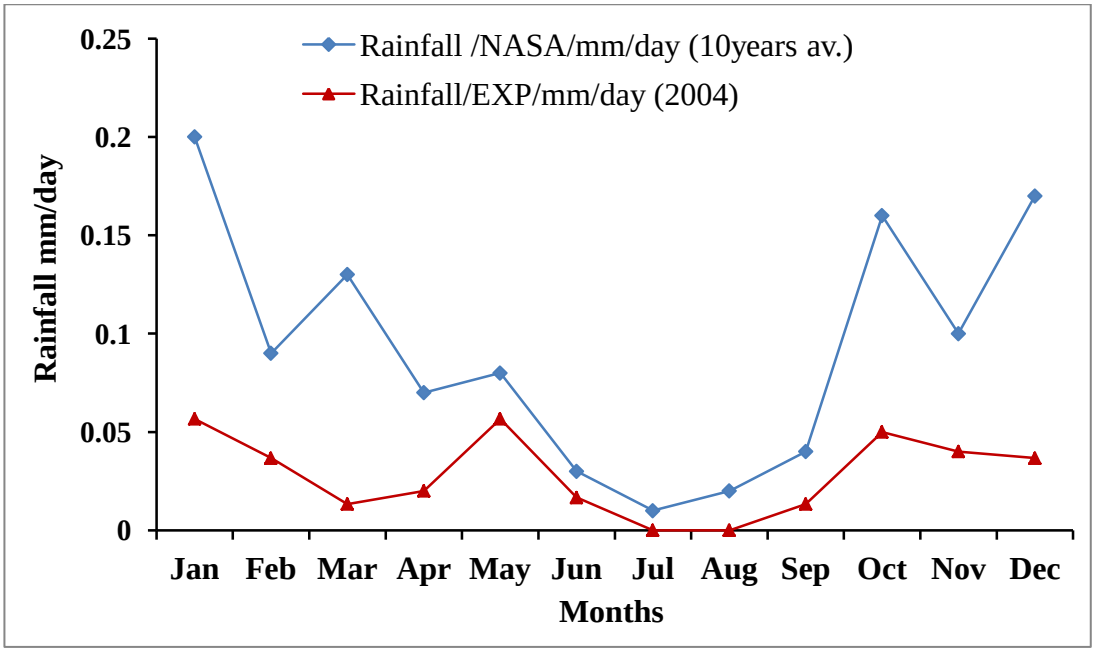

Figure 4.14 Sabha daily average rainfall

The yearly average wind speed is presented in Figure 4.15 with an average estimated at 4.5 m/s/day. The average yearly clouds amount shows that an almost clear sky during the year with a monthly average of 28.4%, as illustrated in Figure 4.16 [131].

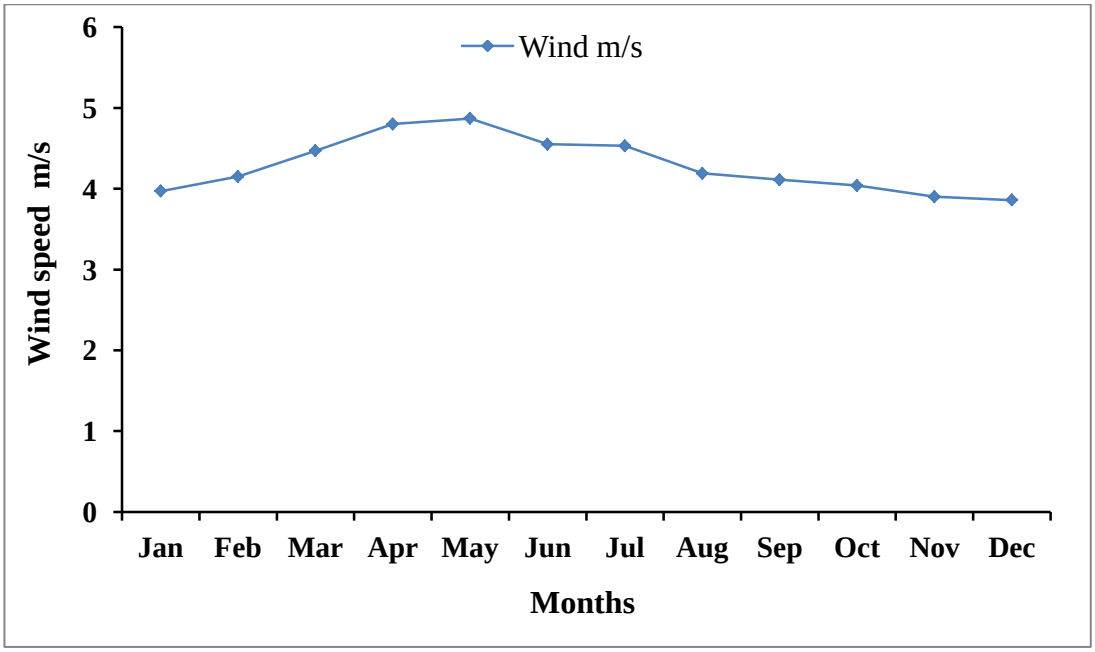

Figure 4.15 Sabha average monthly wind speed

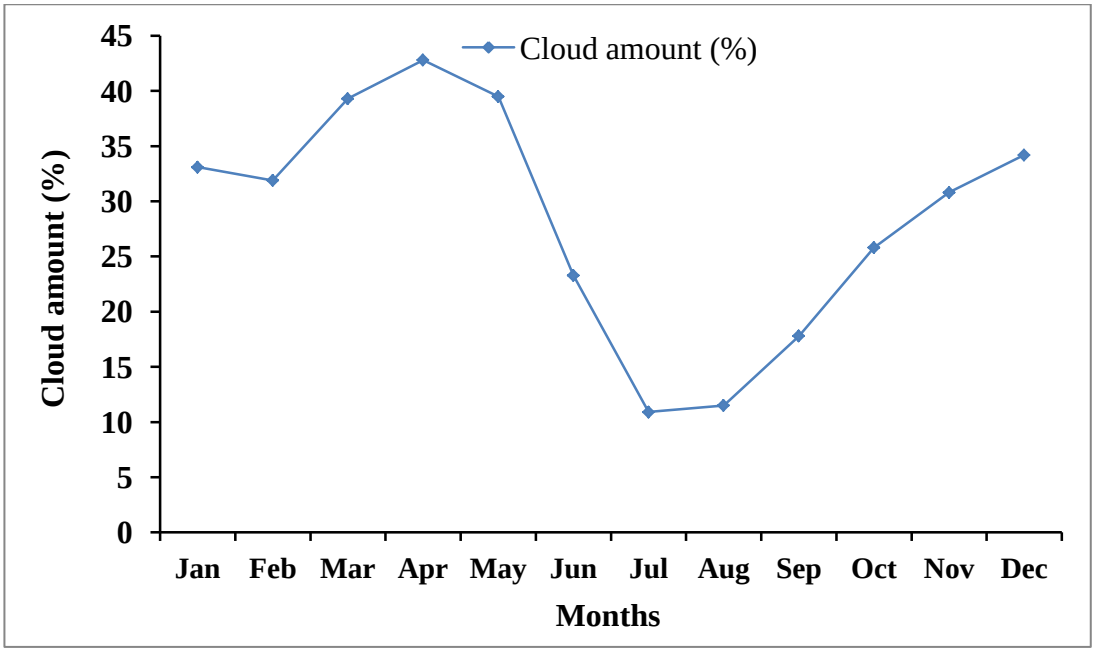

Figure 4.16 Amount of cloud in Sabha

4.7 Newcastle Solar data

The monthly average optimum angle during the year for Newcastle is shown in Figure 4.18 and table 4.10 using different sources with a mean value estimated at 41°. Data for the optimum (Hopt) and horizontal (Hh) real sky solar intensity in kW/h/m^2/day collected for Newcastle from NASA and compared with data from PVGIS are presented in table 4.10 and Figure 4.17.

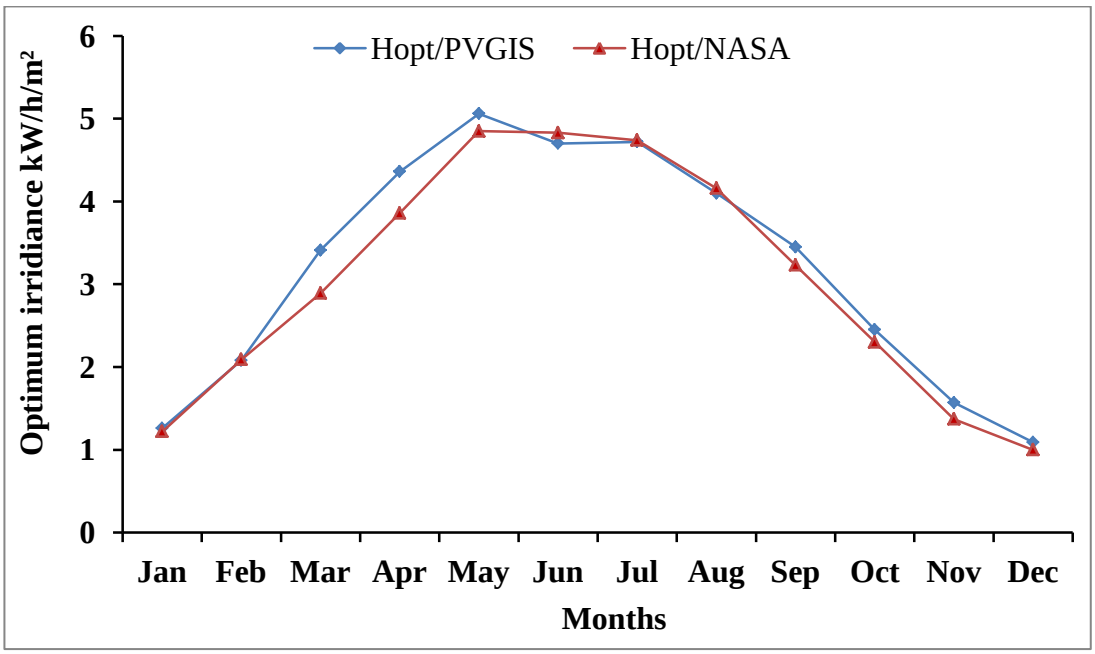

Figure 4.17 Newcastle monthly average solar intensity

It is clear that the maximum solar intensity received by a system in Newcastle is almost less than half the amount received by the same system installed at Sabha with an average hourly solar intensity during the year calculated as 0.75 kWh/m^2 as presented in table 4.10. However, the daily average sunshine duration during the year for Newcastle is estimated as 4.2 hours daily [135].

Month	Hh/ PVGIS	Hopt/ PVGIS	OPTANG/ PVGIS	TD/ PVGIS	OPT ANG/ NASA	Hh/ NASA	Hopt/ NASA
Jan	0.598	1.26	72	4.800	68	0.63	1.22
Feb	1.210	2.08	64	5.600	60	1.31	2.09
Mar	2.420	3.41	53	6.700	46	2.31	2.89
Apr	3.780	4.36	37	8.600	31	3.53	3.86
May	4.940	5.06	24	11.30	18	4.67	4.85
Jun	4.880	4.70	16	13.90	11	4.73	4.83
Jul	4.800	4.72	19	160.0	15	4.62	4.74
Aug	3.780	4.10	30	16.50	26	3.92	4.16
Sep	2.710	3.45	45	14.60	42	2.72	3.23
Oct	1.560	2.45	60	11.50	57	1.57	2.30
Nov	0.766	1.57	71	7.700	66	0.77	1.37
Dec	0.465	1.09	75	4.900	71	0.47	1.00
Year	2.670	3.19	41	10.20	41	2.61	3.05
Day-av		0.76					0.73

Table 4.10 Newcastle solar intensity from different sources

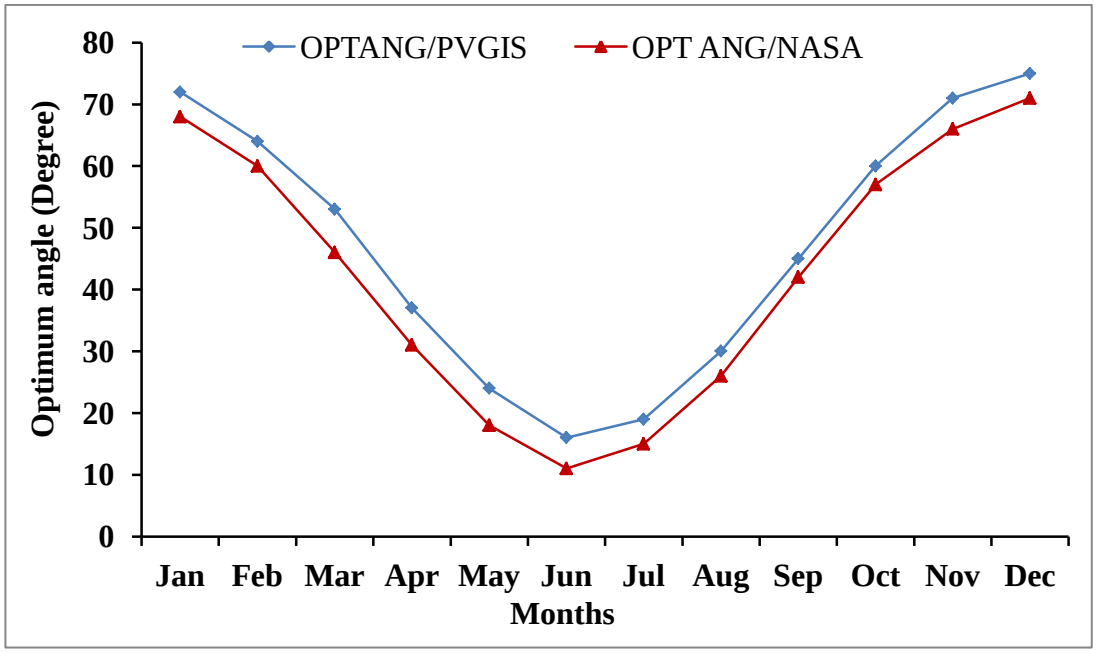

Figure 4.18 Newcastle monthly average optimum angle

4.7.1 Newcastle weather data

The main meteorological parameter collected for Newcastle is presented in table 4.11. The average daily rainfall collected by NASA is estimated as 4.8 mm, while the yearly average wind speed was around 5 m/s and the cloud cover was 73.9%.

Month	22-year Average CLOUD %	10-year Average rainfall (mm)	22-year Average wind m/s	Mini T (°C)	Max T(°C)
Jan	71.3	5.82	2.88	2.78	5.54
Feb	74.6	5.52	2.33	2.49	6.29
Mar	74.8	5.50	2.00	3.10	8.55
Apr	74.1	4.71	2.08	4.05	11.4
May	74.5	4.33	1.71	6.65	15.2
Jun	78.6	4.04	2.10	9.69	18.4
Jul	77.4	3.90	1.90	12.4	21.0
Aug	73.2	4.08	2.16	13.3	21.2
Sep	72.4	4.71	2.25	11.2	18.0
Oct	77.0	5.14	2.85	8.58	13.3
Nov	70.0	5.33	2.86	5.70	8.74
Dec	69.0	5.59	3.07	3.87	6.44
Year	73.9	4.88	2.35	6.90	12.8

Table 4.11 Meteorological data for Newcastle

4.8 Conclusion

Weather and solar energy data for Misurata, Sabha and Newcastle have been collected and illustrated using different sources. The most important key climate parameters for the investigation of any solar system are solar intensity, ambient temperature, sunshine duration, cloud amount and wind speed. Data collected using satellite, radar images and software analysis such as PVGIS and NASA database are given along with varies and a wide range meteorological features and solar information for any specific site compared to ground station and monitoring data. An over estimation of the main key parameters values will lead to costly design, incorrect evaluations and output results for the system. Data collected for the Libyan cites indicates that they are optimal sites for solar energy production during the whole year, while Newcastle solar and meteorological information will involve limited productivity for any solar system. An hourly average solar intensity during the year estimated at 0.67, 0.70 and 0.75 kWh/m^2 has been

calculated for Sabha, Misurata and Newcastle respectively. The daily average sunshine duration for the three cities can be predicted to be 9.6, 8.8 and 4.2 hours respectively. The average daily ambient temperatures for the three sites of Sabha, Misurata and Newcastle are 28.5, 23.0 and 10.0 ^{o}C. In addition, the daily average wind speed during the year for the three sites is around 5 m/s, measured in an open field at 10 m above the ground.

CHAPTER FIVE

Chapter Five

Description of the simulation tool (IPSEpro)

5.1 Introduction

A literature survey of work on solar hydrogen systems indicates that there are only few SHS projects that have been installed, mainly for study purposes all over the world up to date. In addition, SHS technologies are still immature and costly, providing a boost for more studies and investigations to improve performance and reduce equipment costs. Consequently, using actual systems for experimental examinations and studying purposes is also costly and time consuming. In contrast, software modeling and simulation analysis are proper tools that save time and money for system pre design, optimization, evaluation and prediction of performance and outputs. However, choosing a model from those which are available and ready to use as software or whether to develop a new one is a decision which depends mainly on the advantages and disadvantages of these models as well as their simulation purposes. Furthermore, there are many criteria controlling the model and software selection decisions for any energy system. These criteria can be summarized in terms of the area of interest (methodology), the state of the model (dynamic or steady), details and dimensions of complexity, speed, accuracy, flexibility, source code availability, time step, graphical representation, libraries of thermodynamic properties and system units, documentation and model validation [109]. The commercially available models and software related to SHS and its units are mostly theoretically based and detailed or programs with a specific purpose. These models are mainly based on a specific coefficients and semi-empirical relations that could be used only for a particular unit or a region in the system. Furthermore, none of the commercially available energy or SHS software models such as, Hydrogems[39]. Homer [48], Simplorer [42], Hyprid2 [45], TRANSYS [82], Visual Pascal [36], Mat-lab, and IPSEpro have been developed based on a thermo-economic analysis of SHS. However, I. Giglmayr et al. [136] indicated that IPSEpro is one of the most famous 16 commercially available developed software for thermodynamic processes analysis and evaluations. They compare a list of programs including Aspen Plus 10.0, Prosim 3.3, Thermoflex 4.0/-6, STEAM PRO-STEAM, Gate Cycle 5.22.0.r and Cycle Tempo 4.14. The authors show that, as the requirements to be met by these programs are different; the program selection is a tool for the potential user according to his or her specific needs [136]. However, in this study, the commercially available energy analysis software package IPSEpro has been adopted because of its reliability, open source code,

low cost, graphically and friendly user interface, ease of use, wide range of applications and short implementation time [136,137]. The software was successfully applied to the model and investigate several energy systems such as, refrigeration, desalination, solar thermal and power thermal plants as well as its components [136,137,138,139,140,141,142]. Many leading companies including DLR, Abengoa Solar, Epuron, SunTechnics, Flagsol, Ciemat-PSA, Rolls-Royce and Iberdrola used IPSEpro to build their own model libraries for different applications including solar thermal [139]. In the following paragraphs the software; structure, working principle and abilities as well as the components of modules and libraries will be introduced and clarified.

5.2 IPSEpro system's structure

The IPSEpro is a highly flexible, easy, open source code and comprehensive software package with a friendly interface that can be used for designing, simulating and evaluating any engineering processes. With IPSEpro, the processes can be represented and structured graphically as a network of components using their mathematical equations and physical behavior. The software package consists of several modules and libraries that are be briefly described in the following paragraphs [138,144,145].

5.2.1 IPSEpro Modules

IPSEpro provides well-organized data management, powerful mathematical methods and an intuitive graphic user interface [138]. Using the following IPSEpro Design and processing modules it is possible to create and simulate any energy process model graphically:

-MDK Module

Module development kit MDK uses a model description language (MDL) to build a new or modify component model libraries according to its specific mathematical equations and user requirement.

-PSE Module

Processes simulation environment PSE is a friendly-user interface flow sheet using graphically and pre-defined library components to simulate, represent and connect the process or the unit.

-PSLink Module

Provides a link between MS-excel and PSE-projects enabling exchange of data in both directions, and creates a sensitivity analysis and parametric study for the unit or system parameters.

-PSEasy Module

Used to transform and calculate any PSE pre simulation models into a standard and fixed cycle layout.

-PSValidate Module

IPSEpro-PSValidate uses statistical methods to remove the redundancies and check the accuracy of a measured data used in the simulation processes.

-PSOptimize Module

The module selects the best and optimum operations and design parameters for any project according to the user's pre-defined criteria.

-PSEconomy Module

This module allows studying and evaluating the IPSEpro processes economically through a life cycle cost and profitability analysis.

5.2.2 IPSEpro Model Libraries

The development of energy systems' module libraries using IPSEpro-MDK kit has been carried out by the software main developer company Sim-tech and many other researchers and companies according to their own requirements [138,142]. However, the software founder Sim-tech usually provides the following libraries with the main licences for the program package:

-General Power Plants (App_Lib)

The library consists of fifty-six component models such as; turbines, heat exchanger, compressor, boilers, combustors and pump. This library model and its units or components can be used alone or in combination with other model libraries. It could be used with desalination, and refrigeration libraries to simulate the power thermal and cogeneration plants as well as combined cycle plants and many other energy systems.

-Refrigeration (Frigo_Lib)

The refrigeration processes library enables one to calculate and access around fifty refrigerants thermodynamic properties. With (Frigo-Lib) alone and in combination with other model libraries it is possible to simulate many refrigerant systems and thermal compression processes such as absorption chillier, heat pump, organic Rankin cycle

systems and complete tri-generation systems as well as evaluating different environmental refrigerants.

-Desalination (Desal_Lib)

The desalination process library can be applied to simulate and investigate different types of desalination methods such as:

-RO – reverse osmosis

-MSF – multi-stage flash

-MED – multi-effect distillation

-MVC – mechanical vapour compression

-TVC – thermal vapour compression

5.2.3 IPSEpro architecture and working principle

The main IPSEpro modules that could be seen as the software's core are the MDK and PSE modules, whereas the other modules are extensions and complementary modules. The program's flexibility is referred to by the independency and unlimited applications to create or modify any model library. This processes using the tow level steps; MDK for model building and PSE for model processes and simulation. The architecture and the interaction between the main MDK and PSE modules are presented in Figure 5.1.

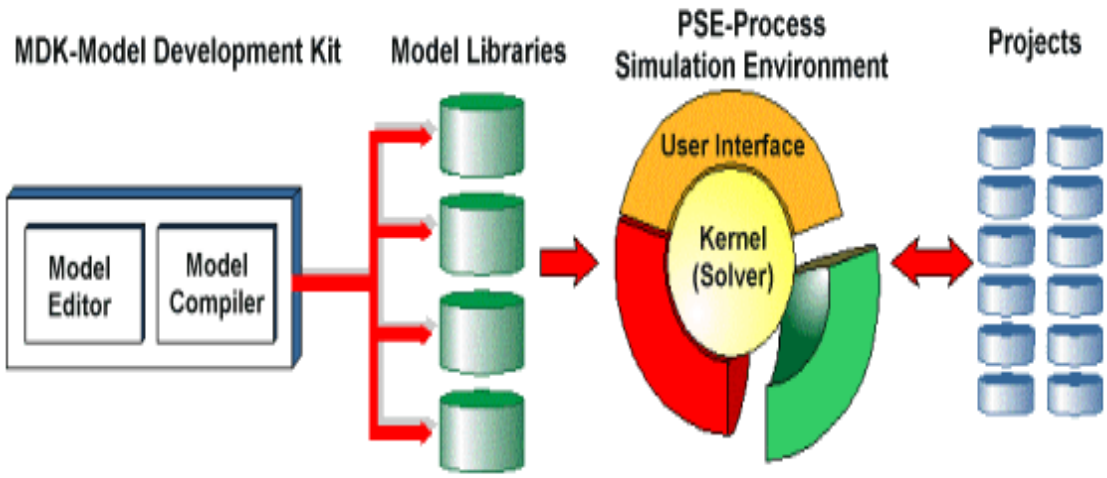

Figure 5.1 IPSEpro's structure and modules interacts [145]

IPSEpro uses some expressions, definitions, typographic conventions in the software construction that can be summarised as:

-process scheme, flow sheet: is the graphical representation of the IPSEpro project in the PSE window.

-model, process model, component: are defined as the mathematical representations of a process scheme or a component within the process.

-project: a collection of several process model files containing all available information about the process model.

-icon, unit icon: an expression of the graphical representation of a component or equipment in an IPSEpro library.

IPSE pro also defines three types of models;

-Units: The nodes in the network frame represent actual pieces of equipment such as heat exchangers or pumps. Units reference connections and globals, whereas they cannot reference other units.

-Connections: A connection represents the information about the substance or fluid that is transferred between the units such as streams.

-Globals: Globals representing information that is shared by an undefined number of other objects, such as chemical composition. Connections and units can reference globals, but globals cannot reference any other objects. However, as shown in Figure 5.2, IPSEpro restricts how objects of different components can reference each other to a hierarchical structure.

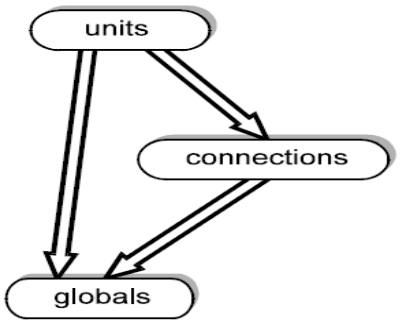

Figure 5.2 Hierarchical structures of IPSEpro models[145]

In this study, the IPSEpro-MDK, PSE and PSElink modules, as well as the App_Lib library were used to build, simulate and evaluate the SHS and its components thermo-economically. Therefore, in the following sections, a general description of the main modules principles will be presented.

5.3 Model development kit MDK principles

MDK is IPSEpro's model development kit, which is used for developing new component models or modifying existing ones in a library. It is used as model editor, complier and a source of the model description language (MDL) in order to build the

model libraries according to the user requirement and the mathematical equations representing the physical behaviour of any component. MDK's model compiler translates the model descriptions into a binary format including all the necessary information to be used in the PSE solving process. Unlike PSE, MDK requires practice and qualified persons to operate it [138,145].

5.3.1 Component model structure

In the previous sections, it was explained that IPSEpro process is structured and represented by a network of discrete components. However, the elements that are described by the component model can be classified as follows:

-Items : defined as the basic elements used for editing the mathematical equations represents the component model including the data provided by the user such as; variables, parameters, curves, tables and switches, as well as built–in and external functions.

-**Equations:** describes the actual behaviour of a model. IPSEpro uses the normal form of traditional equations and notation starting with a label to identify an equation that can contain conditional statements and sub-equations.

-**Tests:** are conditions for invalid calculated results; a warning is issued if the conditions are not satisfied.

-**References:** define the interaction with other models. These are defined in terms of its name and type of object referenced.

5.3.2 Model description language MDL

Unlike the traditional languages like FORTRAN or Pascal, the MDL language depends on a straightforward block of written equations with no sequence relevance in the process. The basic elements used to construct the equations in the MDK include the following expressions[145]: tokens, comments, arithmetic operators (-,+,/,*),relational operators (<,>,==,>=,<=), logical-operators (||,&&),equality-operator(+), negation-operator(!), reference operator, mathematical functions(abs(x), sin(x)), identifiers.

5.3.3 Implementing a model library using MDK

The content of the MDK model library is displayed in a window as a tree, with a sub-tree, marked by (+) for the expanded ones, for each of the model class types; including connections, globals and units, as presented in Figure 5.3. All the information and description of the library is stored in the MDK file. In addition, MDK creates several

files in the same directory that all share the same file name. Nevertheless, to develop any MDK library the library contents; including connections, globals and units have to be edited with the necessary information. Depending on the model type, MDK opens a window including several panes to allow the user to edit specific information according to each model, as presented in Figures 5.4, 5.5, 5.6. These panes can be classified as:

-Item panes: These are displayed in all models' windows in order to switch between the available models of model class and to have access to editing the available items in the model such as the parameters and variables.

-Equation pane: These are also displayed in all models' windows to edit the mathematical equations for each model (equations, tests,…etc.).

-Data cross pane: Displayed only with the connection model's windows that are used to select the type and appearance place with reference to the properties of the connections such as enthalpy and entropy.

-Icon pan: Displayed only with the unit model in order to draw and represent the unit and create its connectors graphically using the icon editor.

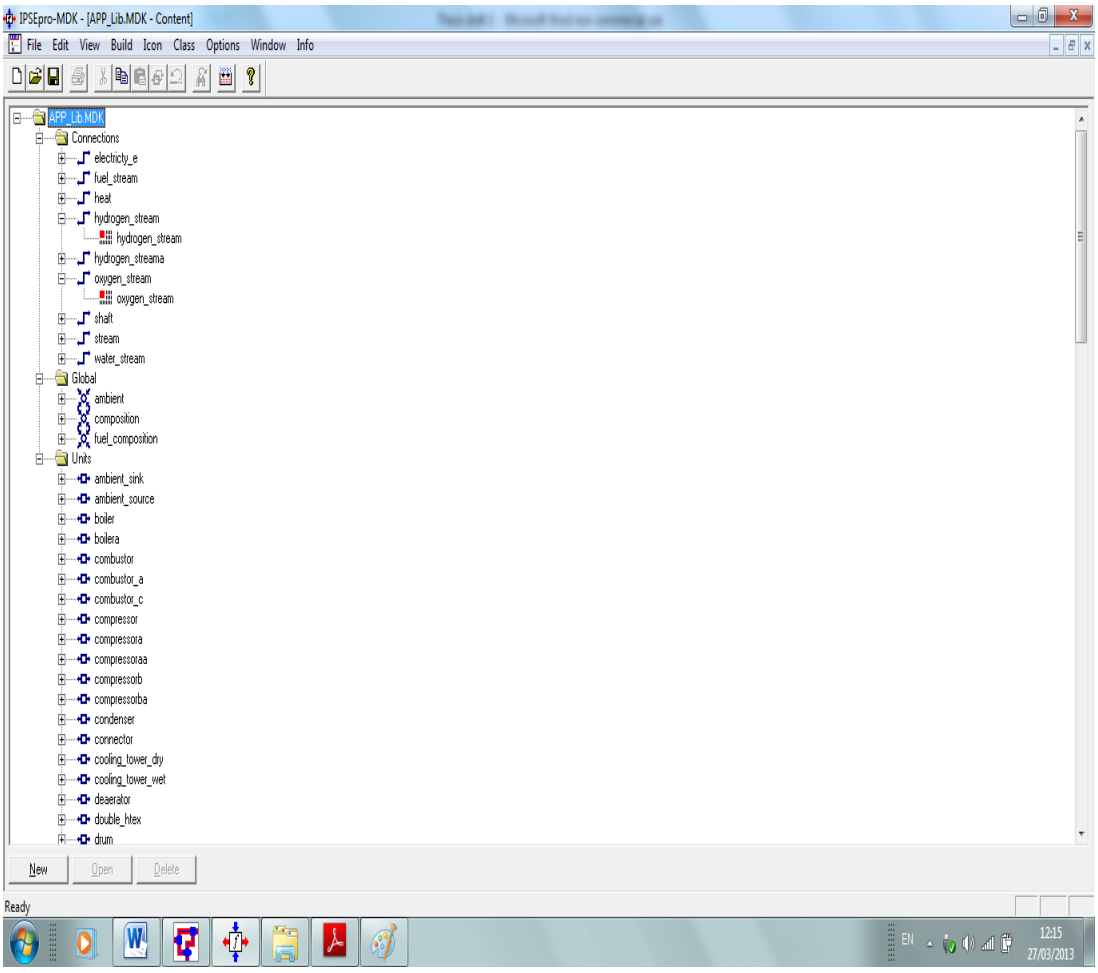

Figure 5.3 Print screens for window's content of MDK-Library

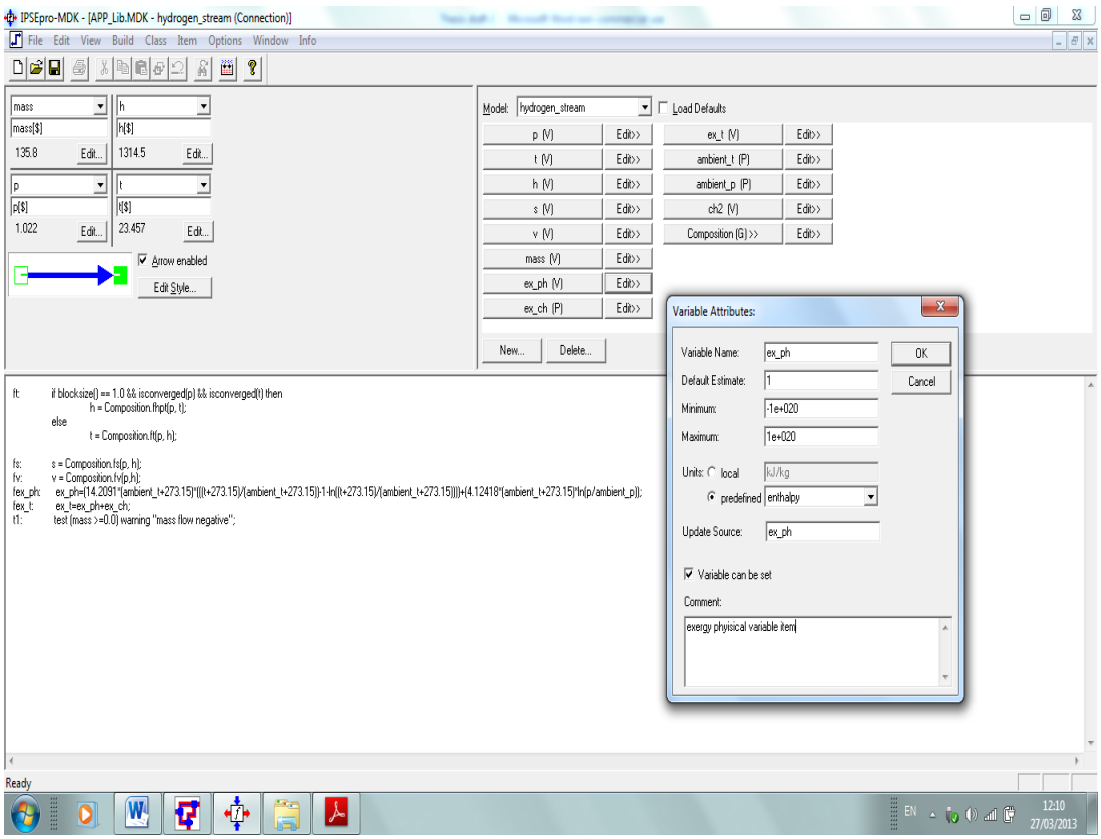

Figure 5.4 Window for editing hydrogen stream connection and a variable

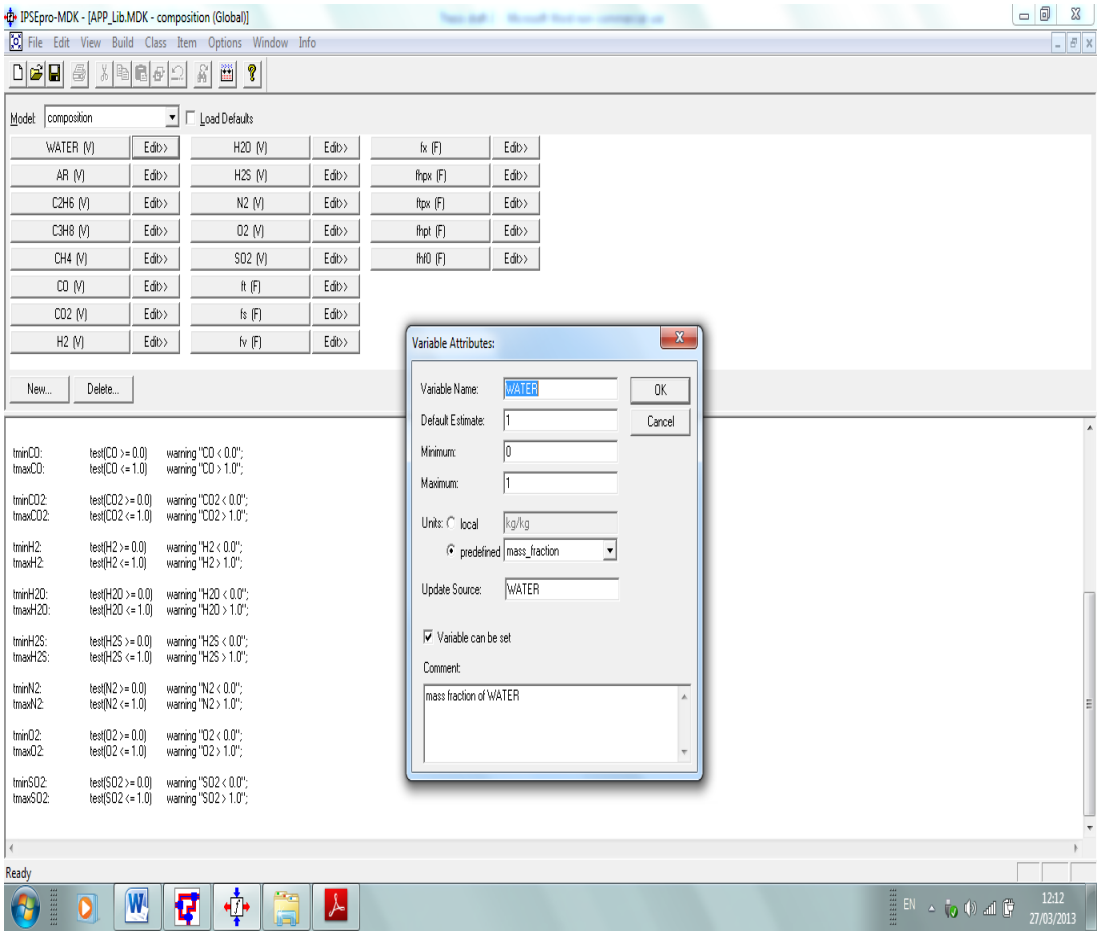

Figure 5.5 Window for editing globals and a variable

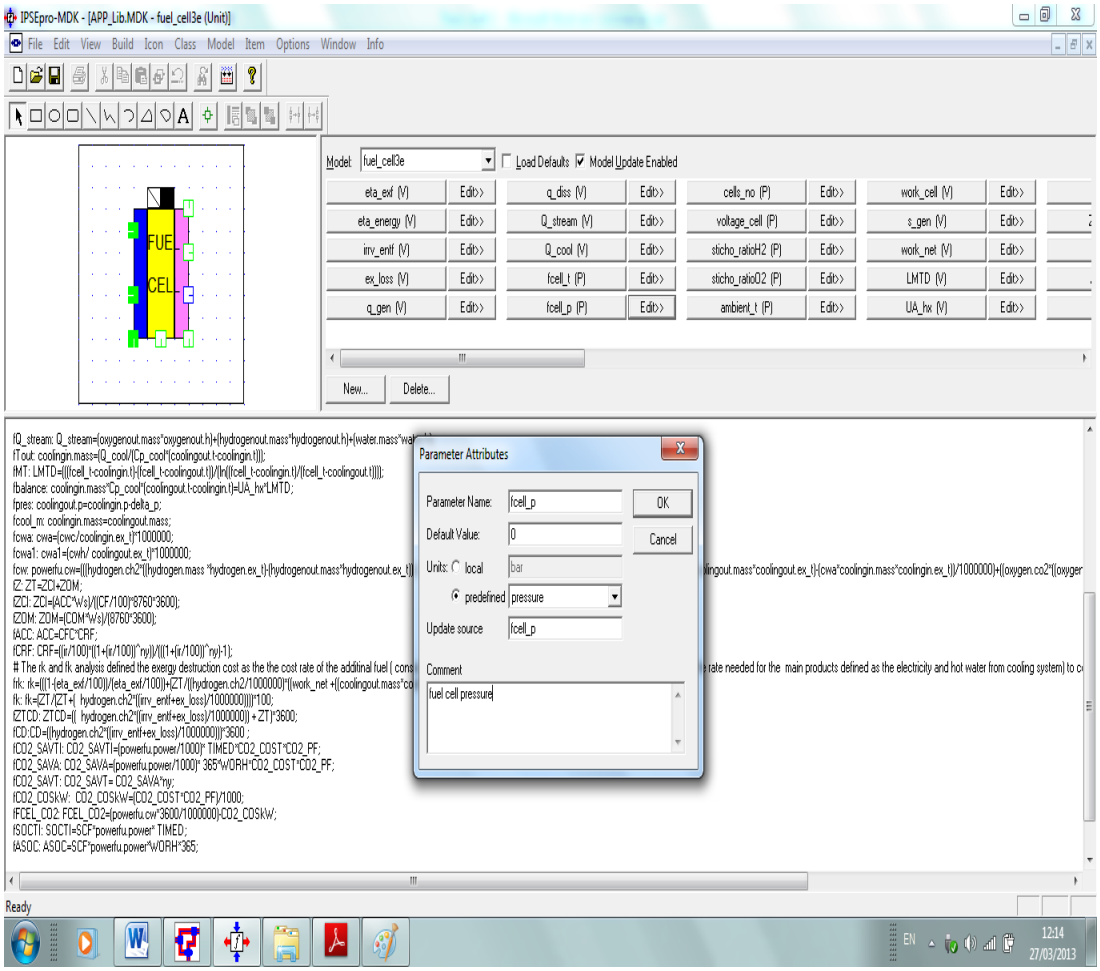

Figure 5.6 Window for editing fuel cell unit and a parameter

5.4 Processes simulation environment PSE principles

The process simulation environment module in IPSEpro provides a user-friendly interface flow sheet editor which can be used to build a process model. The PSE opens a project window enabling the user to choose the proper unit icon from the library's menu and dragging the theme into the window in order to form the process. The process can be several models or one model, representing equipment with its details such a turbine included its valves or pipes. The models were connected together by the suitable connection and the proper data and necessary information are inserted interactively and directly to the model. PSE running an equation oriented approach based on an initial iteration values and numerical analysis method. The variables and equations are grouped and solved simultaneously using numerical methods of analysis. In the analysis PSE firstly, issued a warning and running a protocol for any existed calculation errors and the displayed cross data is coloured red or blue according to the type of error.

5.4.1 PSE window screen details

The main elements of the PSE windows presented in Figure 5.6 can be described as follows:

-Work space: This is similar to many other MS-windows programs used to edit the models. However, it could be fill with one or more project windows and process.

-Project windows: This is used to provide an interface for editing the project and displaying its contents.

-Icon bar: This shows all the available components in the library needed to build the process.

-Menu bar: Menu bar offering the commands which are used for handling and editing the projects.

-Function bar: Allows fast access to the most frequently used commands.

-Object bar: This displays the name of the object currently being used.

-Data frame bar: Used to implement and format data frames.

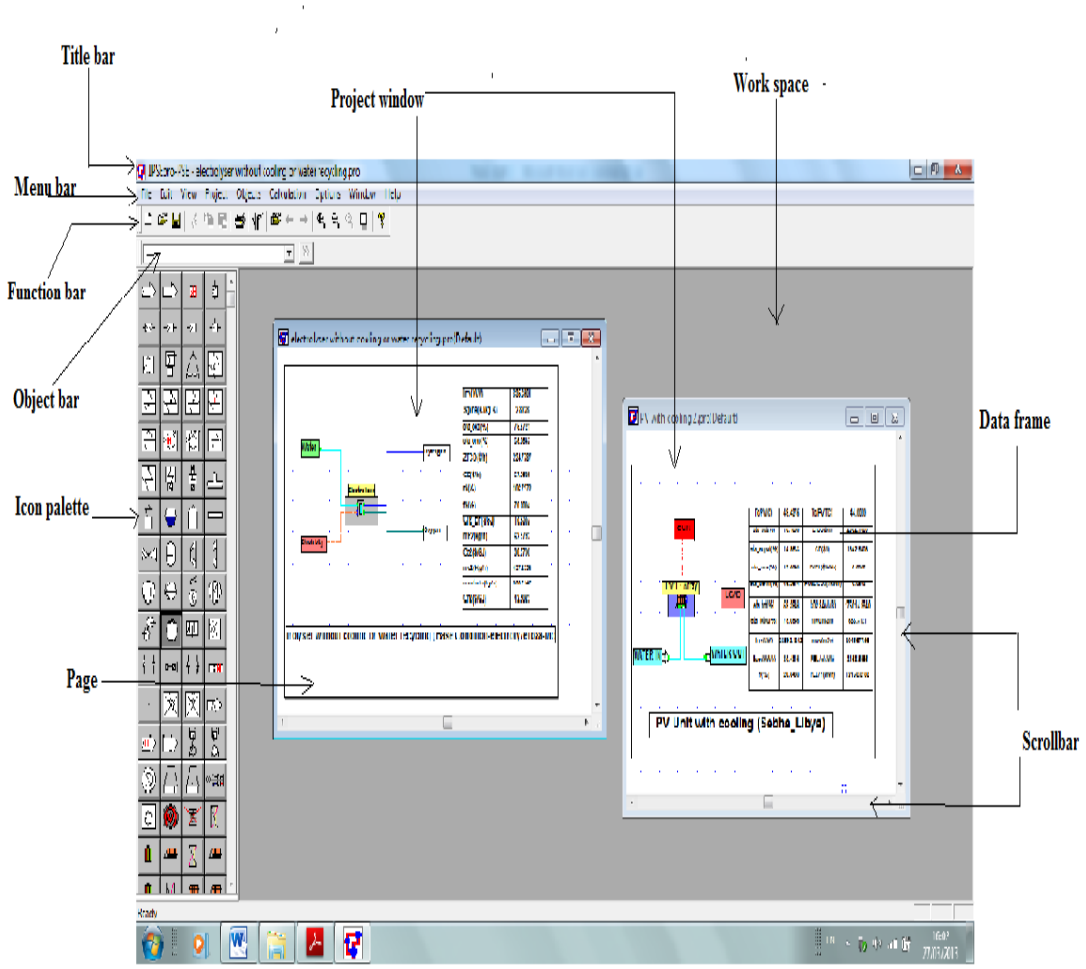

Figure 5.7 PSE window print screen for two opened projects

CHAPTER SIX

Chapter Six
Methodology

6.1 Introduction

The road towards SHS economy and competitiveness increases the necessity to develop more practical, simple and friendly interface software tools in order to investigate, evaluate and reach an optimum level of design and operation of these systems. The system feasibility can be improved by increasing its efficiency or by reducing its component cost whereas the most important question is how to do both of them at the same time and which one of these processes is more feasible. Furthermore, system efficiency can also be improved by reducing exergy losses, which require knowledge of its location, causes and costs as well as the necessary improvement cost to reduce them in each component of the system. This approach emphasises the importance of the combination of the thermodynamic (energy and exergy) and economic analysis for the system and its components, which is called thermo-economic analysis. This methodology has been widely used in the last decade in order to evaluate renewable energy systems and help them become more competitive [146]. Thermo-economic analysis is the main methodology used in this study to develop a software model for SHS analysis and for efficiency enhancement with proper cost using the energy software package IPSEpro, as illustrated in chapter five. The cost of environment impact and the cost of natural resources consumed for the production of the same power produced from the SHS and its components have been considered in the model. In this chapter, the main fundamentals, definitions and relations governing the energy, exergy and thermo-economic concepts used to study and develop an IPSEpro models for the SHS and its components are illustrated. However, details of the IPSEpro MDK equations and configurations of these models are presented in the next chapter and appendixes.

6.2 Fundamentals of energy and exergy analysis

The energy crisis in 1970 encouraged the search for more energy efficient and sustainable development systems. This led to a new ways and technologies to develop more active and improved thermodynamically procedures for the power system [147]. Energy analysis is based on first law of thermodynamics, law of conservation energy (eq. 1) and deals only with the quantity of mass, heat transfer and work or power flow into and out of the system. This has been the traditional method for many years. Energy

analysis doses not distinguish the quality of energy e. g. 1W of heat equals 1W of work or electricity, whereas a unit of electricity unit has a higher quality and economic value than a heat unit. As an example, a compressed air process maintains its energy (enthalpy) to equal zero, whereas its useful energy or ability to do work (exergy) is greater than zero [6]. Many researchers now suggest that the exergy analysis method, in place or in addition to energy analysis, needs to be used to evaluate, design and improvement of energy systems. In addition, it is a useful tool aid decision making regarding allocation resources [6]. Exergy is a measure of the maximum capacity of a system, substance or stream to perform work when it is brought from a specified state (pressure, temperature, elevation, velocity and chemical potential) to be in equilibrium to its surroundings at reference environment or dead state. A system in a reference environment or dead state has zero exergy, which indicates that it has no ability to do useful work at this point. Unlike energy, exergy can be partially or totally destroyed or consumed, as stated by the second law of thermodynamics (eq. 2). The last term of the left side of this equation is called exergy destruction or irreversibility ($\mathbf{I}$), which is proportional to the entropy generation in the system. Increasing the exergy destruction and losses for a system or plants which use fossil and toxic fuels means reducing its efficiency and increasing the pollutant emissions [6]. Thus, in exergy analysis the system is optimized so that it can reduce its exergy losses and destruction, or in other words to minimize its entropy generation (EGM). The main reasons which make exergy analysis, rather than energy analysis, a suitable tool for energy system analysis can be summarised in the following key points [147, 6];

1- It is an effective method for using the conservation of mass and energy together with second law of thermodynamics for the design and the analysis of energy systems.

2- With exergy analysis it is possible to compare, on a common basis, different interactions (inputs, outputs, work, heat, losses) taking in consideration the variation and affection of many other operation and design parameters in the system boundary.

3-It is suitable method to pinpoint the location, types, and amount of exergy destruction and losses in the system leading to draw a map of it for more efficient energy resources use.

4- Exergy analysis enables designing cost effective and environmentally benign systems Figure 6.1.

The first and second law of thermodynamics in a steady state can be expressed respectively as:

$$\sum_{in} en_{in}\ \dot{m}_{in} - \sum_{out} en_{out}\ \dot{m}_{out} + \sum \dot{Q}_K - \dot{W} = 0 \quad (1)$$

$$\sum_{in} ex_{in}\ \dot{m}_{in} - \sum_{out} ex_{out}\ \dot{m}_{out} + \sum ex^{\dot{Q}} - ex^{\dot{W}} - I = 0 \quad (2)$$

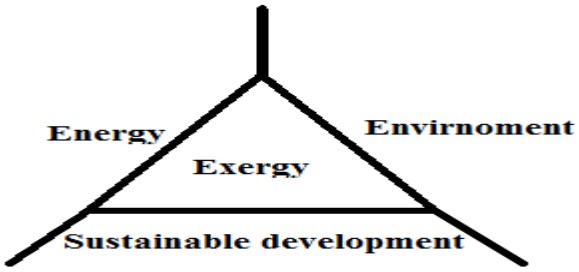

Figure 6.1 The interdisciplinary triangle of exergy [6]

6.2.1 Exergy mathematical model

There are several types of exergy such as physical, kinetic, chemical, potential, nuclear, electrical….etc. In this section the fundamentals of the physical ($e_{x,phy}$), chemical ($e_{x,ch}$), kinetic ($e_{x,kn}$) and potential ($e_{x,pt}$) exergies are described. The total exergy and total specific exergy on mass basses can be expressed as:

$$\dot{E}_x = \dot{E}_{x,phy} + \dot{E}_{x,ch} + \dot{E}_{x,kn} + \dot{E}_{x,pt} \quad (3)$$

$$ex = ex_{phy} + ex_{ch} + ex_{kn} + ex_{pt} \quad (4)$$

The second law of thermodynamic (eq. 2) states that the exergy rate transferred into the system must exceed that which is transferred out from it. The difference is the total exergy destruction (I) caused by irreversibility and losses. The general exergy balances equations at steady state can be rewritten in a general way for any system as in [146, 149]:

$$\dot{E}_{x,in} = \dot{E}_{x,out} + \dot{E}_{x,D} + \dot{E}_{x,loss} \quad (5)$$

$$I = \dot{E}_{x,D} + \dot{E}_{x,loss} = T_o S_{gen} \quad (6)$$

$$\dot{E}_{x,in} = \sum_{in} \dot{m}_{in}\, ex_{in} + \dot{W}_{in} + \sum_{in} \dot{Q}_{in} \left(1 - \frac{T_{amb}}{T_{in}}\right) \quad (7)$$

$$\dot{E}_{x,out} = \sum_{out} \dot{m}_{out}\, ex_{out} + \dot{W}_{out} + \sum_{out} \dot{Q}_{out} \left(1 - \frac{T_{amb}}{T_o}\right) \quad (8)$$

Where, $\dot{E}_{x,in}$ denotes the exergy entering the system in the form of work, heat or incoming streams; $\dot{E}_{x,out}$ denotes the exergy leaving the system in the form of work, heat or outgoing streams with a further use; $\dot{E}_{x,D}$ is associated with the destruction of exergy due to irreversibility and exergy loss $\dot{E}_{x,loss}$ represents the exergy associated

with streams through to surroundings without further use. The exergy efficiency for any system can be expressed as:

$$\eta_{ex} = \frac{\dot{E}_{x,out}}{\dot{E}_{x,in}} = 1 - \frac{\dot{E}_{x,D} + \dot{E}_{x,loss}}{\dot{E}_{x,in}} \quad (9)$$

6.2.2 Kinetic and potential exergies

The kinetic and potential exergies which are mainly based on the velocity V and the elevation Z of the system concerned are in principle fully convertible to work as the system is brought to rest relative to environment ($ex_{kn} = ex_{pt} = 0$). However, the effect of these parameters on SHS is not significant and these types of exergies are neglected in this research study. Furthermore, these exergy terms can be calculated by using the following formulas:

$$ex_{kn} = \frac{1}{2}V^2 \quad (10)$$

$$ex_{pt} = g\,Z \quad (11)$$

6.2.3 Physical exergy

The physical exergy can be defined as the maximum amount of work which can be achieved when a stream, substance or a system is brought to a state of equilibrium (P_o, T_o) from an initial state at (P, T), by being involved only in thermal interaction with its environment. It is calculated using the general following formula [149]:

$$ex_{phy} = (h - h_o) + T_o(S - S_o) \quad (12)$$

o = reference environment (restricted)

As special case, the physical exergy for an ideal gas with a constant specific heat ratio (k), can be calculated as:

$$ex_{phy} = Cp\,T_o\left[\frac{T}{T_o} - 1 - ln\frac{T}{T_o}\right] + Cp\,T_o \quad ln\left(\frac{P}{P_o}\right)^{\frac{K-1}{K}} \quad (13)$$

6.2.4 Chemical exergy

The chemical exergy component is the exergy amount gained or lost when the process involving heat transfer and exchange of chemical potential and composition of a substance, a stream or a system when brought to a reference state (unrestricted) from its initial state. It can be expressed in a molar basis as [149]:

$$ex_{ch} = \sum_j X_j \left(\mu_{j,o} - \mu_{j,oo}\right) \quad (14)$$

Where:

- Xj = is the mole fraction of species j in the flow.
- $\mu_{j,o}$ = is the chemical potential of species j in the flow at (P_o, T_o).
- $\mu_{j,oo}$ = is the chemical potential of species j in the flow at (P, T).

The chemical exergy component for streams will be neglected in a general exergy balance analysis, if there is no change of the chemical composition or no change of substance when it is crossing the control volume considered in the analysis. However, it may become important to consider the value of the chemical exergy for such streams if it is used to enter or leaving any other unit in the control volume considered in the system [146]. For simplicity, standard chemical exergy values are calculated based on a standard reference substance commonly considered in exergy system analysis. The values for the standard chemical exergy for hydrogen, oxygen and water used for studying SHS in this research have been taken from pre tabulated data Model II in reference [149].

6.3 Fundamentals of thermo-economic analysis

Exergy analysis and optimization processes provide answers to engineering questions related to the quantity, location, reasons for and the values of the thermodynamic inefficiencies in the system. It is also indicated their proper structure, arrangement and geometry with regard to the optimum efficiency of the system components [149]. After this process, a thermo-economic analysis that combined the concepts of exergy method and economic analysis is used. Thermo-economic analysis provides a measure of the cost of inefficiencies in the system, and/or the costs of individual process streams, including intermediate and final products [116]. Moreover, the optimization process gives a trade off balance between system efficiency improvement and the necessary investments and exergy costs in order to create a cost-optimal structure and the cost-optimal values of the thermodynamic efficiencies in each component and minimum product cost. The thermo-economic analysis method is nowadays a powerful tool that has been successfully applied to evaluate and optimize power plants, cogeneration plants and renewable systems. It helps in investment decisions, and in comparing alternative techniques and operating conditions, in a cost effective way for improvement of these plants [146,149,150]. Various names have been given to the thermo-economic methods procedures proposed in the past, which include the following [149, 151]:

-Exergy Economics Approach (EEA)

-First Exergoeconomic Approach (FEA)

-Thermo-economic Functional Analysis (TFA)

-Exergetic Cost Theory (ECT)

-Engineering Functional Analysis (EFA)

-Last-In-First-Out Approach (LIFOA)

-Structural Analysis Approach (SAA)

-SPECQ Method (SPECOM)

The main differences between these approaches refer to the definitions of exergetic efficiencies, definitions of products and fuels, the development of auxiliary equations and productive structures.

6.3.1 History of thermo-economics

The first person to discuss the principles of combining exergy and the stream in a system was Keenan in 1932. He revealed that the value of the stream and the electricity rests in its availability rather than in their energy. In 1950, Tribuls and Eurns applied the idea of exergy costing to a desalination process and introduced the term "thermo-economics". However, since the 1980s, several studies, papers and theoretical approaches to this field had been published, whereas the most contribution to achieve greater standardization and formulism was carried out in the 1990s and later [151]. In 1985 Kotas [146] published one of the main reference books in thermo-economic field including some of the collecting works and data in this area. Bejan, Tsatsoronis and Moran introduced the use of the second law of thermodynamics and thermo-economic variables and evaluation method for thermal system design and operation in their book published in 1996. This method and expressions was used in this study as explained in the following sections [149].

6.3.2 Exergy costing and thermo-economic model

The cost of each stream entering or exiting a system in terms of its exergy rate is called exergy costing. A general balance thermo-economic equation for a k_{th} component in an energy system or unit receiving heat transfer and generating power, can be expressed by [149]:

$$\sum_{out}(C_{out}\,\dot{E}_{x,out})_k + C_{w,k}\dot{W}_k = C_{q,k}\dot{E}_{q,k} + \sum_{in}(C_{in}\,\dot{E}_{x,in})_k + \dot{Z}_k \qquad (15)$$

As a basis of fuel used to generate products in any system, equation (15) can be rewritten as:

$$\dot{C}_{P,tot} = \dot{C}_{F,tot} + \dot{Z} \quad (16)$$

Where:

-C_e, C_i, C_w and Cq are denote the exergy costs related to each exergy stream rate leaving, entering, generating power and heat transfer in the system or a k_{th} component considered respectively in ($/GJ).

-$\dot{Z}$ *or* ZT is the annualized investment cost in ($/unit time).

-$\dot{C}_{P,tot} = C_{P,tot}\dot{E}_{P,tot}$ is the total cost rate ($/unit time) for any products in the system, although the product for any component is defined according to its purpose and operation procedure.

-$\dot{C}_{F,tot} = C_{F,tot}\dot{E}_{F,tot}$ is the total fuel cost rate ($/unit time), whereas the fuel represents the resources or streams expended in generating the products.

Equation (15) can be used to determine the cost of the power (C_w), if the value of all other parameters in the equations is known. In the case of more than one product existing in the system, an auxiliary equation is required to determine the unit costs of the different products. This equation is depends on the number of output products; in general, it is necessary to formulate (N_P-1) auxiliary equations to solve any system thermo-economic balance equations, which have (N_p) number of output products. There are several methods which can be used to determine the auxiliary equations for a system according to its functions and operations definition. As an example, the following procedures can be applied to a turbine producing both power and exhaust gas [149, 152]:

- The equality method

The generation of the two products has the same priority and the unit cost of the high temperature exhaust gas is charged to the two products, in proportion to their exergies.

-The extraction method

Considering only the shaft power unit cost as a main product, the exergetic unit cost of the leaving exhaust gas is charged the same as the one entering the turbine.

The by –product method

The unit exergetic cost of the output power is calculated by considering the value of the exhaust gas leaving the unit as a known value, which is valued as if it was produced from a diesel engine in the same operation conditions.

6.3.3 Thermo-economic optimization and evaluation factors and principles

The exergy costing and thermo-economics principal suggests as proper tool for thermal system design and evaluation. This method is identifying technical options that may improve the cost effectiveness of the system. Furthermore, this technique could be used for evaluating and optimizing the system for the following purposes [146, 149]:

-Pinpointing the exergy destruction within the entire system and/or the system components.

-Creating a trade-off between the exergy destruction (exergy efficiency) and investment cost of each component in the system.

-Understand the cost formation process and the flow of costs in the system.

-Determine the costs of each product generated by the system.

-Optimize the entire system or a specific variables in a single unit.

Several variables and factors are used in completing thermo-economic evaluation and optimization process for any energy system and its components. The definitions and concepts of the key factors used for this process will be illustrated in the following sections.

- Cost rate of exergy destruction

This is a measure of the exergy destruction cost in a component or a system. It can be calculated approximately in terms of the fuel unit cost ($C_{F,k}$) as the additional fuel supplied to the unit to cover the rate of exergy destruction considering the product exergy rate ($\dot{E}_{P,k}$) is fixed as:

$$\dot{C}_{D,k} = C_{F,k}\dot{E}_{x,D} \quad (17)$$

Alternately it could be considered as the monetary value of the product losses as exergy destruction taken the value of the product cost rate ($C_{P,k}$) as basis and the fuel exergy is fixed ($\dot{E}_{F,k}$) as:

$$\dot{C}_{D,k} = C_{P,k}\dot{E}_{x,D} \quad (18)$$

- Costing of exergy loss streams

The cost balance equation for any system including a rejection of exergy streams ($\dot{C}_{L,k}$) to its surroundings can be written for a k_{th} component as:

$$\dot{C}_{P,k} = \dot{C}_{F,k} - \dot{C}_{L,k} + \dot{Z}_k \quad (19)$$

In general, very few components have exergy losses that, for costing purposes, need to be distinguished from exergy destruction. The loss in exergy cost is charged zero in a thermo-economic optimization or evaluation process when the losses streams are finally discharged into the environment without further use. However, if the thermo-economic evaluation or optimization is for a single unit including a losses stream it could be further used in the system or the considered control volume, therefore its exergy cost should be considered. Its cost could be calculated based on the exergy cost of the fuel or alternately the product as for the cost of the exergy destruction cost above, using the following expression respectively:

$$\dot{C}_{L,k} = C_{F,k}\dot{E}_{L,k} \quad (20)$$

$$\dot{C}_{L,k} = C_{P,k}\dot{E}_{L,k} \quad (21)$$

- Relative cost difference

The relative cost difference (r_k) for the k_{th} component is defined by:

$$r_k = \frac{C_{P,k} - C_{F,k}}{C_{F,k}} = \frac{1-\eta_{ex}}{\eta_{ex}} + \frac{\dot{Z}_k}{C_{F,k}\dot{E}_{P,k}} \quad (22)$$

This variable expresses the relative increase in the average cost per exergy unit between fuel and product of the component. If the cost of the fuel in this unit changes extremely from one iteration to the next, the designers will be concerned to minimize the relative cost difference of a component instead of minimizing the cost per exergy unit of the product.

- Exergoeconomic factor

The exergoeconomic factor (f_k) can be defined as the contribution of non exergy-related cost ($\dot{C}_{D,k} + \dot{C}_{L,k}$) to the total cost increase and calculated for a k_{th} component by:

$$f_k = \frac{\dot{Z}_k}{\dot{Z}_k + C_{F,k}\left(\dot{E}_{x,D} + \dot{E}_{L,k}\right)} \quad (23)$$

A low value of f_k indicated that there is room to spend more money on minimizing its level of exergy destruction, while a higher value of f_k means that the priority is to decrease its investment cost rather than to increase its efficiency.

- Exergy efficiency

The exergy efficiency for any system as in (eq. 9) can also be expressed in terms of the total production or outputs and the total fuels consumed or inputs streams to generate it:

$$\eta_{ex} = \frac{\dot{E}_{P,k}}{\dot{E}_{F,k}} = \frac{\dot{E}_{ex,out}}{\dot{E}_{ex,in}} = 1 - \frac{\dot{E}_{x,D}}{\dot{E}_{F,k}} \quad (24)$$

Where, the total exergy destruction ($\dot{E}_{x,D}$) included the losses is :

$$\dot{E}_{x,D} = \dot{E}_{F,k} - \dot{E}_{P,k} \quad (25)$$

- Exergy destruction ratio

The exergy destruction ratio represents the total exergy destruction of the component in the system to the total exergy of the fuel or stream resources to generate the products in the system and it can be described as:

$$Y_{D,K} = \frac{\dot{E}_{x,D}}{\dot{E}_{F,k}} \quad (26)$$

6.4 The levelization value and economic analysis

The total annual cost ($\dot{Z}_k$) of the components presented in the general thermo-economic balance equation (15) is calculated based on the total fixed (ZCI) and operation and maintenance cost (ZOM) of the unit. The calculations consider the time value of money concepts during the time life of each unit (levelized value) according to the effect of the discount rate or effective rate (i_{ef}). The discount rate includes the normal interest, escalation (change of value caused by factors such as resource depletion, increased demand, and technological improvement) and inflation rates during the unit life years. The capital and maintenance cost of the SHS are expected to be decline in the time due to the currently impressive improvement in this technology. This can lead to dismissing the effect of the inflation and escalation rate with regard to the unit cost, taking the internal rate of return or the normal banking interest rate (ir) for calculating the time

value of money expended for the unit cost during its lifetime. The PV units could be used in an open area within the fields or in the desert in a country such as in Libya without any extra cost. However, most of the SHS equipment can be operated in an open area or under a steel structure umbrella, so the cost of the construction, installations and engineering can be estimated and included in the unit cost in this study. The salvage value that represents the replacement cost of any unit in the system during the expected lifetime is neglected as the lifetime of all system units is adopted as 25 years according to its manufactures data sheet. The total annual cost ($\dot{Z}_{k,tot} or\ ZT$) is calculated usually in a cost per time units ($/s) by:

$$\dot{Z}_{k,tot} = ZT = ZCI + ZOM \tag{27}$$

$$ZCI = \frac{ACC * Ws}{CF * 8760 * 3600} \tag{28}$$

and the annual operation and maintenance cost ZOM is calculated in terms of the annual maintenance cost factor (COM) as a percentage of the capital unit cost depending on the nature of each unit as:

$$ZOM = \frac{COM * Ws}{8760 * 3600} \tag{29}$$

Where, Ws is the unit designed rated (produced or consumed) power or capacity and the capacity factor (CF) represents the unit yearly parentage of operation. The annual capital cost (ACC), is calculated in terms of the unit capital cost CFC and the capital recovery factor (CRF). The capital recovery factor is used to determine the equals' value of the present capital cost value of each unit in the system at the end of its lifetime (money transaction for (ny) years). ACC is calculated in ($/ kW yr) as:

$$ACC = CFC * CRF \tag{30}$$

and,

$$CRF = \frac{ir(1+ir)^{ny}}{(1+ir)^{ny} - 1} \tag{31}$$

6.5 Environmental impact and costs of resources consumed

The environmental damage can be represented by the avoidable cost of CO_2 emission reduction by the SHS plant, compared with a similar fossil fuel plant. This cost can be calculated in terms of estimated CO_2 damage cost to the environment (CO2-COST) per tons produced from traditional plants ($/ton) and the average amount of CO_2 emission per ton for each MW produced by a fossil fuel plant (CO2-PF) [153]. The cost of the

CO_2 damage has been estimated and considered as (24$/ton) [60], whereas the emissive CO_2 per each MW produced is estimated to be between (0.4 to 0.8 ton/MW) and this is depending on the technology and type of fuel used [2, 58, 154]. This value is the least when a natural gas is used and the highest when a coke or heavy fuel is used to produce the power or heat, however in the analysis an average value of (0.6 ton/MW) is suggested. The monetary saving from using the SHS instead of using traditional power plants form the environmental point of view can then be calculated. It could be calculated per unit time during the day (CO2-SAVTI), annually (CO2-SAVA), or during the plant total lifetime (CO2-SAVT) as well as its effect on the cost of the output electricity or product for each unit (ELEL-CO2) using the following relations respectively:

$$CO2 - SAVTI = W * TIMED * CO2 - COST * CO2 - PF \quad (32)$$

$$CO2 - SAVA = W * 365 * WORH * CO2 - COST * CO2 - PF \quad (33)$$

$$CO2 - SAVT = CO2 - SAVA * ny \quad (34)$$

$$ELEL - CO2 = C_w - (CO2 - COSkW) \quad (35)$$

Where:

TIMED is the considered time during the day.

W is the unit output power or product.

WORH is the working hours of the unit during the day.

ny unit lifetime

C_w is the unit output cost.

CO2-COSkW is the cost of the CO_2 damage in the unit output cost unit calculated as:

CO2-COSkW=CO2-COST*CO2-PF (36)

The resources consumed value represents the saving implemented by the cost of the fossil fuel has to be used to produce the same quantity of SHS output production. This saving can be calculated for each system unit by a specific time interval (SOCTI), annually (ASOC) and for the total lifetime of the unit (TSOC) by using the following equations:

$$SOCTI = SCF * W * TIMED \quad (37)$$

ASOC=SCF*W*WORH*365 (38)

TSOC=ASOC*ny (39)

Where;

SCF is the shared percentage unit cost of the total output production cost in relation to the cost of the fossil fuel used to produce this unit cost. This value is estimated as 0.05 $/kW [60] in this study as the average fuel cost to produce one kW of electricity in the

traditional power plants was estimated to be 40-70% of the total production unit cost [155]. This value is depending on the fossil fuel type, price and the used technology. In general, the total SHS unit output production cost could be estimated by subtracting from it the cost of the CO_2 damage reduction cost alone or in addition to the resource consumed saving cost.

6.6 Thermo-economic evaluation and optimizing technique

Thermodynamic analysis for energy systems is extracted firstly in order to pinpoint the energy efficiencies, exergy efficiencies and the exergy destruction for the system components as well as the entire system. To enable an optimum system design a parametric study, according to the mathematical model and system boundary, has to be implemented. The parametric study is carried out to investigate the effect of the main operating parameters along with changing the system; structure management, configurations, size, material composition and specification on the entire system and its units performance and production. The next step is to evaluate and optimize the entire system and its components thermo-economically using the factors introduced in this chapter, which can be sequenced for each k_{th} component as follows:

1- Energetic and exergetic efficiencies, η_{en} , η_{ex} .

2- Exergy destruction rate,$\dot{E}_{D,k}$.

3- Exergy destruction ratio, $Y_{D,K}$.

4- The total annual cost, $\dot{Z}_k$.

5- Cost rate of exergy destruction, $\dot{C}_{D,k}$.

6- The relative cost difference (r_k).

7- The exergoeconomic factor (f_k).

The following processes have to be conducted to evaluate and optimize the thermal systems thermo-economically [152]:

1- The system components have to be ranked according to its cost importance order from the highest to the lowest using the sum of $(\dot{Z}_k + \dot{C}_{D,k})$.

2- The components have the highest values for factor in step1, high relative cost difference r_k factor, low exergy efficiency or high exergy destruction ratio should be considered firstly for design changes and performance improvement.

3- The exergeconomic factor (f_k) gives an indication and trade-off for the most important cost source between investment cost and the exergy destruction cost. However, the highest f_k leads to pay more attention to reduce the investment cost first,

while the low value indicates that there is a room for more investments to improve the component exergy efficiency.

4- Any sub processes or streams with non-contribution to the unit cost investment reduction or fuel cost have to be eliminated.

6.7 Solar hydrogen system components mathematical models

In the following sections the assumptions and the basics that used to develop a mathematical model for the SHS components, (the photovoltaic, photovoltaic thermal, electric heater, fuel cell, heat exchanger, and hydrogen and oxygen storage tanks are analysed. The mass, energy, exergy and thermo-economic balance equations of each unit in addition to an electro-thermal model for some units are explained in detail. The mathematical models of SHS supplementary components such as, connections, mixers, compressors, pumps, and power models, developed using the existing IPSEpro energy are explained.

6.7.1 Photovoltaic model

The photovoltaic phenomena can be defined as the processes of transfer of the sun's heat energy (photon energy) directly to electric energy. This leads to the necessity of illustrating the electro thermal nature of the process in order to estimate its output and evaluate its performance. The voltage-current relationships of a PV cell can be represented by a one diode electric circuit as presented in Figure 6.2 [52] and it can be used to model a unit consists of a number of cells in series [53,156,157].

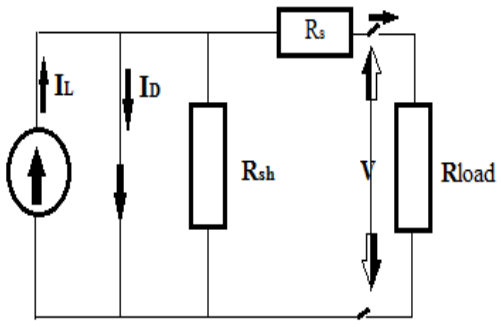

Figure 6.2 One diode electric equivalent circuit of PV solar cell

The one diode model characteristics current voltage equation is:

$$I = I_L - I_D - I_{sh} = I_L - I_o\left[e^{\left(\frac{U+I*R_s}{a}\right)} - 1\right] - \frac{U + I * R_s}{R_{sh}} \qquad (40)$$

Where:

I_L = the light generated current is proportional to solar irradiance, A.

I_o = the diode saturation current density, A.

R_s *and* R_{sh} = the series and shunt resistance respectively, Ω.

a = curve or slope fitting parameter.

V= operation voltage, V.

I = operation current, A.

However R_{sh} can be assumed to be too large compared to the series resistance R_s particularly for the crystalline solar cells, then equation (40) can be rewritten as:

$$I = I_L - I_o \left[e^{\left(\frac{U + I * R_s}{a}\right)} - 1 \right] \quad (41)$$

The (I-V) cell characteristics mainly depend on the weather conditions, particularly solar radiation, cell temperature and wind speed during the day. However to predict the power output of the unit at any time it is necessary to determine the corresponding rated voltage and current. In this research study, the PV unit is assumed to be working at its maximum allowable power, whereas an MPPT (maximum power tracking) convertor is used to maintain this goal during the day. The maximum allowable power can be produced by the unit can be defined in terms of its maximum power I_m and maximum voltage V_m as presented in Figure 6.3 and the following:

$$P_m = I_m * V_m \quad (42)$$

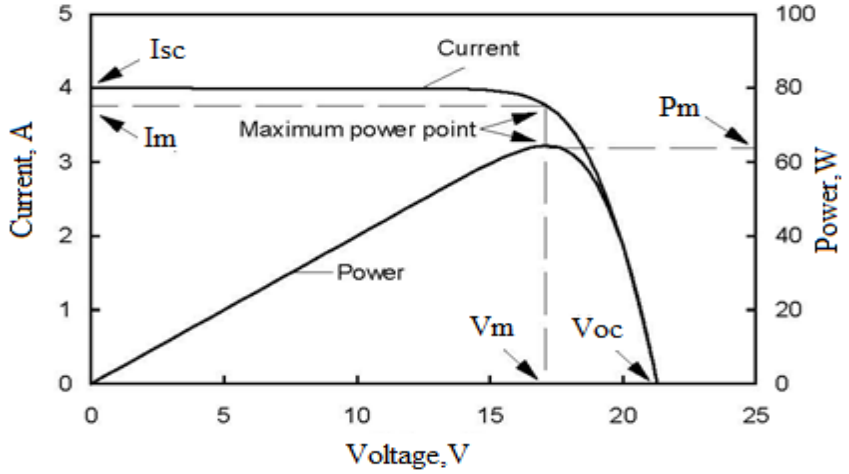

Figure 6.3 I-V and P-V characteristics curve for a PV unit

The effect of cell surface temperature T_c for a typical PV on the unit maximum power point, voltage and current at constant solar irradiance is illustrated in Figure 6.4. It is clear that as the surface temperature decreased the maximum power point is increased while short-circuit current I_{sh} (V=0) is slightly decreased and the open circuit voltage

V_{oc} (I=0) is significantly increased. However, the effect of the solar irradiance variation on the PV cell maximum power point at a constant surface temperature is presented in Figure 6.5. The figure shows that the maximum power point is increased as the solar irradiance increases, while the maximum voltage (Vm) is slightly increased. This figure also clearly illustrates that the maximum current (Im) decreases extremely as the solar irradiance decreases.

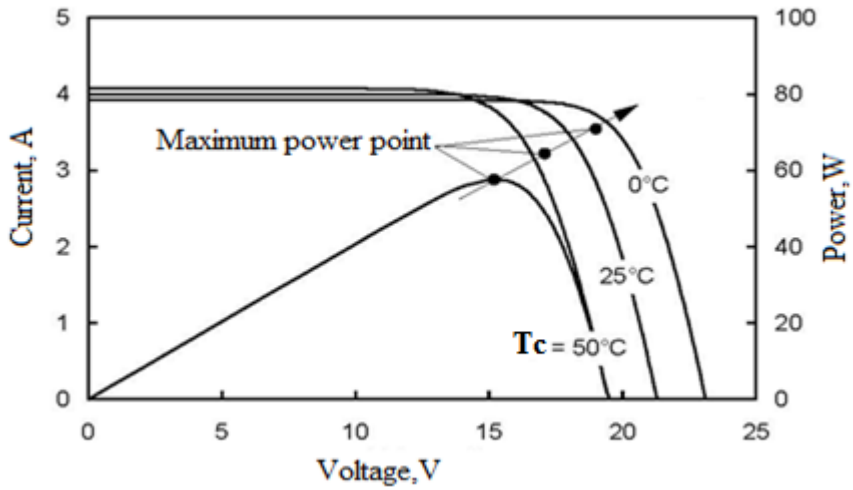

Figure 6.4 I-V Characteristics curve and the maximum power point line at different PV unit surface temperature and constant solar irradiance

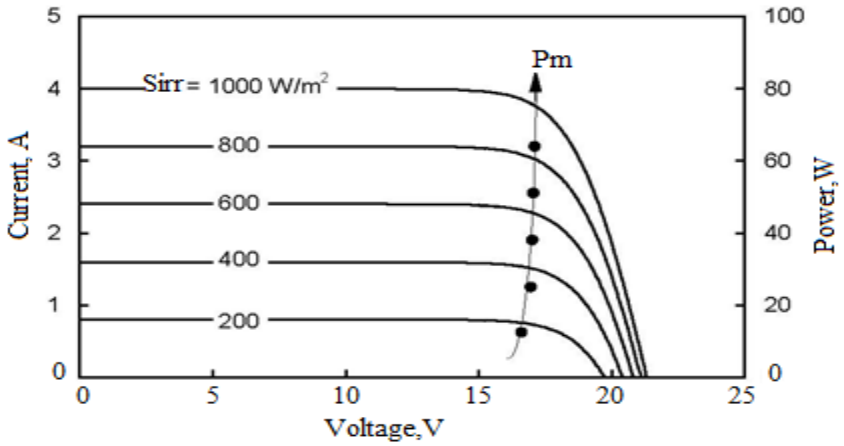

Figure 6.5 Variation of PV power (Pm) with solar irradiance (Sirr) at constant surface temperature

The manufacture of the PV modules normally provides information about the short circuit current ($I_{sc,}$), the open circuit voltage (V_{oc}) , the maximum voltage (Vm), the maximum current (Im), the maximum power (P_m) and the temperature coefficients of the short circuit and open voltage (μ_{Isc} , μ_{Voc}) , for a given set of reference conditions usually Standard Test Conditions (STC). These indoor test conditions is performed at a

solar global irradiance of 1000W/m^2 with a spectral distribution compatible to the AM 1.5 spectrum and a PV surface temperature T_c of 25 ºC. The provided (STC) parameters can be used to predict the crystalline silicon PV module outputs and performance at any time of the day using the following simple relations and algebraic method as illustrated and presented by many references [52, 53, 62, 69,70,156, 157,158]:

The PV power output can be expressed as:

$$P_{el} = IV \quad (43)$$

Moreover, the maximum output power is given by

$$P_m=(IV)_m=V_{oc}\ I_{sc}\ FF \quad (44)$$

The energy conversion efficiency at STC is given by

$$\eta_{sta}=(V_m\ I_m / P_{in})_{sta} = (V_{oc}\ I_{sc}\ FF\ / P_{in})_{sta} \quad (45)$$

Where the energy absorbed by the module surface is

$$P_{in}=Sirr\ Am \quad (46)$$

The absorbed energy can also be calculated in more details based on the type of the transparency and absorption factors for the glass and cover (αG) and the cells (αC) of the modules as well as the area factor of the cells to the module area (β) as:

$$P_{in}=[(\ \alpha G\ \alpha C\ \beta\ )+(1-\beta)\ (\ \alpha G\ \alpha C)]\ Sirr\ Am\ mn \quad (47)$$

$$\text{and } \beta=Ac(mn/\ Am) \quad (48)$$

The exergy output of the photovoltaic system can be calculated as [70,160] :

$$\dot{E}_{ex,out}= V_{oc}\ I_{sc} - [\ (V_{oc}\ I_{sc}\ - V_m\ I_m\ ) + Q_{loss}\ (1 - T_a/T_c\ )\ ] \quad (49)$$

The surface temperature T_c can be treated as an input measured value or it is estimated using one of the following known formulas:

$$T_c=T_b+(Sirr/Sirr\text{-}sta)\ \Delta T \quad (50)$$

Where;

T_b is the module backside temperature.

ΔT: is the temperature difference between the PV cells and the module back surface depends on the PV material, type and configurations. However, this value for crystalline cells is estimated as 3 ºC. The cell temperature can also be estimated using the $T_{C,NOCT}$ values usually provided by the manufacturing. $T_{C,NOCT}$ is a measure of the assumed homogeneous surface temperature of the cells at an ambient conditions (Sirr=800 W/m^2 , $T_{R,NOCT}$ = 20 ºC and 1 m/s wind speed). The $T_{C,NOCT}$ value is around 46 ºC for stand free modules whereas it is increased by 15 to 20 ºC for building integrated modules as a result of less or no ventilation on the module's back [75,157,160]. However, the following formula is used to calculate the cell temperature in this study;

$$T_c=T_a+(T_{C,NOCT}-T_{R,NOCT})(Sirr/0.8) \quad (51)$$

The heat loss (Q_{loss}) can be calculated as:

$$Q_{loss}= h_{ca} A_m (T_c - T_a) \quad (52)$$

The convective and radiation heat transfer coefficient (h_{ca}) can be adopted as a pre-defined constant input parameter or calculated using a build in empirical formula. Different formulas and correlations existed in the literature gives noticeably varying predictions for (h_{ca}) values. However, producing an accurate and universal formula is a continued research challenge task [64,161,162,163]. Consequently, users of famous energy simulations software such as EnergyPlus [164] and TRNSYS[82], given the options to insert their own model or pre calculated / measured values as well as using one of the offering built in formulas. For example, some models of TRANSYS used the built in liner form proposed by McAdams [165] and Duffie and Beckman [52] (eq, 53). The formula in (eq. 53) that has been widely used today for modelling solar panels was adopted to be used in this study for modelling PV/IPSEpro unit [64, 70, 161, 163]. The IPSEpro users also have the option to supply the (h_{ca}) values as constant parameters for some models:

$$h_{ca}=5.7+3.8(v) \quad (53)$$

The exergy input of the photovoltaic system (exergy of solar energy) can be calculated approximately as:

$$\dot{E}_{x,solar}= \dot{E}_{x,in} =Sirr\ A\ (\ 1– T_a/T_{sun}) \quad (54)$$

Thus, the exergy efficiency of the photovoltaic system can be defined as

$$\eta_{pv,ex}= \dot{E}_{ex,out} / \dot{E}_{x,in}= [V_m I_m- (1- T_a/T_c) [h_{ca} A(T_c-T_a)]]/ \dot{E}_{x,in} \quad (55)$$

The irreversibility of the system (exergy destruction) can be expressed as:

$$\dot{E}_{x,D}=I=(1-\eta_{pv,ex})\dot{E}_{x,in} \quad (56)$$

The total area of a photovoltaic system could be calculated as:

$$A_t=Cn\ mn\ A_c\ 1.54 \quad (57)$$

Where: (1.54 is the PV array space factor)

The PV system performance parameters are affected by the ambient conditions and can be calculated by using the following equations:

$$\eta_{act}=[\eta_{sta}(1-\mu(T_c-T_r)]+[Sirr-_{coeff} \log(Sirr)] \quad (58)$$

$$(P_{el,act})=\alpha\tau\ \eta_{act}\ Sirr\ mn\ (Am / \eta_{conv}\ ) \quad (59)$$

$$V_{oc\_act}=V_{oc\_sta}–[(\mu_{Voc}\ V_{oc\_sta}\ (T_c – T_r)] \quad (60)$$

$$I_{sc\_act}=I_{sc\_sta}\ (Sirr/Sirr_{sta})[1+\mu_{Isc}\ I_{sc\_sta}(T_c–T_r)] \quad (61)$$

$$FF_{act}=P_{el,act} / (V_{oc\_act}\ \ I_{sc\_act}\ ) \quad (62)$$

The module energy efficiency and the maximum electric efficiency are expressed respectively by:

$\eta_{en}=[V_{oc\_act}\, I_{sc\_act}+Q_{loss}]/Sirr\ Am$ (63)

$\eta_{el\text{-}max}=(V_{oc\_}act\ Isc_{\_act})/\ Sirr\ Am$ (64)

The entropy generation in any unit in the SHS can be calculated by:

$S_{gen}=I\ /T_o$ (65)

The thermo-economic, environmental and resource consumed costs equations (15-39) were used to calculate the PV parameters (ZT, COM, ZCI, CRF, ACO2-SAVTI, CO2-SAVA, CO2-COSkW, SOCPT, ASOC, TSOC, PVELT, fk, rk ZTCD,CD). Additionally, the PV electricity output unit cost C_w is calculated using equation (15) considering that the cost of the input energy from the sun is free and the only output is the electricity (P_{el}), as:

$C_w=ZT/P_{el}$ (66)

6.7.2 Photovoltaic thermal model (PV/T system)

The PV/T system suggested in this study works to cool the PV cells using water pumped through the back of the unit system that is designed to enhance the unit efficiency, lifetime and reduce the production cost. However, the output hot water can be utilized directly for domestic use or using low thermal utilization facilities such as organic Rankin cycle or absorption chillier. A simple thermo-economic model is developed to evaluate and analyse the system as well as to optimize its functional use for hot water and electricity production. The analysis considers a constant output water temperature and varying mass flow rate as it is recommended for the industrial sector and most applications. The constant output water mass flow rate with a varying output water temperature mode could also be considered as an option in the model. The steady state analysis assumed that the unit has a homogeneous cell surface temperature, neglecting pressure drop and fully developed water throughout. The analysis assumed also that the water output temperature ($T_{wt,out}$) is following the cell temperature (T_c)by 4 ^oC. However, the PV/T model equations and its parameters' values were adopted from the references [79,80,81,86,89,98,99] that almost similar to the PV model except for the following:

$T_{wt,out}\ = T_c - 4\ ^oC$ (67)

$$\dot{E}x_{out} = \left(\frac{P_{el}}{\eta_{conv}}\right) + \left[\left(\dot{m}_{wt}\ C_{p-wt}\ (T_{wt-out} - T_{wt-in})\right)\left(1 - \frac{T_a}{T_{wt-out}}\right)\right] \quad (68)$$

The thermal efficiency can be expressed as:

$$\eta_{th} = \frac{\dot{E}n_{th}}{S_{irr}\ Am\ mn} \tag{69}$$

The thermal energy $(\dot{E}n_{th})$ and the water mass flow rate $(\dot{m}_{wt})$ can be calculated using the unit energy balance equation as:

$$\dot{E}n_{th} = P_{in} - \left[\left(\frac{P_{el}}{\eta_{conv}}\right) + \dot{Q}_{loss}\right] \tag{70}$$

$$\dot{m}_{wt} = \frac{P_{in} - \left[\left(\frac{P_{el}}{\eta_{conv}}\right) + \dot{Q}_{loss}\right]}{C_{P-wt} * (T_{wt-out} - T_{wt-in})} \tag{71}$$

An expression for the total efficiency (η_{total}) and the total equivalent efficiency or the energy-saving efficiency $(\eta_{tot-equiv})$ calculated in terms of the efficiency of a traditional fuel power plants assumed as (η_{power} =0.4) is considered using the following equations [81]:

$$\eta_{total} = \eta_{th} + \eta_{el-act} \tag{72}$$

$$\eta_{tot-equiv} = \left(\frac{\eta_{el-act}}{\eta_{power}}\right) + \eta_{th} \tag{73}$$

The output electricity unit cost of the PV/T system (C_w) is calculated based on a specific (input or cold) water cost $(C_{wa1})\ or\ (C_{wc})$ and for hot water as $(C_{wa})\ or\ (C_{wh})$ in ($/GJ) as:

$$C_w = \frac{\left[ZT - [\dot{m}_{wt}((C_{wa})ex_{w-out} - (C_{wa1})ex_{w-in})]\right]}{P_{el}} \tag{74}$$

In addition to the above equations all the relations used in the different purposes PV and PV/T IPSEpro-MDK models included a detailed heat transfer balance equations for the unit layers are given in the Appendix D.

6.7.3 Electric heater model

The main purpose of the photovoltaic system is to produce electricity. However, using a photovoltaic thermal system may help to reduce the cell temperature leading to enhancing the lifetime and the performance of the system. In the meantime, hot water as a by-product is produced by the PV/T system. The output water temperature is depending on the operation and weather conditions. A trade–off analysis between the electricity and hot water production is necessary for the optimum performance and cost according to the main function of the unit and the weather condition. The output of hot water can be used directly for domestic and human use or it can be utilized for cooling or producing power using low thermal energy source devices such as absorption chillier

or an organic Rankin cycle. The low thermal source device requires a source with at least 70°C [166], so for the PV/T system it is necessary to increase the output temperature. For this purpose a simple electric heater energy model, as illustrated in Figure 6.6, needs to be developed to evaluate and trade-off analysis of the PV/T system. The electricity consumed by the electric heater (P_{el-he}) can be calculated based on the enthalpies and the mass flow rate of the hot water:

$$P_{el-he} = \frac{\left[(h_{wt,out} - h_{wt,in})\dot{m}_{wt}\right]}{\eta_{el-h}} \quad (75)$$

and the mass balance equation is:

$$\dot{m}_{wt,in} = \dot{m}_{wt,out} = m_{wt} \quad (76)$$

Where: η_{el-he} is the electric heater efficiency assumed as 98% [167].

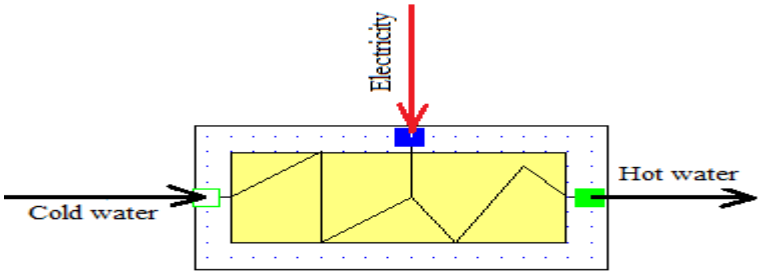

Figure 6.6 Electric water heater schematic

6.7.4 Fuel cell model

A fuel cell is an electrochemical energy converter that converts the chemical energy of a fuel and an oxidant to electrical current (DC). In the case of a $H_2 - O_2$ fuel cell, H_2 is the fuel, and O_2 is the oxidant and the only product is pure water and heat as illustrated in Figure 6.7. A simple basic model depends on the data usually provided by the manufacturers is used for the energy, exergy and thermo-economic analysis of the fuel cell based on the following assumptions [104,116].

-The fuel cell is operating at or near its rated capacity under specific steady state temperature, pressure and voltage.

-The flow of reactants is steady, incompressible, and laminar.

-The theoretical amount of hydrogen is calculated based on the power produced.

-All gases are ideal gases.

-Kinetic and potential exergy are neglected.

-Chemical exergy values are taken from literature as standard values.

-20% of the total heat generated by the fuel cell is lost via convection and radiation from the fuel cell [108, 116].

-The water mass flow rate for humidification the reactants are neglected, so it has a small exergy amount and it does not affect the analysis result [6].

- The water leaving the unit is at saturated liquid condition.

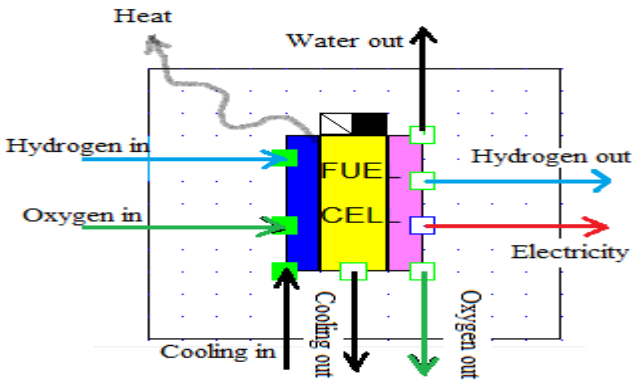

Figure 6.7 Schematic for PEM fuel cell with cooling

According to equations 1 and 2, the irreversibility (exergy destruction) of a fuel cell without cooling and recycling the output streams could be calculated as

$$I = (1-(T_a / Tc)\, \dot{Q}_{loss} - \dot{W}_{net} + [(\dot{m}_{H2}\, ex_{H2in}) + (\dot{m}o_2\, ex_{o2in})] - [(\dot{m}_{H2\_out}\, ex_{H2out}) + (\dot{m}o_{2\_out}\, ex_{o2out})] - [\dot{m}_{wt}\, ex_{wt}] \quad (77)$$

However, the energy, exergy and thermo-economic relations used to build the model can be represented by the following equations [110,112,113,114,116,168,169,170];

The exergy efficiency is calculated by:

$$\eta_{ex} = [1-I/[(\dot{m}_{H2}\, ex_{H2in}) + (\dot{m}o_2\, ex_{o2in})]] \quad (78)$$

and the heat generated within the cell defined as:

$$\dot{Q}_{gen} = (1.481-V_c)\, C_n \dot{W}_c / V_c \quad (79)$$

The heat losses from the unit can be calculated based on the unit geometry and the overall heat transfer coefficient and thermal resistance as an input parameters or it could be estimated for a unit with cooling as [108,114,116]:

$$\dot{Q}_{loss} = RHL\ \dot{Q}_{gen} \quad (80)$$

Where RHL is the heat losses factor estimated as 0.2 in this study.

$$\dot{W}_{net} = P_{el} - \dot{W}_{acc} \quad (81)$$

$$P_{el} = \dot{W}_c C_n \quad (82)$$

The total specific exergy of any stream in the unit is expressed as:

$$ex_t = ex_{ph} + ex_{ch} \quad (83)$$

The chemical exergy is taken from literature as a constant value at reference condition [149], and the physical exergy for H_2,O_2 are treated as ideal gases, with constant specific enthalpy, and is calculated respectively as:

$$ex_{ph\_H2} = 14.2091\ T_o\ [(T_{H2}/T_o) - 1 - \ln(T_{H2}/T_o)] + 4.12418\ T_o \ln(P_{H2}/P_o) \quad (84)$$

$$ex_{ph\_o2} = 0.9216\ T_o\ [(To_2/T_o) - 1 - \ln(To_2/T_o)] + 0.25983\ T_o \ln(Po_2/P_o) \quad (85)$$

and the water physical exergy is given by:

$$ex_{ph\_wt} = (h_{wt} - h_{wt\text{-}o}) - T_o\ (S_{wt} - S_{wt\text{-}o}) \quad (86)$$

The energy efficiency related to the high heating value of hydrogen is [118]:

$$\eta_{en} = \dot{W}_{net} / 141860\ \ \dot{m}_{H2\_in} \quad (87)$$

The hydrogen, oxygen and water mass flow rate for an individual unit is calculated based on its stoichiometric ratios (S_t) defined as the theoretical amount to the actual amount consumed, cell numbers (C_n) and the corresponding power and voltage values as:

$$\dot{m}_{H2\_in} = 1.05\ e^{-0.5}\ S_{t\_H2}\ (C_n\ \dot{W}_c / V_c) \quad (88)$$

$$\dot{m}_{H2\_out} = (S_{t\_H2} - 1)\ \ \dot{m}_{H2\_in} \quad (89)$$

$$\dot{m}_{o2\_in} = 8.29\ e^{-0.5}\ S_{t\_o2}\ (C_n\ \dot{W}_c / V_c) \quad (90)$$

$$\dot{m}_{o2\_out} = (S_{t\_o2} - 1)\ \dot{m}_{o2\_in} \quad (91)$$

$$\dot{m}_{wt} = 9.34\ e^{-0.5}\ (C_n\ \dot{W}_c / V_c) \quad (92)$$

The power output of a fuel cell integrated in a solar hydrogen system where the hydrogen amount is known and coming from an electrolyzer directly or from a tank can be calculated as

$$P_{el\text{-}FC} = \dot{m}_{H2\_in} V_c / 1.05\ \ e^{-0.5}\ \ S_{t\_H2} \quad (93)$$

The energy balance equation for a fuel cell unit at steady state with cooling and streams recycling can be written as:

$$\dot{Q}_{gen} = \dot{Q}_{loss} + \dot{Q}_{cool} + \dot{Q}_{strem} \quad (94)$$

where the cooling energy can be expressed as:

$$\dot{Q}_{cool} = \dot{m}_{cool}\ \ C_{p,cool}\ (T_{cool\text{-}in} - T_{cool\text{-}out}) \quad (95)$$

The cooling, discharges, and recycling streams have to be considered in the exergy and thermo-economic balance equations according to the chosen boundary conditions. In addition, the model equations (15-39) have to be used in order to calculate the unit production cost as well as evaluate the unit and its performance environmentally and thermo-economically.

6.7.5 Electrolyzer model

As discussed in chapter 3, hydrogen can be produced in many ways and many factors affect its production such as source availability, cost, quality and purity. It can be produced from fossil sources as well as from renewable sources. One of the most

important technologies used is water electrolytic, which is proposed for this research project. Hydrogen is produced by the decomposition of water into hydrogen and oxygen by passing an electric current between two electrodes separated by an electrolyte, as illustrated in chapter 3 and Figure 6.8.

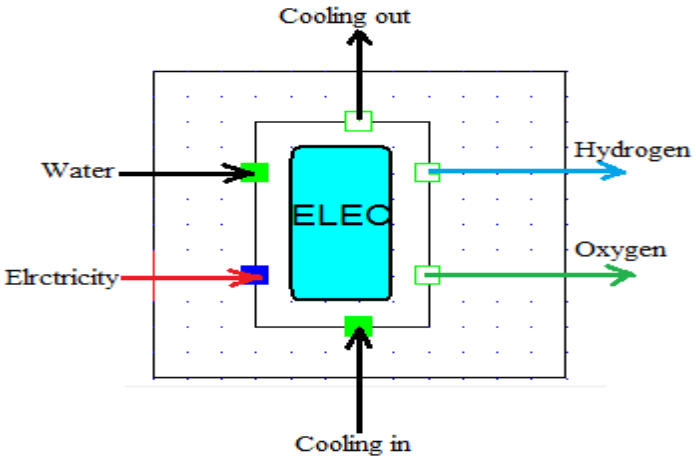

Figure 6.8 Schematic for alkaline electrolyzer unit

A simple thermodynamic model for energy, exergy and thermo-economic analysis of an alkaline electrolyzer cell and unit, similar to the one used for the fuel cell, is applied except for the following changes:

$$\dot{Q}_{gen} = (V_c\text{-}1.481)\,(P_{in\_el} - \dot{W}_{acc}) / V_c \quad (96)$$

The total heat generated at steady state is assumed to be dissipated as heat to surrounding by radiation and convection. However, for a unit without cooling system and neglecting the heat transferred with the output streams it is:

$$\dot{Q}_{loss} = \dot{Q}_{gen} \quad (97)$$

The heat losses from an electrolyzer unit with cooling and recycling streams at steady state can be calculated by using the same energy balance equations (94). The analysis could depend either on the unit geometry and the overall heat transfer coefficient and thermal resistance or on an known and predefined input heat transfer coefficient. In addition, the heat losses could be estimated for the unit as a percentage of the total heat generated (RHL) based on experimental results for a similar unit. However, for the current study it is assumed as 10% of the total heat generated in the unit [126] and the other parameters can be calculated as:

$$\dot{W}_c = (P_{in\_el}\text{-}\dot{W}_{acc})\, C_n \quad (98)$$

$$\eta_{en} = 141860\, \dot{m}_{H2\_in} / \dot{W}_{net} \quad (99)$$

and the exergy destruction can be expressed by:

$I=(1-(T_a/T_c)\ \dot{Q}_{loss}+\dot{W}_{net}-(\dot{m}_{H2}\ ex_{H2in})-(\dot{m}_{o2}\ ex_{o2in})+(\dot{m}_{wT}\ ex_{wt})$ (100)

According to the chosen boundary, the analysis considers all the cooling, discharges, and recycling streams in the exergy and thermo-economic balance equations. The analysis also considers the calculations of the environment and the resources consumed costs and the thermo-economic parameters in order to evaluate the unit and its performance using equations (15-39).

6.7.6 Hydrogen and oxygen storage tank models

Hydrogen and oxygen tanks mathematical models designed to optimize the system storage capacity and its performance according to each weather conditions are presented here. The model is based on the necessary relations used to calculate the tank volume and thermo-economic evaluations parameters that based on the specifications of the entering $(\dot{m}_{st,in})$and exiting $(\dot{m}_{st,out})$ streams gases to the tanks Figure 6.9. The ideal gas, mass, exergy and thermo-economic balance equations in addition to the general form relations presented in the previous sections are applied to investigate the tanks thermo-economically.

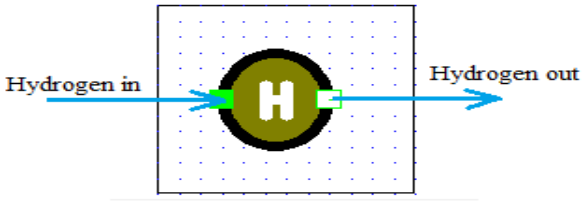

Figure 6.9 Hydrogen tank

The mass balance is :

$\dot{m}_{st,in}=\dot{m}_{st,out}$ (101)

The tank volume in (m^3/s) is:

$\dot{V}_{tank}=v_s\ \dot{m}_s$ (102)

and the required total tank volume in (m^3) according to the total working hours is:

$V_{tank-total}=\dot{V}_{tank}\quad X_{days}*3600*X_{hrs}$ (103)

The irreversibility and the exergy efficiency of the tank can be calculated as:

$I=\dot{m}_s\quad (ex_{tank-in}-ex_{tank-out})$ (104)

$$\eta_{ex}=\frac{\dot{E}x_{tank-out}}{\dot{E}x_{tank-in}}$$ (105)

The tank thermo-economic balance equation can be written as:

$C_{w\text{-}h2\text{-}out}\ (\dot{m}_s*ex_{t-in})=C_{w\text{-}h2\text{-}in}\ (\dot{m}_s*ex_{t-out})+\dot{Z}$ (106)

Where; $C_{w\text{-}h2\text{-}out}$ is the unit cost of the hydrogen stream exit the tank.

6.7.7 Compressor model

The compressor is used to increase the pressure of the electrolyzers' output gases in order to store them in a high-pressure tank Figure 6.10. The existing energy IPSEpro compressor model (APP-Lib) based on the mass balance, pressure ratio (P_{out}/ P_{in}), entropy and enthalpy analysis was developed for exergy and thermo-economic analysis. Two models for both oxygen and hydrogen gas streams were developed using similar thermo-economic equations model illustrated in the previous sections except the following;

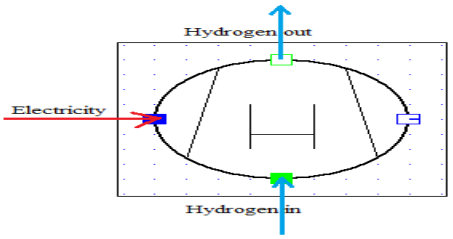

Figure 6.10 Hydrogen gas compressor

The electricity consumed by the shaft power ($P_{el-comp}$) considered for an adiabatic diaphragm single stage process can be calculated as :

$$\dot{W}_{comp} = \dot{m}\frac{\Delta h}{\eta_c} \tag{107}$$

or

$$\dot{W}_{comp} = \frac{\dot{m}}{\eta_{comp}} * \frac{K\ R\ T_1}{K-1}\left[\left(\frac{P_2}{P_1}\right)^{\frac{K-1}{K}} - 1\right] \tag{108}$$

Where:

$\dot{m} = \dot{m}_{in} = \dot{m}_{out}$

η_{comp} is the mechanical efficiency assumed as (0.98).

Δh is the streams enthalpy difference

K is the specific heat ratio of the gas (for hydrogen=1.4)

R is the gas constant (for hydrogen =4.1243 kJ/kg K)

T_1 and P_1 are the intial temperature (K)and pressure (Pa)

P_2 is the outlet gas pressure (Pa)

The outlet gas temperature is increased based on the compression ratio value and can be calculated as:

$$T_2 = T_1 - \left(\frac{P_2}{P_1}\right)^{\frac{K-1}{K}} \tag{109}$$

The exergy efficiency ($\eta_{ex-comp}$) based on the exergy rate of the fuel and product definition according to the compressor function [155] can be calculated as:

$$\eta_{ex-comp} = \frac{\dot{m}(ex_{out} - ex_{in})}{P_{el-c}} \quad (110)$$

and the exergy irreversibility:

$$I = \dot{m}(ex_{in} - ex_{out}) + P_{el-c} \quad (111)$$

The thermo-economic equations (15-31) are used to calculate the thermo-economic parameters, whereas the unit cost of the output hydrogen stream ($Ch2_{out}$) is calculated as:

$$Ch2_{out} = \frac{\dot{Z} + \dot{m} * Ch2_{in} * ex_{in} + C_{w-power} * P_{el-comp}}{ex_{out} * \dot{m}} \quad (112)$$

6.7.8 Heat exchanger model

The compressor's outlet gas temperature has to be cooled in order to be stored in the high-pressure tanks at nearly ambient temperature. Counter flow (tube and shield) heat exchangers are usually used for cooling hydrogen and oxygen gases. Figure 6.11 is a schematic diagram for a counter flow heat exchanger unit.

IPSEpro adopts a method based on mass and energy equations using the UA formation along with the mean temperature difference to specify the size and the performance of a heat exchanger.

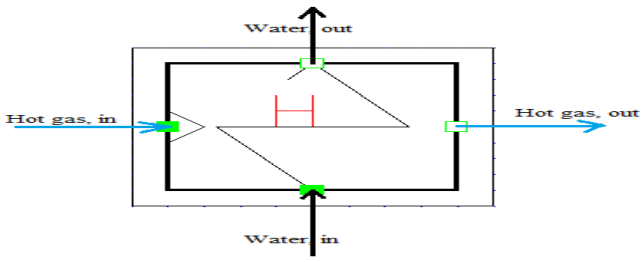

Figure 6.11 Schematic for counter flow heat exchanger

The heat transfer of heat exchanger can be calculated as:

$$\dot{Q} = UA * (LMTD) \quad (113)$$

Where:

$$LMTD = \frac{(T_{hot,in} - T_{cold,in,}) - (T_{hot,out} - T_{cold,in})}{\ln\left(\frac{(T_{hot,in} - T_{cold,in,})}{(T_{hot,out} - T_{cold,in})}\right)} \quad (114)$$

The effectiveness-number of transfer unit (ε-NTU) method has been adopted for heat exchanger model validation, the definitions and details of these method is described in the next chapter. The heat exchanger IPSEpro energy model has been developed to evaluate the unit thermo-economically and the following equations is used [152]:

The irreversibility of the heat exchanger can be expressed as:

$$I = \dot{m}_{hot} * \left(ex_{hot,in} - ex_{hot,out}\right) - \dot{m}_{cold} * \left(ex_{cold,out} - ex_{cold,in}\right) \quad (115)$$

and the unit exergy efficiency (η_{ex-hex}) calculated as:

$$\eta_{ex-hex} = \dot{m}_{cold} * \left(ex_{cold,out} - ex_{cold,in}\right) - \dot{m}_{hot} * \left(ex_{hot,in} - ex_{hot,out}\right) \quad (116)$$

A thermo-economic analysis and evaluation is conducted using the general thermo-economic balance and parameter equations (15-31) illustrated in the previous sections, whereas the output gas unit cost ($C_{w,hot,out}$) can be calculated as:

$$C_{w,hot,out} = \frac{\left(Cw_{hot,in} * ex_{hot,in} * \dot{m}_{hot,in} + \dot{Z}\right)}{\left(ex_{hot,out} * \dot{m}_{hot,out}\right)} \quad (117)$$

6.7.9 SHS supplementary models (connections, mixers, splitter and pump)

The existing IPSEpro-APP Library supplementary unit models such as pumps, mixers, splitters and connections are based on mass and energy balance equations in order to work with the other units. In this study these units have been developed based on exergy and thermo-economic methodology in order to successfully connect with the SHS units. In this section, the functions and the structure of the models are illustrated. More details of the IPSEpro MDK equations of these models are presented in the appendix D.

- Connections

The model structure of the IPSEpro units requires that each unit have to define IN and OUT connections. A connector, as described in chapter five, indicates the positions where a connection can be attached to the instances of the respective unit model class. Connectors are not only graphical elements but also include information that is relevant for the models. Figure 6.12 illustrated general graphical structure of a connection stream. The basic IPSEpro MDK applied library has only three types of connections (streams, fuel stream and shaft). However, for SHS thermo-economic analysis the

following connections models have been developed based on the gas or substance involved in the processes, these connection models are;

Figure 6.12 Graphical structure of stream connection

1- Hydrogen stream, Oxygen_ stream and Water_ stream connections

These stream models are used to identify the oxygen and hydrogen gases as well as the water stream transferred between the units. A composition object and the mathematical equations in the model present the chemical composition of the transferred medium. The input parameters to the model (temperature, pressure and mass) are used to calculate its characteristics such as (enthalpy, entropy and volume). The physical exergy of the streams is calculated based on the mathematical equations (6.12) for water and (6.13) for hydrogen and oxygen. Figures (6.13 and 6.14) represent the graphical structure of the developed hydrogen and oxygen class units. These units are developed based on a general model existing in the IPSEpro APP-Lib in order to enable the specific connection streams in SHS to connect to each unit in the system. In addition to the exergy equations, the model considered also the cost term of the hydrogen (Ch2), oxygen (CO_2). However, the mathematical equations representing the cost unit of each specific stream have been pre-defined in each unit or connection model based on the general thermo-economic equation (6.15).

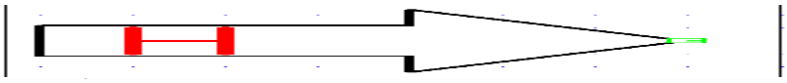

Figure 6.13 Graphical structure of hydrogen source unit

Figure 6.14 Graphical structure of oxygen sink unit

2- Eelectricity_e and Heat connections

The (electricity_e) connection model is used to transfer the output power to the next unit in the system or the final user. The power amount (kW) and the power unit cost term (C_w) in ($/GJ) are predefined as variables or parameters in the model class. The

heat model connection is used to transfer the heat from the sun (Sirr_Sun) in (kW/m^2) to the photovoltaic unit in the SHS model processes.

- Pump

The pump unit in the SHS is used to feed and recycle the water in the system units. Figure 6.15 illustrates the graphical structure of the IPSEpro modified model. The model considered the unit electricity cost (C_w) and the exergy concepts of the unit inlet and outlet connecters' class model are developed in order to calculate the exergy terms of the inlet and outlet streams. These terms are compatible with the similar pre-defined terms in the connected units or streams to the pump. However, the model of the pump unit ignores the exergy and thermo-economic analysis of the pump due to the very low amount of power consumed in the unit compared with the electrolyzer and other SHS units. In addition, the IPSEpro APP-lib estimates default values of 98% and 70 % for the pump mechanical and entropy efficiency respectively, which is similar to the values estimated for the compressor unit. The power consumed is calculated based on the mass and energy balance equations of the inlets and outlet streams existed in the basic IPSEpro APP- Lib that is similar to the one used for the compressor unit.

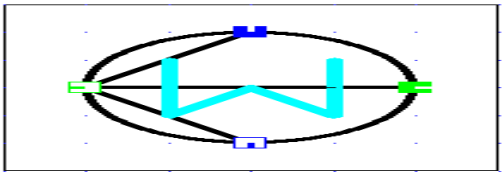

Figure 6.15 Graphical structure of the water pump unit

- Mixers

The graphical structure of the three developed mixer units for recycling and mixing the hydrogen, oxygen and water streams in the SHS is illustrated in Figure 6.16. The basic mixer unit exists in the IPSEpro applied library based on the energy, mass and pressure balance of the inlet and exit streams to the unit have been developed. The development includes a definition of the exergy parameters, cost terms for each feed, and drain connection class in the model, in order to enable it to be successfully connected to the other units in the SHS.

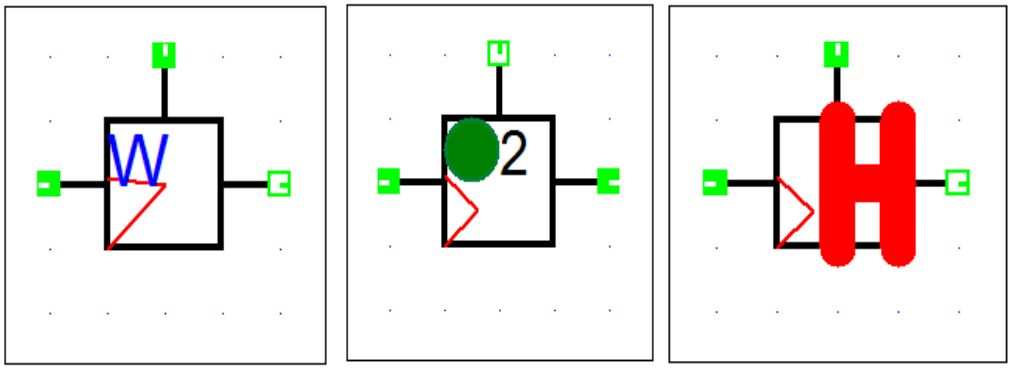

Figure 6.16 Graphical structures for water, oxygen and hydrogen mixer units

- Splitters

A simple splitters IPSEpro models have been developed to distribute the system input electricity to all units in the system such as (electrolyzer, pumps and compressors). The IPSEpro graphical structure of the nine and two branches splitter models are presented in Figure 6.17. The two-branch model is used to distribute the total PV electricity according to a pre-defined percentage to cover both the load in the daytime and the required electricity of the SHS. However, the nine-branch model is used to distribute the input electricity according to the real consumption of each connected unit in the SHS.

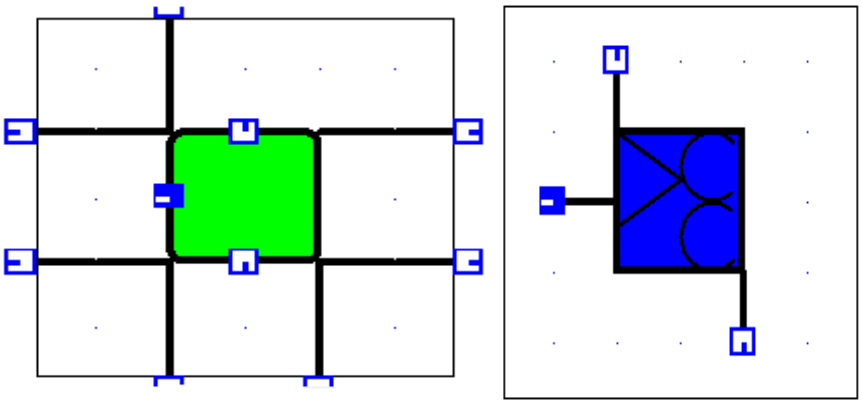

Figure 6.17 Graphical structures of nine and two branches splitter units

CHAPTER SEVEN

Chapter Seven

IPSEpro Models configurations and validation

7.1 Introduction

In this chapter, the configurations and the validation processes of the developed IPSEpro library models for the solar hydrogen system components will be introduced. The validation of these models that based on a real data provided by the manufacturers of the chosen components and the previous study is also presented. Meanwhile, the models output results have been compared theoretically, experimentally and with other simulation tool results.

7.2 The Developed IPSEpro Applied Library

As described in chapter five the IPSEpro Applied Power Library (APP_Lib) is used for the energy analysis of the traditional thermal power plants, and has to be developed in order to apply for the thermo-economic analysis of the SHS. The IPSEpro-MDK kit package has been used for the library development, which is one of the main subjects of this study. Figure 7.1 depicts the existing IPSEpro model library, while Figures 7.2 and 7.3 illustrate print screens of the developed IPSEpro-MDK and part of PSE libraries respectively. It is clear from the figures that many new model components have been developed and integrated for use with the existing IPSEpro APP-Lib. The developed library can be used to optimize, investigate and simulate SHS and its units thermo-economically individually or as a system which is integrated with any other energy power units in the library. The methodology and the equations govern the development of these models was outlined in chapter six. The model's inputs and design parameters used in this study will be described in the next chapter. In the following sections, descriptions, details configurations and validation of some of the developed SHS components models (photovoltaic (PV), electrolyzer, fuel cell, heat exchanger, tanks, compressor and other complementary units) are outlined. However, due to limited space all the configurations of the models and IPSEpro-MDK equations are presented in appendix D.

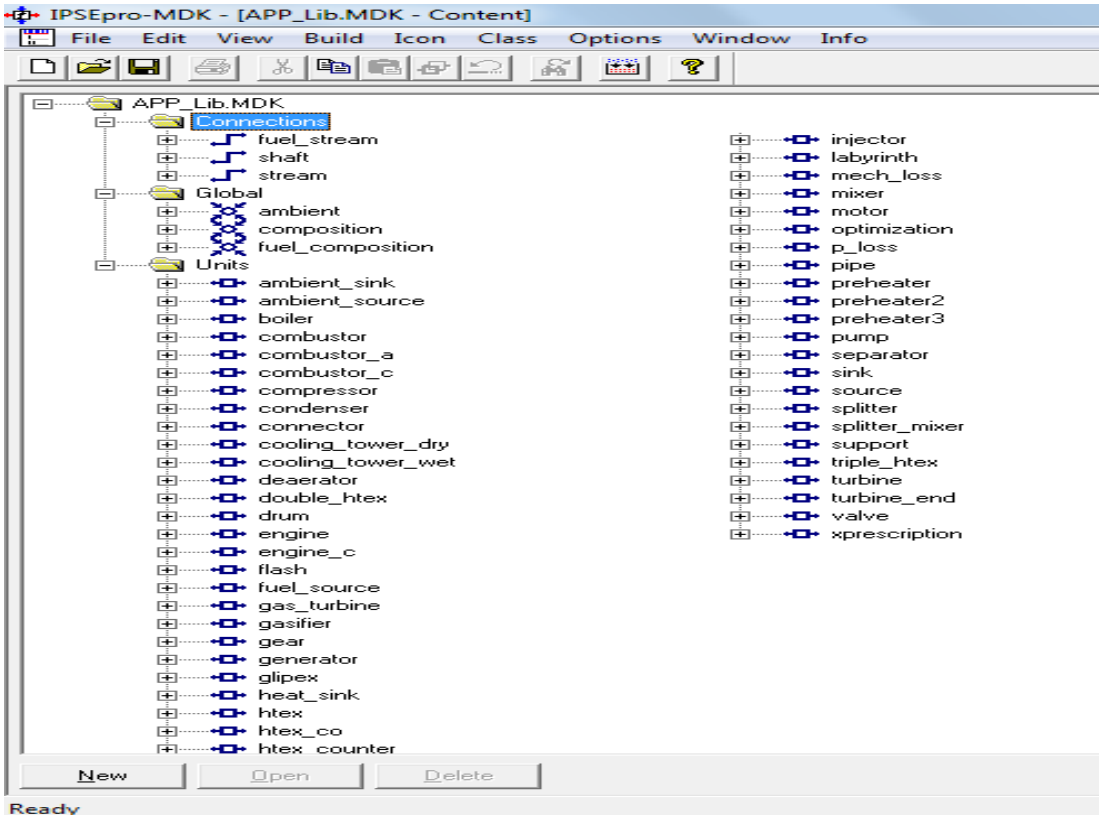

Figure 7.1 The existing IPSEpro library (APP-Lib.MDK)

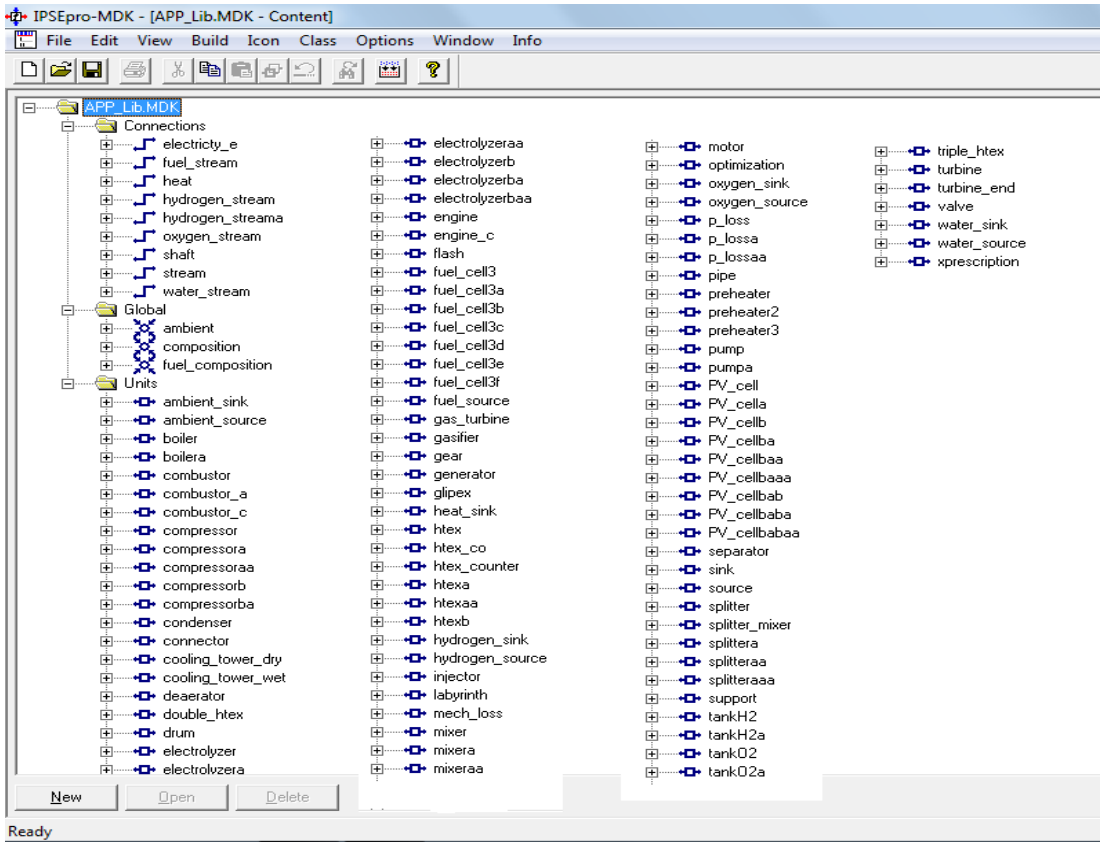

Figure 7.2 The developed (APP-Lib.MDK) included the SHS models

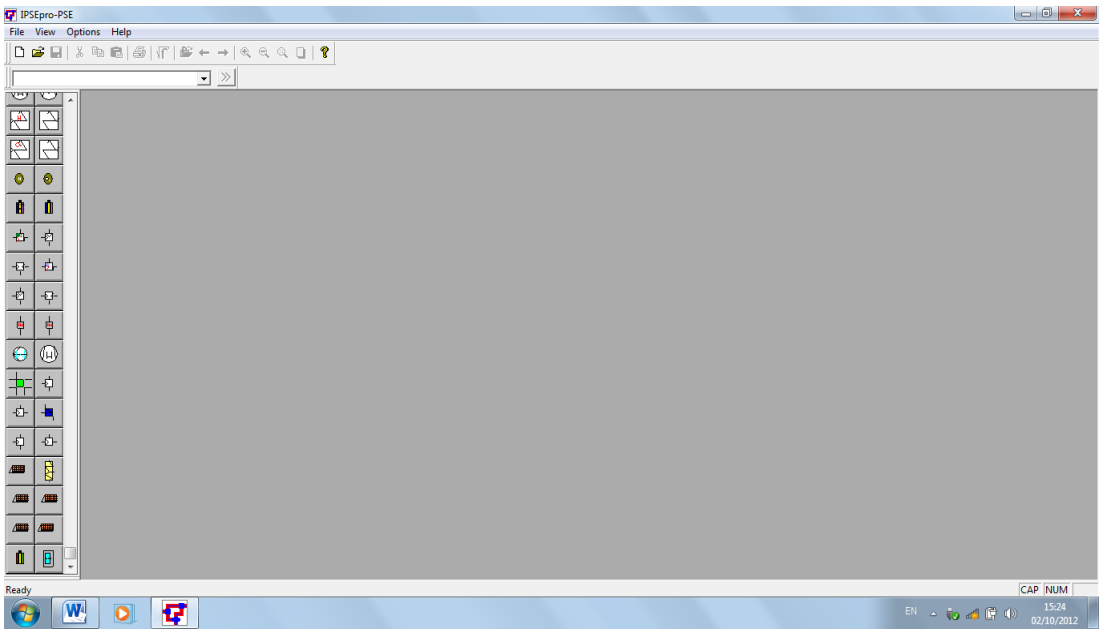

Figure 7.3 Part of the developed (APP-Lib.PSE) included the SHS units

7.3 Photovoltaic IPSEpro models

The modified model library presented in Figure 7.1 was developed using IPSEpro.MDK and consisting of many new connections, globals and units. The main unit in the SHS is the photovoltaic unit (PV) and different PV models have been developed according to the accuracy, detailed and the purpose of these units. A simple unit (PV_cell) as presented in Figure 7.4 is used for energy and exergy analysis whereas Figure 7.5 presented a print screen for the model (PV_cellba) used for the thermo-economic analysis of a unit using the thermal analysis equation (6.53).

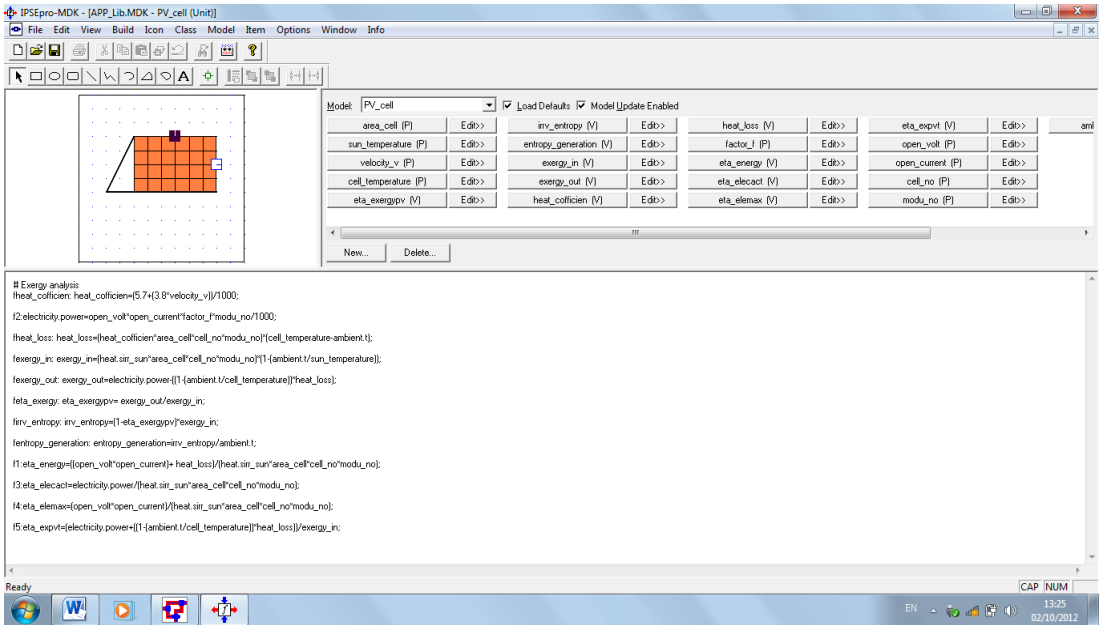

Figure 7.4 Energy and exergy analysis (PV_cell) IPSEpro_MDK model

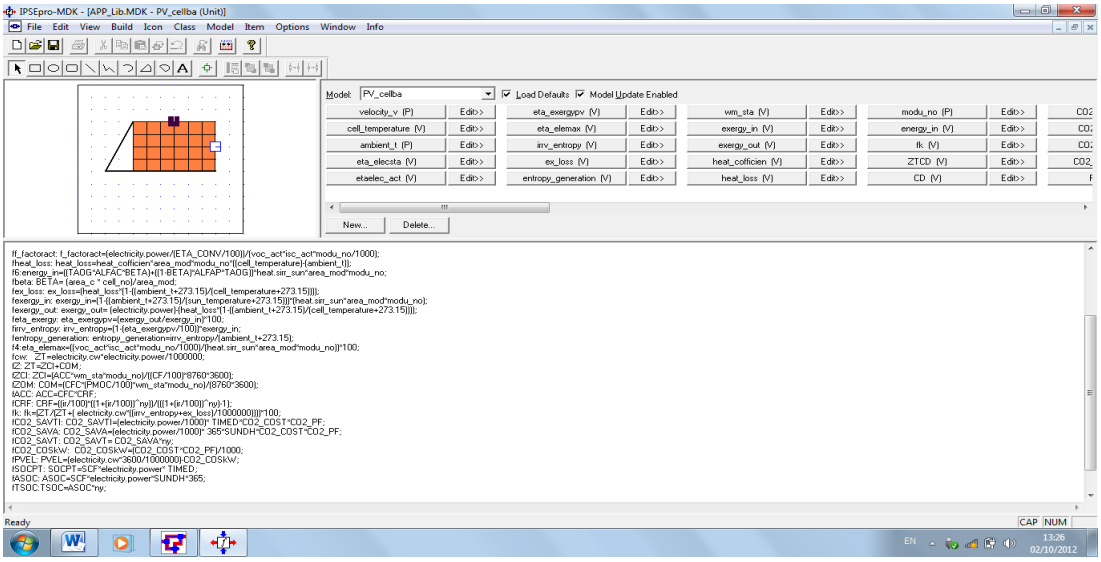

Figure 7.5 Thermo-economic analysis using equation (6.53) (PV_cellba) IPSEpro_MDK model

Figure 7.6 represents a print screen for the (PV_cellbabaa) IPSEpro_MDK model for a detailed thermo-economic analysis of the unit. The model used a general thermal balance equations method included the heat transfer coefficients from the bottom and the top of the unit. The model (PV_cellbaaa) for the detailed thermo-economic analysis of the PV/T unit with water cooling system is illustrated in Figure 7.7. Due to space limitations, the mathematical models and all model configurations of the PV and PV/T models IPSEpro_MDK are presented in appendix D.

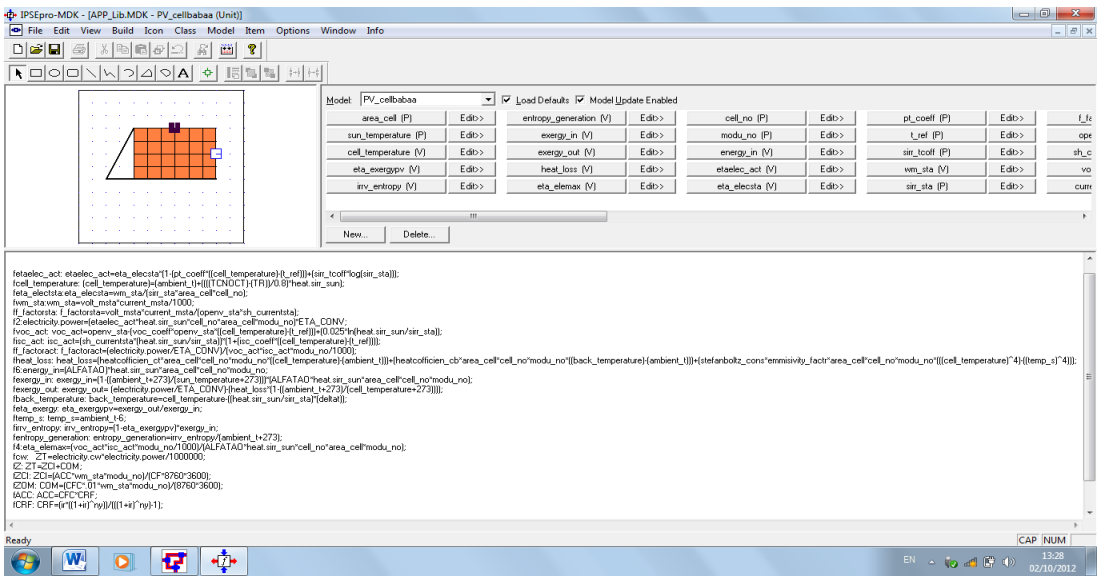

Figure 7.6 Detailed thermo-economic analysis (PV_cellbabaa) IPSEpro_MDK model

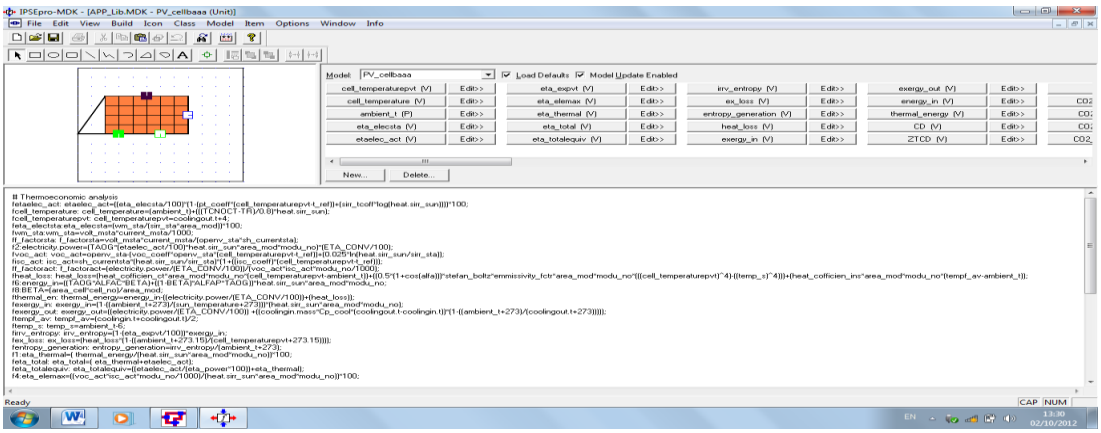

Figure 7.7 Detailed thermo-economic analysis (PV/T) (PV_cellbaaa) IPSEpro_MDK model

7.3.1 PV Model validation

The accuracy of the IPSEpro-PV model results has been examined using three different types of validation. The model output results have been calibrated theoretically using a tested data at standard conditions provided by the manufacturer of the photovoltaic modules. The calibration processes compares the technical data provided by the company with the results of the IPSEpro model for the same inputs at (STC) conditions. The analysis used the technical data presented in (appendix A) for a PV module produced by a2 peak company type (power on P220-6*10 glass/ back-sheet) module [171]. Figure 7.8 presents the IPSEpro print screen output results of the PV performance parameters such as the module electric efficiency (eta-elec), power output, open voltage (Voc) and shunt current (Isc) at STC. The figure reveals that the IPSEpro results agree with the measured data (with +-2% tolerance) provided by the manufacturer.

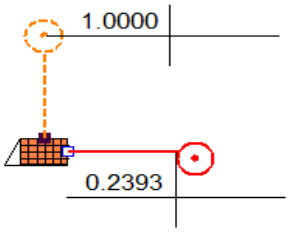

Parameter	IPSEpro (STC)	Measured (STC)
Tc(℃)	25.000	25.000
Sir-Sun (kW)	1.000	1.000
Wind (m/s)	1.000	1.000
Power-STC (kW)	0.239	0.240
eta_elec_actual %	14.400	14.400
Isc-STC (A)	8.100	8.100
Voc_STC (V)	37.750	37.750

Figure 7.8 Calibration of IPSEpro PV model using measured data at STC

As described earlier in this study, the nature of the PV unit that transformed the photo energy directly to electricity, leading to the necessity of inclusion the unit I-V

characteristics in the analysis. These phenomena, along with the significant effect of the climate conditions on the unit performance as well as the steady state nature of the IPSEpro package, forced to checking the accuracy of the IPSEpro model results to be carried out on an hourly basis. Consequently, the results of the experimental study of Barker and Norton [172] with regard to the analysis of a PV array module at rank-mounted and specific hourly conditions as presented in Figure 7.9 were adopted for the validation processes. In addition, the results for studying the same PV module using MATLAB software and five parameter PV mathematical model were chosen to verify the IPSEpro model results [73]. The analysis used a PV module produced by Siemens company type SM55 according to the module design parameters and operation data presented in Appendix E.

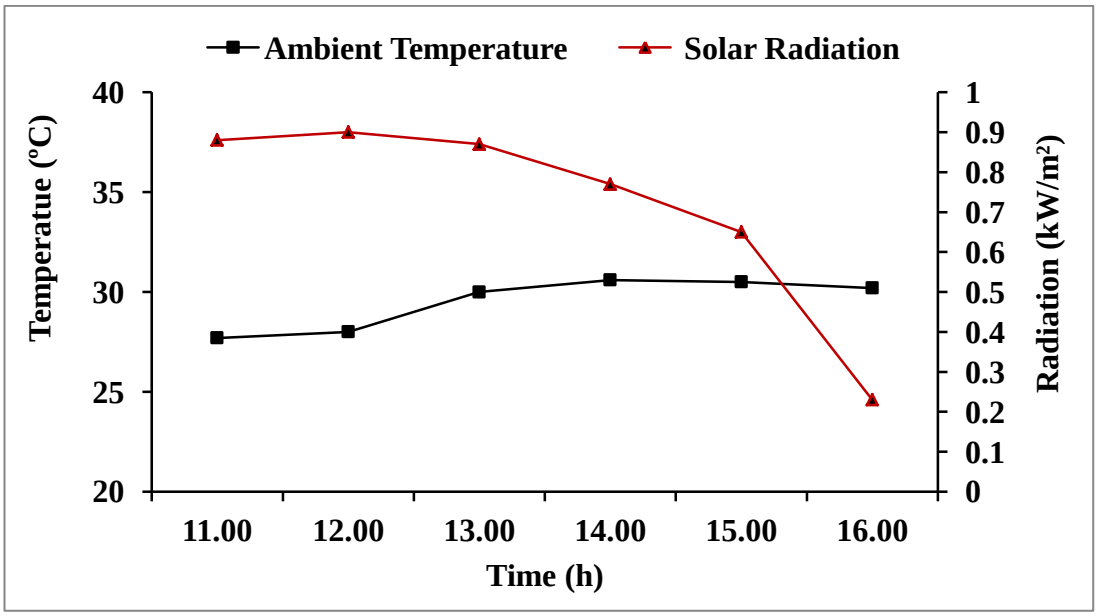

Figure 7.9 Variation of solar radiation and ambient temperature during the test day

The same data for the SM55 module were used as inputs for the IPSEpro model (PVCellba) except for the wind speed where it is considered as 1 m/s instead of 0.5 m/s as in Ref. [73] and its neglected in Ref. [172]. Also 2% of the power output losses were considered in the IPSEpro model, due to the expected losses from the wires, mismatching and non-homogeneous of cell structure.

The analysis considered the main PV module performance parameters such as the unit power output, cell temperature, electrical and energy efficiency, open voltage and open

current. These parameter's IPSEpro simulation results was compared with a previous simulated (sim) [73] and experimental studies (exp) [172] results as showed in Figures 7.7 to 7.12. The root mean square percentage deviation (RMS) has been considered for the comparison between the previous studies results and IPSEpro results using the following equation:

$$RMS = \sqrt{\frac{\sum\left[100 * \frac{X_{exp,i} - X_{sim,i}}{X_{exp,i}}\right]^2}{n}} \quad (7.1)$$

Where: n is the number of experiment records.

The IPSEpro simulated values for the PV surface temperature compared with the measured and MATLAB simulated values are presented in Figure 7.10. It is clear from the figure that the IPSEpro results agreed with the experimental values with RMS percentage deviation = 1.83%. This percentage deviation is less than the one recorded as 4.82 % when the difference between the MATLAB (sim) and experimental (exp) results is considered.

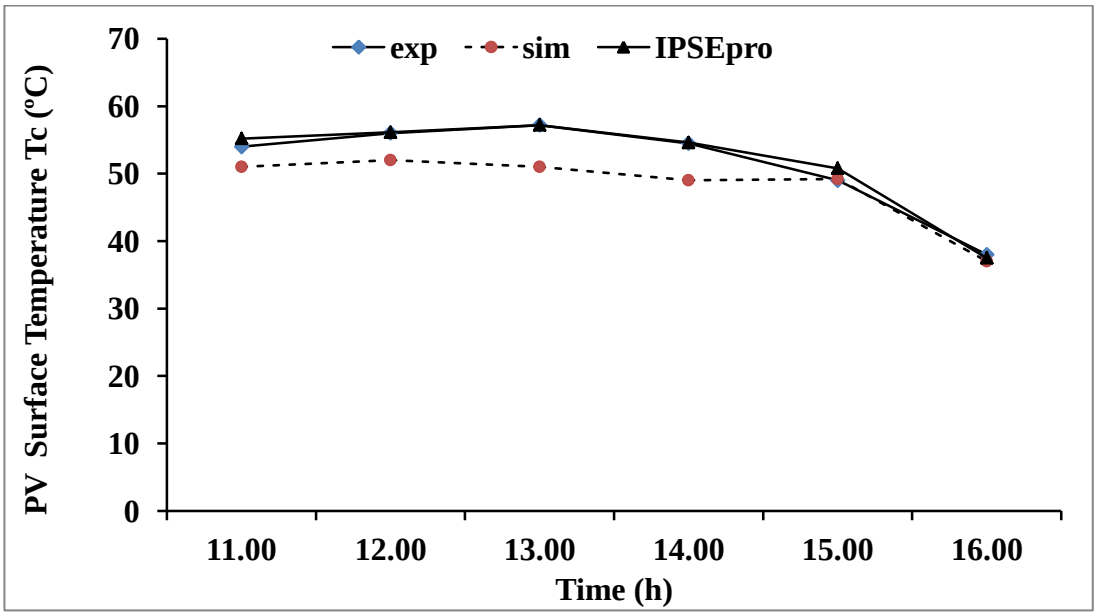

Figure 7.10 The measured PV surface temperatures compared with the IPSEpro and MATLAB simulated results

The IPSEpro simulated values for PV power output, open voltage (Voc) and open current (Isc) compared with an experimentally tested and MATLAB simulated values have been shown in Figures 7.11, 7.12 and 7.13 respectively. It is observed from the figures that there is a good agreement between the experimental and the simulated

results with RMS percentage deviation between the IPSEpro and measured values as (2.2%, 3.9%, and 1.3%) for these parameters respectively. These deviations percentages are less than the RMS percentages deviation values for the same parameters that calculated for the experimentally tested values compared to the MATLAB results recorded as (2.8%, 2.4%, 4.6%) respectively.

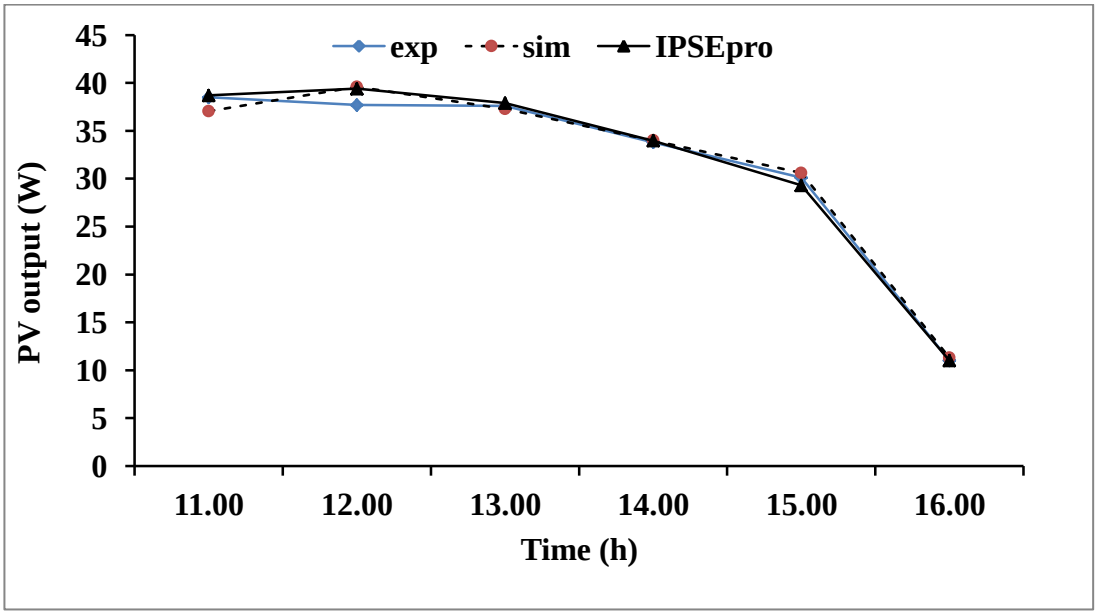

Figure 7.11 The tested PV output values compared with the IPSEpro and MATLAB simulated results.

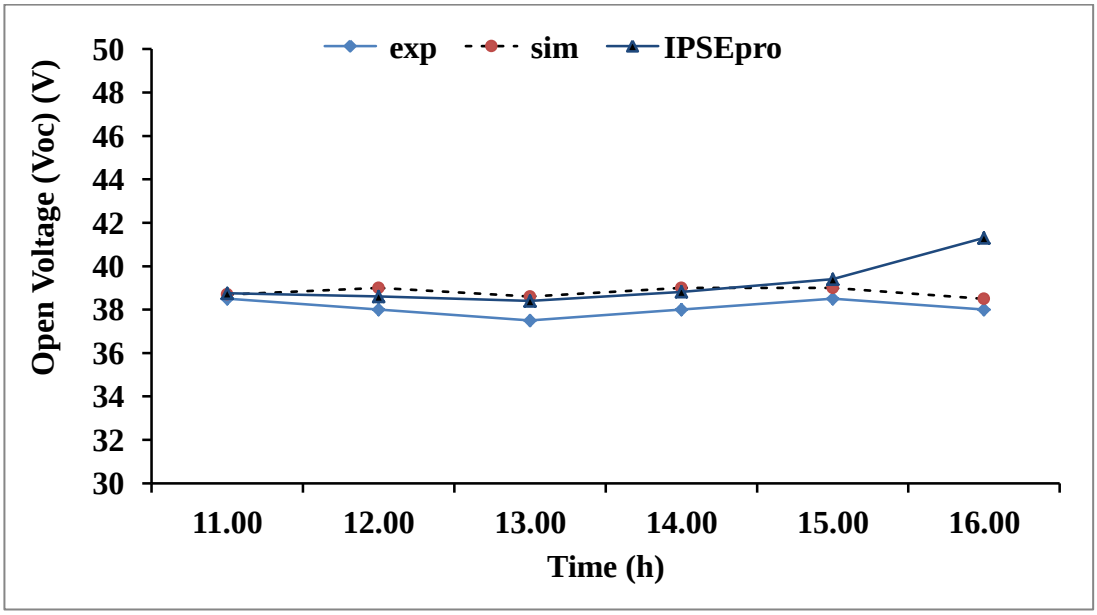

Figure 7.12 The tested open voltage values compared with the IPSEpro and MATLAB simulated results

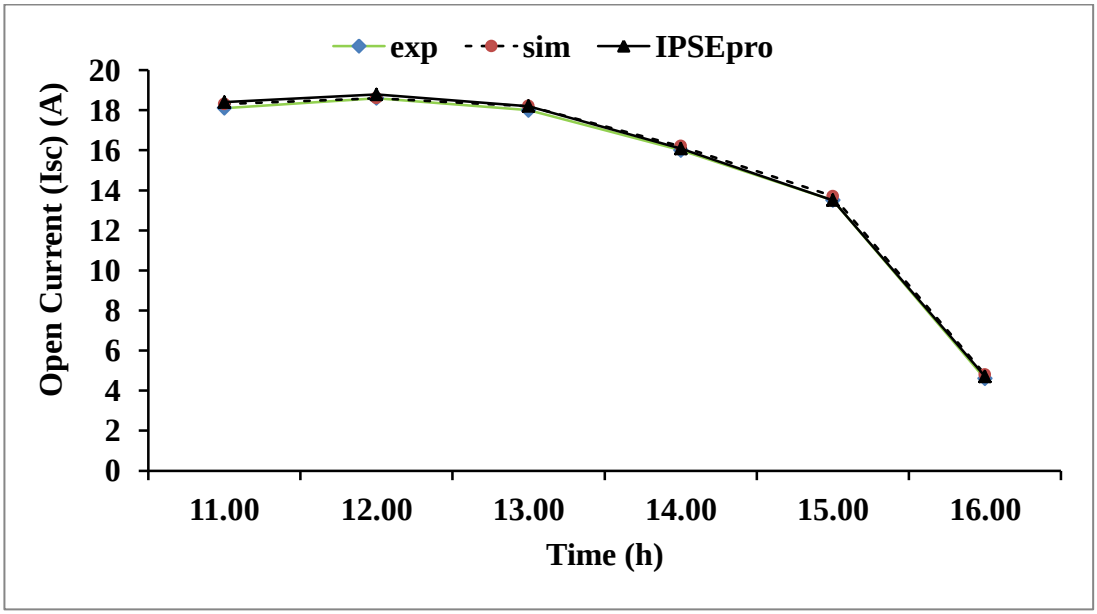

Figure 7.13 The measured open current values compared with the IPSEpro and MATLAB simulated results

The simulated IPSEpro, MATLAB and experimental electrical and energy efficiency values during the day are shown in Figures 7.14 and 7.15 respectively. It can be seen from the figures that there is a good agreement between the IPSEpro values and the experiment one for both efficiencies with RMS percentage deviation calculated as (2.8%, 4.8%). These RMS percentage difference are less the one calculated as (3.58%, 5.88%) respectively for the MATLAB results to the experimental results for the two parameters.

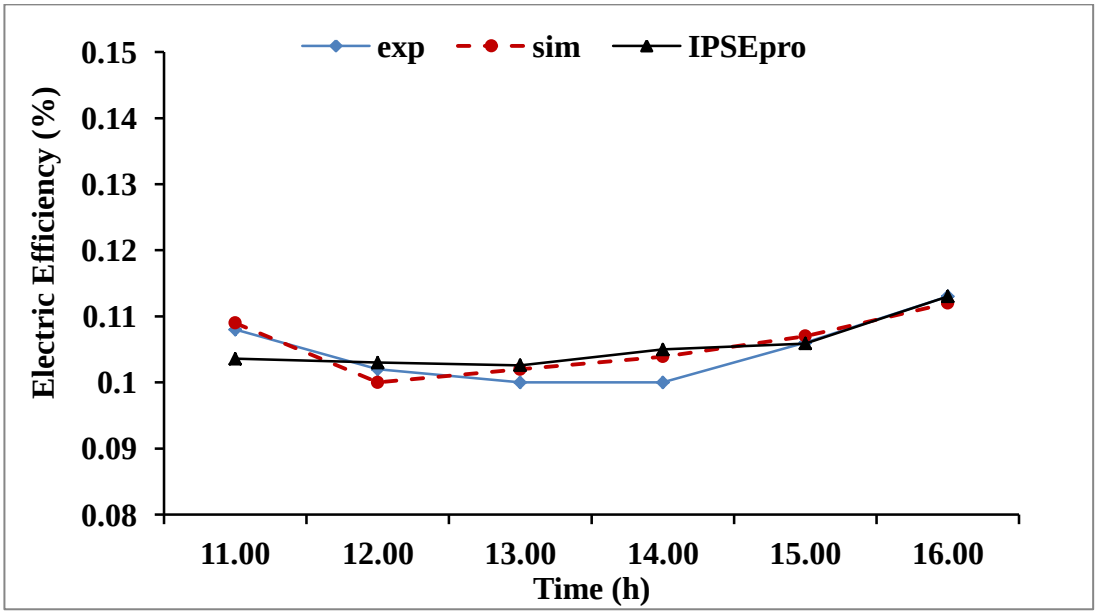

Figure 7.14 The experimental electric efficiency values compared with the IPSEpro and MATLAB simulated results

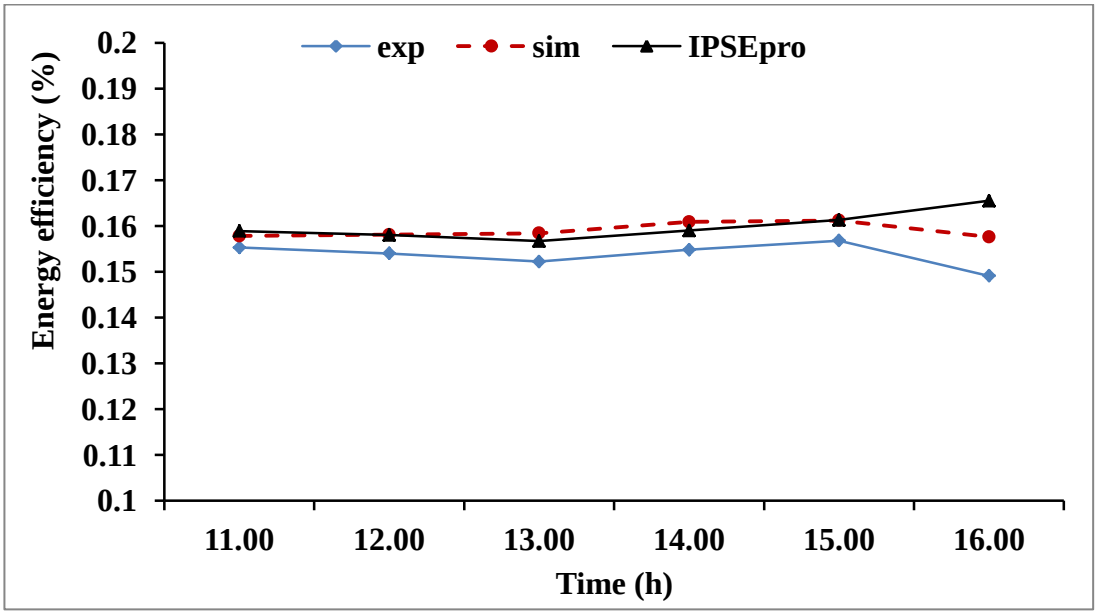

Figure 7.15 The experimental energy efficiency values compared with the IPSEpro and MATLAB simulated results

The agreement of the IPSEpro model results with the measured and MATLAB simulated results, indicating the accuracy of the IPSEpro model in predicting the PV module performance in different climate conditions, particularly for solar intensity over 200 W/m^2. However, the existing difference in appearance between the results may refer to the inaccuracy of obtaining the measured values from the curves presented in references [73,172]. In addition, some of the parameters have been considered constant such as the current and voltage temperature coefficients, and wind speed while in practice it is slightly fluctuation during the day.

7.4 Electrolyzer and Fuel cell IPSEpro Models

The electrolyzer and fuel cell IPSEpro model was developed based on a steady state thermo-economic methodology at a constant and a given operational conditions. The steady state thermal analysis of these units has been carried out at specific operation parameters, particularly for unit temperature, pressure and the corresponding rated voltage and power as provided by the manufactures. However, the electrochemical nature, over potential losses as well as the current density change has not been considered in the analysis. Furthermore, the effect of varying the unit operation conditions particularly the power, voltage, pressure and cell temperature on the unit's thermo-economic parameters and performance will be examined in the next chapter. In

the following sections the models' configurations and validation will be generally described and presented, while more details are provided in appendix D.

7.4.1 Electrolyzer IPSEpro models

The electrolyzer unit adopted for this study is used to produce hydrogen and oxygen from water using electricity produced from the solar panels or any other source. Six IPSEpro electrolyzer models for different analysis and purposes have been developed as presented in Figure 7.2. Figure 7.16 shows an IPSEpro print screen for (elecrolyzer) model used for energy and exergy analysis of standalone unit without cooling or streams recycling, whereas the model (electrolyzerb) is used for the energy and exergy analysis of a unit with a cooling system, as presented in Figure 7.17.

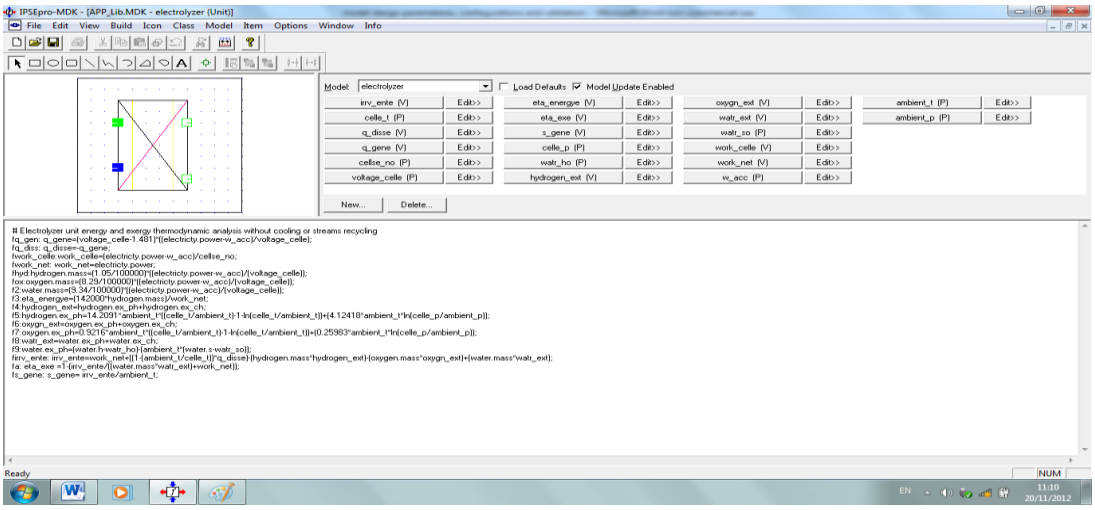

Figure 7.16 IPSEpro electrolyzer model (electrolyzer) for energy and exergy analysis without cooling or stream recycling

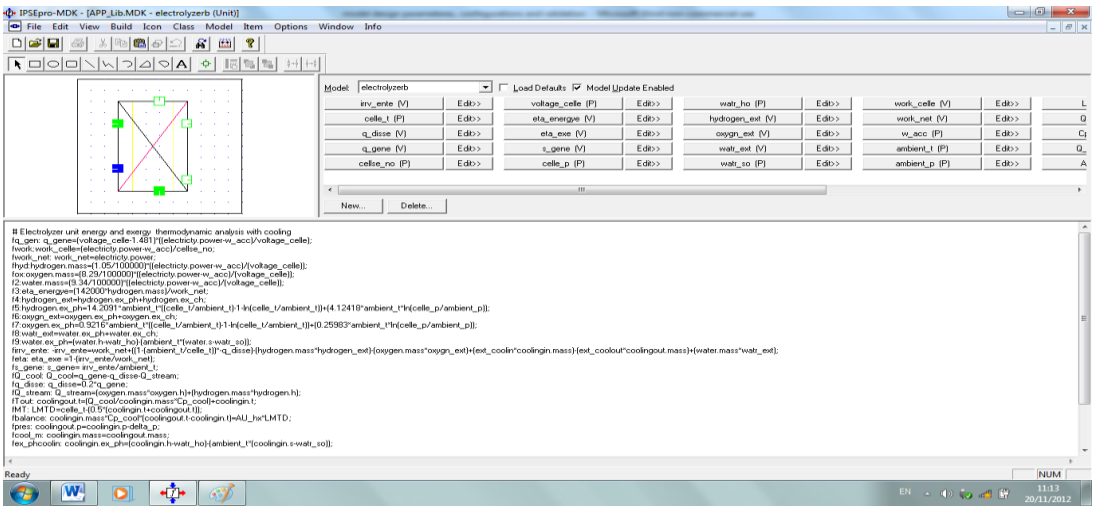

Figure 7.17 IPSEpro electrolyzer model (electrolyzerb) for energy and exergy analysis with cooling

The thermo-economic analysis of an electrolyzer unit with cooling and streams recycling system, as integrated with SHS, can be carried out by using the model library (electrlyzerba) as presented in Figure 7.18. However, theIPSEpro library model presented in Figure 7.19 (electrolyzerbaa) can be used for the thermo-economic analysis of the unit without a cooling or recycling system.

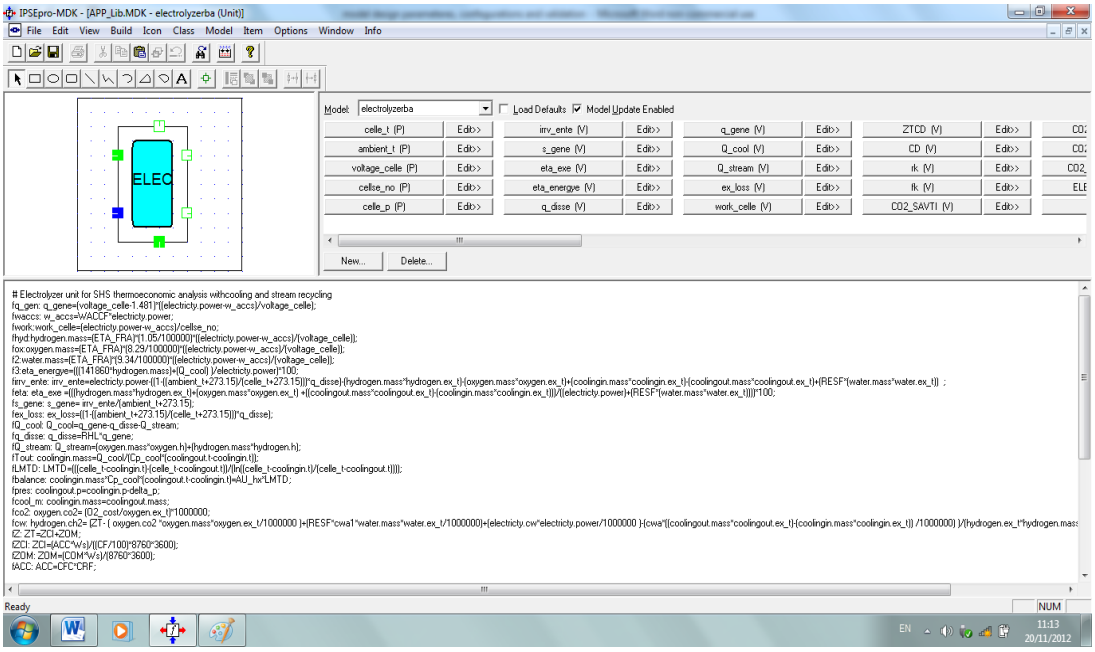

Figure 7.18 IPSEpro electrolyzer model (electrolyzerba) for thermo-economic analysis with cooling and recycling system integrated in SHS

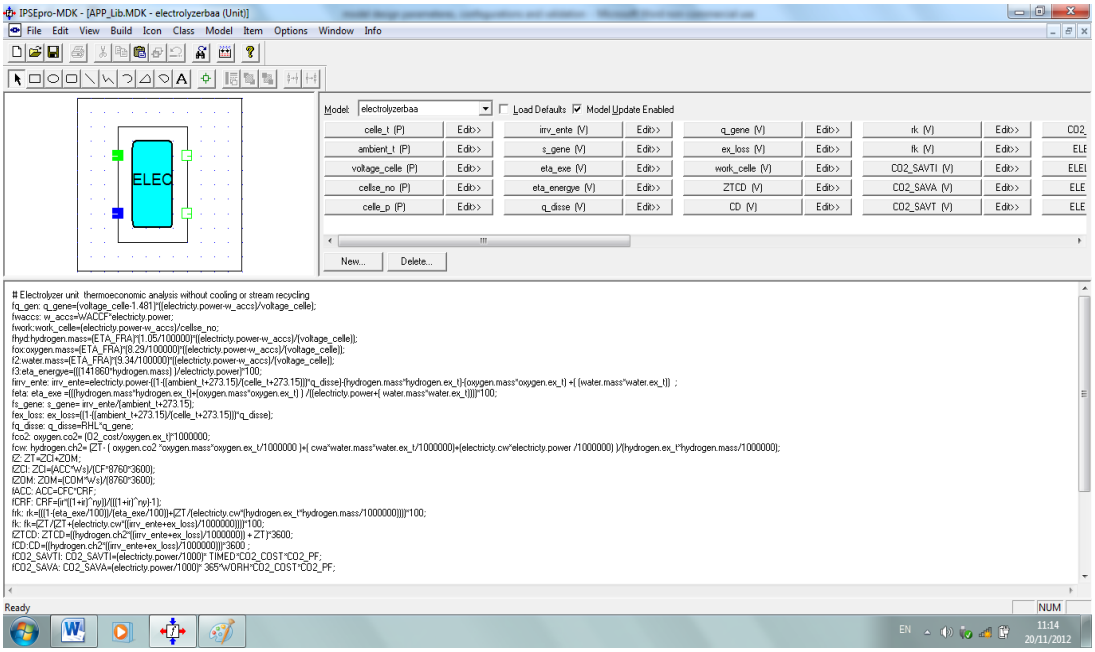

Figure 7.19 IPSEpro electrolyzer model (electrolyzerbaa) for unit thermo-economic analysis without a cooling or recycling system

7.4.2 IPSEpro Electrolyzer model validation

The developed electrolyzer model library is calibrated theoretically by using actual data from a hydrogen and renewable integration project installed at West Beacon Farm, Leicestershire, UK, known as the HARI-project. The alkaline electrolyzer unit in the project was modelled by the IFE (Institute of energy technology, Norway) and the HARI-project evaluation team [173]. The unit consists of 1 stack, 32 cells, 0.1 m^2 cell area operated at 65 ^{O}C, 450 A, 25 bar, 1.815 V, 26.1 kW, and the hydrogen and oxygen output are 6 Nm^3/h and 3 Nm^3/h equivalent to 0.522 kg/h and 4.12 kg/h respectively. The efficiency existing at these conditions is 79.6 %. The obtained results using IPSEpro for the same operation conditions give an identical output and results, as shown in Figure 7.20.

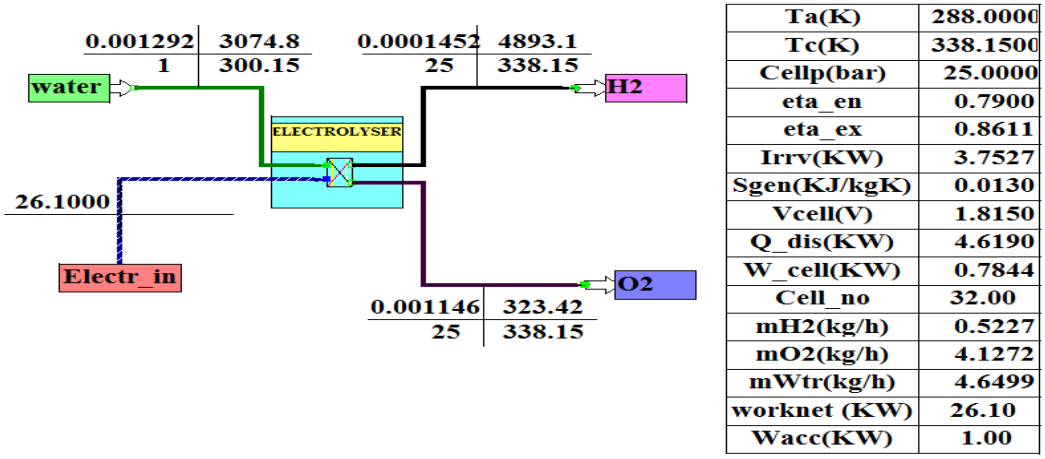

Figure 7.20 Simulation results screen of electrolyzer unit (IPSEpro) based on a real project operation data [173]

The current simulation study has adopted an alkaline water electrolyzer type HYSTAT 60 produced by Hydrogenics company [174]. The technical data provided by the manufacturer to produce the rated capacity (+-2% tolerance) hydrogen flow rate (60 Nm^3/h) is presented in appendix C. The unit operated at 10 bar, 70^{o}C and 1.815 V with a specific total consumed power 5.2 kWh/Nm^3 for the entire system including the treatment, purification, control panel and cooling system and 4.2 kWh/Nm^3 for the unit stack with an efficiency 80%. The IPSEpro model library (electrolyszrba) is used to verify the unit performance and output using the same operation parameters and

assumed 20% of the total consumption input power consumed for the auxiliary equipment. The IPSEpro output results particularly for the hydrogen and oxygen production amount and electricity and water consumed agrees with the provided data as presented in Figure 7.21.

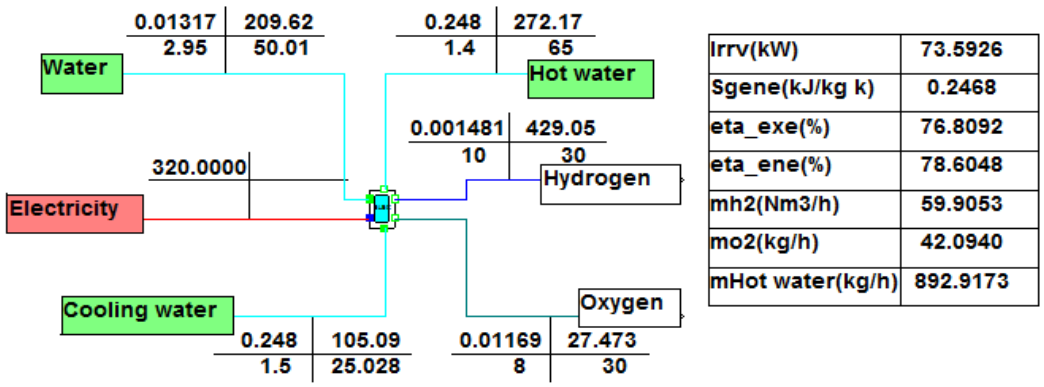

Figure 7.21 Calibration of IPSEpro (electrolyzerba) model results

7.4.3 Fuel cell IPSEpro models

The PEM fuel cell unit used in the analysis at the current research study uses the hydrogen and oxygen produced from the water electrolyzer or any other sources. Six different IPSEpro fuel cell models have been developed for different purposes according to the methodology described in chapter six. Figure 7.22 represents a print screen of the model (fuel-cell3) used for unit energy and exergy analysis without cooling.

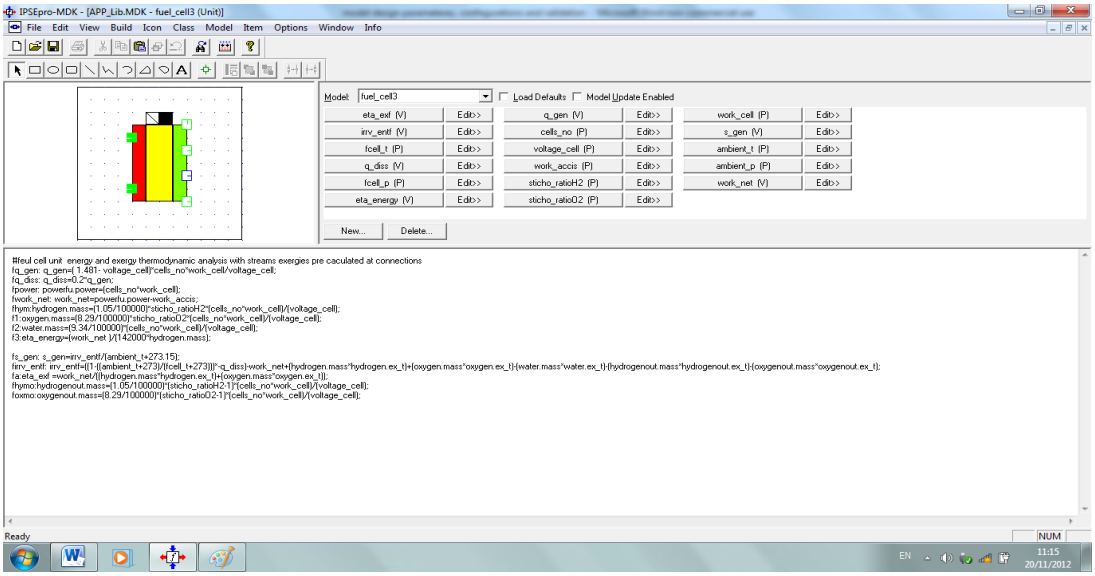

Figure 7.22 IPSEpro model (fuel-cell3) for unit energy and exergy analysis

The model (fuel-cell3d) presented in Figure 7.23 is used for energy and exergy analysis of a unit in a SHS with cooling and recycling system.

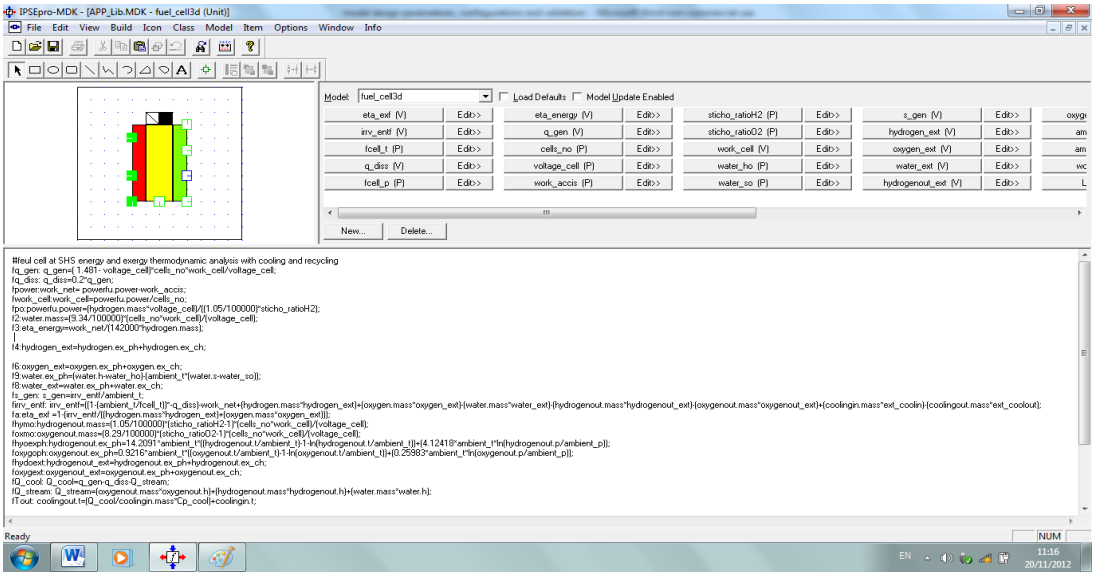

Figure 7.23 IPSEpro model (fuel-cell3d) for a unit energy and exergy analysis integrated in a SHS with cooling and streams recycling

Detailed thermo-economic analysis of a fuel cell unit with cooling and recycling system integrated with a SHS can be performed using the model (fuel-cell3e) presented in Figure 7.24. Detailed model MDK equations and configurations of the all fuel cell IPSEpro models are presented in appendix D.

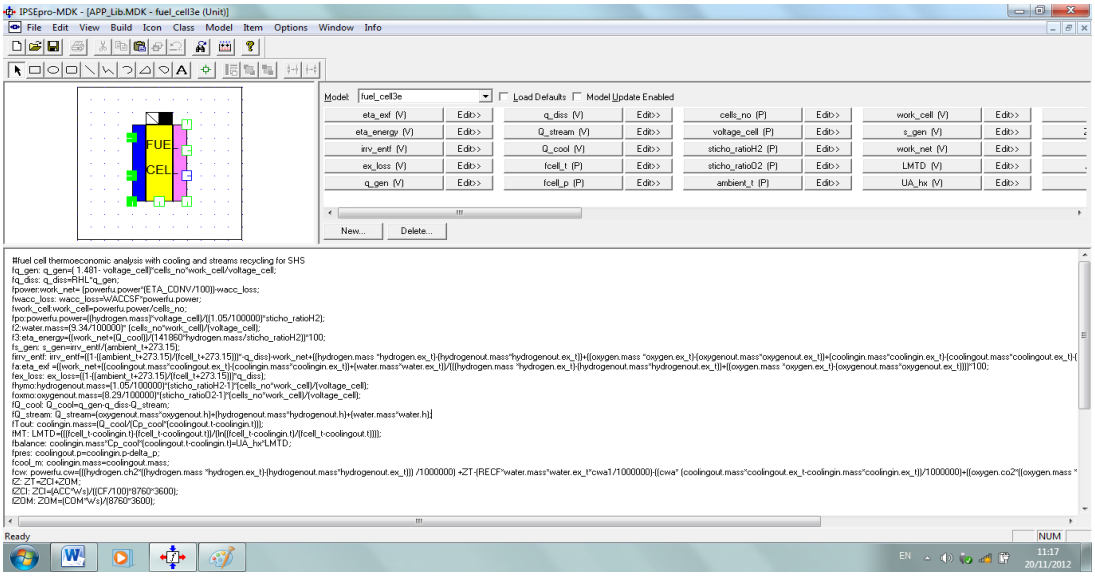

Figure 7.24 IPSEpro model (fuel-cell3e) for a unit thermo-economic analysis integrated in SHS with cooling and streams recycling

7.4.4 Fuel cell IPSEpro model validation

The accuracy of the fuel cell IPSEpro model results needs to be calibrated by comparison with test results. The technical data provided by Ballard Company for the 1 MW fuel cell (+- 2% tolerance) that adopted for the analysis in this study is used to validate the IPSEpro model results (appendix C). The unit operates at 70 ^{o}C, 3 bars and 0.6 V/cell and consumed 63 kg/h hydrogen to produce the full capacity and 1100 kW heat load with voltage efficiency as +- 48% and energy efficiency (without cooling) of +- 40%. The IPSEpro model library unit (fuel cell3e) simulation results in the same operation conditions of the tested unit are presented in Figure 7.25. The results show a good agreement with the manufacturer technical data as presented in appendix B, revealing the accuracy of the model and the assumption of the heat loss factor as (RHL=0.2) and the auxiliary loads as 10 kW.

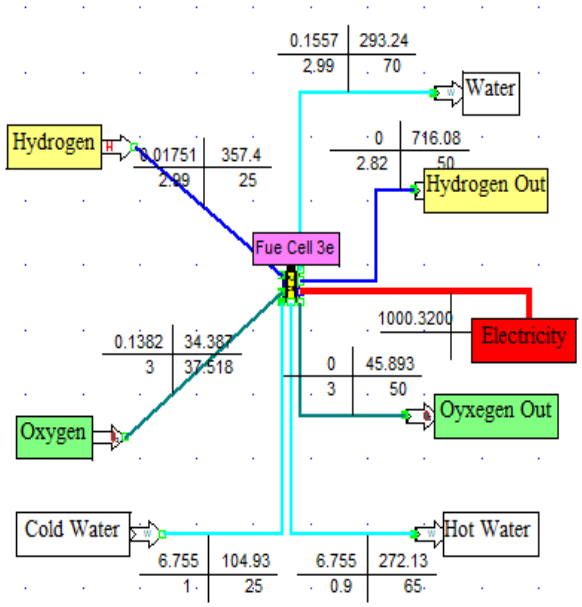

Parameter	IPSEpro	DATAsheet
eta-evoltage(%)	50.4	+- 48
H2-mass (kg/h)	63	63
Qcool (kW)	1129	1100
Tc (C)	70	65-70
pressure(bar)	3	2-4
power (kW)	1000.3	1000
RHL	0.2	
Wacc (kW)	10	
Voltage (V)	0.6	
eta-energy(%)	83.3425	
eta-exe (%)	35.6860	

Figure 7.25 IPSEpro (fuel cell 3e) model results compared with the data provided by the manufacture of Ballard 1 MW

7.5 IPSEpro Heat exchangers models configurations

Based on the existing IPSEpro-MDK library and the used gas, two types of heat exchangers were developed for the unit's thermo-economic analysis. The IPSEpro model (htexaa) presented in Figure 7.26 is used for the thermo-economic analysis of a heat exchanger with oxygen as hot stream, while the model (htexa) presented in (appendix D) is used for energy and exergy analysis only. Figure 7.27 illustrated the

print screen of IPSEpro model library (hetxb) used for the thermo-economic analysis of heat exchangers used hydrogen as a hot gas. In addition the model (htex) presented in (appendix D) is used for the exergy analysis of heat exchanger unit using hydrogen gas.

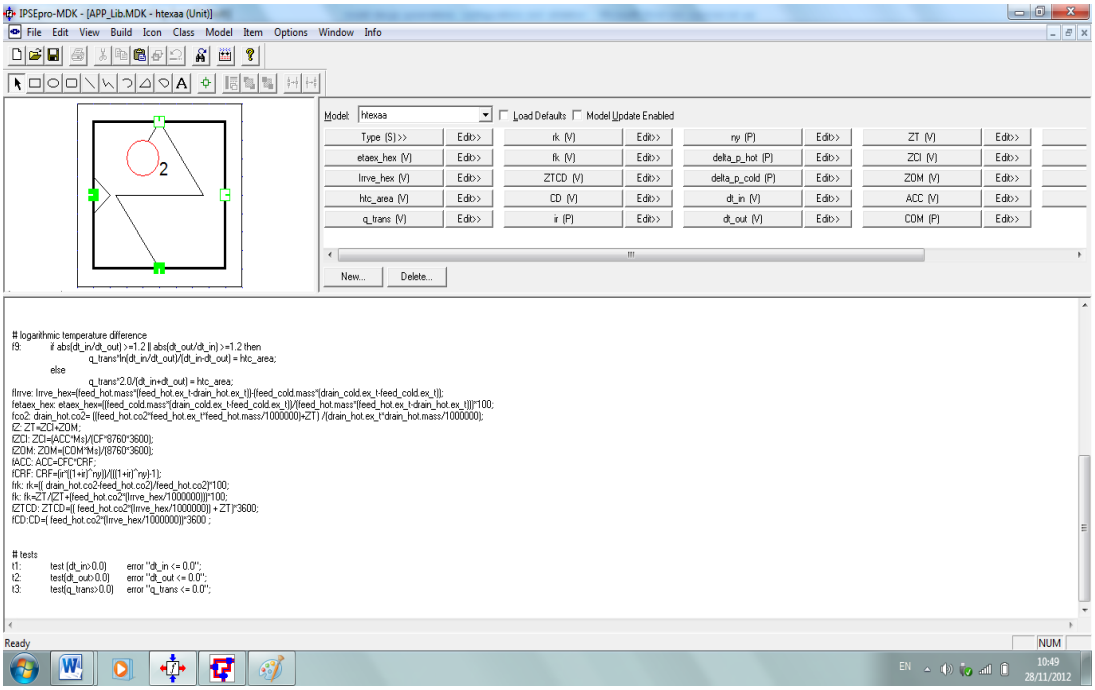

Figure 7.26 IPSEpro MDK (hetxaa) model for Oxygen heat exchanger thermo-economic analysis

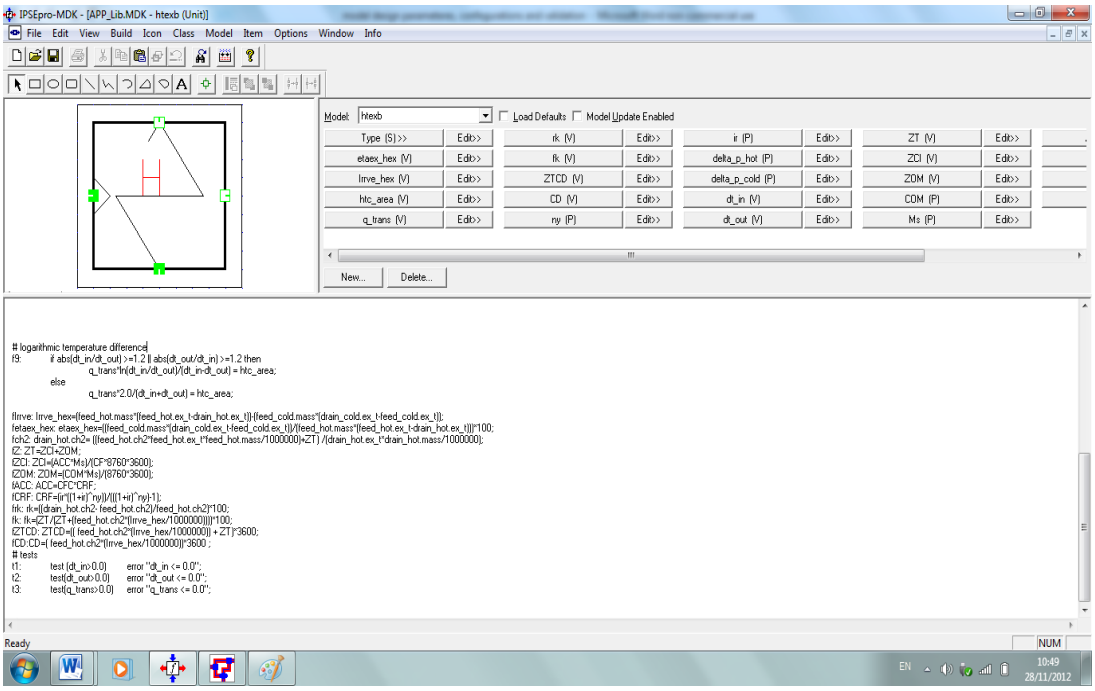

Figure 7.27 IPSEpro MDK (hetxb) model for Hydrogen heat exchanger thermo-economic analysis

7.5.1 IPSEpro Heat exchangers models validation method

Counter flow tube and shell heat exchangers are acceptable ways to cool hot gases by using unmixed water as a cooler fluid. The specifications, design parameters and costs of such types are clarified in terms of the selection and costing of heat exchangers guidelines published by the ESDU UK [175,176]. However, it is necessary to validate the heat exchanger to work in a valid thermodynamically range. The Ɛ-NTU method is used to validate the heat exchanger thermally using the following relations:

The effectiveness (Ɛ) defined as the actual amount of heat transferred ($\dot{Q}$) to the maximum possible amount of heat that could be transferred with an infinite area ($\dot{Q}_{max}$):

$$\text{Ɛ} = \frac{\dot{Q}}{\dot{Q}_{max}} \tag{7.1}$$

Where:

$\dot{Q}$= The heat transferred=$\dot{m}_{hot} C_{p\ hot}(T_{hot\ out} - T_{hot\ in})$ (7.2)

or

$$\dot{Q} = \dot{m}_{cold} C_{p\ cold}\left(T_{cold,out} - T_{cold,in}\right) \tag{7.3}$$

and;

$\dot{m}$ is the mass flow rate of the fluid.

T is the temperature of the input or output hot or cold fluid.

C_p is the heat capacity of the fluid.

The non-dimensional expression called number of transfer units (NTU) defined as:

$$NTU = \frac{UA}{(\dot{m}_{Cp})min} \tag{7.4}$$

Where:

$(\dot{m}_{Cp})min$ = the lower of the two streams heat capacity.

U is the overall heat transfer coefficient.

A is the heat exchanger surface area.

The capacity ratio C_R is the non-dimensional ratio defined as:

$$C_R = \frac{(\dot{m}_{Cp})min}{(\dot{m}_{Cp})max} \tag{7.5}$$

Where:

$(\dot{m}_{Cp})max$ = the higher of the two streams heat capacity.

The effectiveness (Ɛ) is a function of the NTU and C_R as:

Ɛ=Ɛ (NTU, C_R)

Physically, a heat exchanger with a large product of UA and a small $(\dot{m}_{Cp})min$ should have a high degree of energy recovery and a high effectiveness. This is restricted by the additional cost for the higher unit surface area and the system input and output streams characteristics and values. However, for industrial use of the hydrogen and oxygen gases counter flow heat exchangers, an effectiveness of between (0.8 to 0.9) is recommended [125].This can lead to optimizing the units in the system to work thermodynamically in the valid region, taking in considerations the UA factor and the working temperatures of the input and output streams. The experimental results consist of pre plotted relations for the corresponding heat exchangers for the NTU values, set against the effectiveness values at a different amounts of capacity ratios C_R are figured in many previous studies and references [177, 178]. These figures and methods will be used in the next chapter to validate the IPSEpro heat exchanger models simulation results according to each operation conditions and working fluid temperatures and values.

7.6 IPSEpro SHS complementary models configurations

As described in chapter six some complementary units have to be used with the main SHS components to complete the generation cycle. These include pumps, compressors, connectors, mixers, splitters and tanks. These models are designed for energy and exergy analysis only or for thermo-economic analysis based on the methodology described in chapter six. It is also developed with reference to the type of input streams and mainly depends on the existing IPSEpro-MDK-APP-Library models except for the tanks, which were developed as new unit library using the IPSEpro- MDK package. Due to limited space only some of the IPSEpro models configurations of the SHS complementary units can be presented here, while more details of the all units model configurations and their IPSEpro- MDK equations are presented in Appendix D. Figure 7.28 represents a print screen for the (compressorb) IPSEpro-MDK model used for the thermo-economic analysis of the hydrogen compressors. However, the PSEpro-MDK model (tankO2a) used for thermo-economic analysis of oxygen tanks is presented in Figure 7.29. The library includes also many other models for specific purpose such as models (tankO2), (tankH2), (compressorba) for energy and exergy analysis as well as (compressor) for the thermo-economic analysis of oxygen compressor. It is also included models developed for mixers and splitters for different uses as appears in appendix D.

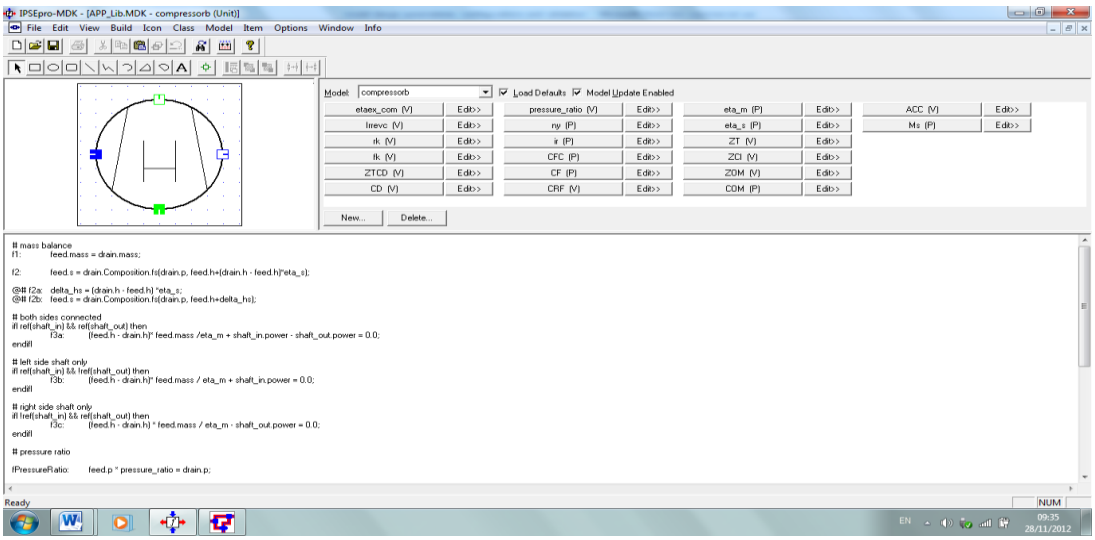

Figure 7.28 Print screen for the (compressorb) IPSEpro-MDK model used for thermo-economic analysis of hydrogen compressors

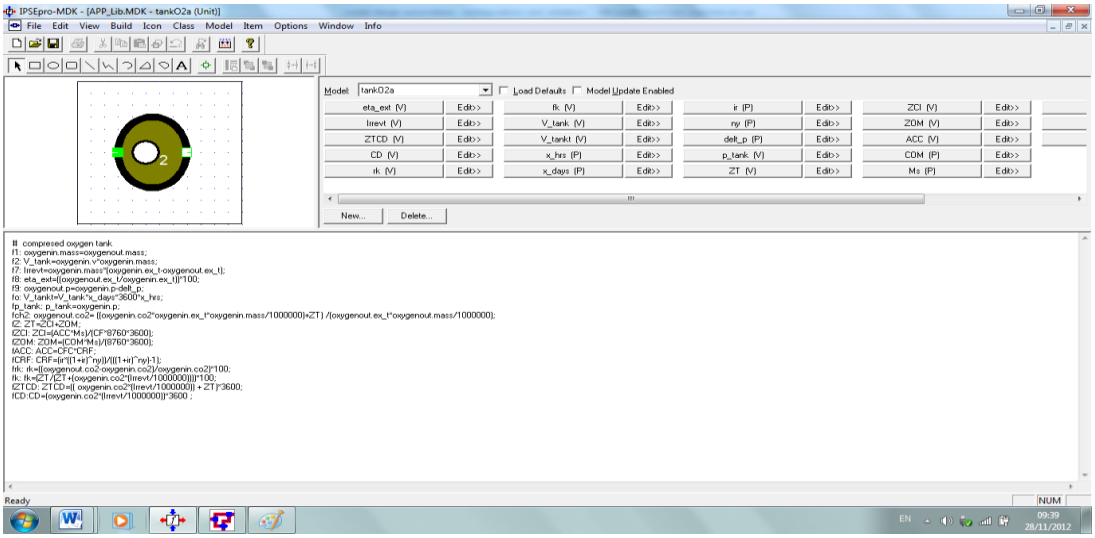

Figure 7.29 The IPSEpro-MDK model (tankO2a) used for thermo-economic analysis of Oxygen tanks

7.7 Closing remarks

The configurations of the IPSEpro models library developed for the solar hydrogen system based on energy, exergy and thermo-economic methodology are presented in this chapter. The developed models have been validated using experimental and previous simulations data in order to check the model results at different operation conditions. The analysis shows that the SHS IPSEpro models results are agree with the tested and previous simulated results. In the next chapter, a parametric study and thermo-economic analysis of the SHS and its components is carried out. The effect of varying the operation parameters and the environment conditions on the system performance is investigated and discussed.

CHAPTER EIGHT

Chapter Eight

Energy, exergy and thermo-economic study of SHS and its components

8.1 Introduction

In this chapter, the SHS IPSEpro model developed in the previous chapter is used to design, optimize and evaluate the system and its components based on energy, exergy and thermo-economic method. The system has been designed and optimized to meet the energy requirements of a small community with an hourly peak load day and night as one MWh. A parametric study is conducted to investigate and evaluate the effect of the environmental, operational, design and economic parameters of each unit on the entire system and on each unit's performance. The collected average yearly and daily weather data for selected case studies in Sabha, Misurata and Newcastle, as presented in chapter four, is used in the analysis and the results have been tabulated, figured and discussed. The photovoltaic thermal model PV/T and its ability to enhance the system's performance and provide heat energy to the community are discussed. In addition, a trade-off analysis between the hot water output quantity and temperature against the produced electricity of the PV/T system is also carried out and discussed taking in consideration the main purpose of the unit. The utilization of the PV/T system outlet hot water in a low thermal energy system is also investigated.

8.2 The SHS design parameters and optimization

The solar hydrogen system is a system used to provide the user's energy demand particularly electricity and hot air or water. In addition, the hydrogen gas and the system output thermal energy can be used directly or indirectly to meet some of the user's energy requirement. In this study, the developed IPSEpro models for the SHS are used to design and optimize the system to meet the daily energy requirement of small community at Sabha city in Libya. The system assumed to produce one MWh using the solar panels directly in the day light time and the fuel cell during the night or absences of the solar energy. The weather and solar data at the optimum angle collected for Sabha presented in chapter four is used to simulate and evaluate the system. Table 8.1 represents the operations and design parameter's values adopted or assumed to investigate the PV unit using the (PV-Cellba) IPSEpro model. The system in its initial stage, as illustrated in the table, is designed and simulated for a base condition with (Sirr =1000 W/m^2, ambient temperature=25 ^{o}C , wind velocity =1 m/s) and taking the yearly

average sun shine duration of Sabha as 9.6 hours in consideration. The analysis estimating the cost of the unit as 3000 $/kW included the panel, wires, convertor and the installations and land cost according to the cost of the selected solar panels from the manufacturer and the average price index of crystalline panels in December 2012 [56]. However, the unit costs declined over time and the effect of the variation of the CFC on the unit and system performance is considered in the following sections. The interest rate (ir) or the effective rate (ieff) when the inflation rate is estimated as 4%. The ETA-CONV defined as the PV power reduction caused by the convertor, soil, wires and cells mismatching, which is dependent on the site and the type of convertor is estimated as 95% [69]. The capacity factor CF defined as the percentage of the working hours of the unit during the day is estimated as 40% according to the average yearly sunshine duration at Sabha. The yearly maintenance and operation cost factor of the PV unit has been estimated as 0.7% of the capital cost for this capacity, although previous studies assumed this for small PV units as <1 % [36, 57, 61, 157]. The other design and operations parameters have been adopted from the unit manufacture's data sheet (appendix A) and previous studies [86,157]. The system optimization processes for the assumed peak load production revealed that 26201 solar panels from the type chosen in this study were required to produce around 4850 kWh at base condition to cover this load day and night.

Sirr (kW/m^2)	1	$V_{OC\text{-}coeff}$ ($1/^{\circ}C$)	0.00344	TCNOCT ($^{\circ}C$)	45	ETA-CONV (%)	95
V (m/s)	1	$Isc\text{-}_{coeff}$ ($1/^{\circ}C$)	0.000548	Timed (h)	9.6	CO2-COST $/ton)	24
Ta (^{o}C)	25	$Sirr\text{-}_{coeff}$	0.0012	Sund (h)	9.6	CO2-PF(ton/MW)	0.6
modno	26201	$Pt\text{-}_{coeff}$	0.0046	Sun_temp($^{\circ}C$)	5526	TAOG	0.95
V_{OCsta} (V)	37.72	ir (%)	4	Areamod(m^2)	1.667	ALFAC	0.9
I_{OCsta} (A)	8.10	ny(years)	25	Cell-no	60	T_{sun}	5526
V_m (V)	31.49	T_{ref} (^{o}C)	25	CFC($/kW)	3000	Sirr-sta(kW/m^2)	1
I_m (A)	7.62	TR(^{o}C)	20	SCF($/kW)	0.05	PMOC (%)	0.7

Table 8.1 Design and operation parameters of PV unit at base condition (Sabha yearly average)

8.2.1 The electrolyzer model design and operation parameters

Table 8.2 presented the operation and design parameters' inputs for the alkaline electrolyzer unit adopted to evaluate and build a SHS at base conditions for Sabha average data using the (electrolyzerba) IPSEpro model. The unit has to be optimized to produce the sufficient amount of hydrogen and oxygen required to produce the one MWh power from the fuel cell to cover the community demand during the night. It received the electricity produced from the PV system during the daytime, whereas the

rest of PV produced electricity will cover the assumed user demand during the daytime. The capacity factor CF for the unit is estimated as 30 % of the total unit capacity according to the working hours during the day as 9.6 hours. This estimation also takes in consideration that a part of the 12 (HySTAT60) units will be offline during this period due to the variation of PV electricity input to the units. The yearly operation and maintenance factor is estimated to be 3% of the unit capital costs (CFC) [111], while the other parameters have been estimated from the manufacturer data sheet (appendix C) and previous studies [26,51,111,126,179, 180]. The temperature and the pressure of the output streams are assumed to have had almost the same cell temperature and pressure with a 10-15 % reduction due to piping, purification and filtration process losses. The electrolyzer is assumed to use the recycled hot water output from the fuel cell for its water Input. In the next sections a parametric study is carried out on an individual electrolyzer unit to investigate the effect of varying the operation, economic and design parameters such as CFC, CF, ny, ir and Vc on the unit performance.

Cellt (^{o}C)	70	RHL (%)	10	O2-COST ($/kg)	0.011
Cellp (bar)	10	Ws (kW)	3850	deltap	0.1
Ta (^{o}C)	25	ETA-FRA	1	CO2PF	0.6
Vc (V)	1.815	RESF	0	WORH (h)	9.6
ir (%)	4	Cwa ($/GJ)	187	COSRESF	0.05
ny (years)	25	TIMED (h)	9.6	Cp (kJ/kg.K)	4.18
CFC ($/kW)	1500	WACCF (%)	20	Cwa1($/GJ)	373
CF (%)	30	COM ($/Kw.yr)	45	CO2-COST ($/ton)	24

Table 8.2 Design and operation parameters of electrolyzer unit at base condition and Sabha yearly average weather data

8.2.2 The fuel cell model design and operation parameters

The one MW Ballard unit adopted for the SHS analysis in this study has been simulated at the base conditions at Sabha using yearly average data. Table 8.3 illustrated the operation and design parameters adopted and estimated from the manufacture's data sheet and the previous studies [51,110,179,180] and uses as inputs for the IPSEpro model (fuel cell3e). The capacity factor CF is estimated as 50 % according to the unit working hours during the night-time, solar energy unavailability and load variations particularly at sleeping time. The unit CFC, estimated at 3000 $/kW, was offered by the producer (Appendix B), while the operation and maintenance cost factor was estimated as 2 % of the CFC cost. The unit heat losses ratio RHL were estimated as 20% of the total heat generated whereas it operated at 70 ^{o}C, 3 bars, and 0.6 V with stoichiometric ratios for hydrogen and oxygen as 1.2 and 2 respectively [36,108,114]. The other unit parameters are similar to the one considered for the PV and electrolyser units or adopted

from the manufacturer's data sheet. The temperature and the pressure of the output streams are assumed to have almost the same cell temperature and pressure with around 10-15 % of reduction losses being due to piping, purification and filtration process losses. The values of the Cwa and Cwa1 parameters are optimized by the IPSEpro based on the estimated cost of the cooling system input and output water.

Cellt (^{o}C)	70	RHL (%)	20	CO2-COST ($/ton)	24
Cellp (bar)	3	Ws (kW)	1000	deltap	0.1
Ta (^{o}C)	25	ETA-CONV (%)	95	CO2PF	0.6
Vc (V)	0.6	Cwa($/GJ)	197	WORH (h)	9.6
ir (%)	4	Cwa1 ($/GJ)	309	COSRESF	0.06
ny (years)	25	TIMED (h)	9.6	Cp (kj/kg.k)	4.18
CFC ($/kW)	3000	WACCF (%)	1	S_{to2}	2
CF (%)	50	COM ($/Kw.yr)	60	S_{th2}	1.2

Table 8.3 Design and operation parameters of fuel cell at base condition (Sabha yearly average)

8.2.3 The Compressor and heat exchangers models design and operation parameters

Two types of compressors and heat exchangers IPSEpro models for hydrogen (compressorb and htexb) and for oxygen (compressoraa and htexaa) are used in the SHS to raise up the pressure gases from 10 bars to the required storage tanks pressure and cool it to the storage temperature. The CFC of the hydrogen compressor is estimated as 615 $/kg for the (65 kg/h) unit capacity as (40000$ for the unit) and 60 $/kg for the oxygen unit at a unit capacity of 500 kg/h as (30000$ for the unit) [181]. Moreover, the cost of the heat exchanger was estimated according to the simulated UA factor of each unit, using the guidelines and procedures for selecting and costing of heat exchangers prepared by Engineering Sciences Data Unit (ESDU) in UK) [175,176]. However, an updating and inflation factor percentage for the reported 1992 prices to the current prices as 100% was considered. According to this procedure the inline hydrogen heat exchangers cost was estimated at 7000 and 4000$, while for oxygen it was 5000 and 4000$. In addition, the compressors' mechanical efficiency (etam) and the entropy efficiency (etas) were estimated, as the IPSEpro general model suggested, as being 0.98 and 0.7 respectively. The other parameters for the compressors and the heat exchanger models such as ny, ir, CF and the operation and maintenance factors were considered similar to the one estimated for fuel cell unit.

8.2.4 The storage tanks models design and operation parameters

The IPSEpro models (tankH2a) and (tankO2a) for hydrogen and oxygen tanks at low pressures have been used to simulate the SHS. The maximum tank pressure is

considered to be (34 bars) due to the maximum limit allowed by the IPSEpro package for hydrogen and oxygen gases integrated specification as ideal gases. The models have to be optimized for the necessary capacity volume according to the system's maximum output and the site weather conditions. The storage capacity for Misurata and Sabha in Libya is respectively estimated as 3.273, 3 days of the electrolyzer rated capacity, and for Newcastle it is estimated as 30 days. This estimation takes in consideration the sunshine duration time and weather conditions at each site, as well as the ability to cover the customer load using the fuel cell in the absence of solar energy. The operation and maintenance factor is estimated to be 1% of the total tank cost (CFC), whereas the other parameters are similar to the heat exchanger model inputs. However, the tanks costs are estimated as 400 $/kg for hydrogen and 26 $/kg for oxygen, based on the current low gas pressure tank prices of around 1200$/$m^3$ produced by the Libyan tracks and tanks company and the prices for similar tanks mentioned in the previous study [25,180].

8.3 IPSEpro simulation analysis of SHS at base condition

The IPSEpro model units developed for the SHS analysis were used to design and optimize a system for an average one MW peak load demand during the day and night. The load will be covered by the free stand PV system output during the daytime and using the fuel cell during the night and solar unavailability time as illustrated in Figure 8.1. The system analysis considering the unit's operation and design parameters at base conditions was presented in the previous sections for the yearly average sunshine duration for Sabha. The total installed capacity of the PV units at base conditions (Sirr=1000W/m^2, Ta= 25 ^oC, V=1m/s) is 6.287 MWh uses 26201 PV panel. However, the actual output at base condition is 4.858 MWh, assuming an ETA-CONV factor as being 95% for the PV output losses due to the DC/DC or MPPT convertor, wires, cell mismatching and soil losses. The analysis estimated a space factor of 1.54 of the total PV area, which means that the PV system required an open field area of 67262 m^2 to produce the total PV rated capacity. A two branches splitter unit (splittera) is used to distribute the PV output electricity according to the load demand during the day and the required electrolyzer input electricity to produce the sufficient amount of hydrogen for the fuel cell. Under these system operation conditions it was found that 79% of the total PV output is required for the electrolyzer input and other system units and the rest transferred directly to cover the one MW peak load. Moreover, a nine-branch splitter unit (splitteraa) is used to distribute the electricity to the system units (electrolyzer,

compressors and pumps) according to its consumptions during the operation process. Underground or municipality water at (20 to 25 ^{o}C) is assumed to be used in the cooling system. It was found that the cooling system could be produced up to 37.85 m^3/h of the hot water. The output hot water of the fuel cell and electrolyzer system represented 96% of the total produced amount. The hot water is assumed to be reused partially or totally for domestic use or utilized in a low thermal energy system and it is considered as an energy and exergy output for the unit and system analysis. The output hydrogen, oxygen and water streams of the fuel cell are recirculated and reused in the system using an IPSEpro model mixers (mixer),(mixera), and (mixeraa) for each stream type respectively. It is suggested that 3 days of the rated output capacity of the electrolyzer output are necessary to store in order to cover the load during the winter and solar unavailability time for Sabha site. The analysis shows that for the base condition at (9.6 hours) sunshine duration the total capacity volume of the hydrogen storage for 3 days is 659.78 m^3 and 327.3 m^3 for oxygen storage.

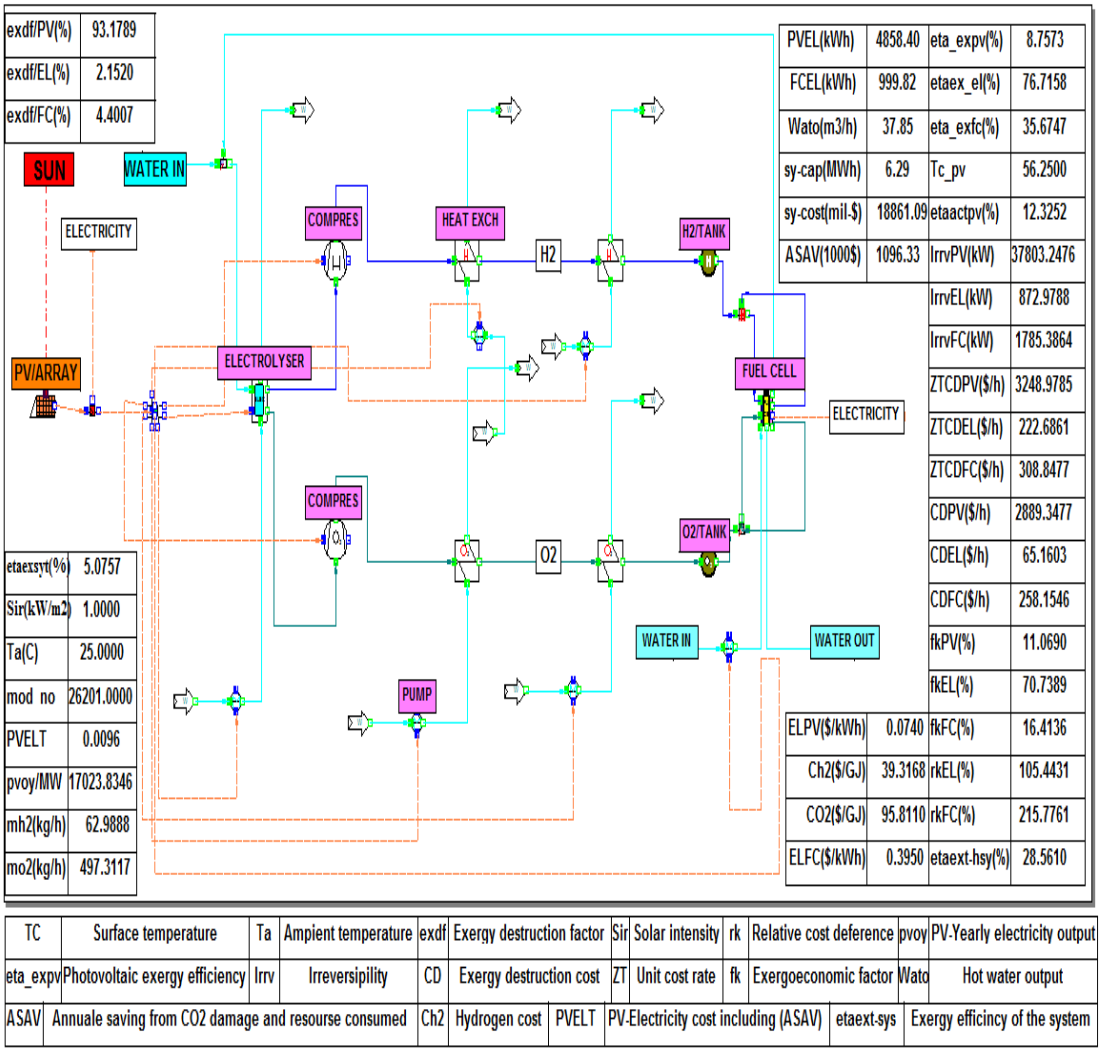

Figure 8.1 IPSEpro simulation results print screen for SHS at base condition

Two heat exchangers for each gas stream are suggested to be used to cool down the gases to the storage temperature at (25 ^{o}C) after the compression process. These heat exchangers have been shown to be working within the thermally acceptable and recommended performance range using the methodology described in section (7.4.1). It was found that in these operational conditions (base condition) a one stage heat exchanger will not be working within the recommended performance (effectiveness 80-90%) as shown in Figure 8.2.

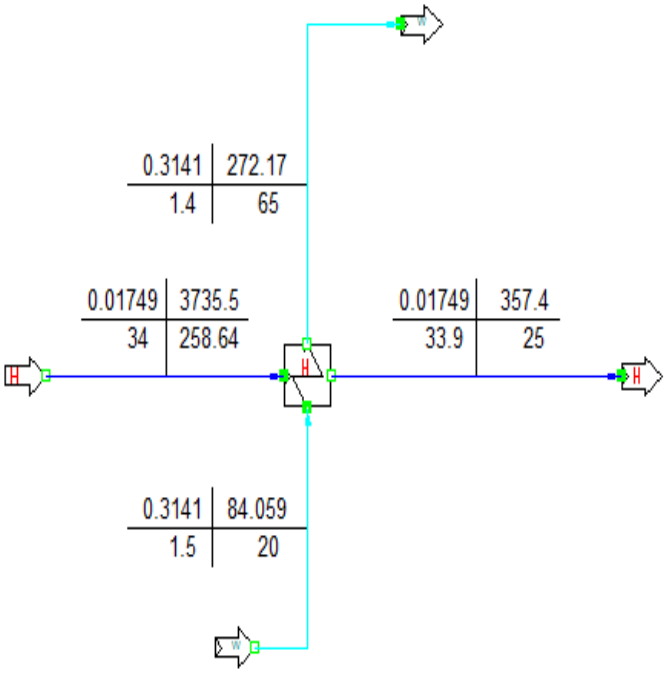

UA (kW/K)	1.145
Qtrans (kW)	59.082
Ccold (kW/k)	1.313
Chot (kW/K)	0.248
CR	0.189
Qmax (kW)	59.268
NTU	4.611
E (effectiv)(%)	100

Figure 8.2 Validation of one stage hydrogen heat exchanger working in a SHS at base condition

8.3.1 Energy and exergy analysis of SHS at base condition

The exergy destruction factor for the main SHS units presented in Figure 8.1 was calculated as 93.17% , 4.40% and 2.15% for the PV, fuel cell and the electrolyzer units respectively, whereas it was just 0.27% for the complementary units as illustrated in Figure 8.3. It is clear that the photovoltaic unit has the highest exergy destruction factor followed by the fuel cell and the electrolyzer. This is due to the high irreversibility of these units, leading to reductions in its exergy efficiencies (eta-ex) to 8.75%, 35.67% and 76.71% for the main system units respectively, as shown in table 8.4. However, the entire system exergy efficiency is calculated as 5.07 % and it is reduced to 3.35% when the total PV output is totally used to cover the load using the electrolyzer and the fuel cell. The hydrogen system exergy efficiency includes the electrolyzer and the fuel cell

and the complementary units only are found to be 28.56%. In addition, the simulation analysis shows that the actual and maximum electrical efficiency of the PV unit is 12.32% and 16.63% respectively, whereas the energy efficiency of the fuel cell and electrolyzer is raised up to 83.17 and 78.60 % if the cooling load is utilized.

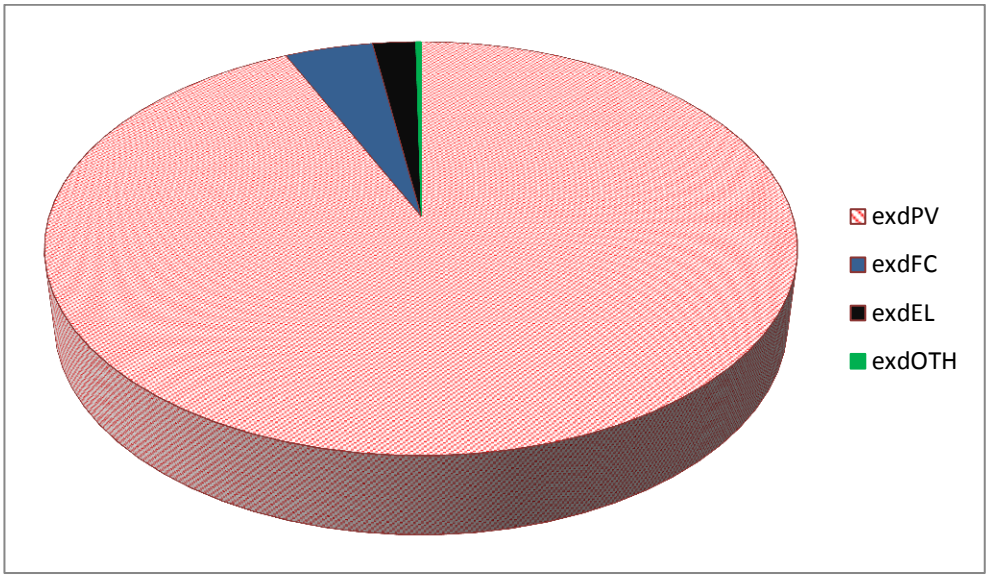

Figure 8.3 Exergy destruction factors for SHS units at base conditions

	PV	FC	EL	COMP/ H2	COMP/ O2	HEX H2/1	HEX H2/2	HEX O2/1	HEX O2/2	H2/O2 TANK
IRRV (kW)	37803	1785	872	10.09	5.93	7.46	0.63	5.16	0.3	53.43/ 25.94
eta-ex (%)	8.75	35.67	76.71	78.41	79.02	19.46	46.16	18.30	48.07	98.13/ 52.68
Sgen (kW/K)	126.70	5.988	2.92							
ex-loss (kW)	1230	38.5	7.29							
eta-energy (%)		83.17	78.6			69.94	92.80	75.47	91.93	
$\dot{Q}$-cool (kW)	0	1124	489	0	0	33.23	13.82	21.33	7.01	

Table 8.4 Energy and exergy simulation results of SHS at base condition

8.3.2 Thermo-economic evaluation of SHS at base condition

The thermo-economic evaluation parameters of the system main units and complementary units are presented in tables 8.5 and 8.6 respectively. These parameters are studied in order to evaluate and optimize the system thermo-economically for the optimum thermo-economic unit and system production costs. The units have the higher

parameter for the summation of investment and exergy destruction cost (ZTCD) is considered first for more attention and improvement possibility. The other thermo-economic evaluation parameters such as fk, rk, eta-ex, CD, ZT, and the streams exergy and unit output costs also play a significant role in the effective cost improvement of the system output.

	PV	FC	EL
ZT ($/h)	359	50	157
CD ($/h)	2889	258	65
ZTCD ($/h)	3248	308	222
C_f ($/GJ)	0	39.31	20.56
rk (%)		215	105
fk (%)	11.06	16.41	70.74
Ch2-EL ($/GJ)			38.19
Ch2-FC ($/GJ)		39.31	
CO2-EL ($/GJ)			38.57
CO2-FC ($/GJ)		91.70	
CO2-SAVA ($)	245143	50448	190758
ASOC ($)	851191	175168	662357
ELC ($/kWh)	0.0740	0.3945	0.0740
ELC-CO2 ($/kWh)	0.0596	0.3800	0.0596
ELC-ASOC ($/kWh)	0.0096	0.3300	0.0096

Table 8.5 Thermo-economic evaluation results of SHS main units

	COMP/ H2	COMP/ O2	HEX-H2/1	HEX-H2/2	HEX-O2/1	HEX-O2/2	H2/ TANK	O2/ TANK
ZT ($/h)	0.821	0.615	0.112	0.284	0.061	0.166	6.32	3.16
CD ($/h)	0.746	0.439	1.024	0.088	0.684	0.037	7.30	3.01
ZTCD ($/h)	1.568	1.055	1.1368	0.37	0.75	0.201	13.63	6.17
C_f ($/GJ)	20.56	20.56	38.12	38.04	36.80	34.15	37.96	32.28
rk (%)	57.81	63.80	-	-	-	-	3.55	184
fk (%)	52.37	58.40	9.87	76.37	8.25	81.64	46.41	51.19

Table 8.6 Thermo-economic evaluation results of SHS complementary units

The simulation results for the SHS at base conditions presented in tables 8.5, 8.6 shows that the ZTCD factor for the PV unit is the highest, followed by the fuel cell and the electrolyser. Furthermore, the low ZTCD factors of the complementary units as

presented in Table 8.6 indicate that it has not had a significant impact on the cost structure of the system production exergy cost. It is also clear that the high unit production cost of the fuel cell (ELC= 0.3945 $/kWh), compared with the current electricity cost of the traditional power plants, encourages more improvement in these systems, particularly for the main units. The low f_k factor of the PV and FC units indicates that there is a plenty of room for more investments to increase the exergy efficiency of these units and reduce its exergy destruction cost. However, the high f_k factor of the electrolyzer indicates that it is more effective to reduce the cost of the unit, even if this involves a further reduction in its exergy efficiency. On the other hand, the high relative cost difference factor r_k of the fuel cell and electrolyzer units shows that more investigation is required to pin point the most cost effective parameter (C_f , eta-ex or ZT) which needs to be improved in order to reduce its unit production exergy cost. The average exergy cost of the hydrogen and oxygen streams exiting the electrolyzer in ($/GJ) are 38.19 and 38.57 respectively. These values are increased to 39.31 and 91.70 $/GJ respectively at the entrance to the fuel cell after the cooling and the compression processes. However, the most important factor affecting the output stream exergy cost of the storage tanks is the volume and the stored pressure. Furthermore, the compression ratio as well as the electricity input value and its exergy cost have the significant impact on the compressor thermo-economic evaluation and the stream output average exergy cost.

8.3.3 The SHS environmental and resources consumed costs

The total cost of the SHS presented in Figure 8.1 according to the current prices is 28.754 m$, whereas the cost of the PV unit is 18.86 million $ and 3 million $ and 5.67 m $ for the fuel cell and the electrolyzer respectively. However, the PV output electricity cost can be reduced by 19.40% if the CO_2 direct impact cost has been considered in the analysis as presented in Table 8.5. This impact also decreases the fuel cell unit production cost by around 4%. The total annual saving cost of the SHS working at base condition relating to the CO_2 damage cost for the traditional systems has been estimated at $295,592. This also represents 25.70 % of the total system cost during its lifetime. The fossil fuel has to be consumed to produce the same quantity of power produced by SHS can be considered as a saving to be reserved as a reservoir or to cover the cost of the subsidized-tariff, as illustrated in the previous chspter. As example in Libya, the fuel and electricity are priced at around 10 to 20 % of its international price. In the SHS analysis at base condition, a factor for fuel resources consumed cost

SCF=0.05 $/kW is assumed. This factor is used to cover a part of the average fuel cost necessary to produce the same SHS power in traditional power plants, taking in consideration that the fuel cost in such plants is estimated at 40 to 60 % of the total unit output cost. The total annual resource consumed saving cost for the SHS as presented in Figure 8.1 is calculated as ASOC=1.026*10^6 $. This value, if considered along with the CO_2 damage cost, will reduce the cost of the PV output electricity unit from 0.07 to only 0.01 $/kWh and the fuel cell output electricity unit cost from 0.3945 to 0.33 $/kWh. The analysis shows also that the electrolyzer hydrogen unit thermo-economic cost will be reduced from 39.16 $/GJ to 16.69 $/GJ if the same hydrogen quantity has been produced using fossil fuel instead of solar electricity and the SCF and CO_2 damage reduction factors are considered in the analysis of standalone electrolyzer unit.

8.3.4 The effect of varying solar intensity and ambient temperature on SHS performance at base condition

The two main environment parameters affecting the performance and outputs of the SHS are the solar intensity and ambient temperature. A parametric study to investigate the effect of varying these parameters on the performance and thermo-economic factors of SHS was carried out and the results were tabulated and discussed. Tables 8.7 to 8.10 show the effect of varying (Sirr) at a constant (Ta) temperature, while Tables 8.11 until 8.21 present the effect of varying the (Sirr) and (Ta) together with regard to the SHS performance. Table 8.7 and Figures 8.4 and 8.5 show the simulation results of varying the solar intensity from 0.2 to 1 (kW/m^2) at a constant ambient temperature (Ta) on the PV energy and exergy performance factors. The results indicated that the PV power output had increased by 341% from 1.10 MWh to 4.85 MWh, whereas the irreversibility (PV-Irrv) and entropy generation (PV-Sgen) increased from 7.20 MW to 37.80 MW and from 24.27 to 126.79 (kJ/kg.K) respectively. The increase in the irreversibility was mainly caused by increasing the cell temperature from 31.50 ^oC to 56.25 ^oC and the exergy loss, leading to decreasing the exergy efficiency of the unit by 30.70% for the same range. However, the electric or actual efficiency (etaelec-act) and the maximum electrical efficiency (eta-elemax) also decreased by 11.74 and 7.50 % respectively when the solar intensity increased from 0.2 to 1 kW/m^2, as presented in Table 8.7 and figure 8.4.

Sirr (kW/m^2)	PV-power (kWh)	PV-Tc (^oC)	PV-Sgen (kW/K)	PV-eta_ elemax (%)	PV-eta_ ex (%)	PV-etaelec_ act (%)	PV-ex_ Loss (kW)	PV-Irrv (kW)
0.2	1101	31.25	24.27	17.97	12.64	13.96	53.24	7238
0.3	1627	34.37	36.62	17.81	12.14	13.76	118.58	10920
0.4	2137	37.50	49.11	17.64	11.64	13.55	208.70	14643
0.5	2632	40.62	61.73	17.48	11.14	13.35	322.84	18406
0.6	3109	43.75	74.49	17.31	10.65	13.14	460.31	22209
0.7	3571	46.87	87.37	17.14	10.17	12.94	620.42	26051
0.8	4016	50.00	100.35	16.97	9.69	12.73	802.51	29931
0.9	4445	53.12	113.52	16.80	9.22	12.53	1005.95	33848
1	4858	56.25	126.79	16.63	8.75	12.32	1230.13	37803

Table 8.7 Effect of varying (Sirr) on the PV energy and exergy factors

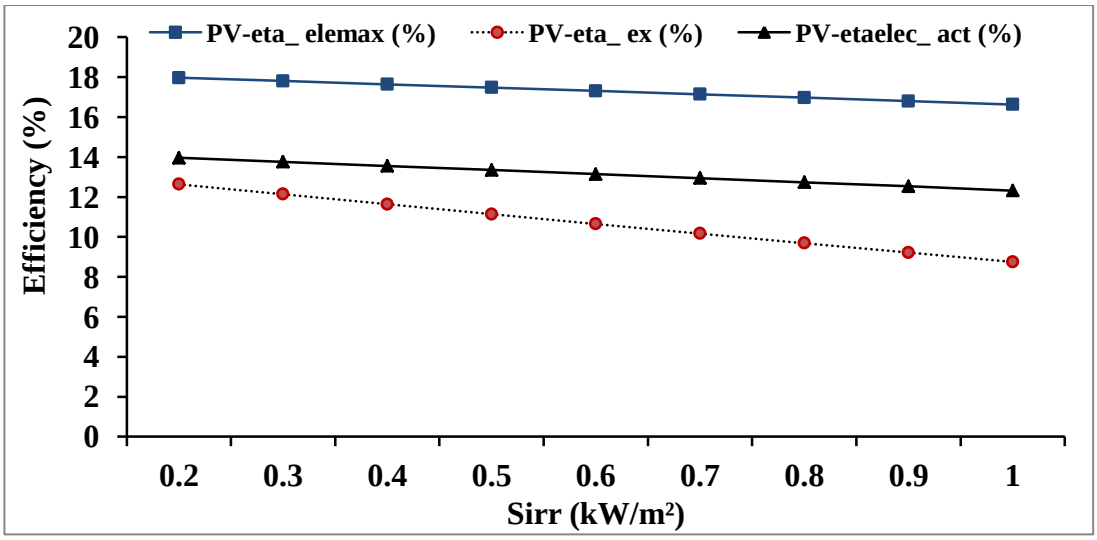

Figure 8.4 Variation of PV efficiencies with solar intensity

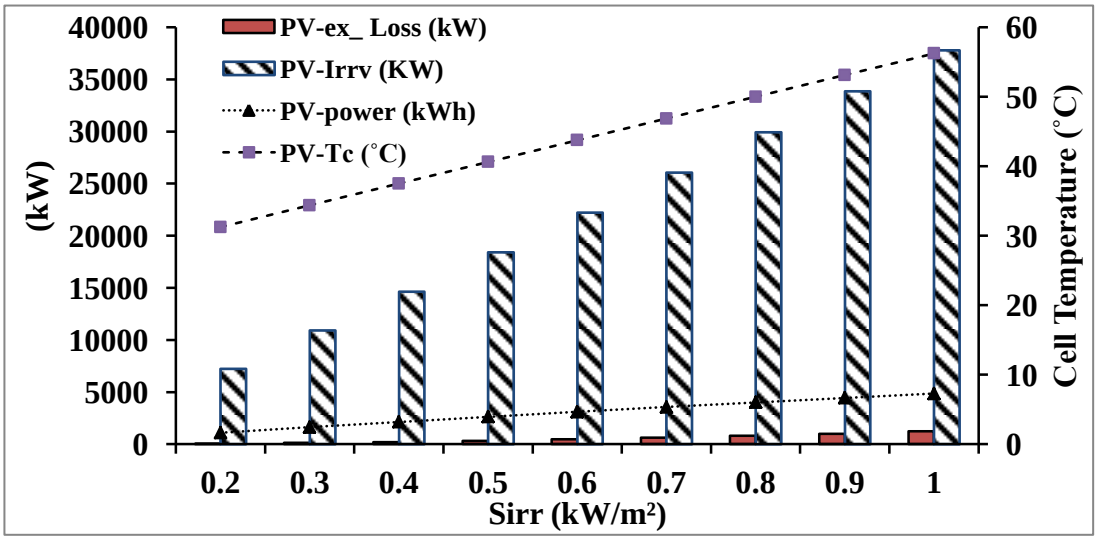

Figure 8.5 Variation of PV (power, irrv, ex_los and Tc) with solar intensity

Increasing the power output from the PV unit by increasing the solar intensity will increase the power input to the electrolyzer and the power output from the fuel cell in the same (Sirr) range, as shown in Table 8.8.

Sirr (kW/m^2)	FC-power (kWh)	FC-irrv (kW)	FC-S_gen (kJ/kg.K)	El-irrv (kW)	El-S_gene (kJ/kg K)	El-power (kWh)	EL-O2 Mass (kg/h)	EL-H2 mass (kg/h)
0.2	226.62	404.68	1.35	197.86	0.66	856.91	112.71	14.25
0.3	334.97	598.16	2.00	292.47	0.98	1266.64	166.60	21.09
0.4	439.98	785.68	2.63	384.16	1.28	1663.68	218.84	27.68
0.5	541.65	967.24	3.24	472.93	1.58	2048.12	269.38	34.09
0.6	639.98	1142.86	3.83	558.78	1.87	2419.92	318.31	40.28
0.7	734.95	1312.43	4.40	641.71	2.15	2779.06	365.54	46.29
0.8	826.59	1476.06	4.95	721.72	2.42	3125.54	411.12	52.05
0.9	914.87	1633.70	5.47	798.80	2.67	3459.36	455.04	57.63
1	999.80	1785.37	5.98	872.95	2.92	3780.51	497.26	62.96

Table 8.8 Effect of varying Sirr on the FC and EL energy and exergy factors

The parametric study shows that the power consumption of the electrolyzer presented in Figure 8.1 will increase from 857 kWh to 3780 kWh when the (Sirr) increases from 0.2 to 1 kW/m^2. This power increase will rise the hydrogen and oxygen production mass from 14.25 to 62.96 kg/h and from 112.71 to 497.62 kg/h respectively. This also increases the fuel cell power output from 226.2 kWh to 999.8 kWh for the same (Sirr) range. The power increasing to the electrolyzer and from the fuel cell also increases the unit entropy generation, as shown in Table 8.8 above and the irreversibility from 404 to 1785 kW for the fuel cell and from 197 to 872 kW for the electrolyzer. The analysis shows also that the energy efficiency, exergy efficiency, exergy loss and as a result, the thermo-economic factors of the FC and EL units, do not a significantly change with the Sirr variation. This is due to the steady state operation and constant ambient temperature assumptions and the balance in the difference between the decreasing of the power and the irreversibility reductions in the same (Sirr) range.

The effect of varying the solar intensity on the economic and the thermo-economic factors of the SHS are presented in table 8.9. The analysis shows that the exergy cost of the electricity produced by the PV (PV-EL) can be reduced by 77.33 % from 90.71 $/GJ at 0.2 kW/m^2 to 20.56 $/GJ at 1 kW/m^2. This reduction is mainly caused by the unit high power output at high solar intensity. However, this unit output exergy cost reduction dismisses the adverse effect of increasing the PV exergy destruction cost (CD) by 21 % and the PV exergoeconomic factor (fk) reduction by 16%, due to the unit

exergy efficiency decreasing at high (Sirr). For the SHS presented in Figure 8.1 the fuel cell output exergy cost (FC-EL) decreases by increasing the Sirr from 618 $/GJ to 109 $/GJ and the electrolyzer hydrogen output exergy cost (EL-Ch2) is decreasing from 184 $/GJ to 38 $/GJ for the same range of Sirr variation which appears in Table 8.9.

Sirr (kW/m^2)	PV-EL ($/GJ)	FC-EL ($/GJ)	EL-Ch2 ($/GJ)	PV-CD ($/h)	PV-ZTCD ($/h)	PV-fk (%)	FCELT ($/GJ)	ch2EF ($/GJ)	PVELT ($/kWh)
0.2	90.71	618	184.46	2381	2740	13.12	601.07	162.95	0.262
0.3	61.37	405	123.28	2438	2798	12.85	388.01	101.78	0.156
0.4	46.72	299	92.74	2498	2857	12.58	281.66	71.24	0.103
0.5	37.95	235	74.45	2559	2918	12.32	217.97	52.95	0.072
0.6	32.12	193	62.29	2621	2981	12.06	175.63	40.79	0.051
0.7	27.97	163	53.64	2685	3045	11.80	145.49	32.14	0.036
0.8	24.87	140	47.17	2751	3111	11.55	122.98	25.67	0.025
0.9	22.47	123	42.17	2819	3179	11.31	105.55	20.67	0.016
1	20.56	109	38.19	2889	3249	11.06	91.697	16.69	0.010

Table 8.9 Effect of varying the solar intensity on the economic and the thermo-economic factors of the SHS

The effect of the variation of the (Sirr) on the annual saving if the CO_2 damage and resources consumed costs are considered in the analysis is presented in table 8.10 and Figure 8.6. The results show that the annual saving in the CO_2 damage cost will be increased as the system and its unit power output increases due to increasing the solar intensity. The PV-CO2 SAVA increases from 55,564 $ to 245,139 $ as the Sirr increases, while the PV-ASOC will increase from 192,932 $ to 851,178 $ as presented in table 8.10. This annual saving increasing will result in decreasing the PV output electricity cost (PVELT) from 0.262 to 0.010 $/kWh if the CO_2 damage and fossil fuels resources consumed costs are considered, as presented in table 8.9. The fuel cell output electricity unit exergy cost also decreases from 601 $/GJ to 91 $/GJ as the Sirr increases, if the CO_2 and resources annual saving costs as presented in table 8.10, are considered. Furthermore, the Sirr variation effect on the annual environmental and resources consumed with regard to savings in the electrolyzer unit if the electricity input to the unit is considered as solar electricity instead of burning fossil fuel is presented in table 8.10. The analysis shows that the EL-CO2-SAVA is rising from 43,237 $ to 190,755$ and that the EL-ASOC is increasing from 150,130 to 662,345 $. This leads to reductions in the hydrogen output exergy cost, if the unit working individually using solar energy, from 162.9 $/GJ to 16.6 $/GJ as the (Sirr) varying from 0.2 to 1 kW/m^2 as presented in table 8.9.

Sirr (kW/m^2)	PV-CO2_ SAVA($)	PV – ASOC($)	FC-CO2_ SAVA($)	FC- ASOC($)	EL-CO2- SAVA($)	EL-ASOC ($)
0.2	55564	192932	11434	39704	43237	150130
0.3	82130	285175	16901	58686	63909	221909
0.4	107878	374577	22200	77085	83945	291477
0.5	132806	461134	27330	94897	103343	358832
0.6	156915	544843	32291	112124	122103	423970
0.7	180202	625704	37084	128764	140225	486892
0.8	202669	703713	41707	144818	157707	547595
0.9	224315	778872	46162	160285	174551	606080
1	245139	851178	50447	175165	190755	662345

Table 8.10 Effect of (Sirr) variation on the monetary annual saving from Co2 damage and resources consumed costs of the SHS main units

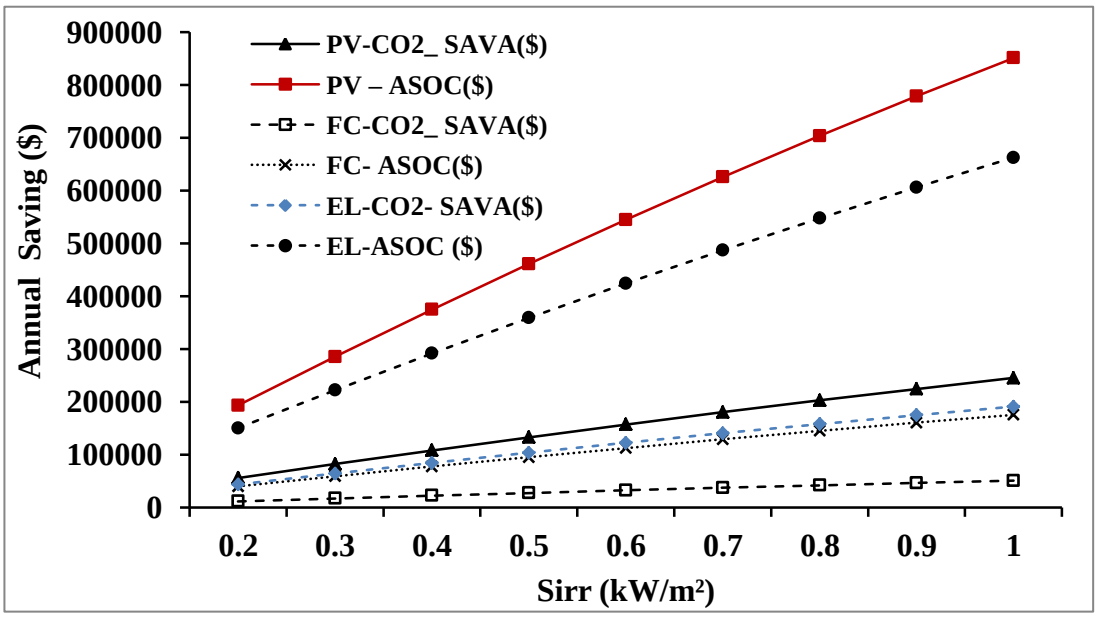

Figure 8.6 Effect of solar intensity on the (CO2_SAVA) and (ASOC)of SHS units

8.3.5 The effect of varying (Sirr) and (Ta) on PV performance and economics

The previous section illustrated the effect of varying the Sirr on the units and system's performance and the product cost at a constant ambient temperature at 25 ˚C. The change in ambient temperature will change the cell temperature, leading to changes in the performance and the unit output. However, practically varying the solar intensity will combine normally with ambient temperature changes. In the next few paragraphs, the SHS simulation results for the effects of the Sirr and Ta on the SHS main unit's performances and cost structure are tabulated and discussed. Table 8.11 illustrates the effect of varying the Sirr and the Ta on the PV surface temperature (Tc). It is clear that Tc is increasing with both Ta and Sirr increasing, but increasing Ta has a more

significant effect on increasing Tc than the effect of increasing Sirr. As an example, increasing Ta from 5 to 45 ^{o}C at Sirr=0.2 kW/m^2 will increase Tc from 11.25 to 51.25 ^{o}C (355%) whereas it will increase from 36.25 to 76.25 ^{o}C at Sirr=1 kW/m^2 (110%). However, at Ta=5^{o}C Tc increases from 11.25 ^{o}C at Sirr=0.2 kW/m^2 to 36.25 ^{o}C at Sirr= 1 kW/m^2 (222%) and by (48.7%) at Ta 45 ^{o}C.

		PV-Ta(˚C)								
PV-Tc	(˚C)	5.00	10.00	15.00	20.00	25.00	30.00	35.00	40.00	45.00
Sirr	0.20	11.25	16.25	21.25	26.25	31.25	36.25	41.25	46.25	51.25
kW/m²	0.30	14.38	19.38	24.38	29.38	34.38	39.38	44.38	49.38	54.38
	0.40	17.50	22.50	27.50	32.50	37.50	42.50	47.50	52.50	57.50
	0.50	20.63	25.63	30.63	35.63	40.63	45.63	50.63	55.63	60.63
	0.60	23.75	28.75	33.75	38.75	43.75	48.75	53.75	58.75	63.75
	0.70	26.88	31.88	36.88	41.88	46.88	51.88	56.88	61.88	66.88
	0.80	30.00	35.00	40.00	45.00	50.00	55.00	60.00	65.00	70.00
	0.90	33.13	38.13	43.13	48.13	53.13	58.13	63.13	68.13	73.13
	1.00	36.25	41.25	46.25	51.25	56.25	61.25	66.25	71.25	76.25

Table 8.11 Effect of varying (Sirr) and (Ta) on the PV surface temperature (Tc)

Increasing the PV surface temperature by increasing (Sirr) and (Ta) is reducing the PV exergy efficiency (PV-etaex) as presented in table 8.12. Unlike the (Tc) effect analysis, increasing the solar intensity has a significant effect on reducing the PV exergy efficiency which is more than the ambient temperature increasing effect. The results shows that PV-(etaex) for a unit at Sirr =0.2 kW/m^2 decreases by 17% when (Ta) changes from 5 to 45 ^{o}C. However this percentage decrease is increased to 21.34 % at Sirr=1 kW/m^2. In addition, the analysis shows that the PV-etaex will decrease by 29.10% when Sirr changes from 0.2 to 1 kW/m^2 at a constant Ta=5 ^{o}C and this percentage increases to 32.86% when the (Sirr) varies at Ta=45 ^{o}C. The results indicate that the best exergy efficiency will be achieved at the least Ta=5 ^{o}C and Sirr=0.2 kW/m^2 as PV-etaex= 13.80%.

		PV_Ta(˚C)								
PV-etaex	(%)	5.00	10.00	15.00	20.00	25.00	30.00	35.00	40.00	45.00
Sirr	0.20	13.81	13.52	13.23	12.94	12.65	12.35	12.06	11.76	11.47
kW/m²	0.30	13.29	13.00	12.72	12.43	12.14	11.85	11.56	11.27	10.98
	0.40	12.77	12.49	12.21	11.93	11.64	11.36	11.07	10.78	10.50
	0.50	12.26	11.98	11.70	11.43	11.15	10.87	10.58	10.30	10.02
	0.60	11.75	11.48	11.21	10.93	10.66	10.38	10.10	9.82	9.54
	0.70	11.25	10.98	10.72	10.45	10.17	9.90	9.63	9.35	9.07
	0.80	10.76	10.50	10.23	9.96	9.70	9.43	9.16	8.88	8.61
	0.90	10.27	10.01	9.75	9.49	9.22	8.96	8.69	8.42	8.15
	1.00	9.79	9.53	9.28	9.02	8.76	8.49	8.23	7.96	7.70

Table 8.12 Effect of varying (Sirr) and (Ta) on the PV exergy efficiency

The analysis also shows that the significant adverse effect of increasing the (Sirr) on the (PV-etaex) will vanished by increasing the unit output power and production cost reduction, as in Tables 8.13 and 8.14. Increasing (Ta) from 5 to 45 ^{o}C at Sirr =0.2 kW/m^2 will reduce the power output and increase the unit output exergy costs by 17.32% and 21% respectively. However these percentages will increase to 19.4% and 24% respectively at Sirr = 1 kW/m^2. In addition, varying Sirr from 0.2 to 1 kW/m^2 at Ta=5 ^{o}C will increase the power output and decrease the unit output exergy costs by 34.60 % and 77.58% respectively, whereas this percentage will decrease to 33% for power increasing and 54% for cost reduction respectively at Ta = 45 ^{o}C. Using this analysis, it is appears that it is recommended to maintain the PV operated at the least ambient temperature and the highest solar intensity to perform the optimum output unit exergy cost.

	Ta (˚C)								
PV-power(kW)	5	10	15	20	25	30	35	40	45
Sirr 0.2	1205.63	1179.51	1153.41	1127.31	1101.21	1075.11	1049.01	1022.91	996.81
Kw/m² 0.3	1784.31	1745.16	1706.01	1666.86	1627.71	1588.56	1549.41	1510.26	1471.11
0.4	2346.80	2294.60	2242.40	2190.20	2138.00	2085.80	2033.60	1981.40	1929.20
0.5	2893.05	2827.80	2762.55	2697.30	2632.04	2566.79	2501.54	2436.29	2371.04
0.6	3423.04	3344.74	3266.44	3188.14	3109.84	3031.54	2953.24	2874.94	2796.64
0.7	3936.77	3845.42	3754.07	3662.72	3571.37	3480.02	3388.67	3297.32	3205.97
0.8	4434.23	4329.83	4225.43	4121.03	4016.63	3912.23	3807.83	3703.43	3599.03
0.9	4915.42	4797.97	4680.52	4563.07	4445.62	4328.17	4210.72	4093.26	3975.81
1	5380.33	5249.83	5119.33	4988.82	4858.32	4727.82	4597.32	4466.82	4336.32

Table 8.13 Effect of varying (Sirr) and (Ta) on the PV power output

	Ta(˚C)								
PV-EL ($/GJ)	5	10	15	20	25	30	35	40	45
Sirr 0.2	82.85	84.69	86.61	88.62	90.72	92.92	95.23	97.66	100.22
kW/m² 0.3	55.98	57.24	58.56	59.93	61.37	62.89	64.47	66.15	67.91
0.4	42.56	43.54	44.55	45.61	46.72	47.89	49.12	50.42	51.78
0.5	34.53	35.33	36.16	37.04	37.95	38.92	39.93	41.00	42.13
0.6	29.18	29.87	30.58	31.33	32.12	32.95	33.83	34.75	35.72
0.7	25.38	25.98	26.61	27.27	27.97	28.71	29.48	30.30	31.16
0.8	22.53	23.07	23.64	24.24	24.87	25.53	26.23	26.97	27.76
0.9	20.32	20.82	21.34	21.89	22.47	23.08	23.72	24.41	25.13
1	18.57	19.03	19.51	20.02	20.56	21.13	21.73	22.36	23.04

Table 8.14 Effect of varying (Sirr) and (Ta) on the PV- output exergy cost

8.3.6 The effect of varying (Sirr) and (Ta) on fuel cell and electrolyzer performance and economics

The variations in the solar intensity and ambient temperature in SHS have a significant and direct effect on PV performance and an indirect effect on the other units. This effect is mainly seen through the variation of the electrolyzer input electricity cost and capacity as well as the hydrogen production mass and cost. The effect of varying the (Sirr) and (PV-Ta) factors of a SHS operated at base conditions on the electrolyzer power input (EL-powerin) and (EL-Irrv) is illustrated in Table 8.15 and Table 8.16. It is clear that the (EL-powerin) and (EL-Irrv) are reduced as the (Sirr) decreasing and (PV-Ta) increases. However, the decrease in the (Sirr) has a significant reduction effect on these parameters compared with increasing (Ta) reduction effect . This reduction has an identical percentage, as the examples and data presented for the PV-power values show in Table 8.13.

		PV-Ta(˚C)								
EL-powerin	(kW)	5.00	10.00	15.00	20.00	25.00	30.00	35.00	40.00	45.00
Sirr	0.20	938.17	917.84	897.53	877.22	856.91	836.60	816.29	795.98	775.67
Kw/m²	0.30	1388.47	1358.00	1327.54	1297.07	1266.61	1236.14	1205.68	1175.21	1144.75
	0.40	1826.16	1785.54	1744.93	1704.31	1663.69	1623.07	1582.45	1541.83	1501.21
	0.50	2251.23	2200.45	2149.68	2098.90	2048.13	1997.35	1946.58	1895.81	1845.03
	0.60	2663.64	2602.71	2541.79	2480.86	2419.93	2359.00	2298.07	2237.14	2176.21
	0.70	3063.41	2992.32	2921.24	2850.15	2779.07	2707.98	2636.90	2565.81	2494.73
	0.80	3450.51	3369.27	3288.03	3206.79	3125.55	3044.31	2963.07	2881.83	2800.59
	0.90	3824.94	3733.55	3642.15	3550.76	3459.36	3367.97	3276.57	3185.18	3093.79
	1.00	4186.71	4085.16	3983.61	3882.06	3780.51	3678.96	3577.41	3475.86	3374.31

Table 8.15 Effect of varying (Sirr) and (Ta) on the (EL- powerin)

		PV-Ta(˚C)								
EL-Irrv	(kW)	5.00	10.00	15.00	20.00	25.00	30.00	35.00	40.00	45.00
Sirr	0.20	216.63	211.94	207.25	202.56	197.87	193.18	188.49	183.80	179.11
kW/m²	0.30	320.61	313.58	306.54	299.51	292.47	285.44	278.40	271.37	264.33
	0.40	421.68	412.30	402.92	393.54	384.16	374.78	365.40	356.02	346.64
	0.50	519.83	508.11	496.38	484.66	472.93	461.21	449.49	437.76	426.04
	0.60	615.06	600.99	586.92	572.86	558.79	544.72	530.65	516.58	502.51
	0.70	707.37	690.96	674.54	658.13	641.72	625.30	608.89	592.47	576.06
	0.80	796.76	778.00	759.24	740.48	721.72	702.96	684.20	665.44	646.69
	0.90	883.22	862.12	841.01	819.91	798.80	777.70	756.60	735.49	714.39
	1.00	966.76	943.31	919.86	896.41	872.96	849.51	826.06	802.61	779.16

Table 8.16 Effect of varying (Sirr) and (Ta) on the (EL-Irrv)

The variation of the (El-powerin) due to varying the (Sirr) and (PV-Ta) will cause variations in the quantity of hydrogen produced and its cost in the same trend as shown in tables 8.17 and 8.18. The hydrogen mass production (ELh2-mass) will be reduced by 21% when the (PV-Ta) increases from 5 to 45 ^{o}C at Sirr=0.2 kW/m^2 due to the reduction of (El-powern). This percentage reduction increases to 24% at Sirr= 1 kW/m^2. In addition, the (ELh2-mass) increases by 346 % when the Sirr increases from 0.2 to 1 kW/m^2 (at Ta=5˚C). This percentage is reduced to 335 % at Ta=45˚C. Reducing the (ELh2-mass) due to increasing (PV-Ta) at the constant of the other parameters will increase its exergy cost (EL-ch2). However, increasing Sirr will reduce (EL-ch2) and this reduction trend will decrease as the (PV-Ta) is increased. As an example, the EL-ch2 increases by 21.50% when Ta is varies from 5 to 45 ^{o}C at Sirr=0.2. This percentage increases to 27.33% at Sirr=1 kW/m^2. In addition, the EL-ch2 is reduced by 393% when Sirr varies from 0.2 to 1 kW/m^2 at Ta =5 ^{o}C and this percentage of reduction will be reduced to 375% at Ta=45 ^{o}C, as shown in table 8.18. The results shows that the best hydrogen production mass and exergy cost will be achieved when the PV-unit operated at Sirr=1 Kw/m^2 and PV-Ta=5 ^{o}C as EL-ch2 =34 $/GJ and a mass of ELh2-mass = 69 kg/h. This optimum exergy cost will be achieved at the unit maximum; power consumed, irreversibility and production capacity as shown in tables 8.15, 8.16 and 8.17 respectively. Consequently, the thermo-economic evaluation technique is the proper tool to investigate which more economically viable and the optimum operation parameters values that can improve the unit in terms of its exergy destruction cost and power input for the optimum production mass and cost.

		PV-Ta(˚C)								
ELh2.mass (kg/s)		5	10	15	20	25	30	35	40	45
Sirr	0.2	0.004342	0.004248	0.004154	0.00406	0.003966	0.003872	0.003778	0.003684	0.00359
Kw/m²	0.3	0.006426	0.006285	0.006144	0.006003	0.005862	0.005721	0.00558	0.005439	0.005298
	0.4	0.008452	0.008264	0.008076	0.007888	0.0077	0.007512	0.007324	0.007136	0.006948
	0.5	0.010419	0.010184	0.009949	0.009714	0.009479	0.009244	0.009009	0.008774	0.008539
	0.6	0.012328	0.012046	0.011764	0.011482	0.0112	0.010918	0.010636	0.010354	0.010072
	0.7	0.014178	0.013849	0.01352	0.013191	0.012862	0.012533	0.012204	0.011875	0.011546
	0.8	0.015969	0.015593	0.015217	0.014841	0.014465	0.014089	0.013713	0.013337	0.012961
	0.9	0.017702	0.017279	0.016856	0.016433	0.01601	0.015587	0.015164	0.014741	0.014318
	1	0.019377	0.018907	0.018437	0.017967	0.017497	0.017027	0.016557	0.016087	0.015617

Table 8.17 Effect of varying (Sirr) and (PV-Ta) on the (ELh2-mass)

		PV-Ta(˚C)								
EL-ch2	($/GJ)	5.00	10.00	15.00	20.00	25.00	30.00	35.00	40.00	45.00
Sirr	0.20	168.08	171.91	175.90	180.08	184.46	189.05	193.87	198.94	204.27
Kw/m²	0.30	112.05	114.67	117.41	120.28	123.28	126.44	129.75	133.23	136.91
	0.40	84.08	86.09	88.21	90.42	92.74	95.18	97.74	100.44	103.29
	0.50	67.32	68.98	70.72	72.54	74.46	76.47	78.59	80.82	83.17
	0.60	56.17	57.60	59.09	60.65	62.30	64.03	65.85	67.77	69.80
	0.70	48.23	49.49	50.81	52.19	53.64	55.18	56.79	58.49	60.29
	0.80	42.30	43.43	44.62	45.87	47.18	48.56	50.02	51.56	53.20
	0.90	37.70	38.74	39.82	40.97	42.18	43.45	44.79	46.21	47.71
	1.00	34.04	35.00	36.01	37.07	38.20	39.38	40.63	41.95	43.36

Table 8.18 Effect of varying (Sirr) and (PV-Ta) on the (EL-ch2)

The variation caused in the electrolyzer hydrogen production mass and exergy cost by varying the solar intensity and ambient temperature will vary the fuel cell output power (FC-powero), irreversibility (FC-Irrv) and its exergy cost (EL-FC) as shown in tables 8.19, 8.20, 8.21. The fuel cell output power will slightly decrease as the (PV-Ta) increases, whereas it will dramatically increase as the (Sirr) increases. The analysis shows that at Sirr = 0.2 kW/m^2 the (FC-powero) decreased from 248 kW at PV-Ta= 5 ^{o}C to 205 kW at PV-Ta = 45 ^{o}C and from 1107 kW to 892 kW at Sirr = 1 kW/m^2. On the other hand, the (FC-powero) increases from 248 kWh at Sirr= 0.2 kW/m^2 to 1107 kWh at Sirr = 1 kW/m^2 at PV-Ta= 5 ^{o}C, while it is increases from 205 kWh at Sirr=0.2 kW/m^2 to 892 kWh at Sirr = 1 kW/m^2 at PV-Ta=45 ^{o}C. The analysis shows that the optimum fuel cell output unit exergy cost is achieved at the maximum production power output at PV-Ta= 5 ^{o}C and Sirr= 1 kW/m^2 as 95.10 $/GJ, as shown in table 8.21.

		PV_Ta(˚C)								
FC-powero	kW	5	10	15	20	25	30	35	40	45
Sirr	0.2	248.11	242.73	237.36	231.99	226.62	221.25	215.88	210.51	205.14
kW/m²	0.3	367.20	359.14	351.08	343.03	334.97	326.91	318.86	310.80	302.74
	0.4	482.95	472.21	461.47	450.73	439.98	429.24	418.50	407.76	397.01
	0.5	595.37	581.94	568.51	555.08	541.65	528.23	514.80	501.37	487.94
	0.6	704.43	688.32	672.21	656.09	639.98	623.87	607.75	591.64	575.53
	0.7	810.16	791.36	772.56	753.76	734.96	716.16	697.36	678.56	659.76
	0.8	912.53	891.05	869.56	848.08	826.59	805.11	783.62	762.14	740.65
	0.9	1011.55	987.38	963.21	939.04	914.87	890.70	866.53	842.36	818.19
	1	1107.23	1080.37	1053.52	1026.66	999.80	972.95	946.09	919.24	892.38

Table 8.19 Effect of varying (Sirr) and (PV-Ta) on the (FC-powero)

FC-Irrv (kW)		PV-Ta (°C) 5	10	15	20	25	30	35	40	45
Sirr	0.2	443.05	433.46	423.86	414.27	404.68	395.09	385.50	375.91	366.32
Kw /m²	0.3	655.71	641.32	626.94	612.55	598.16	583.78	569.39	555.00	540.61
	0.4	862.42	843.24	824.05	804.87	785.69	766.50	747.32	728.14	708.95
	0.5	1063.16	1039.18	1015.20	991.22	967.24	943.26	919.29	895.31	871.33
	0.6	1257.92	1229.15	1200.38	1171.60	1142.83	1114.05	1085.28	1056.50	1027.73
	0.7	1446.71	1413.14	1379.57	1346.00	1312.43	1278.86	1245.29	1211.72	1178.15
	0.8	1629.52	1591.16	1552.79	1514.43	1476.06	1437.69	1399.33	1360.96	1322.60
	0.9	1806.35	1763.19	1720.03	1676.87	1633.71	1590.55	1547.38	1504.22	1461.06
	1	1977.20	1929.24	1881.29	1833.33	1785.37	1737.41	1689.46	1641.50	1593.54

Table 8.20 Effect of varying (Sirr) and (PV-Ta) on the (FC-Irvv)

EL-FC	$/GJ	PV_Ta(°C) 5	10	15	20	25	30	35	40	45
Sirr	0.2	561.92	575.24	589.15	603.71	618.96	634.95	651.74	669.38	687.95
kW/m²	0.3	366.80	375.92	385.46	395.44	405.91	416.89	428.43	440.56	453.35
	0.4	269.36	276.40	283.75	291.46	299.55	308.04	316.97	326.36	336.27
	0.5	211.01	216.79	222.85	229.20	235.87	242.87	250.25	258.01	266.20
	0.6	172.19	177.15	182.35	187.80	193.53	199.55	205.90	212.59	219.65
	0.7	144.54	148.91	153.50	158.32	163.39	168.72	174.34	180.27	186.54
	0.8	123.87	127.81	131.95	136.30	140.87	145.69	150.77	156.14	161.83
	0.9	107.85	111.46	115.26	119.25	123.45	127.87	132.55	137.49	142.73
	1	95.10	98.45	101.97	105.68	109.59	113.71	118.06	122.67	127.56

Table 8.21 Effect of varying (Sirr) and (PV-Ta) on the (EL-FC)

8.4 Parametric study of a stand-alone photovoltaic PV unit

The PV unit can be evaluated thermo-economically and individually in any weather and time conditions by using the IPSEpro model (PV_Cellba). Figure 8.7 represents the simulation results for a unit at Sirr = 0.6 kW/m^2, Ta = 10 ^{o}C and the other parameters are similar to the parameters of the base conditions.

Sirr(kW/m2)	0.60	CD ($/h)	2423.63	ASOC ($)	586166.66	A_cell(m2)	0.0243
Ta(C)	10.00	ZTCD ($/h)	2783.26	CO2-SAVA($)	168816.00	Cell_no	60.00
Tc(C)	28.75	fk (%)	12.9212	PVEL($/kWh)	0.0931	modu_no	26201.00
V_wind(m/s)	1.00	ZT ($/h)	0.0999	PVELT($/kWh)	0.0431	At (m2)	43677.07

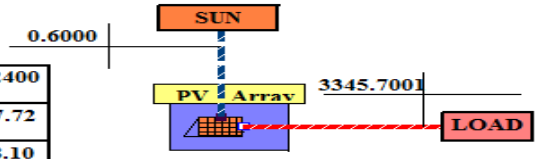

P_sta(kW)	0.2400					eta_expv(%)	11.4837
Voc_sta(V)	37.72					eta_sta(%)	14.3943
Ioc_sta(A)	8.10					eta_elact(%)	14.1460
Vm_sta(V)	31.49	Voc_act(V)	37.221	Irrv (kW)	22064.18	eta_elmax(%)	18.1228
Im_sta(A)	7.62	Ioc_act(A)	4.8700	Sgen(KJ/KgK)	77.92	ex_loss(kW)	483.1884
F_Fsta	0.7854	F_Fact	0.7415	Qloss(kW)	7779.98	CFC ($/kW)	3000.0000

Figure 8.7 Thermo-economic analysis of a PV standalone (Model/PV_Cellba)

The photovoltaic model developed in this study is used to investigate the unit individually or within a system thermo-economically. The model is used to determine; the unit power output, the I-V characteristics change and the performance at any time of the day, as presented in Figure 8.7. The results shows that the exergy efficiency of the PV unit in this condition is 11.48% compared to only 8.75% at the base condition. This is mainly due to the low cell temperature achieved at this condition, leading to decreasing the ex_loss and irreversibility compared to its values at the base condition. However, the power output of 3.345 MWh is less than the one at the base condition at 4.858 MWh, leading to increases in the unit output exergy cost from 0.0740 to 0.0931. In addition, Figures 8.8 to 8.13 present the results of a parametric study which was implemented to investigate the effect of the PV operation and economic parameters on the unit and SHS performance and outputs. Table 8.22 and Figure 8.8 represent the effect of varying the PV capacity factor (CF) and capital cost (CFC) on the unit output electricity cost. The analysis shows that the PV unit exergy cost is increasing from 1.46 $/GJ at CF=100 % and CFC=500 $/kW to 16.03 $/GJ, if the CFC is increasing to 5500 $/kW. Furthermore, the unit output exergy cost will dramatically increase to 146 $/GJ if the CF decreases to 10% at CFC=5500$/kW.

		PV_CF									
	PV-cw($/GJ)	10	20	30	40	50	60	70	80	90	100
PV_CFC($/kW)	500	13.28	6.71	4.52	3.43	2.77	2.33	2.02	1.79	1.60	1.46
	1000	26.55	13.42	9.04	6.85	5.54	4.67	4.04	3.57	3.21	2.91
	1500	39.83	20.13	13.56	10.28	8.31	7.00	6.06	5.36	4.81	4.37
	2000	53.11	26.84	18.09	13.71	11.08	9.33	8.08	7.14	6.41	5.83
	2500	66.38	33.55	22.61	17.13	13.85	11.66	10.10	8.93	8.01	7.28
	3000	79.66	40.26	27.13	20.56	16.62	14.00	12.12	10.71	9.62	8.74
	3500	92.94	46.97	31.65	23.99	19.39	16.33	14.14	12.50	11.22	10.20
	4000	106.22	53.68	36.17	27.42	22.16	18.66	16.16	14.28	12.82	11.66
	4500	119.49	60.39	40.69	30.84	24.93	20.99	18.18	16.07	14.43	13.11
	5000	132.77	67.10	45.21	34.27	27.70	23.33	20.20	17.85	16.03	14.57
	5500	146.05	73.81	49.74	37.70	30.47	25.66	22.22	19.64	17.63	16.03

Table 8.22 Effect of PV-CF and CFC on the PV output exergy cost (cw)

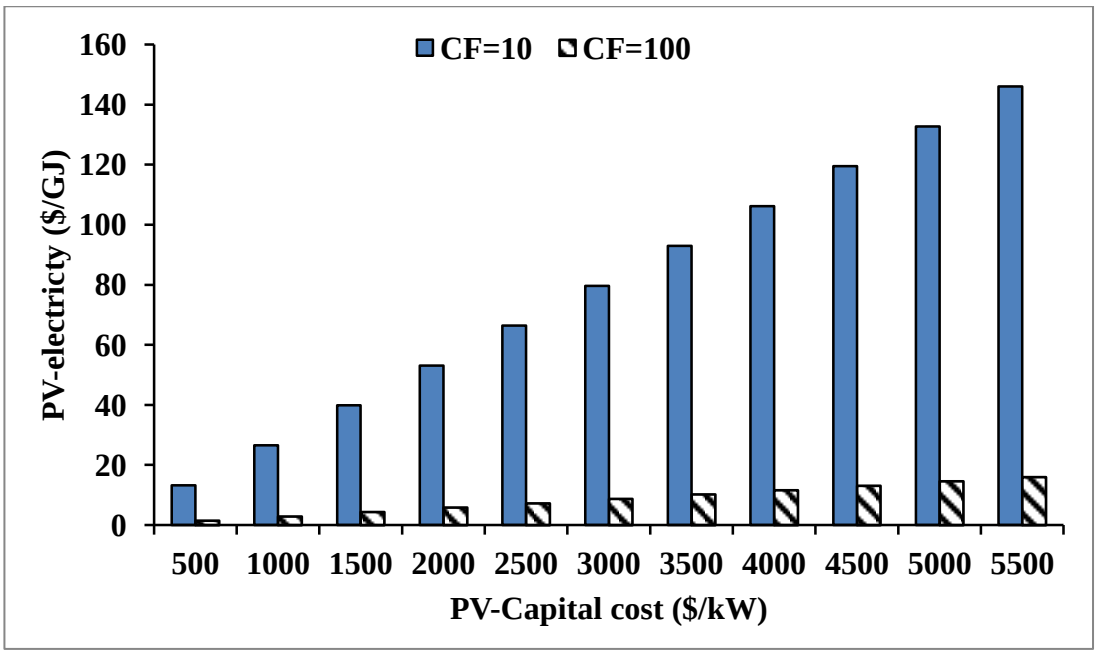

Figure 8.8 Varying of PV output exergy cost with the unit capital cost at different capacity factor

The effect of PV/CF and CFC on the electrolyzer output hydrogen exergy cost and fuel cell electricity output exergy cost is shown in Figures 8.9 and 8.10. The Figures show that decreasing the capacity factor from 100 to 10 % causing an increase in the hydrogen exergy cost by 539 % at CFC=5500 $/kW and by 124 % at CFC= 500 $/kW. The same trend of effect can be conducted by varying these parameters on the fuel cell electricity output exergy cost, as presented in Figure 8.10.

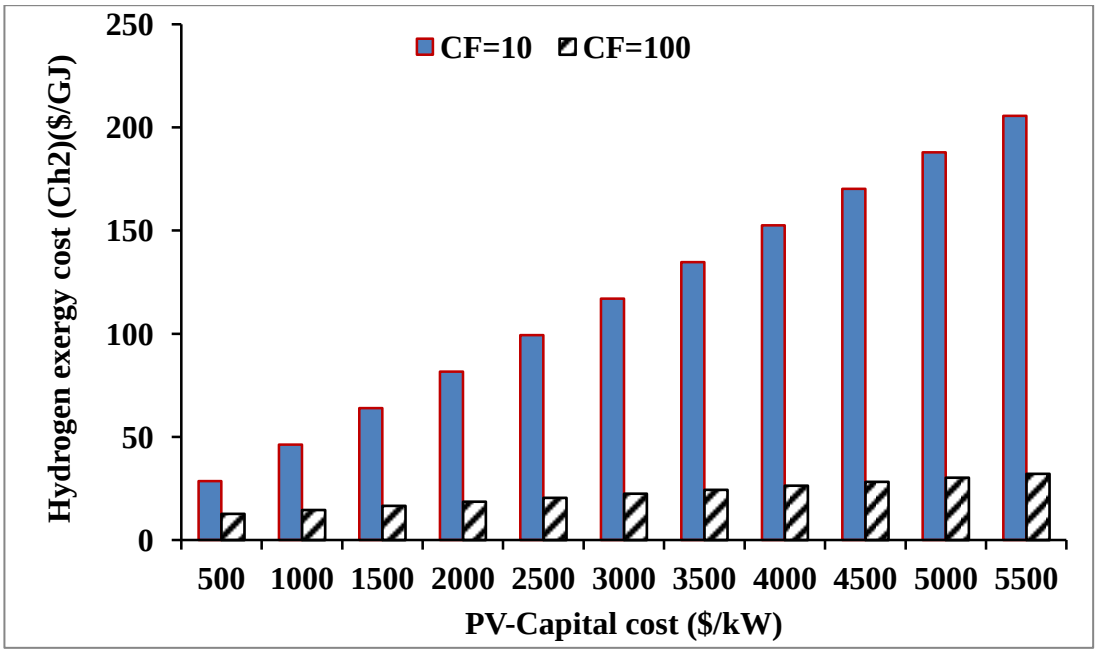

Figure 8.9 Varying of hydrogen exergy cost with varying the unit CFC and CF

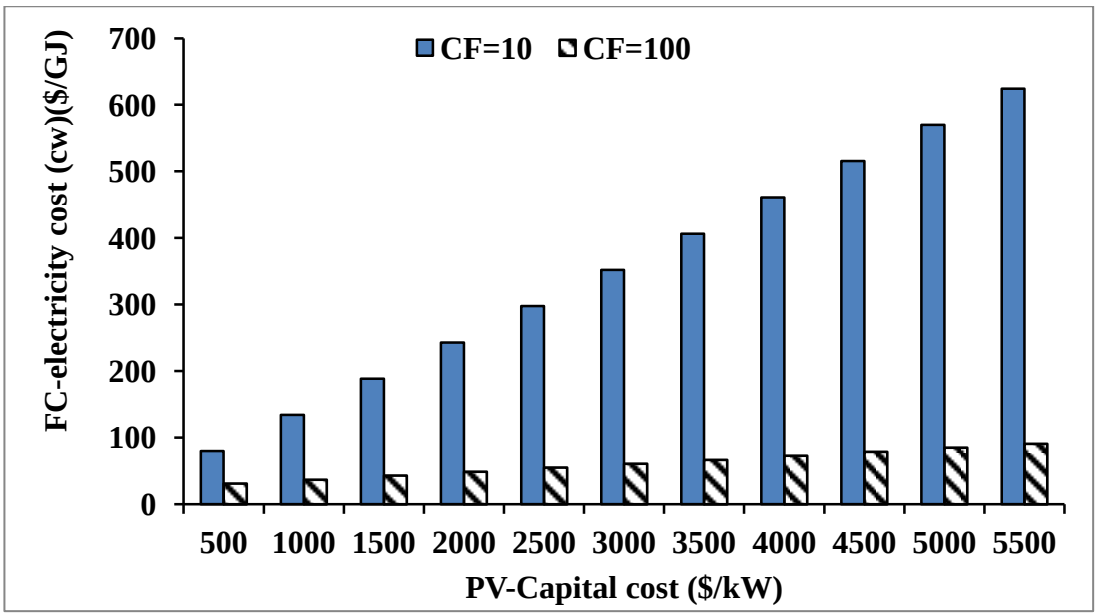

Figure 8.10 Varying of fuel cell electricity cost with varying unit CFC and CF

The effects of the PV unit lifetime (ny) and the interest rate (ir) on the PV and fuel cell exergy unit production electricity cost (cw) and the electrolyzer hydrogen exergy cost (Ch2) are presented in Figures 8.11, 8.12 and 8.13 respectively. These figures show that both parameters (ir and ny) have a significant effect on the unit's production costs. However, increasing the lifetime has a more significant effect than that of increasing the interest rate. As an example, the PV electricity cost (cw) at ny=50 years increases from 8.71 at ir = 1% to 31.91 $/GJ at ir=10 % and to 82 $/GJ if the ny is reduced to 5 years at ir=10%, as presented in Figure 8.11.

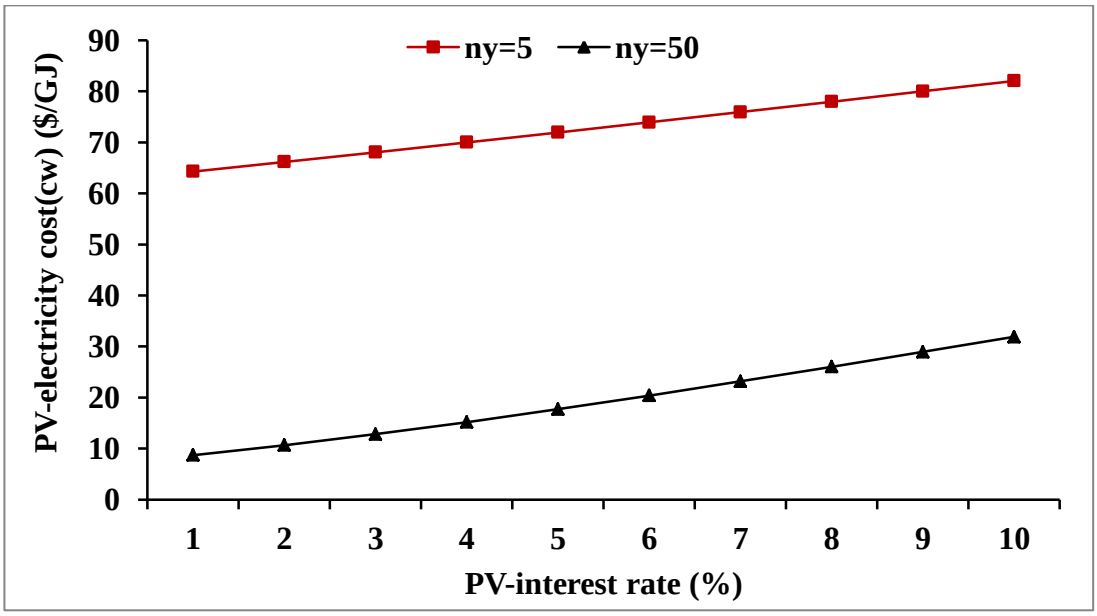

Figure 8.11 Effect of PV (ir and ny) on the unit output electricity cost (cw)

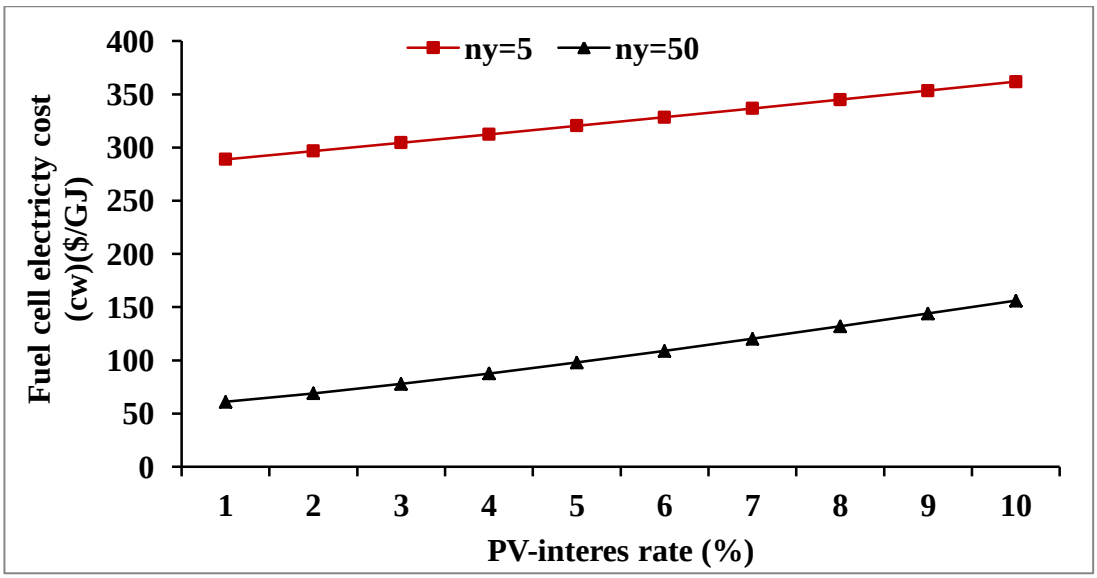

Figure 8.12 Effect of PV (ir and ny) on the fuel cell output electricity cost (cw)

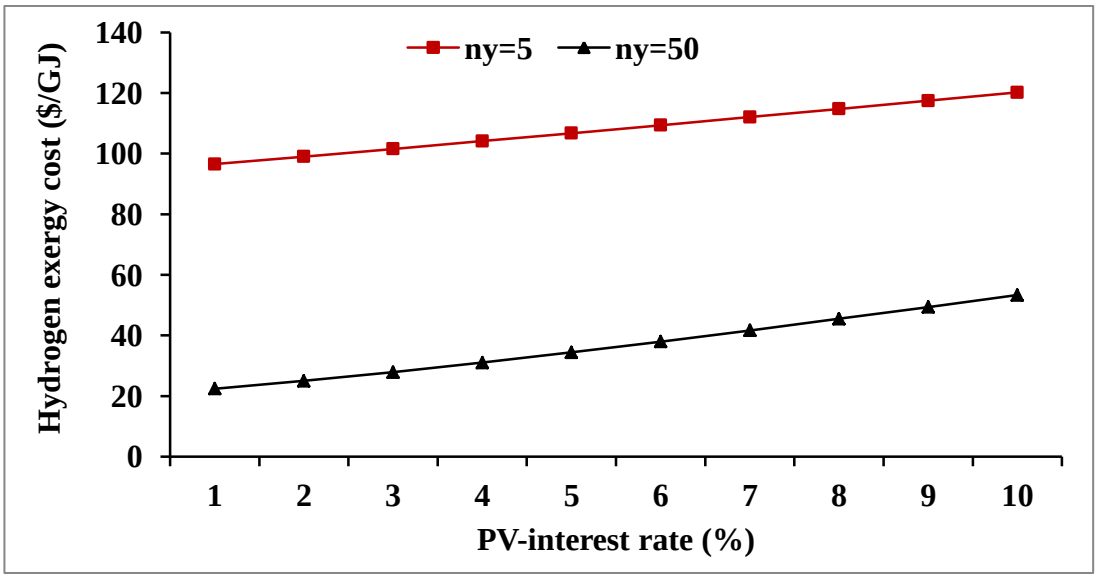

Figure 8.13 Effect of PV (ir and ny) on the hydrogen exergy cost (cw)

8.5 Simulation analysis and parametric study of a stand-alone electrolyzer unit (EL) with and without recycling

The IPSEpro (electrolyzerba) and (electrolyzerbaa) thermo-econmic models are used to investigate a unit individually with and without cooling or recycling water respectively as presented in Figures 8.14 and 8.15. The results shows that the exergy and energy efficiency is increased as well as the hydrogen exergy cost is reduced when a cooling system and a recycled input water is used. The hydrogen exergy cost thus decreases by 10% when cooling and recycled input water is used.

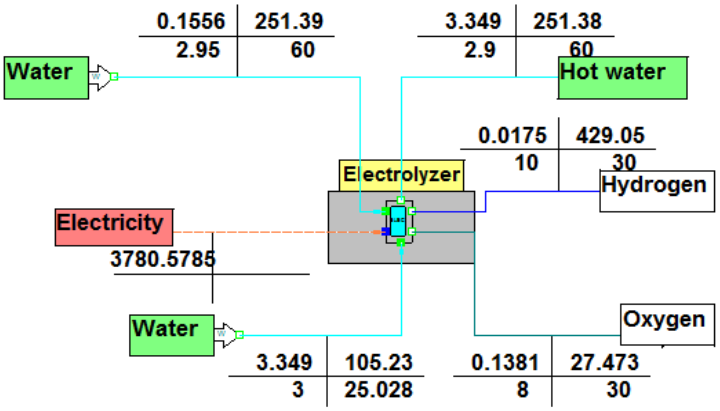

Irrv(kW)	872.9461
Sgene(kJ/kg k)	2.9279
eta_exe(%)	76.7167
eta_ene(%)	78.6048
ZTCD($/h)	222.6837
CD($/h)	65.1579
fk(%)	70.7397
rk(%)	105.4416
Cw($/kWh)	0.0740
mh2(kg/h)	62.9888
Co2($/GJ)	38.5790
mo2(kg/h)	497.3117
mHot water(kg/h)	12057.4350
Ch2($/GJ)	38.1975
Ch2_EF($/GJ)	16.6811

Figure 8.14 Thermo-economic analysis of a standalone electrolyzer with cooling and water recycling (base condition)

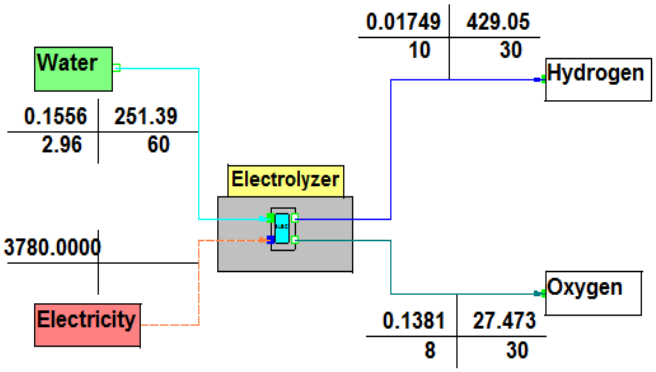

Irrv(kW)	835.6501
Sgene(kJ/kg K)	2.8028
eta_exe(%)	75.9721
eta_ene(%)	65.6542
ZTCD($/h)	224.7787
CD($/h)	67.2529
rk(%)	106.7372
fk(%)	70.0804
Ch2_EF($/GJ)	18.6382
mH2(kg/h)	62.9792
Co2($/GJ)	38.5790
mo2(Kg/h)	497.2356
mwaterin(kg/h)	560.2147
Ch2($/GJ)	42.5023

Figure 8.15 Electrolyzer without cooling or water recycling (base condition)

8.5.1 Effect of operation and economic parameters on electrolyzer performance

Increasing the electrolyzer power input from 1000 kW to 4000 kW at the base condition will reduce the hydrogen output exergy cost by 54%. This reduction is mainly caused by increasing the hydrogen mass by 302% even with the increases of the unit irreversibility and exergy destruction costs, as presented in table 8.23 and Figure 8.16.

EL-power(kW)	Ch2($/GJ)	H2-mass(kg/s)	EL-CD($/h)	EL-rk(%)	EL-Irrv_ente(kW)
1000	81.13	0.0046	17.23	314.24	230.90
1500	61.67	0.0069	25.85	219.61	346.36
2000	51.94	0.0093	34.47	172.29	461.81
2500	46.11	0.0116	43.09	143.91	577.26
3000	42.21	0.0139	51.70	124.98	692.71
3500	39.44	0.0162	60.32	111.46	808.16
4000	37.35	0.0185	68.94	101.32	923.62

Table 8.23 Effect of varying electrolyzer power input on unit performance and outputs

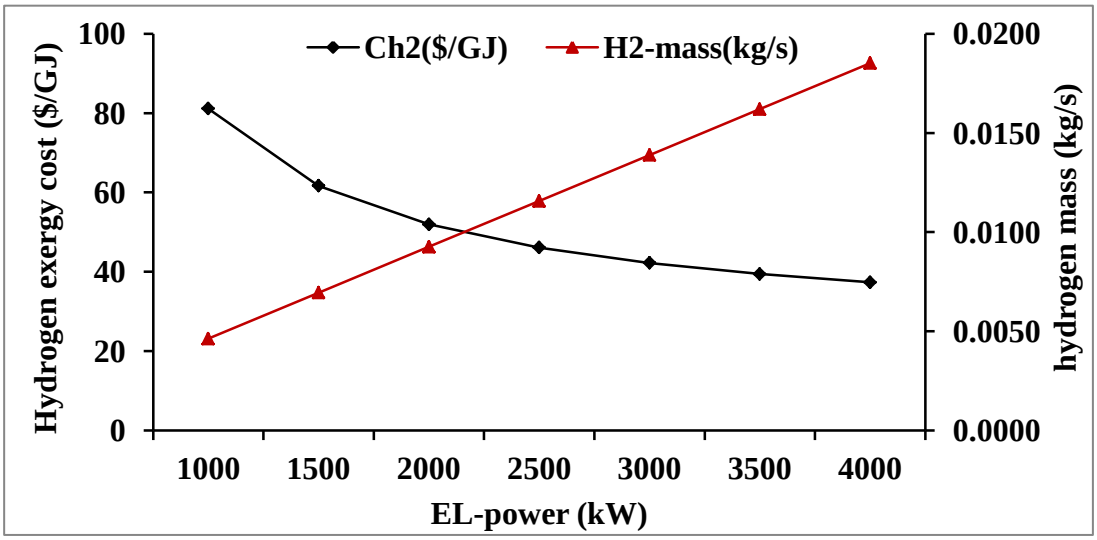

Figure 8.16 Effect of electrolyzer power input on hydrogen mass and cost

The analysis of the SHS and its units at base conditions assumes that it is working at or near to the rated capacity at a specific temperature, pressure and voltage in a steady state condition. However, varying the electrolyzer unit operated cell voltage (Vc) will affect its performance and outputs as presented in table 8.24 and Figure 8.17. The analysis shows that increasing the electrolyzer cell voltage from 1.6 to 2 V at a constant input power will reduce its exergy efficiency by 19% and its energy efficiency by 2%. This is due to increasing its irreversibility by 121%, leading to a decrease in the output hydrogen mass by 19.70% and an increase in the hydrogen exergy cost of 12.22%.

EL-Vc (V)	EL-CD($/h)	EL-eta_exe(%)	EL-eta_energye (%)	EL-Irrv (kW)	Ch2 ($/GJ)	H2-mass(kg/s)
1.6	37.80	86.49	79.49	507.72	35.84	0.0198
1.7	51.39	81.64	79.05	689.08	36.94	0.0187
1.8	63.46	77.32	78.66	850.30	38.03	0.0176
1.9	74.27	73.46	78.31	994.55	39.13	0.0167
2	83.99	69.99	77.99	1124.37	40.22	0.0159

Table 8.24 Effect of varying electrolyzer cell voltage on the unit performance and outputs

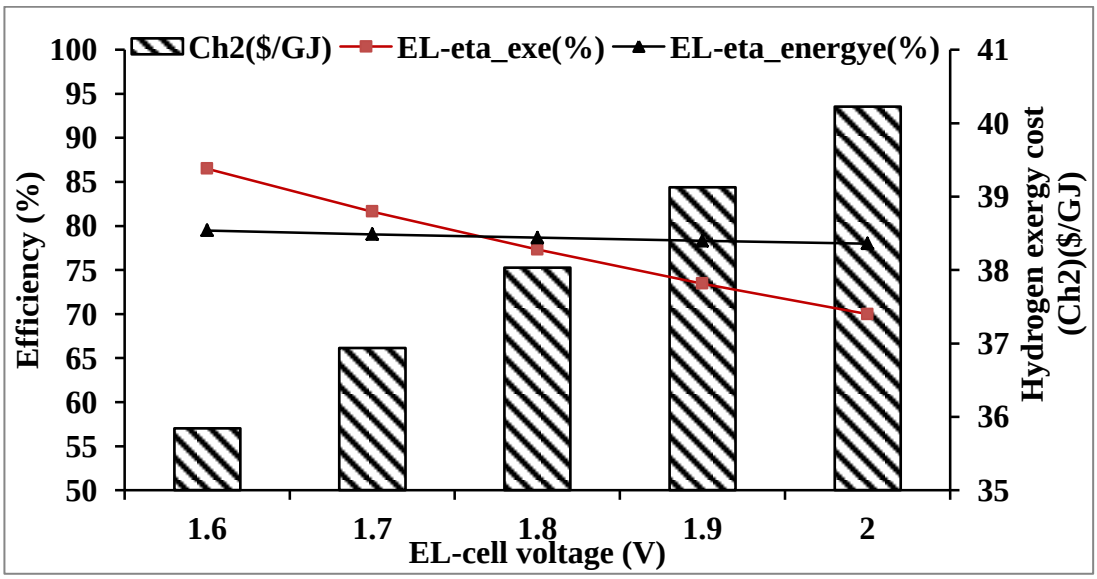

Figure 8.17 Effect of varying electrolyzer cell voltage on the unit exergy and energy efficiency and hydrogen exergy cost

Decreasing the electrolyzer input electricity exergy cost at a base condition from 50 to 5 $/GJ with the constant of the other economic parameters such as CF, CFC, ny, ir will reduce the unit hydrogen output exergy cost by 77.5 %, as illustrated in table 8.2 and Figure 8.18. This reduction will decrease the unit exergy destruction cost (CD) dramatically and increase the exergoeconomic (fk) and relative difference (rk) factors at the constant of a ZT factor. Meanwhile, increasing the (fk) and (rk) factors with decreasing its input fuel cost (cw) at the constant of its exergy efficiency means that more attention has to be focused on reducing the unit investment cost (ZT).

EL-cw($/GJ)	Ch2($/GJ)	EL-CD($/h)	EL-fk(%)	EL-rk(%)
5	17.44	15.84	90.86	339.15
10	24.11	31.69	83.25	184.75
15	30.78	47.53	76.82	133.28
20	37.45	63.38	71.31	107.55
25	44.12	79.22	66.54	92.11
30	50.79	95.07	62.36	81.82
35	57.46	110.91	58.68	74.46
40	64.13	126.75	55.41	68.95
45	70.80	142.60	52.49	64.66
50	77.47	158.44	49.85	61.23

Table 8.25 Effect of varying electrolyzer input electricity exergy cost on the unit performance and output costs

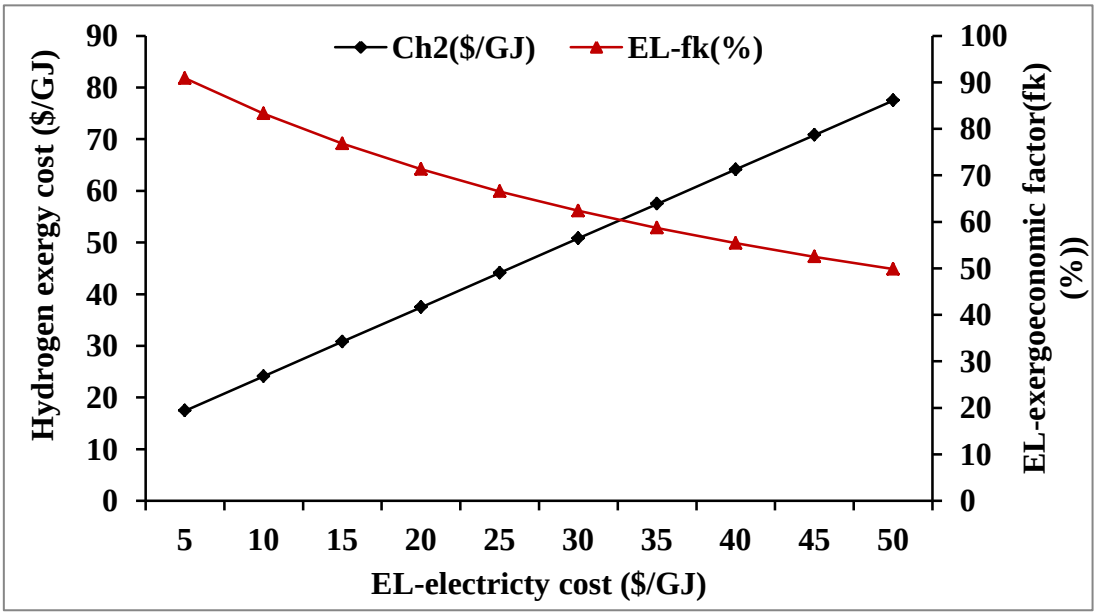

Figure 8.18 Effect of varying electrolyzer input electricity exergy cost on the unit output hydrogen exergy cost and exergoeconomic factor

The capacity factor (CF) of the electrolyzer has a significant effect on the exergy cost of the produced hydrogen, as presented in Figure 8.19, particularly when its value is less than 40%. The figure shows that increasing the unit capacity factor from 10 to 100 % will decrease the produced hydrogen cost by 56%. In addition Figure 8.20 shows that increasing the electrolyzer capital cost (CFC) from 300 to 3300 $/kW at the constant of the other economic parameters will increase the hydrogen exergy cost by 99 %.

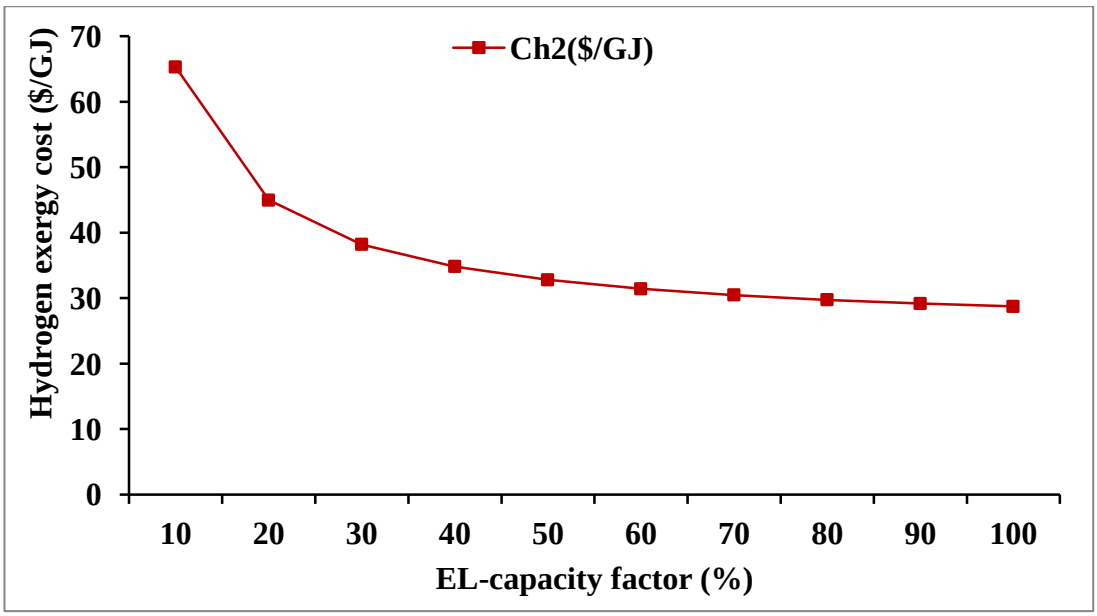

Figure 8.19 Effect of varying electrolyzer CF on hydrogen exergy cost

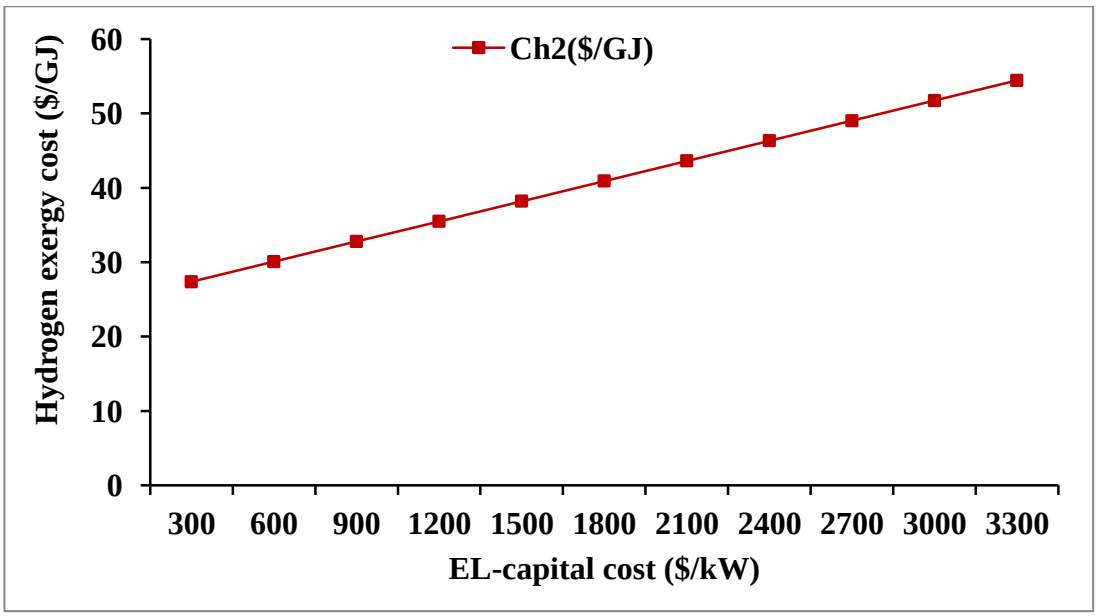

Figure 8.20 Effect of varying electrolyzer CFC on hydrogen exergy cost

The effects of varying the electrolyzer lifetime (ny) and interest rate (ir) on the produced hydrogen exergy cost and the summation of the investment and exergy destruction factor (ZTCD) appear in Figure 8.21 and 8.22 respectively. The analysis shows that increasing the interest rate from 1 to 10% at ny=5 years will increase the hydrogen exergy cost by 17.89%, whereas it will increase by 75% if its lifetime increases from 5 to 50 years at ir =10 %. However, this percentage will increase to 127% if the unit lifetime increases from 5 to 50 years at an interest rate of 1 %. The unit ZTCD factor also increases as the unit lifetime and interest rate increasing, as shown in Figure 8.22.

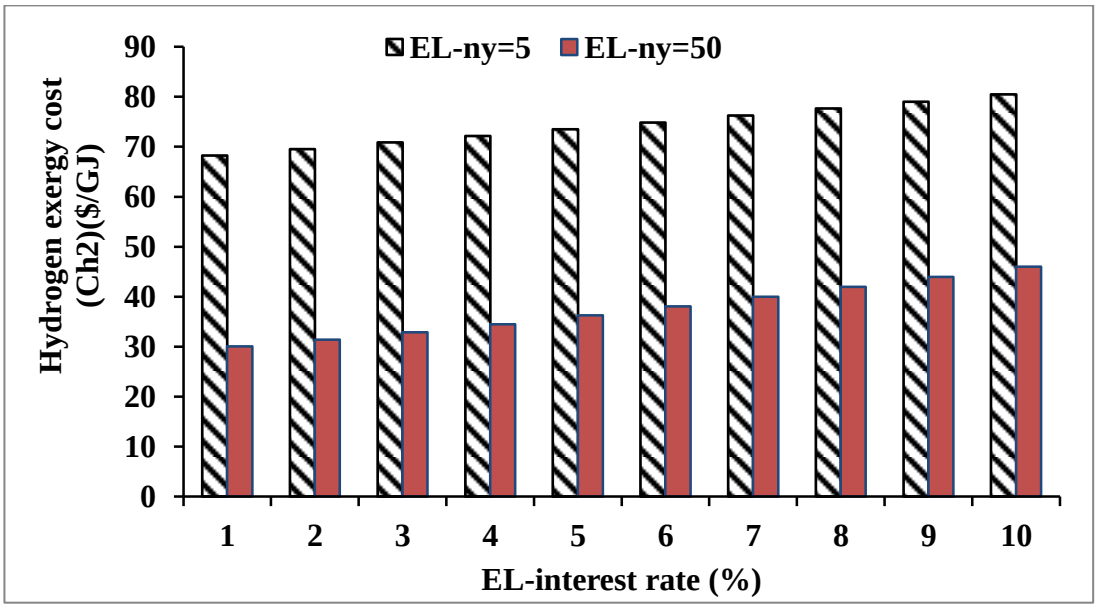

Figure 8.21 Effect of electrolyzer lifetime and interest rate on the output hydrogen exergy cost

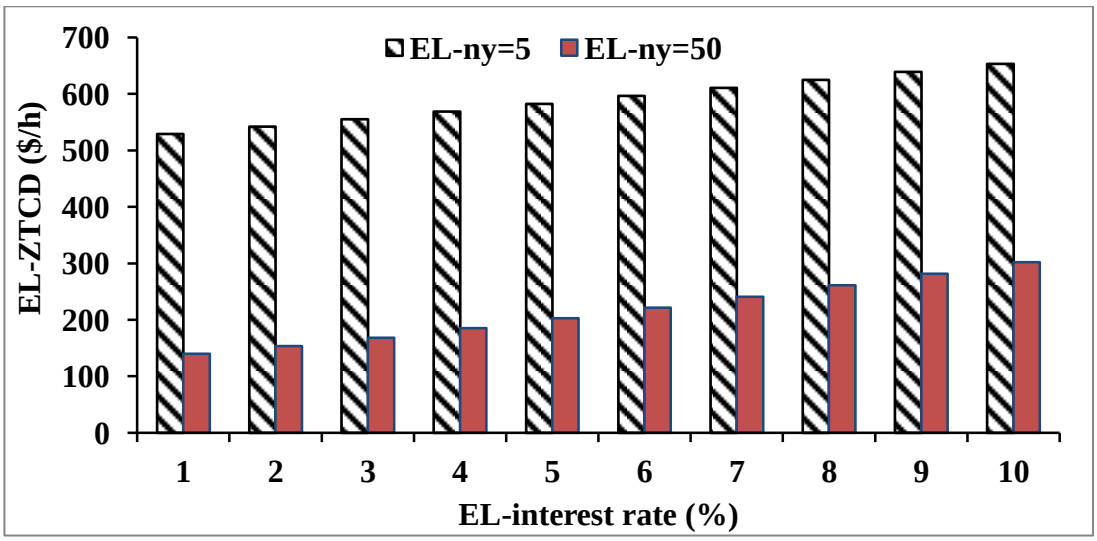

Figure 8.22 Effect of electrolyzer lifetime and interest rate on the electrolyzer ZTCD factor

8.7 Parametric study of a stand-alone Fuel cell (FC) unit with and without recycling

Four different IPSEpro models developed to investigate a standalone fuel cell working at its rated capacity are examined in this section. Figure 8.23 presents a print screen of the simulation results of (fuel-cell3) model used for energy and exergy analysis of a 10 kW rated capacity unit. The analysis is performed on experiment tested 10 kW PEM fuel cell stacks as developed by Energy Partner Inc.

The fuel cell consists of 40 cells with an active cell area of 780 cm^2, capable of generating 10 kW power output at 40 % efficiency at 3 bars and 65 ^oC. The IPSEpro results for the unit performance and outputs agreed with the data provided by the produced company and previous study [110].

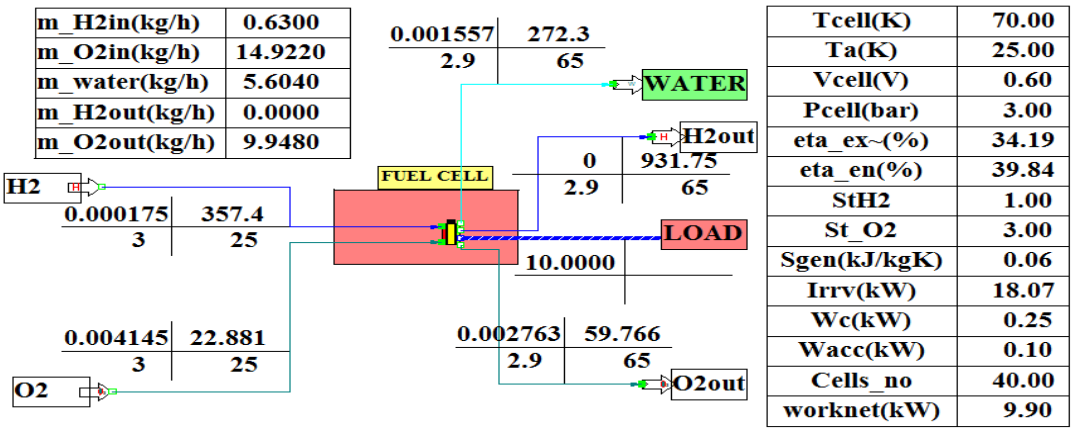

Figure 8.23 IPSEpro model (fuel_cell3) simulation results of 10 kW PEM fuel cell

The IPSEpro thermo-economic model (fuel_cell3e) is used to individually simulate the unit used in the SHS designed at base condition in section 8.2 with a cooling system and stream recycling, as shown in Figure 8.24. The model (fuel_cell3f) is used for a similar unit without gas streams recycling, and the model (fuel_cell3b) used to investigate a unit without cooling and stream recycling system as presented in Figures 8.25 and 8.26 respectively. The analysis shows that the exergy efficiency of the FC unit with cooling and recycling is enhanced by 30% when a cooling and output streams recycling system is used. It will also be enhanced by 21% when the gas streams recycled unit is used. This is due to the reduction of the exergy loss, leading to decreasing the unit output electricity cost and exergy destruction factor and an increase in the exergoeconomic factor, as shown in the Figures. The unit electricity cost increases from 0.3946 $/kWh for a unit at base condition with cooling and recycling system to 0.5614 $/kWh for a unit without a cooling or recycling system. The hydrogen mass required to produce the same quantity of power increases from 63 kg/h for a unit with a cooling and recycling system to 76 kg/h for a unit without a cooling or recycling system.

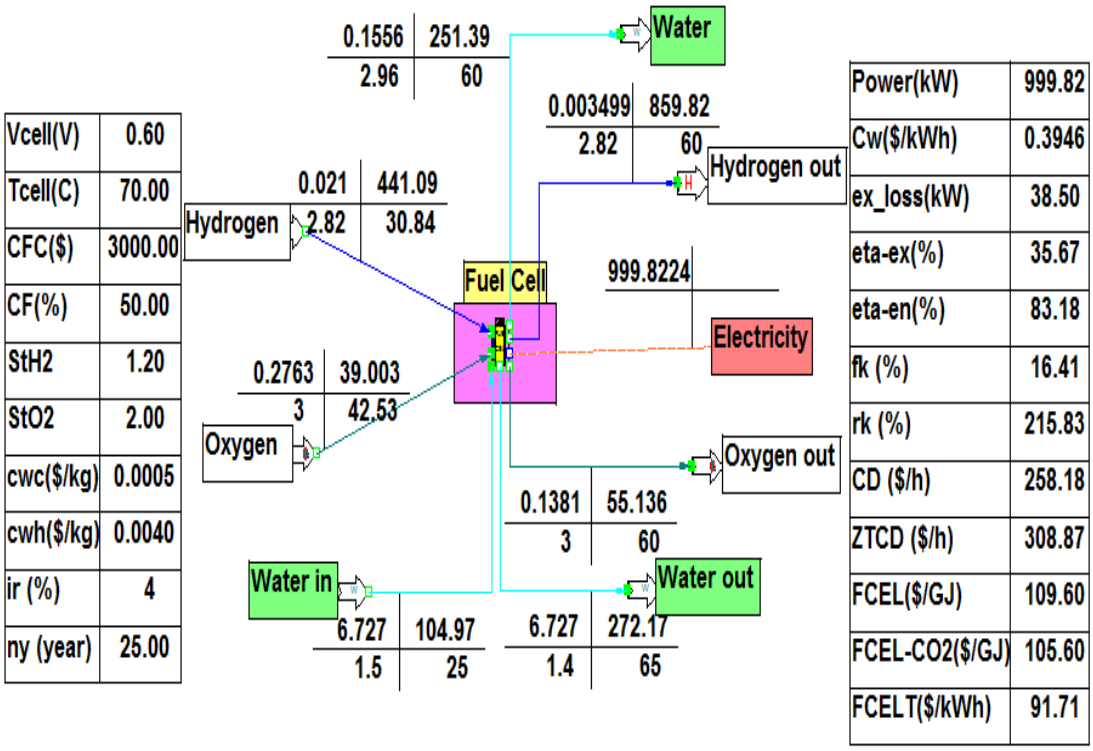

Figure 8.24 Thermo-economic analysis of standalone fuel cell with cooling and recycling (base condition model-fuel_cell3e)

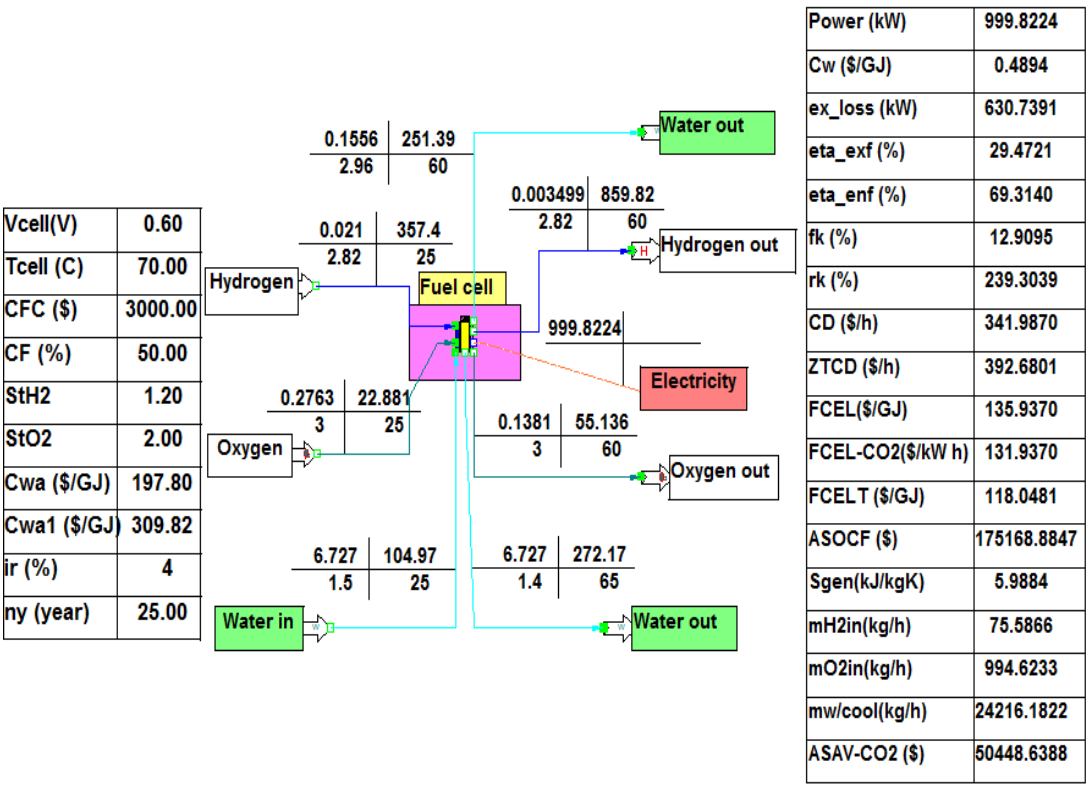

Figure 8.25 Thermo-economic analysis of standalone fuel cell with cooling and without gas recycling (base condition model-fuel_cell3f)

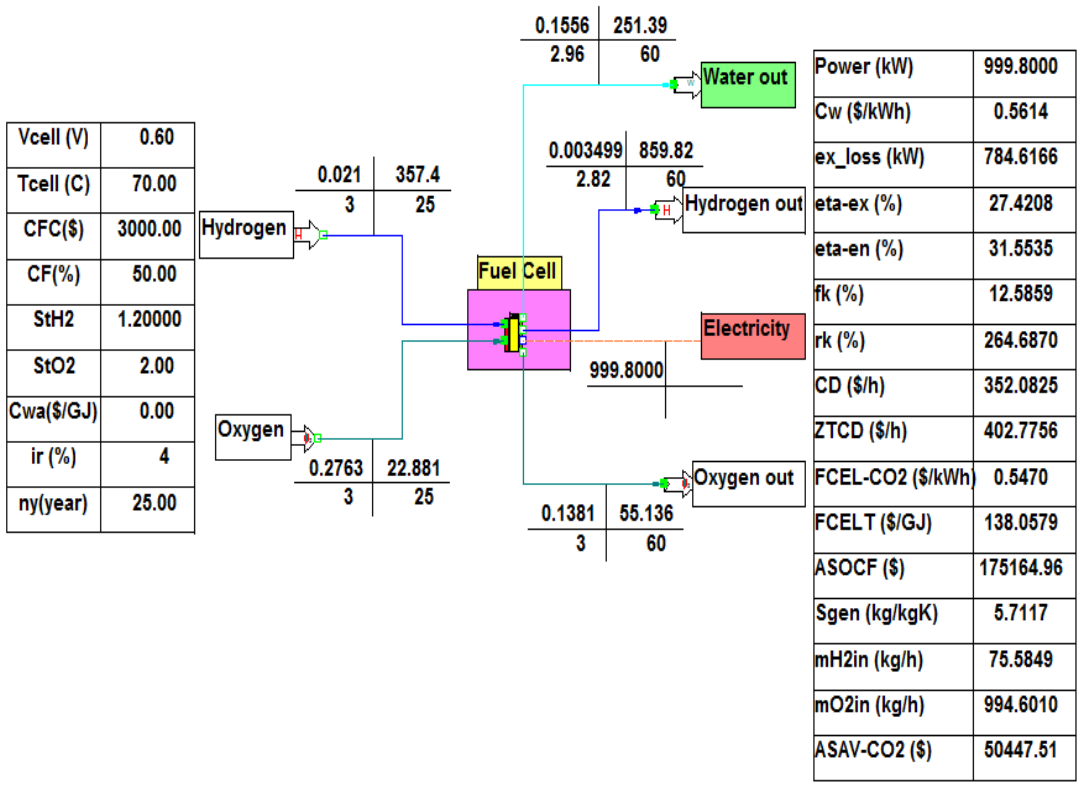

Figure 8.26 Thermo-economic analysis of standalone fuel cell without cooling or output streams recycling (base condition model-fuel_cell3b)

8.7.1 Effect of operation and economic parameters on fuel cell performance

The cell voltage has been considered as a constant value optimized at the chosen unit rated capacity and operation parameters adopted for the analysis of the SHS in this study. However, as mentioned in chapter 6, the voltage loss depends on different operation and design parameters such as the cell temperature, pressure, membrane type, membrane thickness, unit element materials and structure as well as the current density. As shown in Figures 8.27 and 8.28, increasing the cell voltage at a constant output power reduces the heat generated ($\dot{Q}$gen) in the unit and the unit irreversibility, leading to a reduction in the required hydrogen mass consumption needed to produce the same quantity of power. This slightly increases both the energy efficiency and the exergy efficiency, as shown in Figure 8.27. Increasing the exergy efficiency is reflected in reducing the unit output electricity and exergy destruction costs and increasing the exergoeconomic factors with constancy of the other parameters such as the investment cost. Increasing the cell voltage from 0.6 V to 0.7 V will increase the exergy efficiency by 14.30 % and the energy efficiency by 1.10%, while the quantity of hydrogen needed to produce the same quantity of power is reduced by 14.28%.

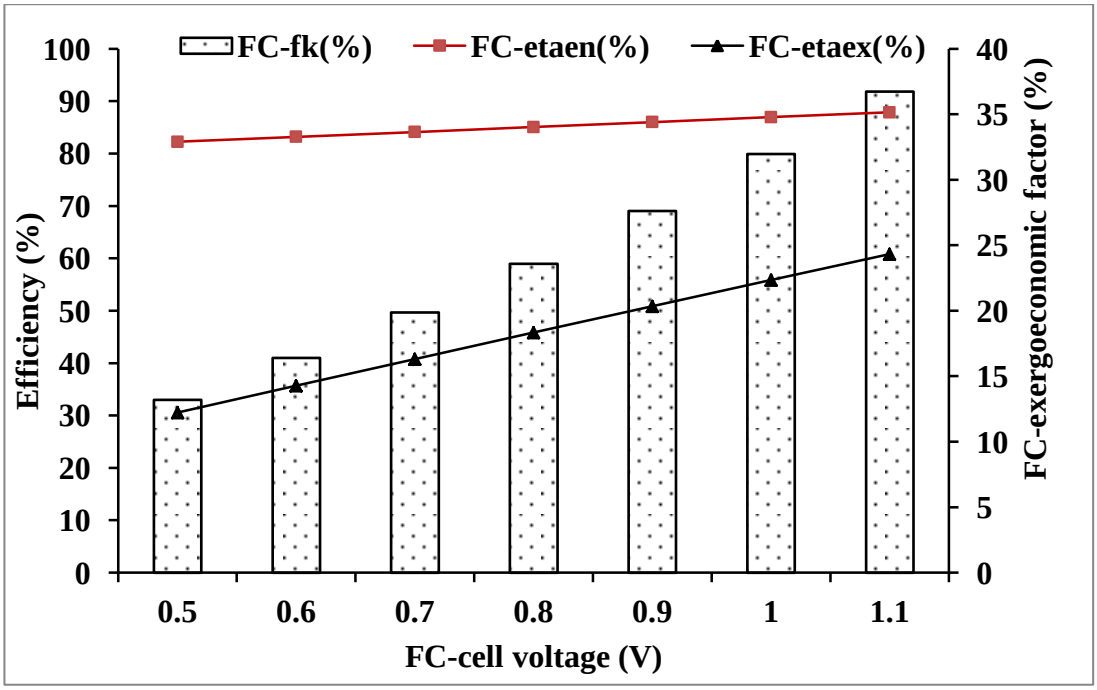

Figure 8.27 Effect of varying fuel cell voltage on the unit exergy and energy efficiency and exergoeconomic factor at constant power

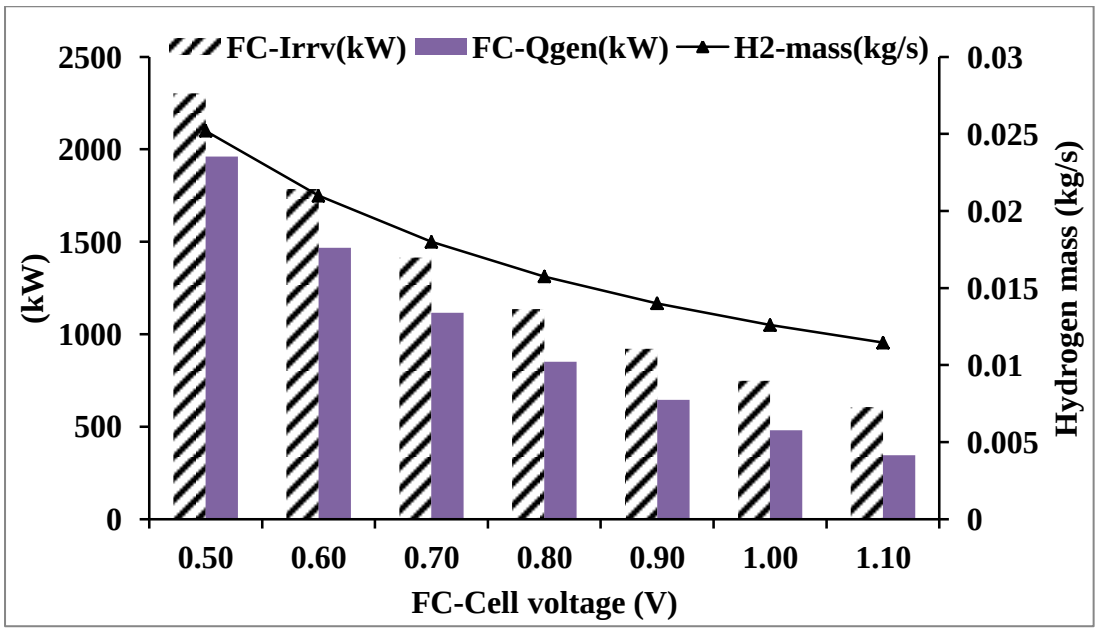

Figure 8.28 Effect of varying fuel cell voltage on the unit irreversibility, heat generated and feed in hydrogen mass at constant power

In addition, for a constant and specific amount of hydrogen mass feed to the fuel cell increasing the cell voltage will increase the power output values. As example, for the unit under study at base condition, increasing the rated cell voltage from 0.6 V to 0.7 V will increase the power output by 16.65 %. Consequently, the unit output electricity cost will be reduced by 11.96 % with constancy of other parameters, as shown in Figure 8.29.

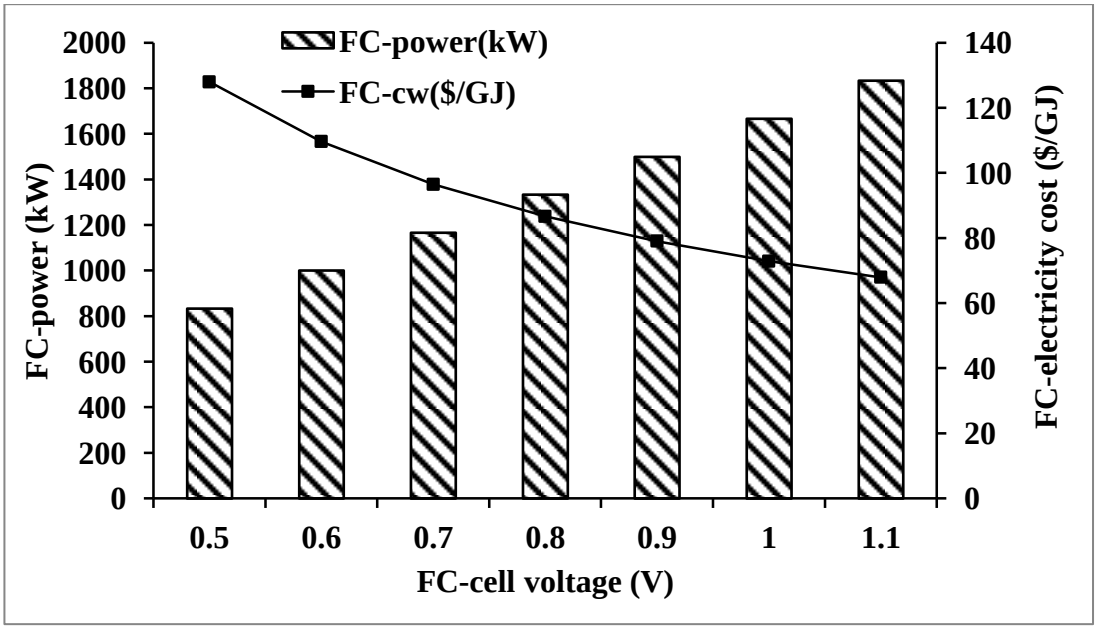

Figure 8.29 Effect of varying fuel cell voltage on the unit output power and exery cost at the constant of feed in hydrogen mass

-Effect of hydrogen and oxygen stoichiometric ratio on the fuel cell performance

The effect of increasing the hydrogen stoichiometric ratio for the fuel cell adopted for this study operating at a base condition on the unit performance and output is presented in table 8.26 and Figure 8.30. It is clear from the analysis that increasing the StH2 ratio over 1 without recycling will increase the hydrogen mass required to produce the same power, leading to a decrease the exergy efficiency and exergoeconomic factor. However, increasing the hydrogen mass will increase the unit output electricity cost and the exergy destruction factor, as presented in table 8.26 and Figure 8.30. Increasing the StH2 ratio by 30% above the theoretical amount will increase the hydrogen mass for the same unit out power by 30%, leading to increasing the unit output electricity and the exergy destruction costs by 31% and 45% respectively. In addition, this percentage of StH2 increments will reduce the exergy efficiency of the unit and the exergoeconomic factor by 23 % and 28% respectively. Besides, the effect of increasing the oxygen stoichiometric ratio is less significant on the unit performance and output than the effect of the StH2 as showed in Figure 8.31. Increasing the StO2 by 100% above the theoretical values of the unit under study at base condition will reduce its exergy efficiency by 0.87% only, while increasing the unit output electricity cost by only 2.24%, as shown in Figure 8.31.

StH2	FC-eta_ex(%)	FC-CD($/h)	fc-fk(%)	FC-cw($/GJ)	FC-power(kW)	H2-mass(kg/s)
1	35.25	262.51	16.19	112.39	999.82	0.0175
1.1	32.11	302.25	14.36	124.16	999.82	0.0192
1.2	29.47	341.99	12.91	135.94	999.82	0.0210
1.3	27.24	381.73	11.72	147.71	999.82	0.0227
1.4	25.32	421.47	10.74	159.49	999.82	0.0245
1.5	23.65	461.21	9.90	171.26	999.82	0.0262
1.6	22.19	500.95	9.19	183.04	999.82	0.0280
1.7	20.90	540.69	8.57	194.81	999.82	0.0297
1.8	19.75	580.43	8.03	206.59	999.82	0.0315
1.9	18.72	620.16	7.56	218.36	999.82	0.0332

Table 8.26 Effect of StH2 on the fuel cell performance, hydrogen mass and electricity cost at base condition

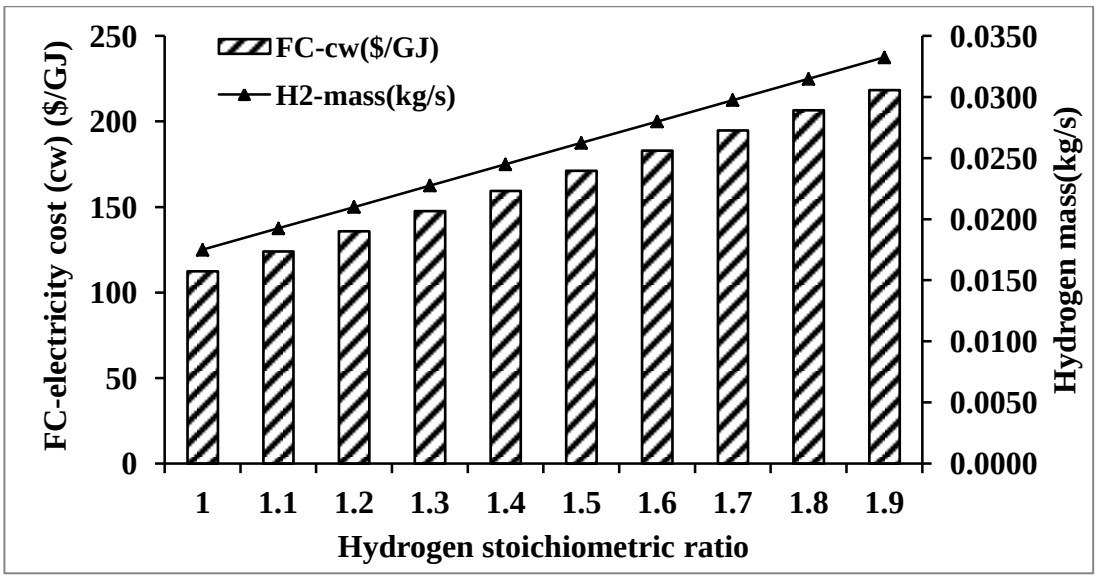

Figure 8.30 Effect of StH2 on the fuel cell hydrogen mass and electricity cost

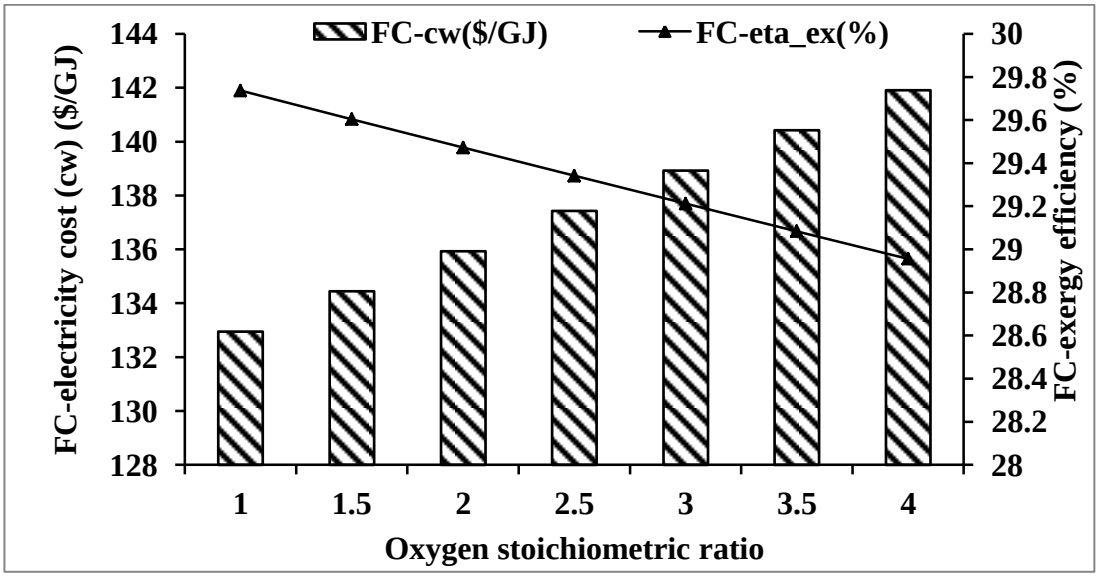

Figure 8.31 Effect of StO2on the fuel cell exergy efficiency and electricity cost

The effects of the fuel cell cooling system input water cost (cwc) and the cost of the output hot water on the unit output electricity are illustrated in Figure 8.32. The cost of the cwc and cwh in the analysis of the unit at base condition are estimated as 0.5 $/m^3 and 4 $/m^3 respectively. However, the values of these parameters may vary from one condition to another, depending on different factors such as the free availability of the input water and its purity as well as its circulation and hot water utilization percentage. The analysis shows that, at the constant of the other parameters for a unit at base condition and an input water charged as 0.4 $/m^3, the fuel cell output electricity cost will be reduced by 33.48% if the output hot water is charged at $7/m^3 instead of $1/m.^{3}

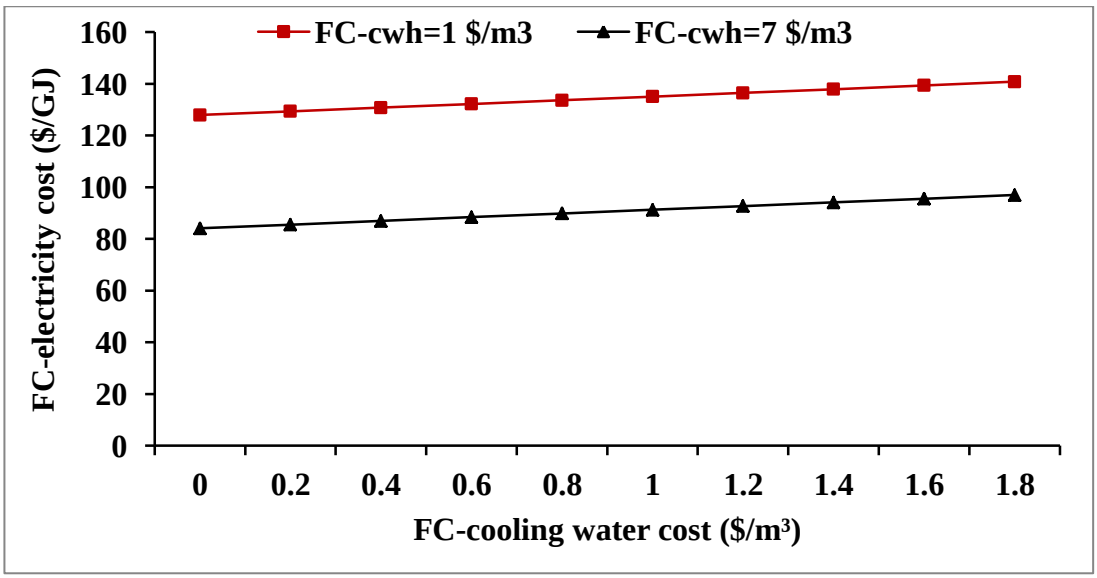

Figure 8.32 Effect of input cooling water and output hot water costs on the fuel cell output electricity cost

Figure 8.33 represents the effect of varying the fuel cell lifetime (ny) and the interest rate (ir) on the unit output electricity cost. The Figure shows that increasing the unit lifetime and decreasing the interest rate will decrease the unit output electricity cost (cw). The analysis also shows that at an interest rate of 4% increases the unit's lifetime from ny=5 to 50 years will reduce the unit output electricity cost by 25%. However, at a unit lifetime of ny=50 years increases the interest rate from 1 to 10% will increase the unit output electricity cost (cw) by 16% and this increment decreases to 9% when the life is decreasing to ny=5 years as illustrated by Figure 8.33.

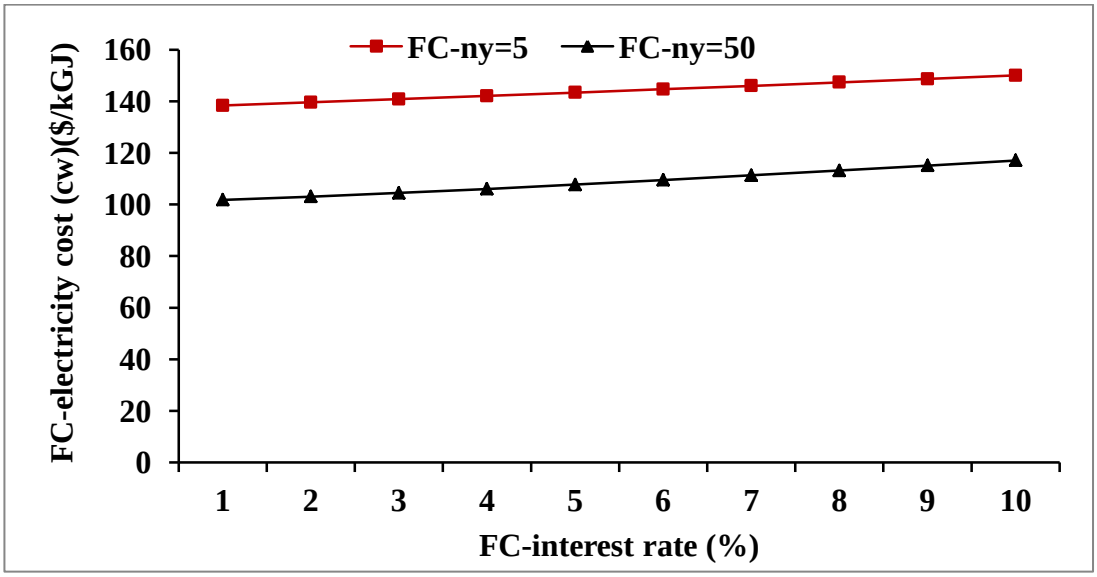

Figure 8.33 Effect of the (FC-ny) and the interest rate on the unit electricity cost

The effect of increasing the (FC-ny) and the interest rate on the unit exergoeconomic factor (fk) is represented in Figure 8.34. The Figure shows that at an interest rate of 4% increases the unit lifetime from 5 to 50 years will reduce the exergoeconomic factor by 66%. However, for a unit lifetime ny=5 years increasing the interest rate from 1 to 10% will increase the unit (fk) factor by 15% whereas this increment will reach 163% if the unit life increases to 50 years.

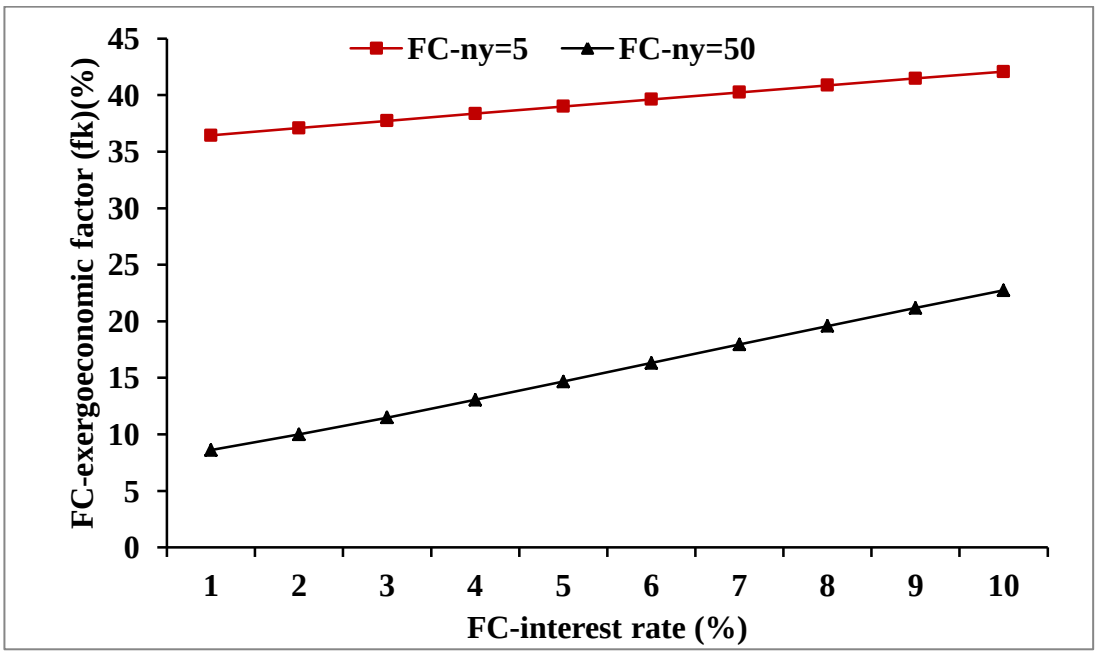

Figure 8.34 Effect of the (FC-ny) and the interest rate on the unit (fk) factor

Increasing the capacity factor (FC-CF) of a fuel cell unit has a significant effect on decreasing the unit output electricity cost at high capital unit costs (FC-CFC), particularly when the unit is working at a CF of less than 50%, as shown in Figure 8.35. The fuel cell electricity cost for a unit working at CF=10% will be reduced by 47% if the unit capital cost is reduced from 5000 to 500$/kW. However, for the same capital cost, the unit electricity cost reduction will be only 9% if it is working at a CF=100%, as shown in Figure 8.35. The same trends of effect will occur if the unit capital cost is decreasing and the capacity factor is increasing while the unit ZTCD factor is being reduced, as shown in Figure 8.36.

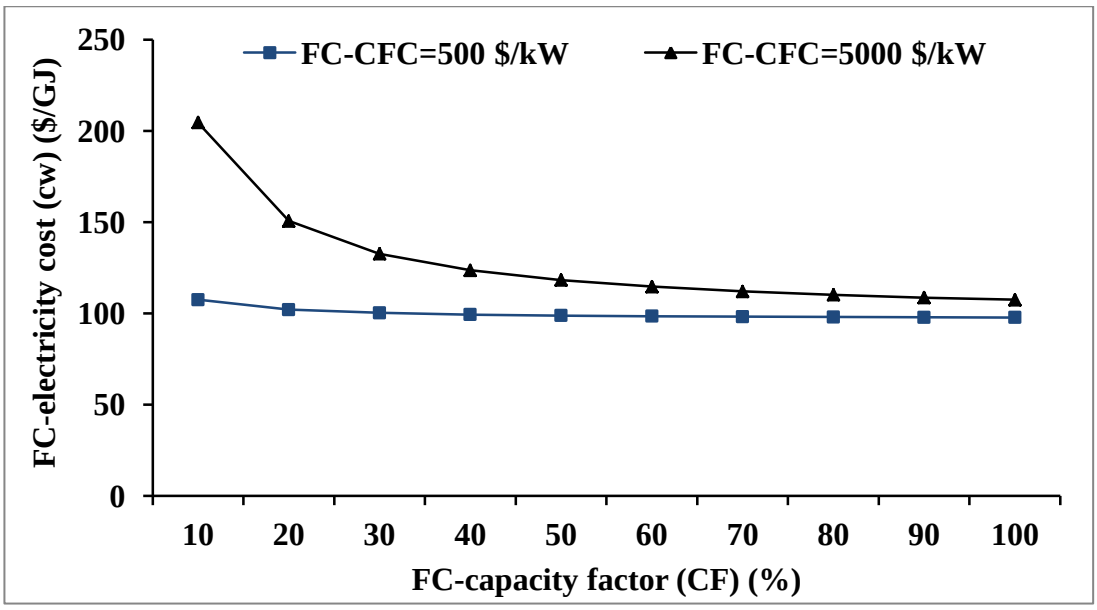

Figure 8.35 Effect of the (FC-CF) and (FC-CFC) on the unit electricity cost

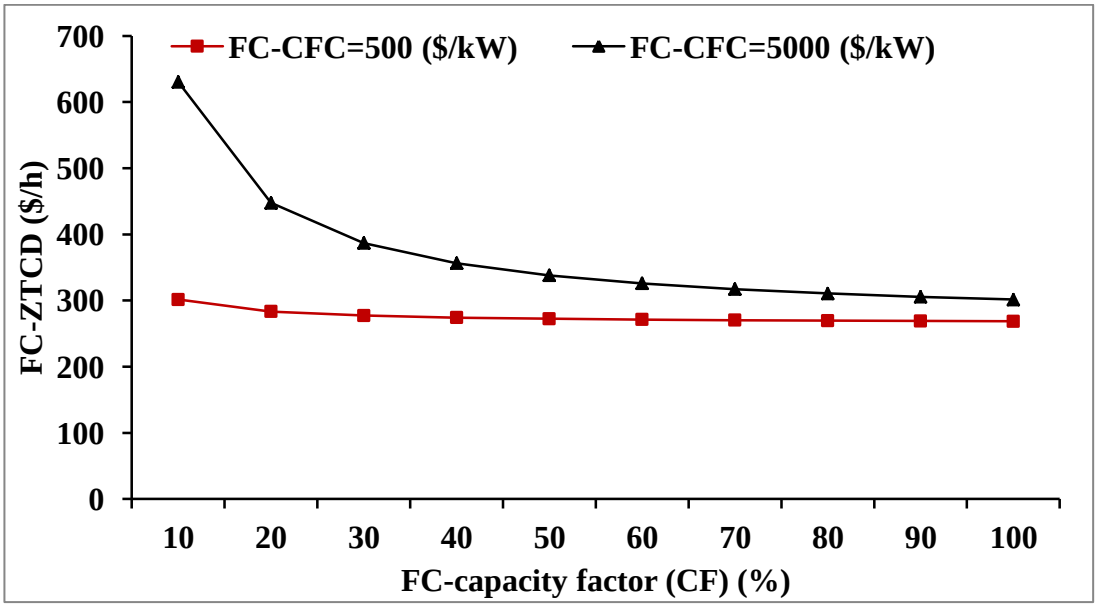

Figure 8.36 Effect of the (FC-CF) and (FC-CFC) on the unit ZTCD factor

8.8 Case study

Three different sites have been chosen to investigate the SHS at a real weather condition and evaluate its performance and output in a daily bases and yearly average mode. Sabha at the southern side and Misurata at the coast side of Libya as hot regions compared with Newcastle as a cold area in United Kingdom are adopted as a case studies in this study. However, the weather and solar data collected and presented in chapter four are used in this analysis.

8.8.1 SHS analysis at Sabha, Misurata and Newcastle using yearly average weather data

In this section, the analysis and evaluation of SHS thermo-economically at Sabha, Misurata and Newcastle is presented and discussed. The hourly average solar intensity during the year for the three sites is estimated as 0.67, 0.7 and 0.75 kW/m^2 for Sabha, Misurata and Newcastle respectively. However, the yearly average ambient temperature is as 28.5, 23 and 10 ^oC for the three sites respectively and the yearly average sunshine hours are estimated as 9.6, 8.8 and 4.2 for Sabha, Misurata and Newcastle respectively, as described in chapter six. The capacity factor (CF) for the PV, HEX, COMP unit is considered to be 40% at Sabha , 37% for Misurata and 20% for Newcastle, according to the unit working hours capacity. In addition, the capacity factor for the fuel cell in Misurata and Sabha is assumed as 50% and 70% at Newcastle as the unit has to be working more hours to cover the load during the absence of solar energy. The capacity factor of the tanks is 100% for all sites and for the electrolyzer at Sabha and Misurata it is assumed 30%, whereas it is 15% at Newcastle. The reduction of CF values is due to solar electricity variations during the day, where part of the SHS units, particularly for the electrolyzer, will be off in some hours of the day, leading to reducing its capacity factor. The output hot water is assumed to be partly utilized and totally recycled for domestic and other purposes with a cost estimated at 2 \$/$m^{3.}$ However a cost of 0.1 \$/m^3 is assumed to cover the cost of the recycled and the substituted water in the cycle. All the other parameters and unit costs in the system are assumed to be similar to the one adopted for the base condition analysis. The IPSEpro thermo-economic analysis and evaluation results of three SHS working to cover the energy demands of a small community at Sabha, Misurata and Newcastle based on yearly average data are presented in tables 8.27, 8.28 and 8.29. The system results tabulated in table 8.27 show that the SHS in Sabha has the best performance and output costs compared with the one installed at Newcastle. It is also clear that there was no significant difference between the Sabha and Misurata sites' output and performance results. The average PV surface temperature Tc increasing at Sabha was 10.2% and 48.0% above the Tc values calculated at Misurata and Newcastle respectively. This led to reductions in exergy and actual efficiency of the unit in Sabha than the one performed in Misurata and Newcastle by 1.50% and 5.68% for exergy efficiency and by 2.29 % and 7.66% respectively for the energy efficiency of the cities. These results agreed with the literature and with observations from previous studies for magnitude of the effect of PV surface temperature increasing with the unit's performance [182]. However, due to the high

solar intensity and long duration of sunshine at Sabha the system there will produce extremely more energy compared with the one in Newcastle and slightly more the one at Misurata. The yearly PV power output and the system's output of hot water as well as the hydrogen output quantity for the system in Sabha was 11820 MWh/y, 92085 m^3/y and 153.22 ton/y respectively. These quantities were over 2% and 88% respectively than the same PV unit and system production output installed in Misurata and Newcastle. Furthermore, fuel cell unit installed in Sabha will produce 2508 MWh/y, which is more than 5% and 95% respectively for the same production units in Misurata and Newcastle, as shown in table 8.27.

	PV-Tc (^oC)	PV-eta-act(%)	PV-eta-ex(%)	PV-P (MWh/y)	eta-ex-sy(%)	mH2 (ton/y)	H2 Tank (m^3)	FC-P (MWh/y)	HW (m^3/y)
Sabha	49.4	12.77	10.12	11820	5.26	153.22	458	2508	92085
Mis	44.8	13.07	10.28	11588	5.38	150.22	490	2384	90289
New	33.4	13.83	10.73	6269	5.68	81.27	2430	1289	48856

Table 8.27 PV and SHS performance and outputs at Sabha, Misurata and Newcastle

The average unit production cost of the PV and fuel cell units, and well as the average hydrogen exergy costs in Sabha were 0.106$/kWh, 0.695 $/kWh and 60.91$/GJ respectively; as shown in table 8.28. These costs are almost the same for the same units' output costs in Misurata and less than the costs of the same unit in Newcastle by 61.55%, 34.24 % and 38.35 % respectively.

The installation of PV and fuel cell units with the capacity adopted in this study in Sabah will save 170,217$ and 35,029 annually from the estimated CO_2 damage which occurred after producing the same quantity of power using fossil fuels. However, this annual CO_2 saving will be reduced to 90,281$ for the PV and 18,579$ for the fuel cell, if these units were installed in Newcastle instead of Sabha, as presented in table 8.28.

	PV-CO2/ SAVA($)	PV-EL($/kWh)	Ch2-($/GJ)	FC-EL($/kWh)	FC-CO2/ SAVA($)
Sabha	170217	0.1066	60.91	0.695	35029
Mis	166878	0.1074	59.69	0.680	34342
New	90281	0.1722	84.27	0.9330	18579

Table 8.28 PV and SHS' outputs electricity and hydrogen costs and annual Co2 damage savings

Table 8.29 shows calculations for the thermo-economic factors for the main SHS components at the three sites. The results show that the SHS units installed at Newcastle had the highiest exergy destruction and ZTCD factors compared with the units installed at Sabha and Misurata. The low PV and FC exergoeconomic(fk) factor for the three

sites meant that more attention has to be focused on increasing the exergy efficiency of these units. However, the high EL (fk) factor at Sabha and Newcastle meant that it was more effective to reduce the unit cost to improve the performance.

	PV-ZTCD($/h)	PV-CD($/h)	PV-fk(%)	EL-CD($/h)	EL-fk(%)	FC-CD($/h)	FC-fk(%)
Sabha	3077	2717	11.68	65.16	70.73	277	15.5
Mis	3250	2863	11.922	70.22	69.16	291	14.83
New	5621	4916	12.52	127	55.24	465	7.57

Table 8.29 Thermo-economic factors for the SHS main components of the three case studies

8.8.2 SHS thermo-economic analysis at typical summer and winter day

The SHS and its components are investigated and evaluated in hourly bases through a selection of an actual weather data for the three case studies sites in a winter and summer day. The data for the hourly solar intensity, wind speed and ambient temperature in the 15th of January 2011 and in the 15th of Aug 2010 recorded at the three case studies sites was collected for the analysis. The hourly energy, exergy and thermo-economic factors for the system and its main components outputs and costs is calculated, tabulated, figured and discussed in the following sections for each site.

- SHS thermo-economic analysis at a summer and winter day at Sabha

The effect of the ambient temperature, solar intensity, wind speed and the PV cell surface temperature on the PV efficiencies during a winter day (15/01/2011) and a summer day (15/08/2010) at Sabha is represented in Figures 8.37 and 8.38. The Figures show that the maximum exergy efficiency, which occurred at the end of 15th of January, was 12.70% while at midday it declined to 10.56% due to an increasing unit surface temperature from 25.28 ^{o}C at 16:00 to 39.18 ^{o}C at midday. However, the actual and electrical maximum efficiencies will be 13.45% and 17.56% at the midday and these increases slightly during the mornings and afternoons. This is due to the decrease in the unit surface temperatures that follow the solar intensity and the ambient temperature at such times. During a summer day (15/08/2010) the exergy, actual and electrical maximum efficiencies at the midday were 8.70%, 11.53% and 15.97% respectively. These low efficiencies compared with those of the 15th of January were mainly due to the high cell surface temperature at that time, which reached 68.25 ^{o}C. This temperature declined to 35^{o}C in the early morning of that day, leading to an increase in exergy efficiency of 12.49% at that time, as shown in Figure 8.38.

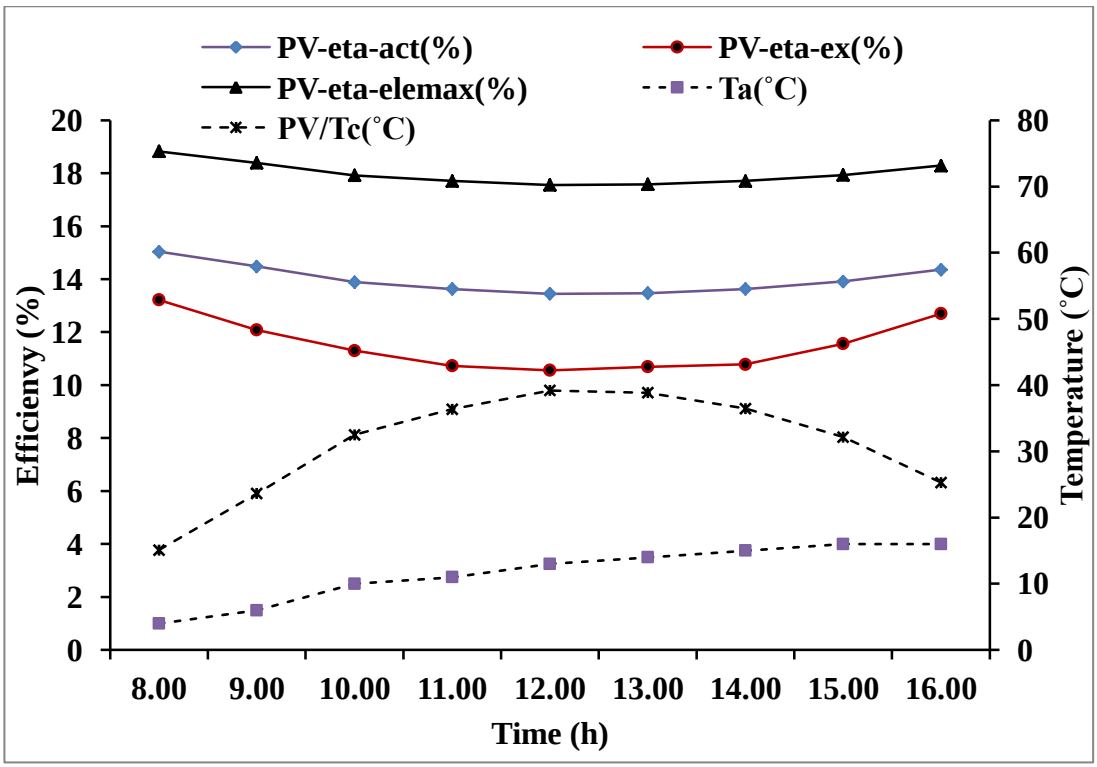

Figure 8.37 Variation of PV efficiency and module surface temperature during the 15th of January 2011 at Sabha with the change of ambient temperature

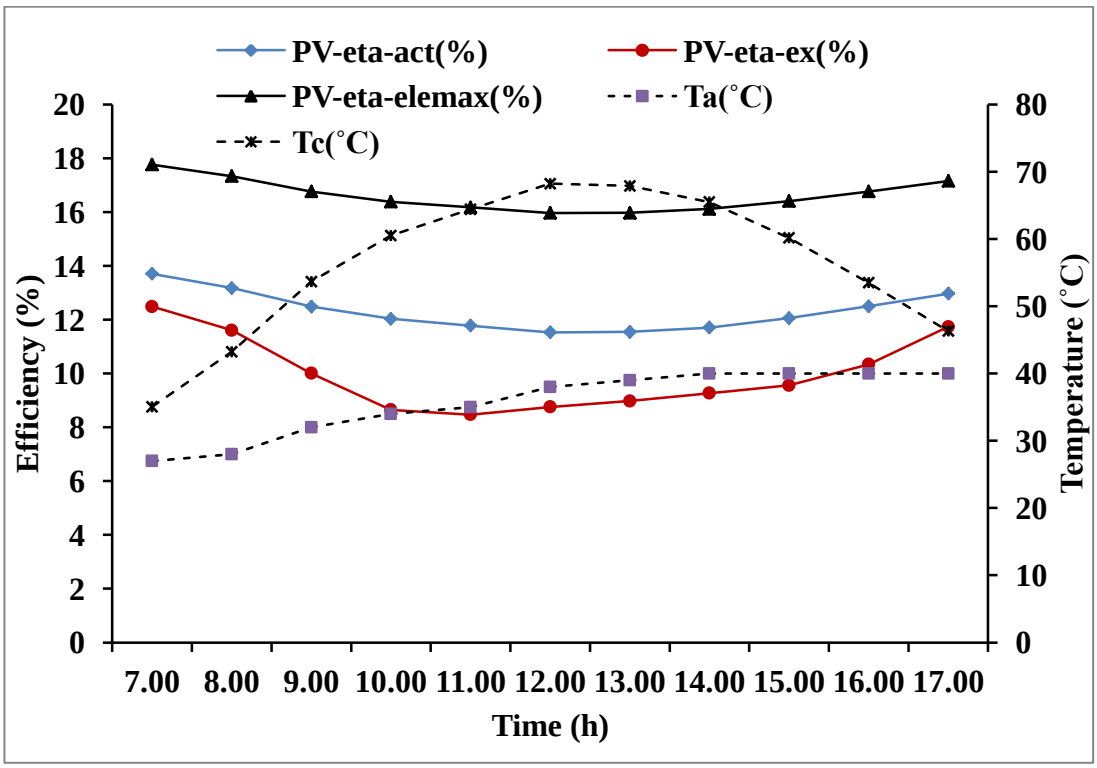

Figure 8.38 Variation of PV efficiency and module surface temperature during the 15th of August 2010 at Sabha with the change of ambient temperature

The wind speed has also had a significant effect on the exergy efficiency of the PV unit as presented in table 8.30. However, with neglecting its cooling effect particularly at low wind speed (<1 m/s), increasing the wind speed above the module surface will reduce the unit exergy efficiency. This is because increasing the heat transfer coefficient's value and the heat transfer from the module surface that leads to an increase in the exergy losses in the unit.

	15 January 2011			15 August 2010		
Time(h)	Sirr(kW/m^2)	Wind(m/s)	PV/ etaex(%)	Sirr(kW/m^2)	Wind(m/s)	PV/ etaex(%)
8:00	0.355	0.66	13.22	0.488	0.05	11.61
9:00	0.564	0.72	12.08	0.694	0.77	10.01
10:00	0.72	0.55	11.3	0.849	1.33	8.65
11:00	0.812	0.66	10.73	0.942	1.02	8.47
12:00	0.838	0.61	10.56	0.968	0.51	8.76
13:00	0.795	0.61	10.69	0.925	0.41	8.98
14:00	0.687	1	10.78	0.816	0.51	9.27
15:00	0.517	1	11.56	0.646	1.05	9.56
16:00	0.297	0.92	12.7	0.432	1.54	10.34
Avr.	0.621	0.75	11.51	0.751	0.8	9.52

Table 8.30 Effect of wind speed and solar intensity on the PV exergy efficiency during a winter and summer day in Sabha

The total power produced by the PV unit during the chosen winter day is 30,325 kWh, whereas 23,738 kWh of this amount is transferred to the electrolyzer unit to produce 6275 kWh by the fuel cell. Moreover, the PV total production power is increased to 34,359 kWh at the summer day whereas 26,734 kWh of this amount is used in the electrolyzer to produce the necessary hydrogen enough to produce 7068 kWh from the fuel cell if it is working and connected directly during the day time. Besides, the PV output during the midday of the 15th of January 2011 is producing 4444 kWh which is above the quantity produced at the same time in August. This is due to the low module surface temperature and irreversibility during that cold time, even with the higher solar intensity as 0.968 kW/m^2 in August compared with 0.838 kW/m^2 recorded at that time in January. The irreversibility of the SHS components is increased by the time of the day until reach its beak value at mid-day time then it is started to be declined. However, the PV unit irreversibility at August midday time reached to 36,505 kW and it is decreased to 31,120 kW in the same time in January as presented in Figures 8.39 and 8.40.

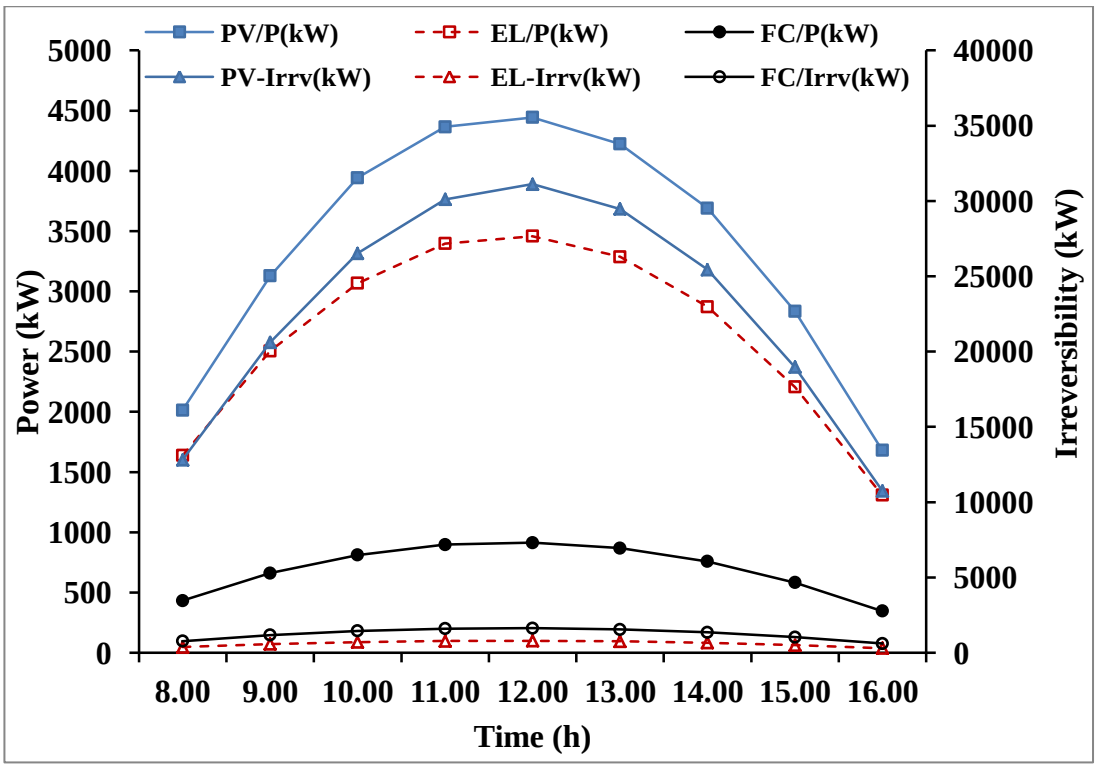

Figure 8.39 Varying of the power and irreversibility of SHS components during the daytime of the 15th of January 2011 at Sabha

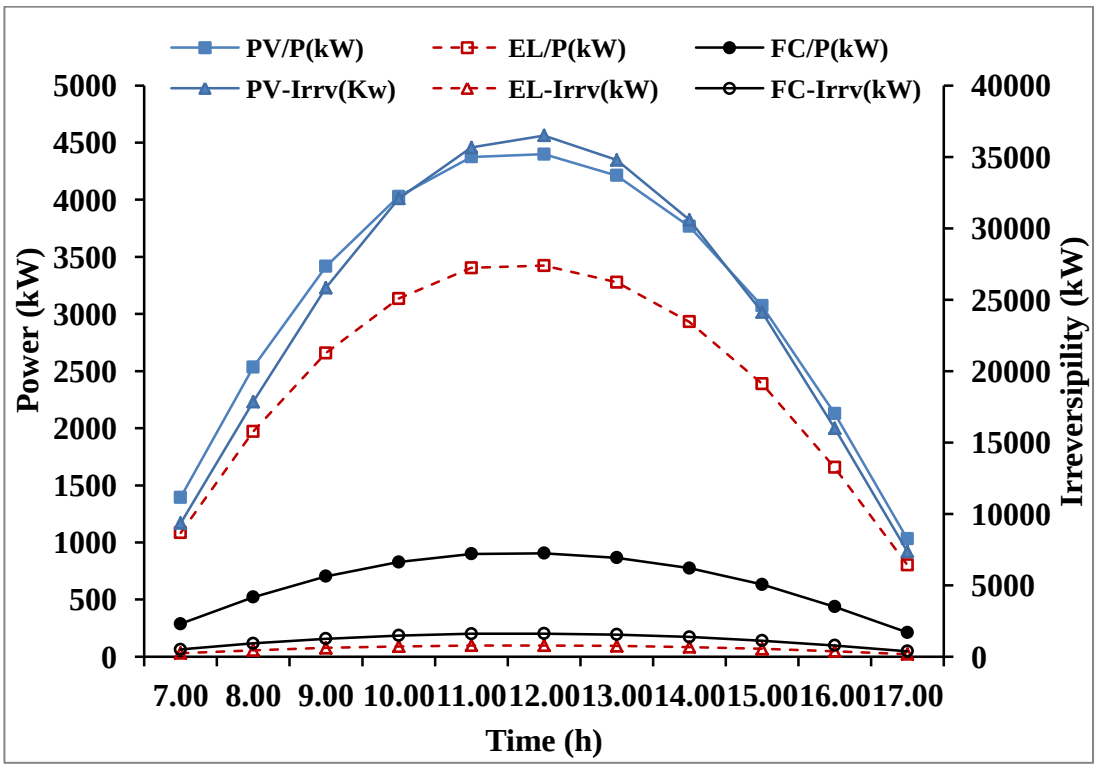

Figure 8.40 Varying of the power and irreversibility of SHS components during the day time of the 15th of August 2010 at Sabha

The average PV and fuel cell output electricity cost at the 15th of January 2010 in Sabha is 0.118 $/kWh and 0.776 $/kWh respectively while it increased to 0.143 $/kWh and 0.960 $/kWh at the 15th of August 2010 as presented in Figures 8.41, 8.42. In addition, the hydrogen exergy cost increased from 67$/GJ in January to 82 $/GJ in August. This is mainly due to the higher average exergy efficiency of the PV unit in January as 11.51 % compared with 9.98% performed at the 15th of August.

The PV electricity cost at the midday in January and August is 0.0809$/kWh and 0.0817$/kWh respectively while it is increased to 0.213$/kWh in January and 0.348 $/kWh in August at the end of the day as presented in Figure 8.41 and 8.42. However, the hydrogen exergy cost is increased from 45$/GJ at midday in January to 125$/GJ at the end of the same day. Meanwhile, it increases from 46$/GJ in August mid-day to 265$/GJ at the end of the same day. Varying the hydrogen exergy cost during the time of the day will vary the fuel cell electricity cost as illustrated in the following figures.

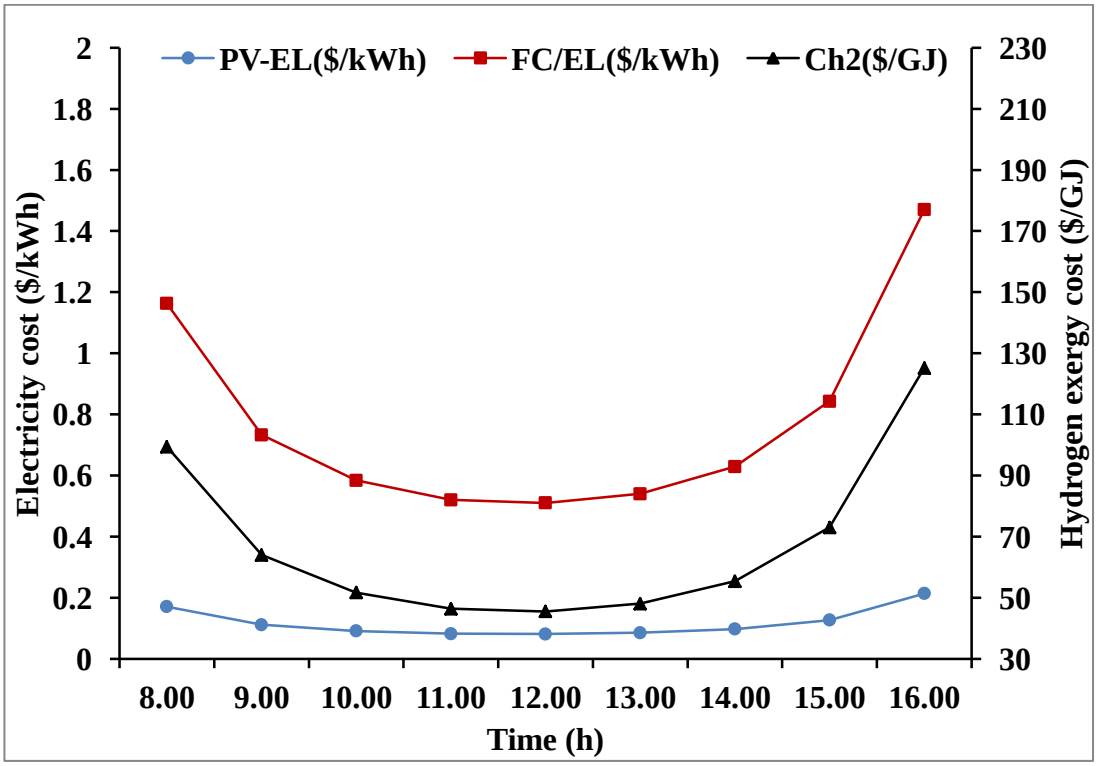

Figure 8.41 Varying of the PV and FC output electricity and hydrogen cost during the day time of the 15th of January 2011 at Sabha

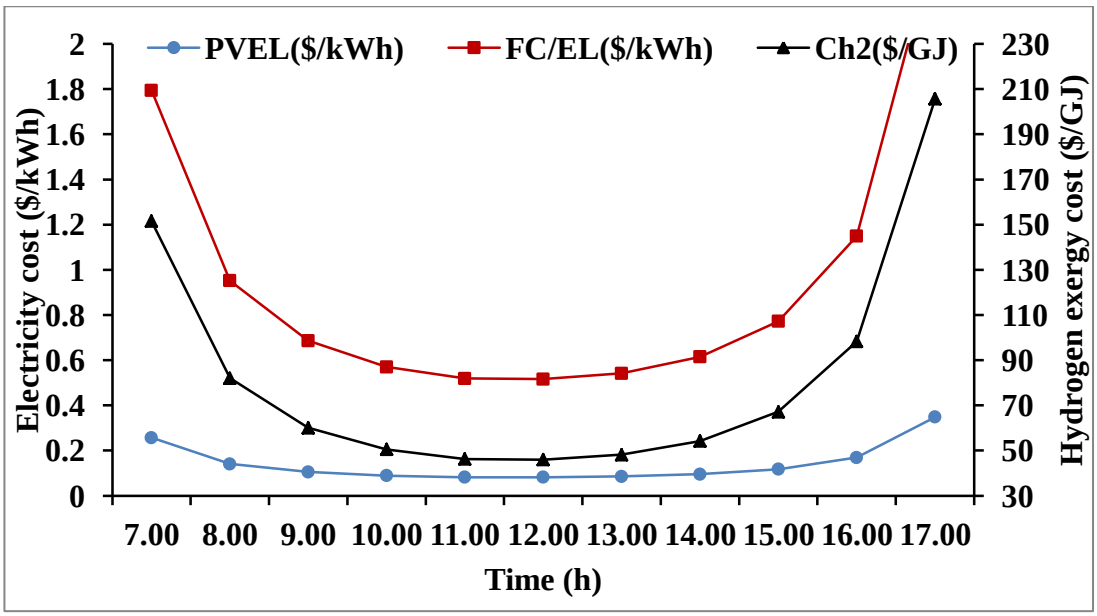

Figure 8.42 Varying of the PV and FC output electricity and hydrogen cost during the day time of the 15th of August 2010 at Sabha

Varying the power output of the PV unit and the power input to the electrolyzer during the time for the selection days will varying the production amount of hydrogen, oxygen and system hot water from the system during the day as presented in Figures 8.43 and 8.44. The total amount of hydrogen, oxygen and hot water produced by the system in the 15th of January is 395(kg/day), 3123 (kg/day) and 273 (m^3/day) respectively. However, these quantities are increased in the 15th of August to 445 (kg/day), 3517 (kg/day) and 268 (m^3/day) for the hydrogen, oxygen and hot water respectively.

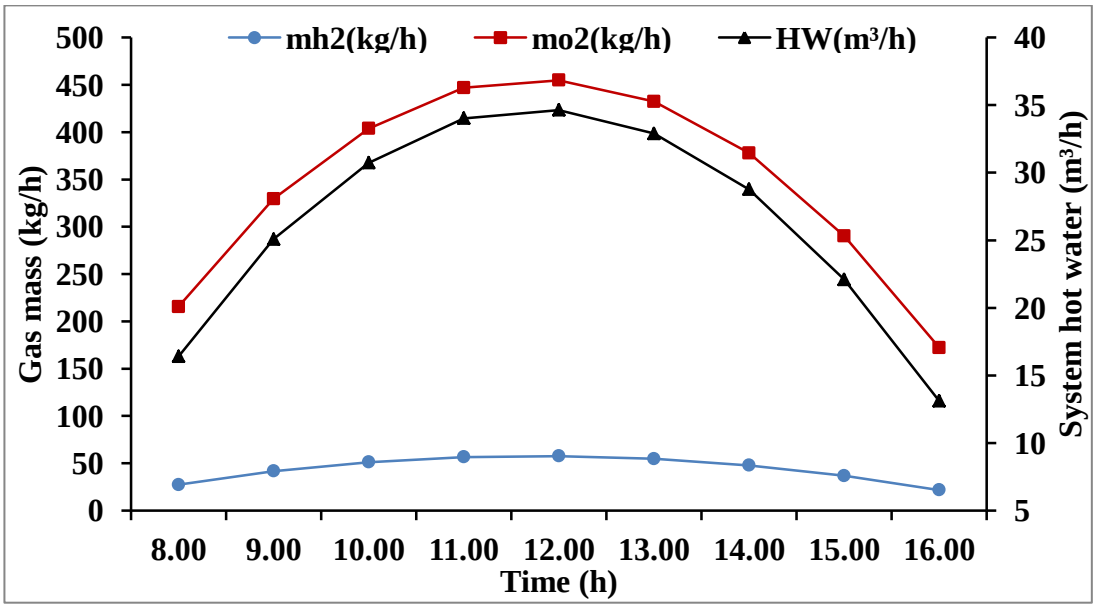

Figure 8.43 Varying of gas mass and hot water outputs during the day time of the 15th of January 2011 at Sabha

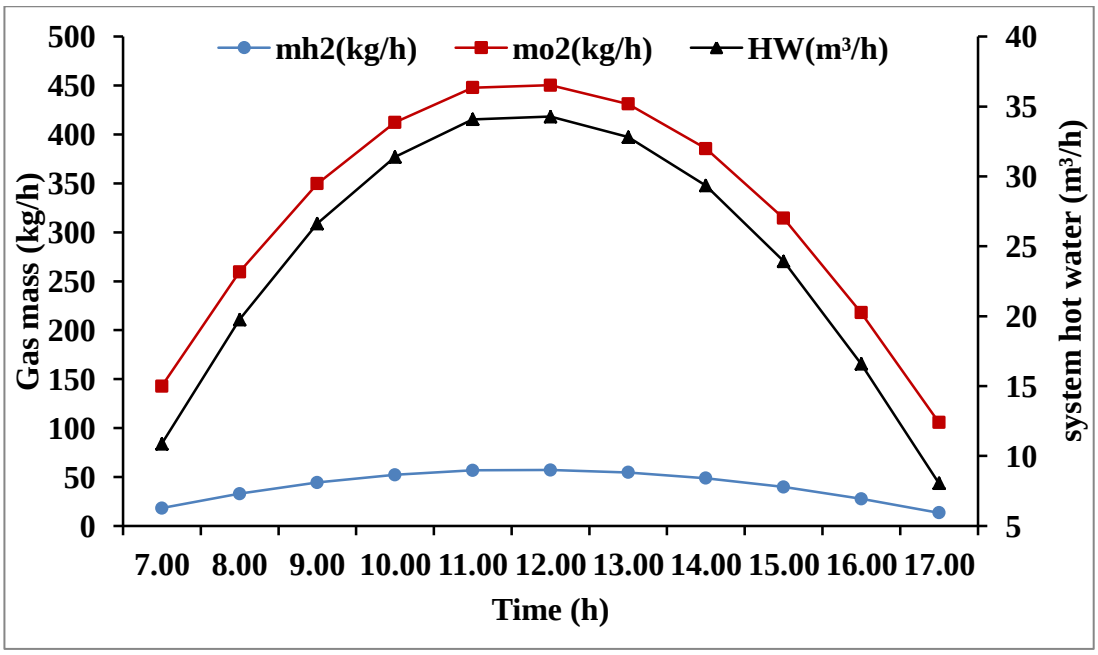

Figure 8.44 Varying of gas mass and hot water outputs during the day time of the 15th of August 2010 at Sabha

The thermo-economic factors of the PV unit at January and August in Sabha are represented in Table 8.31. The results show that the unit exergy destruction factor (PV/exdf) and the exergy destruction cost (PV/CD) calculated in January is above the one calculated for the corresponding hours in August whereas its maximum value was recorded at midday. This is due to the lower exergy efficiency performed at that hour in January than the one performed at the corresponding hour in August. This is also leading to a higher (PV/fk) factor in January than the corresponding one recorded in August as presented in the following table.

	15 January 2011			15 August 2010		
Time(h)	PV/exdf(%)	PV/CD ($/H)	PV/fk (%)	PV/exdf(%)	PV/CD($/h)	PV/fk(%)
8:00	91.44	2215	13.96	92.51	2560	12.31
9:00	91.83	2345	13.29	92.99	2776	11.46
10:00	92.19	2470	12.7	93.32	2951	10.86
11:00	92.37	2541	12.39	93.46	3019	10.64
12:00	92.47	2580	12.23	93.57	3057	10.52
13:00	92.45	2568	12.28	93.54	3036	10.58
14:00	92.36	2538	12.4	93.44	2981	10.76
15:00	92.15	2451	12.79	93.24	2886	11.07
16:00	91.82	2325	13.39	92.95	2750	11.56

Table 8.31 Thermo-economic factors of the PV unit in January and August in Sabha

- SHS thermo-economic analysis at a summer and winter day at Misurata

The thermo-economic simulation analysis of SHS and its components at a winter day (15/01/2011) and a summer day (15/08/2010) in Misurata is representing in the following section. Similar results graphs and tables for Sabha case are also conducted for Misurata to compare the results and evaluate the system. However, for space limited part of the figures and table results will be presented in this section whereas the rest will be presented in the (Appendix F). The results shows that in January for an average solar intensity, wind speed and ambient temperature as 0.539 kW/m^2, 1.2 m/s and 16.88 ^oC respectively the average exergy efficiency, actual efficiency and module surface temperature is 11.28%, 13.85% and 33.74 ^oC respectively. However, for an average solar intensity, wind speed and ambient temperature recorded in August as 0.691 kW/m^2 , 1.1 m/s and 31.31 ^oC the average daily exergy efficiency and the actual efficiency will be reduced to 9.8% and 12.5% respectively. This is due to the increase of the average module surface temperature to 52.92˚C during the summer day. The SHS installed in Misurata will produce 26242 kWh from the PV unit during the day in January and 5399 kWh from the fuel cell when connected and operated directly using the 340 kg of hydrogen produced during the day. These quantities of production will increased to 36,850 kWh for the PV and 7580 kWh for the fuel cell using 477 kg of produced hydrogen when the same system works in August. The system will also produce more hot water output as 287 (m^3/day) in August compared with only 204 (m^3/day) in January. The higher system output production in August decreases the unit thermo-economic cost of the PV, FC and produces hydrogen from 0.149$/kWh, 0.974 $/kWh and 84 $/GJ respectively in January to 0.140 $/kWh, 0.910 $/kWh and 79 $/GJ respectively in August. Table 8.32 represents a comparison between the SHS outputs and performance at Sabha and Misurata during a summer and winter day. It is clear that the system installed in Sabha will produce more PV and FC power, hot water and hydrogen in January than the one installed in Misurata. This reduces the unit thermo-economic cost for the PV, FC and produces hydrogen in January from 0.149 $/kWh, 0.974 $/kWh and 84 $/GJ in Misurata to 0.117 $/kWh, 0.776 $/kWh and 68 $/GJ respectively at Sabha. This is due to the high solar intensity recorded in Sabha at January compared with the one installed at Misurata leading to increase in its exergy efficiency to 11.51 % compared with 11.28% for the system in Misurata. The high solar intensity recorded at Sabha in January is terminated the adverse effect of the higher average module surface temperature recorded at that day due to the high average

ambient temperature and solar intensity. However, for August the system installed in Misurata is producing slightly more PV, FC power as well as hot water and hydrogen than the one installed in Sabha which is mainly due to the higher solar intensity and module surface temperature values recorded at that day in Misurata. This leads to slightly decreasing average unit thermo-economic costs for the PV, FC and hydrogen during the day as presented in the following table.

Daily	15 January 2011		15 August 2010	
	Sabha	Misurata	Sabha	Misurata
Av. eta-ex(PV) (%)	11.51	11.28	9.9	9.8
Av. Tc (^{o}C)	31.05	16.88	56.2	52.92
P/PV (kWh)	30325	26242	34359	36850
P/FC (kWh)	6275	5399	7068	7580
mh2(kg)	395	340	445	477
HW(m^3)	237	204	267	287
Av.PV/EL($/kWh)	0.117	0.149	0.142	0.141
Av.FC/EL($/kWh)	0.776	0.974	0.96	0.91
Av.Ch2($/GJ)	67.6	84	82.7	79

Table 8.32 Comparison between the performance and unit outputs of SHS installed in Misurata and Sabha during a summer and winter day

The varying of the PV exergy efficiency (PV-etaex), electrical actual efficiency (PV-eta-act), electrical maximum efficiency (PV-etaelemax) and PV surface temperature (Tc) during a summer and winter day for a unit installed in Misurata is presented in Figures 8.45 and 8.46. The results show that the low ambient temperature recorded in Misurata during January at high solar intensity leads to a reduction in the module surface temperature and increasing the efficiencies compared with the one performed in August as appeared in the Figures. At midday of January, the module surface temperature reaches 39.4 ^{o}C and declines to 25.8 ^{o}C at the end of the day. This is increasing the unit exergy efficiency from 10.4 % at midday to 12.8 % at the end of the day in January. However, in August the module surface temperature reached to 64.6 ^{o}C and declines to 39.9 ^{o}C at the end of the day. As a result, the unit exergy efficiency will increase from just 8.1% in the midday to 12% at the end of August day. The figures and data representing the results of varying of the SHS components power and irreversibility, hot water production, hydrogen and oxygen mass as well as the cost structure during the summer and winter day for a system installed in Misurata is presented in (Appendix F).

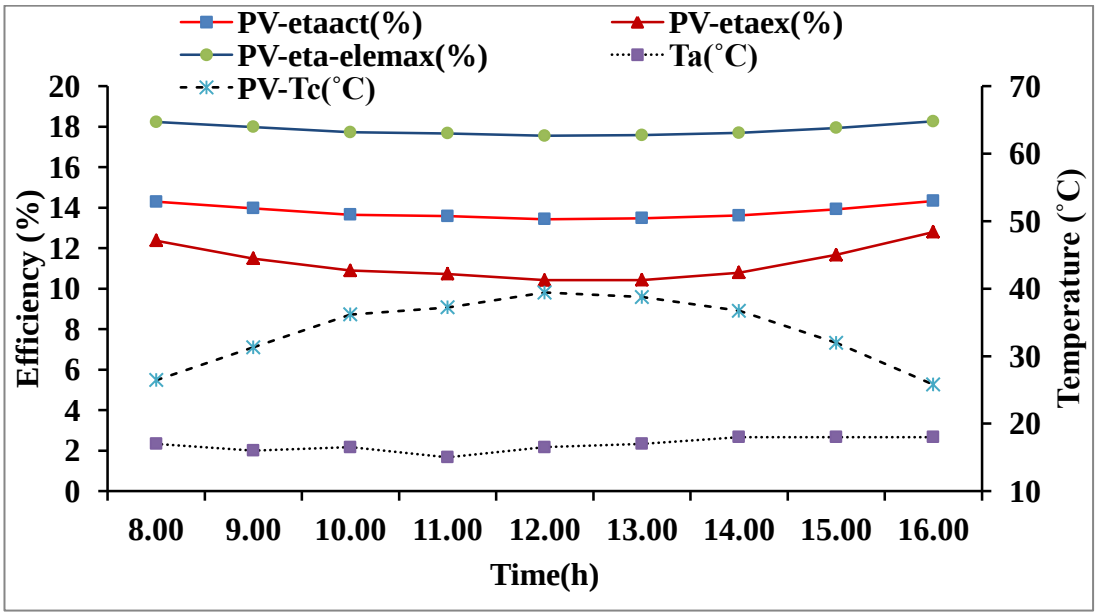

Figure 8.45 Variation of PV efficiency and module surface temperature during the 15th of January 2011 at Misurata with the change of ambient temperature

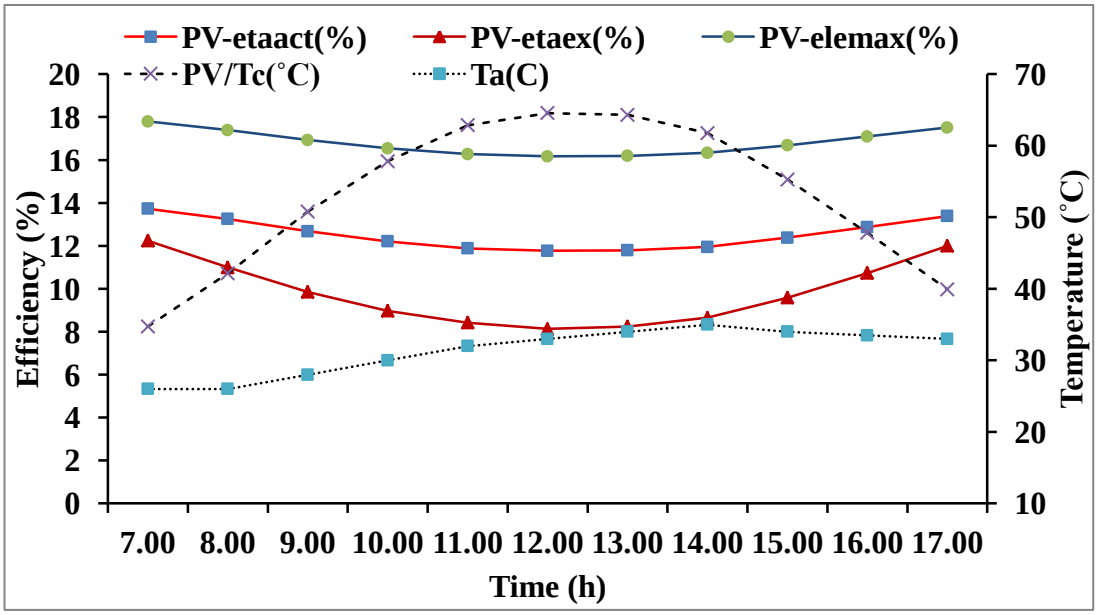

Figure 8.46 Variation of PV efficiency and module surface temperature during the 15th of August 2011 at Misurata with the change of ambient temperature

Table 8.33 represents a comparison between the main thermo-economic factors for the PV unit installed in Sabha and Misurata on a summer and winter day. The results show that the hourly average exergy destruction factor for the unit in the SHS is too high at around 93% during both days. However, in January the unit installed in Sabha has

sligthly higher exergy efficiency and produces more power by 15.55% than the one installed in Misurata with a reduction of a unit thermo-economic cost by 27.35% than the cost performed in Misurata in the same day. This power increases and cost reduction is reflected in reducing the exergy destruction factor and increasing the (fk) factor percentage in Sabha than the one performed in Misurata even with the high irreversibility existed at Sabha unit. In August the unit installed in Misurata with a 4.54% higher daily average solar intensity produces more power by 7.24% than the one installed in Sabha with a 2% less average exergy efficiency during that day. As mentioned earlier in this chapter, the high average wind speeds during the day lead to a decrease in the unit exergy efficiency and an increase in its irreversibility. The adverse effect of the wind speed is terminated by the positive effect of the lower surface temperature and the high solar intensity and power output on the unit thermo-economic cost, which is almost the same for the same August day in Sabha and Misurata as shown in table 8.33.

	15 January 2011		15 August 2010	
PV/Daily Average	Sabha	Misurata	Sabha	Misurata
Ta(^{o}C)	11.66	16.8	35.7	31.3
Wind(m/s)	0.74	1.19	0.766	1.1
Sirr(kW/m^2)	0.62	0.539	0.66	0.69
Tc(^{o}C)	31.05	33.14	56.23	52.9
Power (kW)	30325	26242	34359	36850
etaex(%)	11.51	11.28	9.99	9.8
Irreversibility(kW/h)	22870	19914	24561	25964
EL($/kWh)	0.117	0.149	0.142	0.141
fk (%)	12.82	12.65	11.35	11.46
CD ($/h)	2448	2676	2820	3007
PV/exdf(%)	92.12	92.22	93.07	92.97

Table 8.33 Comparison between the thermo-economic factors of the PV unit installed in Misurata and Sabha during a summer and winter day

- SHS thermo-economic analysis at a summer and winter day at Newcastle

Similarly, to Sabha and Misurata, a simulation analysis and thermo-economic evaluation of a SHS installed in Newcastle is conducted. The results are tabulated, figured, discussed and compared with the results performed for a similar system installed in Sabha. In terms of space limited, some of the result graphs are presented in this section while other results are presented in (appendix F). Figures 8.47 and 8.48 illustrated the variation of the PV unit exergy, actual and electrical maximum efficiencies with the ambient and module surface temperature variation during a winter day (15/01/2011) and a summer day (15/08/2010) respectively. The Figures shows that

the unit exergy, actual and electrical maximum efficiencies in the midday of January are 13.00%, 14.82% and 18.65% respectively and it increased to 13.29%, 14.92% and 18.73% respectively at the end of daylight time. In addition, the unit surface temperature decreased from 18.4 ^{o}C at the midday to 16.8 ^{o}C at the end of January day light time. In the meantime, for August the PV unit efficiencies; exergy, actual and electrical maximum are 12.14%, 13.97% and 17.98% respectively at the midday and it increases to 12.79%, 14.19% and 18.16% at the end of the day. Figure 8.48 representing the variation of the unit surface temperature in August day. The figure shows that the unit surface temperature in August day decreases from 31.97 ^{o}C at midday to 27.81 ^{o}C at the end of day.

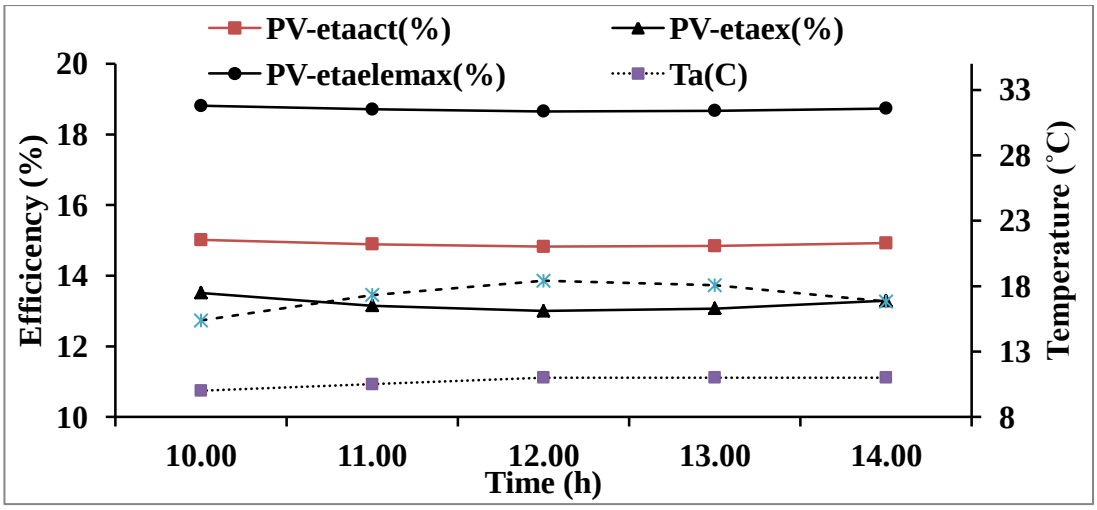

Figure 8.47 Variations of PV efficiency and module surface temperature during the 15th of January 2011 at Newcastle with the change of ambient temperature

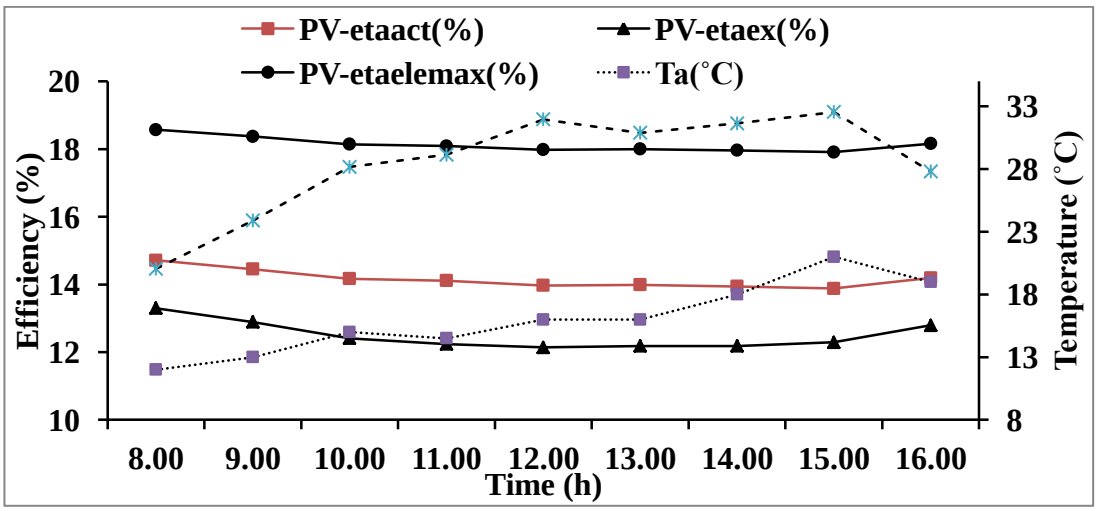

Figure 8.48 Variations of PV efficiency and module surface temperature during the 15th of August 2010 at Newcastle with the change of ambient temperature

A comparison analysis and evaluation of a SHS thermo-economic factors and its units' output and cost structure for a system installed in Sabha with a similar one installed in Newcastle in a summer and winter day bases is presented in Table 8.34. The analysis shows that the system installed in Sabha has extremely better performance and output compared with the similar one installed in Newcastle for both corresponding summer and winter days. In January, the system installed in Sabha is producing 30,325 kW from the PV unit and 6275 kWh from the fuel cell. during the day while, its only produced 6097 kWh from the PV unit and 1253 kWh from the fuel cell for a system installed in Newcastle at January. The system installed in Sabha in January will produce 395 kg/day hydrogen gas and 237 m^3/day hot water compared with only 79 kg/day hydrogen and 47.52 m^3/day hot water produced by a similar system installed in Newcastle at the same date. This high water production in Sabha in January will reduce the PV and FC hourly average unit thermo-economic cost from 0.584 $/kWh and 3.354 $/kWh conducted in Newcastle to 0.117 $/kWh and 0.776 $/kWh in Sabha. In addition, the hydrogen unit exergy cost is reduced from 293 $/GJ in Newcastle to 68 $/GJ in Sabha for the same day. This is because of the low average sunshine duration and solar intensity in Newcastle compared with that recorded in Sabha for the same day. However, the higher PV exergy efficiency and low irreversibility performed in Newcastle than the one performed in Sabha due to its lower average module surface temperature does not have a significant effect on the output unit thermo-economic cost compared with the higher output power and cost in Sabha. The higher PV output unit thermo-economic cost in Newcastle leads to increase in the average daily (CD) and (fk) factors calculated in Newcastle compared with the one calculated in Sabha for the same day. The SHS installed in Sabha in August will also have a higher performance and unit output and costs than the one in Newcastle for the same reasons as in January as appeared in Table 8.34. In August, the system installed in Sabha is producing 34,359 kWh from the PV unit and 7068 kWh from the fuel cell during the day. While, it has only produced 4065 kWh from the PV unit and 19,776 kWh from the fuel cell for a system installed in Newcastle at August. The system installed in Sabha in August will produce also 445 kg/day hydrogen gas and 267 m^3/day hot water compared with only 256 kg/day hydrogen and 154 m^3/day hot water produced by a similar system installed in Newcastle at the same date. This high production in Sabha in August will also reduce the PV and FC hourly average unit thermo-economic cost to 0.142 $/kWh and 0.096 $/kWh respectively compared to Newcastle figures of 0.334 $/kWh and 1.882 $/kWh. In addition, the hydrogen unit exergy cost is reduced from 166 $/GJ in Newcastle to 83

$/GJ in Sabha for the same day of August as presented in table 8.28. The tables showing the results of varying of the SHS components power and irreversibility, hot water production, hydrogen and oxygen mass as well as the cost structure during the summer and winter day for a system installed in Newcastle is presented in (Appendix F).

	15 January 2011		15 August 2010	
Daily Average	Sabha	Newcastle	Sabha	Newcastle
Ta(^{o}C)	11.66	10.7	35.7	16.05
Wind(m/s)	0.74	1.83	0.766	0.37
Sirr(kW/m^{2})	0.62	0.207	0.66	0.39
Tc(^{o}C)	31.05	17.19	56.23	28.46
PV/etaex(%)	11.51	13.2	9.99	12.49
PV/Irrv.(kW/h)	22870	7493	24561	14342
PV/fk (%)	12.82	13.87	11.35	13.19
PV/CD ($/h)	2448	4368	2820	4631.77
PV/exdf(%)	92.12	91.5	93.07	91.94
PV/EL($/kWh)	0.117	0.5848	0.142	0.3338
FC/EL($/kWh)	0.776	3.354	0.96	1.882
Ch2($/GJ)	67.6	293	82.7	166
P/PV (kWh/day)	30325	6097	34359	19776
P/FC (kWh/day)	6275	1253	7068	4065
mh2(kg/day)	395	79.06	445	256.39
HW(m^{3}/day)	237	47.52	267	154.12

Table 8.34 Comparison between the thermo-economic factors and unit outputs of SHS installed in Sabha and Newcastle during a summer and winter day

8.9 IPSEpro photovoltaic thermal model PV/T

The thermo-economic analysis for the SHS reveals that the photovoltaic unit has the highest exergy destruction and exergy destruction cost factors in the system as well as the lowest exergoeconomic factor. The low PV exergoeconomic factor (fk) encourages towards the importance of improving the unit exergy efficiency. However, the analysis also shows that decreasing the PV surface temperature will improve the unit exergy efficiency and its electricity output and cost. The photovoltaic system (PV/T) is a system combined a photovoltaic unit with flat plate or tube collectors using water or air for cooling the PV surface and producing both electricity and heat as described in section 3.3. However, water cooling Photovoltaic thermal IPSEpro model is developed to evaluate and optimize the system thermo-economically, as illustrated in chapter seven. Furthermore, the system has to be optimized between its main function of producing electricity and the hot water as by product according to the operating conditions and the energy and electricity needs at each time and site. Figure 8.49 represents a print screen for an IPSEpro model (PV_cellbaa) simulation results for a

PV/T system installed in Sabah using yearly average data. The analysis has been carried out for a constant water outlet temperature as 45 ^{o}C and the input water at 25 ^{o}C charged as 85 $/GJ included the cost of water recycled, storage and substituted in each cycle (10 to 20%% losses and 1 $/m^3). In addition, it is assumed that 50% of the hot water is utilized in domestic use and it has charged as 100 $/GJ (1.3 $/m^3). The output results of this unit is compared with the results of a similar PV/T unit using water mainly for cooling the module surface rather than producing hot water and its working at an output hot water temperature as 30 ^{o}C. The results were also compared with a similar PV unit working at Sabha yearly average data without cooling, as presented in Table 8.35. The results shows that the exergy efficiency of a PV/T system partly utilizing the hot water was increased by 6% and 48% above the exergy efficiency performed for the same unit operated without utilizing the output water and for a similar PV unit only respectively. Moreover, the PV/T (cooling only) is producing more electricity by 7.7% and 8.0% than the similar system producing electricity and hot water and a PV system only respectively. It is also found that the actual, thermal, total and total equivalent efficiency of the PV/T (cooling) is increasing above the PV/T (hot water) system by 7.7%, 51%, 40% and 32% respectively. Increasing the thermal efficiency of the PV/T cooling system does not contribute in the system's production cost due to the non-utilization of this thermal energy. However, the PV/T (hot water) system has the lowest unit thermo-economic cost as 0.0701$/kWh compared with 0.1152 $/kWh for the PV/T (cooling) and 0.1066 $/kWh for the PV system. This is also leading to decreasing the exergy destruction cost factor (CD) of the PV/T (hot water) system by 38.44% and 37.76% compared with the PV/T (cooling) and PV systems factors respectively.

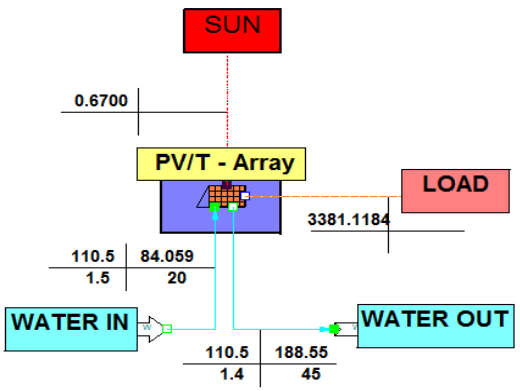

Tc/PV(C)	49.4375	Tc/PV/T(C)	49.0000
eta_act(%)	12.8022	ZTCD($/h)	2110.9656
eta_expvt(%)	14.9884	CD($/h)	1691.3963
eta_max(%)	17.0315	PVEL($/kWh)	0.0701
eta_therm(%)	39.4639	PVEL/CO2($/kWh)	0.0557
eta_tot(%)	52.2661	CO2SAVA($)	170603.1218
eta_toteq(%)	71.4695	mwo(m3/h)	397.8459
Irrv(kW)	23583.4421	mwo(m3/y)	1394052.06
Sgen(kW/k)	80.4484	PEL/h(kWh)	3381.1184
fk(%)	19.8757	PEL/Y(MWh)	11847.4390

Figure 8.49 Print screen of PV/T IPSEpro thermo-economic model results (PV_cellbaa) (Sabha yearly average data)

Due to its low output electricity cost and its high exergy efficiency the PV/T (hot water) is also has the highest exergoeconomic factor compared with the other systems as appeared in table 8.35.

Factor	PV/T (hot water)	PV/T(cooling only)	PV (only)
Tc (^{o}C)	49	34	49.43
eta_act(%)	12.8	13.79	12.77
etaex(%)	14.98	14.13	10.12
eta_th(%)	39.46	59.85	0
eta_tot(%)	52.26	73.65	12.77
eta_toteq(%)	71.46	94.34	31.92
PV/EL(kWh)	3381	3643	3373
HW(m^3/h)	397	1508	0
CD ($/h)	1691	2747	2717
fk(%)	19.87	13.24	11.68
PVEL($/kWh)	0.0701	0.1152	0.1066
CO2/SAVA($)	170603	183838	170217

Table 8.35 Comparison between the thermo-economic factors and performance of PV/T (hot water), PV/T (cooling) and PV only (Sabha average yearly data)

8.9.1 Thermo-economic evaluation of PV/T system at summer and winter days

The performance and outputs of the PV/T system is affected by varying the solar intensity, wind speed and ambient temperature during the day. However, in order to investigate the system, different weather data was provided for a typical summer and winter day data at the 15th of August 2010 and the 15th of January 2011 in the Sabha region. The analysis shows that the system on the summer day will produce 36,432 kWh and 5623 m^3/h hot water at 45^{o}C. This quantity will be reduced to 28,179 kWh/day and 1798 m^3/day on the winter day, as shown in table 8.36. The results also show that the daily average exergy destruction factor (CD) on the winter day increases by 70% more than the one calculated in the summer day. This leads to an increase in the average exergy economic factor (fk) in the summer day by 107 % more than that calculated for the winter's day. However, the exergy efficiency in the winter day increased by 7.27% more than that of the summer day. This is because of the cooling effect of the low average ambient temperature on the winter day, recorded as 12.14 ^{o}C compared with 35.72 ^{o}C on the summer day. Moreover, due to the high quantity of hot water produced on the summer day; the thermal, total and the total equivalent efficiencies on that day is increased by 107%, 68.65% and 44.46% respectively more than the one performed on the winter day.

Daily average	Sabha 15 August 2010	Sabha 15 January 2011
etaex(%)	14.16	15.19
etath(%)	46.72	22.49
etatot(%)	59.52	35.29
etatoteq(%)	78.72	54.49
fk(%)	33.8	16.3
P/PV/T(total)(kWh)	36432	28179
HW(total)(m^3/h)	5623	1798
CD($/h)	1326	2256
PV/T/EL($/kWh)	0.09795	0.09078

Table 8.36 Comparison between PV/T performance in winter and summer days

Figure 8.50 and 8.51 represents the variations in PV/T efficiencies during a summer and winter day in Sabha with regard to ambient temperature. It is clear that the thermal, total and total equivalent efficiencies during the hot day are higher than during the cold day with a highest values being observed at the midday. As an example, the thermal efficiency at mid-summer day is 59.95 % declined to 34.14% on the mid-winter day.

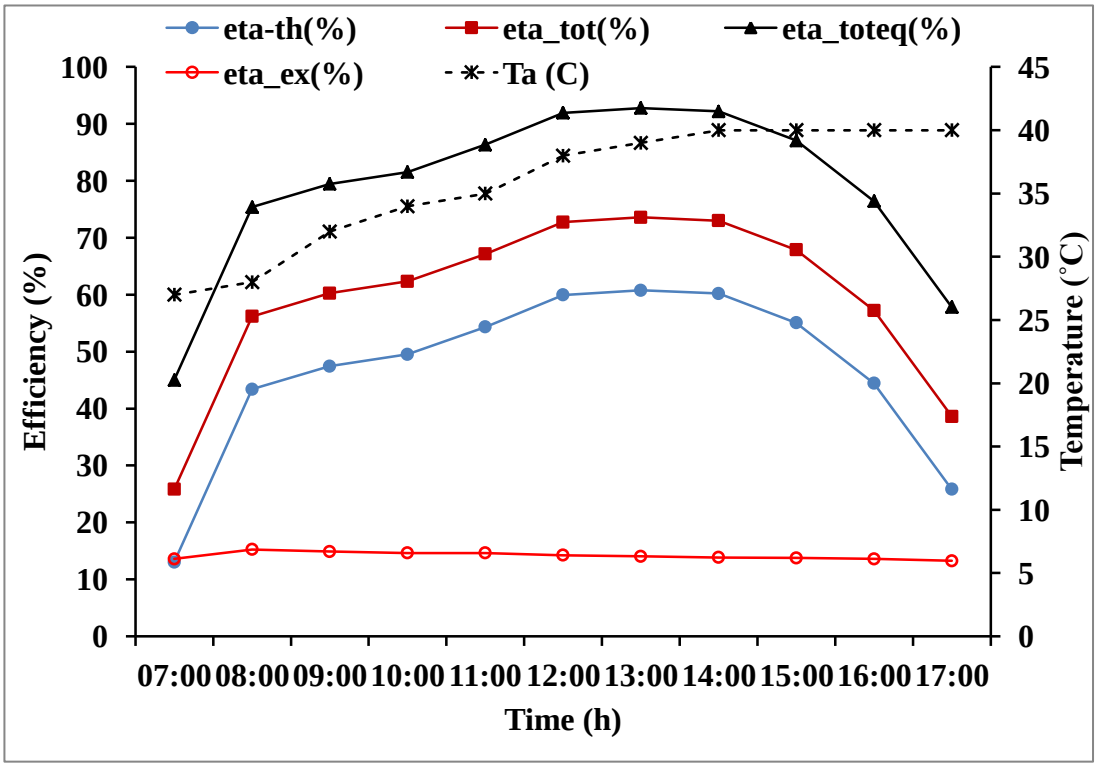

Figure 8.50 Varying of PV/T efficiencies during Sabha summer day

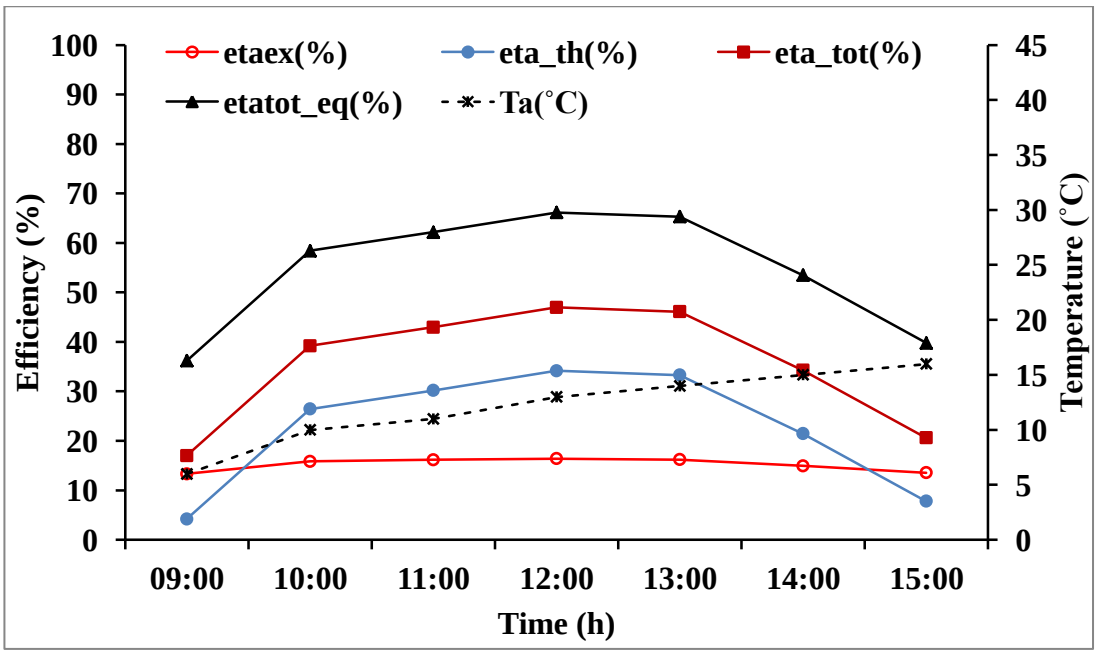

Figure 8.51 Varying of PV/T efficiencies during Sabha winter day

The PV/T power and hot water production during a summer and winter day in Sabha are presented in Figures 8.52 and 8.53. The Figures show that the power produced and the hot water increased up to their peak value at mid-day and then started to decline. The maximum power and hot water values are performed in the mid-summer day as 4886 kWh and 873 m^3/h respectively and this decreased to 1018 kWh and 78 m^3/h by the end of the day. However, these quantities decreased on the mid-winter day to 4229 kWh and 60 m^3/h and to 1498 kWh and 60 m^3/h by the end of that day.

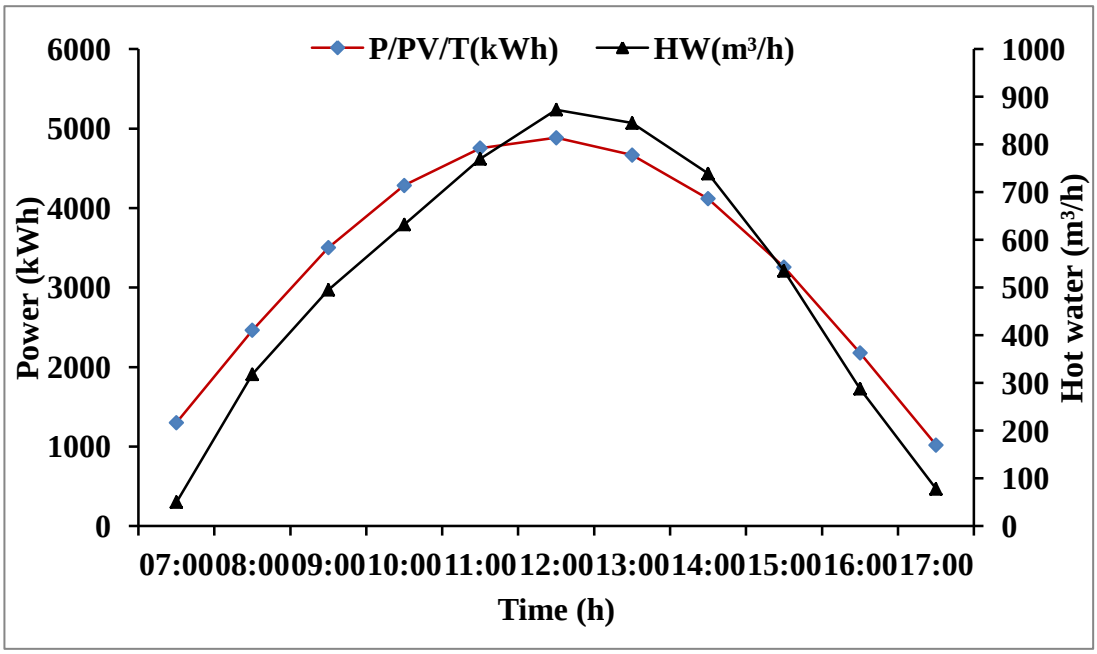

Figure 8.52 Production of PV/T power and hot water during Sabha summer day

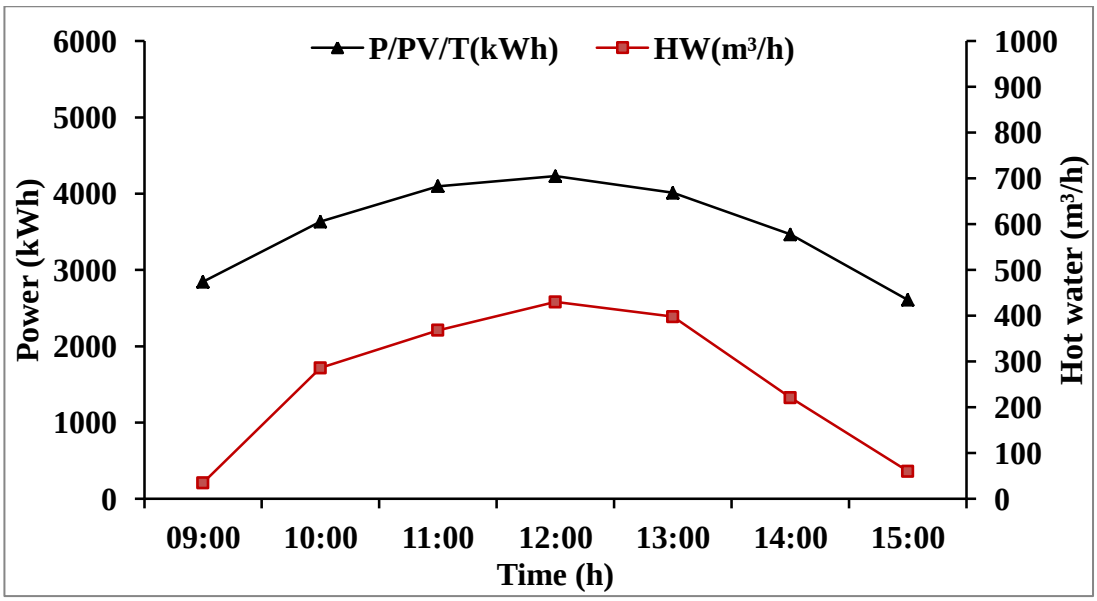

Figure 8.53 Production of PV/T power and hot water during Sabha winter day

The fluctuations in the PV/T electricity and the exergy destruction costs during a summer and winter day in Sabha are illustrated in Figures 8.54 and 8.55. It is clear from the Figures that for the same period of the day the unit working in the summer day has a lower output electricity cost and exergy destruction cost than the one working on the winter day. The analysis shows that the unit output electricity cost and the corresponding exergy destruction cost at the mid-summer day are 0.0039 $/kWh and 134 $/h respectively, which increases to 0.0525 $/kWh and 1600 $/h on the mid-winter day.

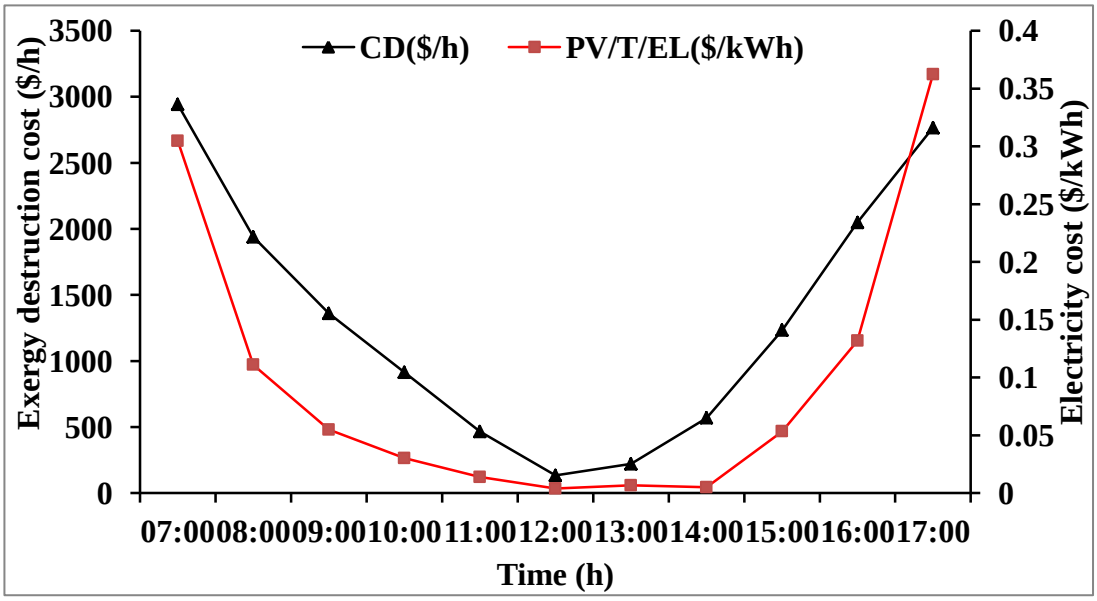

Figure 8.54 Fluctuating of PV/T electricity and exergy destruction costs during a summer day in Sabha

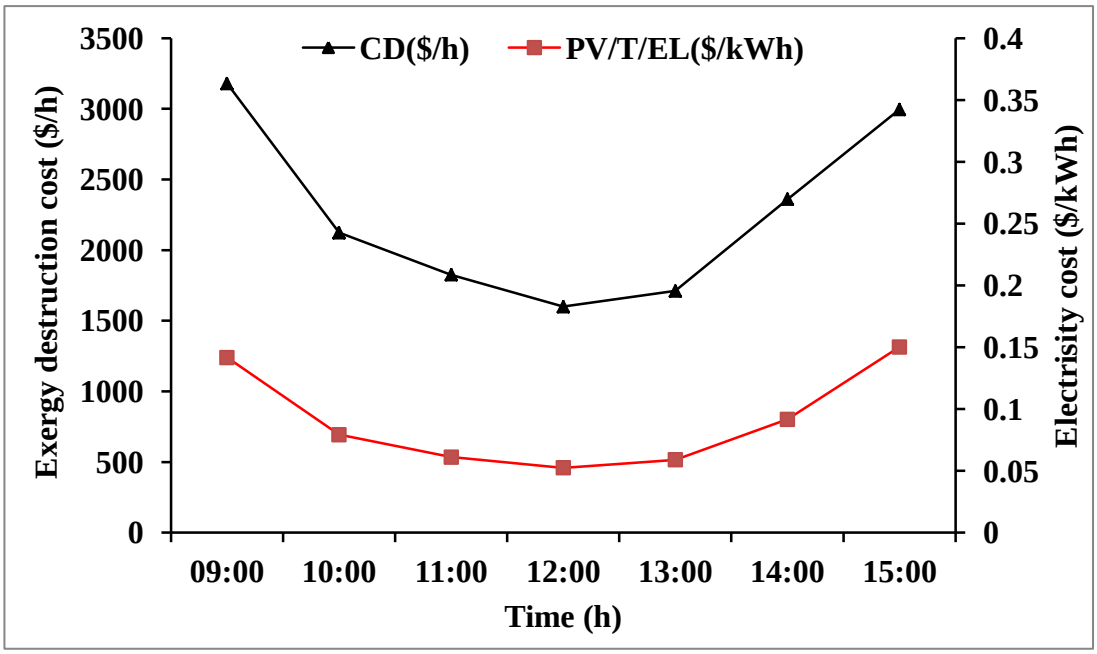

Figure 8.55 Fluctuating of the PV/T electricity and exergy destruction costs during a winter day in Sabha

8.9.2 Parametric study of a stand-alone photovoltaic thermal PV/T system

The analysis of the PV/T system in the previous sections is carried out based on a constant output hot water (T_o= 45 ^oC) with varying mass flow rate. The constant output water temperature mode is suitable for the industrial and domestic uses, whereas this process needs a control system for the input water temperature and mass flow rate. However, the electricity and hot water demands of the users in a community vary according to each site's daily and seasonal weather. The analysis shows that the PV/T systems working at a hot and sunny summer days will produce more hot water and electricity than the one working on a cold day. Unfortunately, the hot water demands during cold days are more than the demands during the hot days. Therefore, the system has to be optimized according to its main function and priority as electricity and hot water production depends on the real demand and the weather condition at that time in each site. This leads to a trade-off analysis to optimize the system for its optimum output electricity and thermal efficiency at an optimum unit output cost at a different output hot water temperature and mass flow rate as presented in table 8.37 and Figure 8.56. The analysis of the PV/T system at Sabha using yearly data shows that increasing the system output hot water temperature from 40 ^oC to 65 ^oC, through reducing the input water mass flow rate, will reduce the system output power. This leads to reducing the

system efficiency, the hot water quantity and increase the output electricity cost. The results show that the exergy, thermal, total and total equivalent efficiencies are decreased by 13.71%, 73.47%, 60%, and 48.11% respectively. Additionally, the power output and the exergo-economic factor are also decreased by 12.60% and 36.03% respectively, while the unit's electricity cost is increasing by 55.86 % by increasing the hot water temperature from 40 ^{o}C to 65 ^{o}C, as illustrated in table 8.37 and Figure 8.56. The PV/T system total equivalent efficiency should exceed 50% to compete the traditional solar hot water systems in terms of energy saving view [81]. Furthermore, the analysis of the PV/T system using a yearly average data as presented in table 8.37, indicating that the total equivalent efficiency is decreasing to less than 50% when the hot water temperature is increased above 55 ^{o}C. In general, the system's main function, the weather and the output utilization percentage and cost governs the decision to use the PV/T system at any specific operation condition.

HW/To(˚C)	ELPV/T($/kWh)	P/PV/T(kWh)	eta_expvt(%)	eta_th(%)	eta_tot(%)	eta_toteq(%)	eta_act(%)	(PV/T)fk(%)	HW/mass(kg/s)
40	0.0691	3468.56	14.95	46.26	59.39	79.09	13.13	20.26	162.66
45	0.0701	3381.04	14.99	39.46	52.27	71.47	12.80	19.87	110.60
50	0.0741	3293.60	14.79	32.67	45.14	63.84	12.47	18.79	76.31
55	0.0815	3206.17	14.37	25.87	38.01	56.22	12.14	17.11	51.79
60	0.0927	3118.73	13.74	19.07	30.88	48.59	11.81	15.09	33.40
65	0.1077	3031.30	12.90	12.27	23.75	40.97	11.48	12.96	19.11

Table 8.37 Effect of varying PV/T hot water temperature on system performance

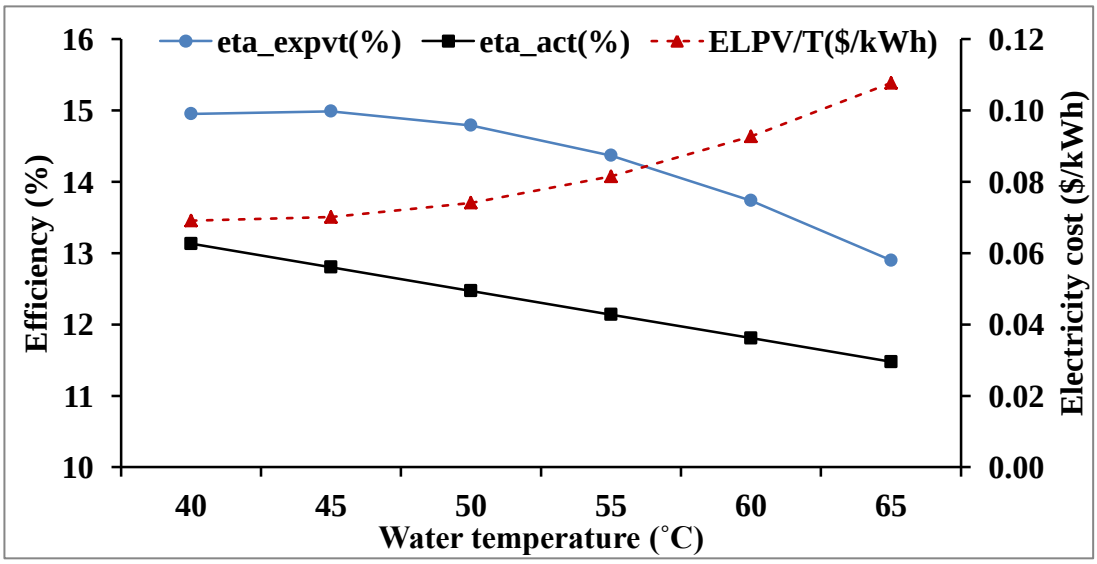

Figure 8.56 Varying of exergy efficiency, actual efficiency and electric cost of PV/T system with varying output hot water temperature

8.9.3 Optimum utilization of PV/T output hot water

The analysis of the PV/T system in the previous sections shows that improvement of the system's thermo-economics and performance factors depends on the percentage of hot water utilization and its mass flow rate, as well as its cost. The hot water at around 45 ^{o}C to 55 ^{o}C as recommended from the energy saving efficiency view is acceptable for used in domestic and human needs. Moreover, the quantity of hot water produced could exceed the needs of the community for such capacity studied in this research and sometimes this is not required for domestic and human needs, particularly at hot regions in the daytime. As an example, the system installed in Sabha produces 873 m^3/h of hot water on a mid-summer day, while the ambient temperature of that day exceeds 38 ^{o}C. However, the economic value of the hot water increases as its temperature and mass flow rate increases to the level where it could be utilized in a low thermal energy systems. However, to use the hot water in low thermal energy systems such as absorption chillers or organic Rankin cycle its temperature has to be raised up to around 70 ^{o}C [166]. Producing a hot water at this level of temperature uses the traditional fuels and power such as in an electric heaters is a non-environmental benign and costing process. For this concept, an IPSEpro model is developed to examine the electricity consumption of an electric heater used to raise up the PV/T output hot water temperature as presented in Figure 8.57. The figure shows that for Sabha, using yearly average data, an electric heater with 98 % efficiency is requiring 11,803 kWh to raise up the water temperature from 45 ^{o}C to 70 ^{o}C at a mass flow rate of 110.60 kg/s, while the PV/T system produce only 3381 kWh. The effect of varying the PV/T output hot water temperature from 40 ^{o}C to 65 ^{o}C on the electricity requirements of the electric heater to raise the water temperature up to 70 ^{o}C is representing in Figure 8.58. The Figure shows that the heater electricity consumption is more than the PV/T electricity production when the output hot water temperature is less than 55 ^{o}C. It is also found that increasing the PV/T hot water temperature from 65 ^{o}C to 70 ^{o}C requires only 407 kWh while the PV/T system is produces 3031 kWh of electricity and the mass flow rate at this situation decreases to 19.11 kg/s. In general, the most important question is how much electricity or cooling load and its unit cost can be produced, using such hot water quantity, in a low thermal energy system.

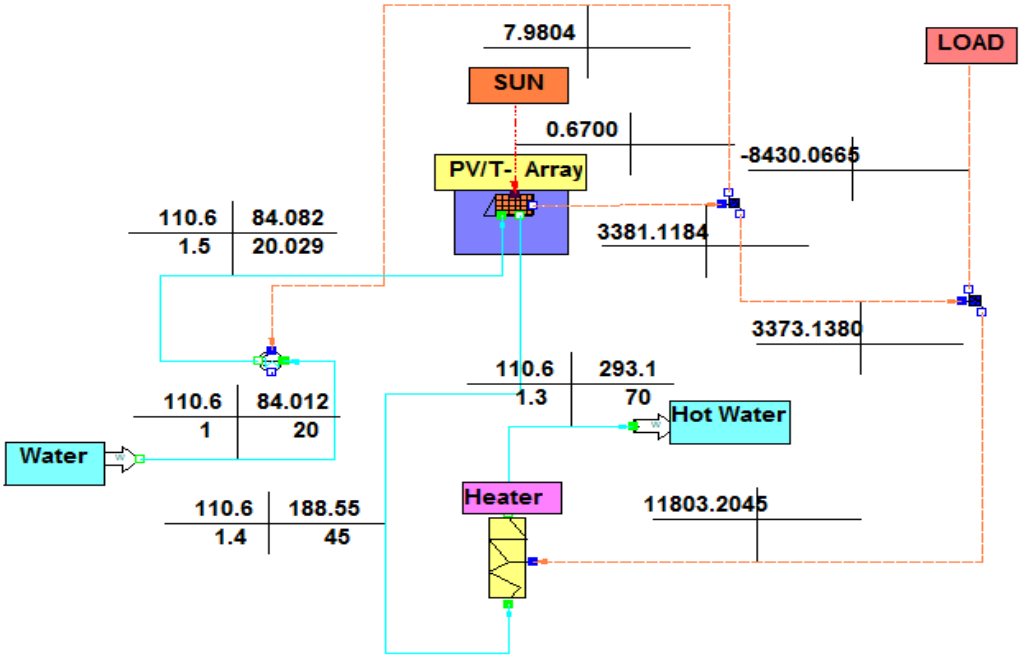

Figure 8.57 IPSEpro model for PV/T system connected to electric heater

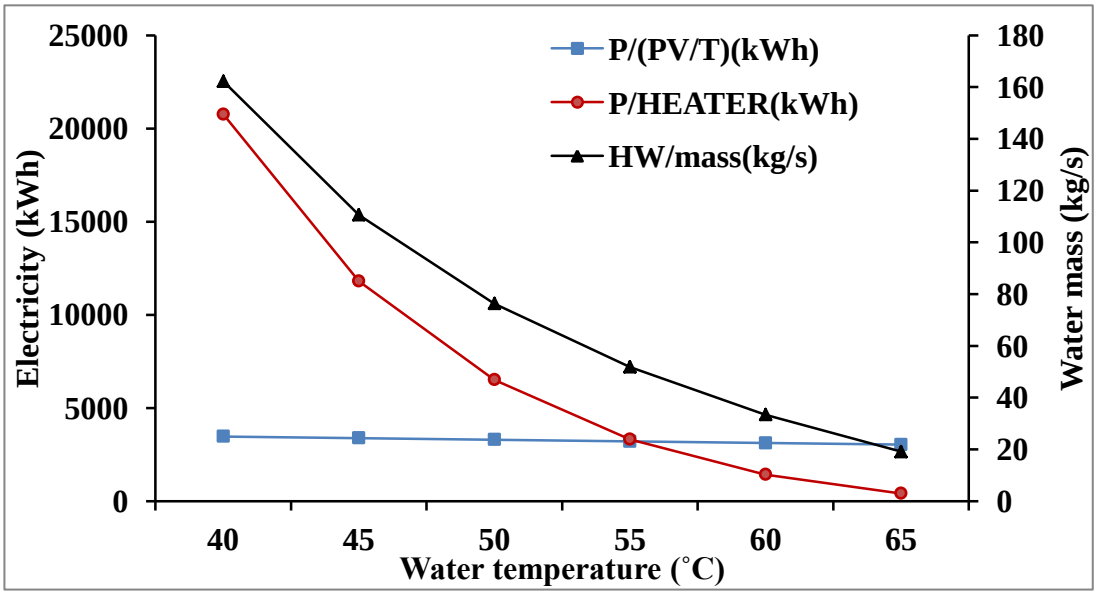

Figure 8.58 Effect of varying PV/T hot water temperature on electricity requirement of electric heater to raise the water temperature up to 70 ^{o}C

CHAPTER NINE

Chapter Nine

Conclusions and recommendations for future work

9.1 Introduction

The rapid depletion of fossil fuels sources and their pollution problems are encouraging governments and scientists nowadays to use reliable, long lasting and environmentally friendly energy sources. New and renewable energy sources such as solar, wind and geothermal are alternative to traditional fossil fuel energy sources. However, the most important challenge in utilizing these sources is their intermittent nature and their utilization costs, particularly for solar energy. Many researchers have suggested that hydrogen is a clean, safe and environmentally benign fuel and an energy carrier used with solar systems instead of using batteries or generators as storage or back-up systems. On the other hand, SHS is still an immature technology, which encourages more efforts in order to improve their performance and output costs. In this study, a thermo-economic model library for solar hydrogen system units such as; photovoltaic, photovoltaic thermal, PEM fuel cell and water electrolyzer were developed using the commercially available energy tool software package IPSEpro. The study takes into considerations the saving of costs from using CO_2 emission damage and fossil fuel resources consumed factors in the analysis. The models were validated theoretically and used the previous experimental studies results as well as the technical and tested data provided by the adopted unit's manufacturing. The developed models, along with the existing IPSEpro model libraries, were used to design, optimize and simulate the entire system to cover one MWh peak load and the energy demand of a small community day and night in Sabha, Misurata in Libya as a hot regions and Newcastle in the United Kingdom as a cold region. The analysis used yearly average and a chosen daily summer and winter real weather data. A parametric study was carried out to investigate the effects of the environmental, main operation and economic parameters on the performance and output of each component and the entire system. In the following sections the main results obtained from this study and some recommendations and suggestions for future work are presented.

9.2 The IPSEpro models

The IPSEpro software packeage was successfully used to develop a new model library to investigate the SHS and its units. An IPSEpro-MDK kit was used to develop these libraries according to their functions and use as presented in table 9.1. These model

libraries along with the IPSEpro developed connections and complementary models were used to simulate and evaluate the SHS and its units individually based on either energy, exergy or thermo-economic methodology. However, these models could also be used along with the existing IPSEpro advanced power thermal library (APP-Lib) or any other available libraries such as the refrigeration library (Frigo_Lib) model units to investigate many energy and refrigeration system. The developed models were successfully validated using experimental and previous simulations data in order to check the accuracy of the results of a model at its rated capacity and at different operation conditions, particularly for the PV unit. Taking in considerations the immaturity of the unit technologies, capacities, costs and the sites evaluated in this study; the simulation and the parametric study revealed that the SHS IPSEpro models are consistent with the tested and previous simulated trends and results.

Model library name	Function
PV_cell	PV-energy and exergy analysis
PV_cellba	PV-thermo-economic analysis using equation (6.53)
PV_cellbabaa	PV-detailed thermo-economic analysis
PV_cellbaaa	PV/T- detailed thermo-economic analysis
electrolyser	EL-exergy analysis without cooling or stream recycling
electrolyserb	EL-energy and exergy analysis with cooling
electrolyzerba	EL-thermo-economic analysis with cooling and recycling system integrated in SHS
electrolyzerbaa	EL- thermo-economic analysis without cooling or recycling system
fuel_cell3	FC-energy and exergy analysis
fuel-cell3d	FC-energy and exergy analysis integrated in a SHS with cooling and streams recycling
fuel_cell3e	FC-thermo-economic analysis integrated in SHS with cooling and streams recycling
hetxaa	Oxygen heat exchanger thermo-economic analysis
hetxb	Hydrogen heat exchanger thermo-economic analysis
compressorb	Thermo-economic analysis of the hydrogen compressors
tankO2a	Thermo-economic analysis of Oxygen tanks
tankH2a	Thermo-economic analysis of Hydrogen tanks

Table 9.1 IPSEpro models developed for SHS components and its function

9.3 SHS analysis at base condition

SHS designed and working in Sabha at a base condition (Sirr=1000W/m^2, Ta=25 ^{o}C, V= 1 m/s) was optimized and sizing as presented in sections 8.2 and 8.3. The system designed, simulated and evaluated to meet the required peak load (1 MWh) day and night using the developed IPSEpro models explained in the previous section. However, in the following paragraphs the main conclusions will be reached.

The analysis indicated that the system required 67262 m^2 in an open field area for the 26201 PV panel with a 6.287 MWh installed capacity in order to produce 4.858 MWh actual powers and 37.85 m^3/h of hot water. The optimization processes show that 79% of the total PV produced electricity was necessary to produce the sufficient hydrogen and oxygen to be used in the fuel cell to cover the load for the rest of the day. The optimization processes also indicated that 659 m^3 and 327 m^3 for hydrogen and oxygen low-pressure tanks' storage capacity was required for three days' suggested storage. It was found that the PV unit had the highest exergy destruction factor percentage at 93.17%, followed by the fuel cell at 4.4 % and the electrolyzer at 2.15%, whereas for the complementary units this was just 0.272%. The calculated exergy efficiency for the PV, fuel cell and the electrolyzer were 8.75%, 35.6% and 76.71% respectively. In addition, the SHS exergy efficiency was calculated at 5.07% and this was reduced to 3.35 % when the total PV output was totally used to cover the load by using the electrolyzer and the fuel cell directly during the day. The exergy efficiency of the hydrogen system only consisting of; the electrolyzer, fuel cell and the complementary units was 28.56%. The analysis also showed that the actual electrical efficiency of the PV was 12.32%, whereas the energy efficiency of the fuel cell and electrolyzer was reached to 83.17 % and 78.6 % respectively when the cooling load was considered.

9.3.1 Thermo-economic evaluation of SHS at base condition

The thermo-economic analysis of the SHS showed that the PV unit had the highest (ZTCD) factor followed by the fuel cell and the electrolyzer. The PV unit also had the lowest (fk) factor at 11.06%, compared with 16.41% and 70.74% for the fuel cell and the electrolyzer respectively. The results also revealed that the PV electricity cost was 0.074 $/kWh while it increased to 0.394 $/kWh for the fuel cell. The low (fk) factors for the PV and FC units indicated that increasing the unit exergy efficiency was a priority. On the other hand, the high (fk) factor for the electrolyzer shows that more attention had to be focused on decreasing the unit cost than increasing its exergy efficiency. However, the high fuel cell and electrolyzer (rk) values pinpoint that more investigation is required to reduce the unit input fuel costs (C_f) in order to reduce the unit production cost. The analysis was also showed that the low ZTCD factors of the complementary units indicated that it had not a significant effect on the cost structure of the system final production cost. However, the hydrogen exergy cost was increased by only 3% between the electrolyzer output and the fuel cell input path. The tank volume and pressure and

the compressor pressure ratio were the most important factors that affected its output exergy cost.

9.3.2 The SHS environmental and resources consumed saving costs

The analysis of the SHS at the base condition showed that the PV and FC electricity costs decreased by 19.4% and 4% if the CO_2 direct impact cost is considered. In monetary values, the annual CO_2 total saving was calculated as $295,592. However, this value of saving was represented 25.7 % of the total system cost during its lifetime. The analysis also showed that considering the fossil fuel resources consumed in addition to CO_2 impact, particularly in fossil fuel subsidised tariff areas as in Sabha, had reduced the PV and fuel cell electricity costs to 0.01$/kWh and 0.33$/kWh respectively.

9.3.3 The effect of varying solar intensity and ambient temperature on SHS performance

The parametric study revealed that increasing solar intensity had a more significant effect on the SHS performance and outputs than increasing the effect of low ambient temperature, particularly for the power output and its cost. The results indicated that the optimum PV exergy efficiency was achieved at the lowest values of Ta= 5 ^{o}C and Sirr= 0.2 kW/m^2 as PV-etaex=13.8%. The parametric analysis also showed that the optimum; hydrogen exergy cost as EL-ch2 = 34 $/GJ, hydrogen production mass as EL-H2mass=69 kg/h and the optimum fuel cell electricity exergy cost as FC-cw= 95.1 $/GJ was achieved when the system was operated at Sirr=1 kW/m^2 and Ta=5 ^{o}C.

9.4 Parametric study of a standalone PV unit

The effect of the economic parameters of the PV such as (ir,ny, CF, CFC) on the unit and entire system performance and outputs was investigated. The analysis showed that at a PV capacity factor as in Sabha case (CF=40%), decreasing the PV-CFC from 5500 to 500 $/kW would decrease the unit output exergy cost from 37.7 $/GJ to 3.43 $/GJ. It was also found that decreasing the PV capacity factor from 100 to 10 % will increase the hydrogen exergy cost by 539 % at CFC=5500 $/kW and by 124 % at CFC = 500 $/kW. The analysis also revealed that increasing the PV lifetime (ny) had a more significant effect on decreasing the PV and fuel cell units' output electricity costs than the effect of reducing the corresponding interest rate (ir) in the analysis.

9.5 Parametric study of a standalone electrolyzer unit (EL)

The simulation analysis of a standalone electrolyzer revealed that using a cooling system, and the fuel cell output water would increase the unit exergy efficiency by 10%. The analysis also showed that increasing the power input from 1000 to 4000 kW at the base condition reduced the hydrogen exergy cost by 54% and increased its mass by 302%. It was found that increasing the operated unit voltage from 1.6 V to 2 V at constant power would reduce the unit exergy and energy efficiencies by 19% and 2% respectively. This voltage increasing would also reduce the hydrogen mass by 19.7% and its exergy cost was increased by 12.22%. The study revealed that, at the constant of other parameters, decreasing the unit input electricity exergy cost from 50 $/GJ to 5 $/GJ will reduce the hydrogen cost by 77.5%. This was leading to decrease the exergy destruction factor (CD) as well as increase the (fk) and (rk) factors. However, increasing these factors with the constant of the unit exergy efficiency means that more attention has to be focused on reducing the unit investment cost (ZT). The parametric study also showed that decreasing the unit capacity factor (CF) has a significant effect on increasing the production cost particularly for a CF factor less than 40%. It was found that increasing the EL-CF from 10 to 100% will decrease the hydrogen cost by 56%, while increasing the unit CFC from 300 to 3300 $/kW will increase the hydrogen cost by 99%. The analysis also showed that increasing the interest rate from 1 to 10% at ny=5 years will increase the hydrogen exergy cost by 17.9% whereas it decreases by 42.8% at ir =10 % if the lifetime increases from 5 to 50 years.

9.6 Parametric study of a standalone fuel cell unit (FC)

Four IPSEpro developed models (fuelcell3, fuelcell3e, fuelcell3f and fuelcell3b) were used to investigate the energy, exergy and thermo-economic analysis with and without water and gas recycling and cooling systems. It was found that the exergy efficiency of the units with cooling and recycling systems and those using recycling system only, working at base condition, would be enhanced by 30% and 21% respectively above the exergy efficiency of a unit without such systems. It was also found that the unit electricity cost and the consumed hydrogen at base condition increased from 0.3946$/kWh and 63 kg/h respectively for a unit with cooling and recycling system to 0.5614 $/kWh and 75.6 kg/h for a unit without recycling and cooling system. The analysis also showed that increasing the cell voltage for a unit working at its rated power from 0.6 V to 0.7 V will increase the exergy and energy efficiencies by 14.3% and 1.1% respectively while the hydrogen quantity will be reduced by 14.3%. The study

also showed that increasing the hydrogen stoichiometric ratio without recycling has a significant effect on the unit performance and output which is greater than the effect of increasing the oxygen stoichiometric ratio. The results also indicated that the unit output electricity cost is affected by the hot water utilization percentage, quantity and its estimated price. The analysis also showed that the effect of increasing the lifetime of the fuel cell was less affected than its increments on the electrolyzer performance. The study revealed also that increasing the fuel cell capacity factor (FC-CF) has a significant effect on decreasing the unit output electricity cost at a high capital unit costs (FC-CFC) particularly when the unit working at a (CF) less than 50%.

9.7 SHS analysis at Sabha, Misurata and Newcastle (yearly average data)

Three SHS installed at Sabha, Misurata and Newcastle were simulated and evaluated based on a yearly average solar and weather data. The results showed that the system installed at Sabha had the best performance and output cost and quantity. However, there was no significant difference between the results of Sabha and Misurata systems as appeared from the simulation results in tables 8.27 and 8.28. The analysis showed that the yearly average PV/Tc calculated in Sabha increased by 10.2% and 48% above the ones conducted at Misurata and Newcastle respectively. This led to a decrease in the yearly average exergy efficiencies of the unit in Sabha by 1.5% and 6% and the energy efficiency by 2.34% and 8.3% respectively below the efficiencies performed at Misurata and Newcastle. However, the total yearly; PV power, hot water and hydrogen mass produced from the system in Sabha was 11820 MWh/y, 92085 m^3/y and 153 ton/y. These quantities were by 2%, and 88% respectively above the levels of the same SHS outputs installed in Misurata and Newcastle. Using the total hydrogen produced during the year the fuel cell unit installed in Sabha produced 2508MWh/y increased up by 5% and 94.5% above the power produced by the same unit in Misurata and Newcastle respectively. The yearly average PV and FC electricity costs, as well as the hydrogen exergy cost in Sabha were 0.1066$/kWh, 0.695$/kWh and 60.91$/GJ respectively. However these costs are almost the same in Misurata and increased in Newcastle to 0.1722 $/kWh, 0.933 $/kWh and 84.27 $/GJ respectively. These values revealed that the SHS output costs were still far away from the current market electricity cost estimated as +- 0.15 $/kWh, unless the CO_2 impact and resources consumed were considered in the analysis.

9.7.1 Thermo-economic analysis of SHS on typical summer and winter days

The analysis showed that in January the PV unit installed in Sabha had slightly higher exergy efficiency and more power produced by 15% than the one installed in Misurata with a reduction of 27.35% in the unit electricity cost. In August, the unit installed in Misurata produced more power by 7.24% than the one installed in Sabha due to the effect of higher solar intensity and low (PV/Tc) recorded at that day in Misurata. The analysis also showed that the system installed in Sabha had much better performance and outputs than the similar one installed in Newcastle for both corresponding summer and winter days. In January, the system installed in Sabha was producing 30325 kWh from the PV unit and 6275 kWh from the fuel cell during the day. It only produced 6097 kWh from the PV unit and 1253 kWh from the fuel cell for a system installed in Newcastle at January. The system installed in Sabha in January also produced 395 kg/day hydrogen gas and 237 m^3/day hot water, compared with only 79 kg/day hydrogen and 47.52 m^3/day hot water produced by a similar system installed in Newcastle on the same date. This high production in Sabha in January reduced the PV and FC hourly average unit thermo-economic cost from 0.584$/kWh and 3.354$/kWh in Newcastle to 0.117$/kWh and 0.776$kWh in Sabha. In addition, the hydrogen unit exergy cost was reduced from 293 $/GJ in Newcastle to 67.7 $/GJ in Sabha for the same day. This reduction was mainly due to the low average sunshine hours and solar intensity in Newcastle, compared with that recorded in Sabha for the same day. However, there was higher PV exergy efficiency and lower irreversibility in Newcastle than in Sabha due to the lower average module surface temperature. This issue have not a significant effect on the output unit's thermo-economic cost values in Newcastle compared with the values conducted in Sabha, due to the higher output power performed in Sabha. The higher PV output unit's thermo-economic cost in Newcastle led to large increases in the average daily (CD) and (fk) factors calculated in Newcastle compared with that calculated in Sabha for the same day. The SHS installed in Sabha in August also had higher performance and unit output costs than the one in Newcastle for the same reasons as in January. In August, the system installed in Sabha produced 34359 kWh from the PV unit and 7068 kWh from the fuel cell during the day. However, it only produced 4065 kWh from the fuel cell unit and 19776 kWh from the PV for a system installed in Newcastle during August. The system installed in Sabha in August would also produce 445 kg/day hydrogen gas and 267 m^3/day hot water compared with only 256 kg/day hydrogen and 154 m^3/day hot water produced by a similar system installed in Newcastle at the same date. These high production in Sabha

in August would also reduce the PV and FC hourly average unit thermo-economic cost from 0.3338 $/kWh and 1.882 $/kWh conducted in Newcastle to 0.142 $/kWh and 0.96$kWh respectively in Sabha. The hydrogen unit exergy cost was reduced from 166 $/GJ in Newcastle to 82.7 $/GJ in Sabha for the same day of August.

9.8 IPSEpro photovoltaic thermal model (PV/T)

The analysis of SHS reveals that decreasing the PV surface temperature will improve the unit exergy efficiency and its electricity outputs and cost. Water cooling PV/T system IPSEpro model was developed and used to optimize and evaluate the system thermo-economically. The system was simulated using yearly average data of Sabha site and it carried out based on a constant outlet water temperature as 45 ^{o}C and assumed that 50% of it was utilized in a domestic use. The results were compared with a similar system used water for cooling only at outlet temperatures of 30 ^{o}C and a PV system. The results showed that the exergy efficiency of the PV/T system (hot water) was increased by 6% and 48% respectively above the exergy efficiency performed for the similar cooling only system and the PV unit only. It was also found that the PV/T (cooling only) produced more power by 7.7% and 8% respectively than the hot water and PV only systems. In addition, the results showed that the hot water system had the lowest output electricity cost as 0.0701 $/kWh compared with 0.1152$/kWh for the PV/T cooling only system and 0.1066 $/kWh for the PV system. The exergy destruction cost (CD) of the (PV/T) hot water system also decreased by 38.44% and 37.76% than the factors calculated for the (PV/T) cooling and PV only systems respectively. It was also found that the (fk) of the (PV/T) hot water system was increased by 50% and 70% respectively above the one conducted for the (PV/T) cooling and PV systems.

9.8.1 Thermo-economic analysis of PV/T system at a summer and winter days

The PV/T system (hot water) installed in Sabha was simulated and evaluated thermo-economically on an hourly basis for a summer and winter days. The analysis showed that the system on the summer day would produce 36432 kWh and 5623 m^3/h hot water at 45^{o}C. This quantity would be reduced to 28179 kWh and 1798 m^3/h in the winter day. The results also showed that the daily average exergy destruction factor (CD) in the winter day was increased by 70% than the one calculated in the summer day. This led to increases in the average exergy economic factor (fk) in the summer day by 107 % than the one calculated in the winter day. However, the exergy efficiency in the winter day increased by 7.27% more than the one performed in the summer day. This was mainly

due to the cooling effect of the low average ambient temperature in the winter day recorded as 12.14 ^{o}C compared with 35.72 ^{o}C in the summer day. Moreover, due to the high quantity of hot water produced in the summer day, the thermal, total and the total equivalent efficiencies on that day is increased by 107%, 68.65% and 44.46% respectively than the ones performed in the winter day.

9.8.2 Parametric study of a standalone PV/T system

Trade-off analysis was carried out to optimize a system working at a different outlet water temperature and varying mass flow rate for its optimum output electricity and thermal efficiency at an optimum output electricity cost. The analysis showed that the system efficiency, water mass flow rate decreased, and the electricity cost increased as the outlet hot water temperature increased. It was found that the exergy, thermal, total and total equivalent efficiencies were decreased by 13.71%, 73.47%, 60% and 64% respectively as the hot water temperature increased from 40 ^{o}C to 65 ^{o}C. In addition, the power output and the (fk) factor also decreased by 12.6% and 36.03% respectively. It was also found that the unit output electricity cost increased by 55.85% with the same range of hot water temperature increases. The results indicated that the total equivalent efficiency had decreased less than the recommended percentage of 50% when the PV/T system output hot water temperature exceeded 55 ^{o}C. In general, the weather and the output water utilization percentage and selling price appeared to be the most important parameters governing the decision to use the PV/T system in specific operation conditions.

9.8.3 Optimum utilization of PV/T output hot water

The quantity of hot water produced by a PV/T system could exceed the needs of the community for such capacity studied in this research. For this concept, an IPSEpro model was developed to examine the electricity consumption of an electric heater. The heater was used to raise up the PV/T output hot water temperature in order to utilize it in low thermal energy systems. The analysis showed that the heater electricity consumption was more than the PV/T electricity production when the output hot water temperature was less than 55 ^{o}C. The electric water heater at this condition was not feasible to use with the PV/T systems. In general, the most important equation is how much electricity or cooling load could be produced by a low thermal energy system using the hot water produced from the PV/T system according to each site and weather condition, and what would it cost be? Thus, more investigation is required to build a

thermo-econmic IPSEpro model for studying a SHS with PV/T unit connected to a solar collector or a backup heater and low energy thermal systems.

9.9 Recommendations and suggestions for future work

The planned proposal and the subject of this research study have been conducted within the available and limited time and space. However, based on the results and the work achieved, some recommendations and additional studies need to be continued and some suggestions as a future work might include the following:

1- It is recommended to develop a thermo-economical IPSEpro models to design, simulate and evaluate a renewable energy and other energy systems such as wind turbine, generator and desalination plants integrated with a SHS.

2- Due to the limited hydrogen specification, data links tables in the existing IPSEpro library to a maximum pressure of 35 bar. It is recommended to use IPSEpro with new linked gases specifications tables to study SHS integrated with different types of storage such as high pressure tanks of up to 700 bar and low pressure metal hydrate tanks.

3- It is also recommended to design and simulate a standalone and grid connected SHS with an hourly control and distribution system for the community energy and electricity hourly and seasonally demands, using a real pattern consumption mode.

4- Develop, design and simulate an IPSEpro thermo-economic model for SHS with PV/T unit connected with a solar collector or backup thermal heater to increase the system output hot water would be useful. It is also suggested to develop an IPSEpro thermo-economic model to utilize the SHS output hot water in an integrated low energy thermal system such as organic Rankin cycle and absorption chillier.

5- Develop, design and simulate an IPSEpro thermo-economic model of PV/assistance heat pump system would be recommended. This system would use the PV/T unit as an evaporator in the heat pump cycle instead of the traditional evaporator.

6- Design, simulate and evaluate SHS thermo-economically with a different capacity and unit types at a different sites using IPSEpro would be a valuable research.

7- The analysis of the PV/T system in this study has assumed that the outlet hot water temperature is homogenous on the unit surface and follows the cell temperature by a $4^{o}C$ reduction according to the previous experimental results. However, for results that

are more accurate it is recommended to develop a model to study a high capacity PV/T system thermo-economically based on a dynamic thermal model for determining the output's hot water temperature.

8- The analysis of the electrolyzer and fuel cell units in this study was carried out under the assumption that the units were working near or at their rated capacity in a steady state condition and a specific pressure, temperature and voltage. For more accuracy particularly in hourly basis results of individual units, it is recommended to develop a thermo-economic model taking in consideration the unit's voltage variation and losses with the current density, temperature and pressure changes. In addition, it would also be useful to develop an exergy analysis model including some other important units design parameters such as cell material, cell thickness, electrode type and specifications.

REFERENCES

References

1- U.S. Energy information administration, *Country analysis brief overview for Libya*, (2013). available at: www.eia.gov/countries/country-data.

2- British Petroleum (BP), June 2011, *Statistical review of world energy*, available at: www.bp.com/statisticalreview.

3- Veziroglu T., Sahın, S. (2008) "21st Century's energy: Hydrogen energy system", *Energy conversion and management*, 49, pp. 1820–1831.

4-. Hefner, R. (2009), *The hydrogen transition age*, John Wiley & Sons.

5- Verizoglu, T. (1987) "Hydrogen technology for energy needs of human settlements", *International journal of hydrogen energy*,12, (2).

6. Dincer, I. (2002) "Technical, environmental and exergetic aspects of hydrogen energy systems", *International journal of hydrogen energy*, 27, pp. 265-285.

7- U. S. Department of energy, *Energy efficiency and renewable energy*, available at: www.eere.energy.gov/hydrogenfuelcells/production/index.html.

8- Yilanic, A., Dincer, I., Oztuk, H. (2009) "A review on solar-hydrogen/fuel cell hybrid energy systems for stationary applications", *Progress in energy and combustion science*, 35, (3), pp. 231-244.

9-. Deshmukh, M. , Deshmukh, S. (2008) "Modelling of hybrid renewable energy systems", *Renewable and sustainable energy reviews*, 12, (1), pp. 235-249.

10- Joshi, S., Dincer I., Reddy, B. (2011) "Solar hydrogen production: A comparative performance assessment", *International journal of hydrogen energy*,36, (17), pp. 11246-11257.

11- Negrue, B., N., Settue, N., Dokkar B. (2011) "Valuation and development of the solar hydrogen production", *International journal of hydrogen energy*, 36, pp. 4110-4116.

12- Belgen, E. (2001) "Solar hydrogen from photovoltaic-electrolyser systems", *Energy conversion and management*, 42, pp. 1047-1057.

13- Tani, T., Sekiguchi, N., Sakai, M., Ohta, D. (2000) "Optimization of solar hydrogen systems based on hydrogen production cost", *Solar energy*, 68, 2, pp.143-149.

14- Wang, C., Nehrir, M. (2008) "Power management of a stand-alone wind/photovoltaic/ fuel cell energy system*", IEEE Transactions of energy conversion*, 23, 3.

15- Calderon, M., Calderon, A., Gonzalez, J., Gonzalez, I. (2011) "Evaluation of hybrid photovoltaic-wind system with hydrogen storage performance using exergy analysis", *International journal of hydrogen energy*, 36, pp. 5751-5762.

16- Shabani, B., Andrew, J. (2011) "An experimental investigation of a PEM fuel cell to supply both heat and power in a solar-hydrogen RAPS system*". International Journal of hydrogen energy*, 36, pp. 5442-5452.

17- Zini, G., Marazzi, R., Pedrazzi, S., Tartarini, P. (2010) "A solar hydrogen hybrid system with activated carbon storage ", *International Journal of hydrogen energy*, 35, pp. 4909-4917.

18- Hacatoglu, K., Dincer, I., Rosen, A. (2011) "Energy analysis of a hybrid solar hydrogen system with activated carbon storage*", International Journal of Hydrogen energy*, 36, 10, pp. 3273-3282.

19- Yilanci, A. Ozturk, H., Dincer, I., Yilmaz, E., Cetin, E., Ekren, O. (2011) "Exergy analysis and environmental impact assessment of a photovoltaic-hydrogen production system ", *International journal exergy*, 2011, 8, 2, pp. 227-246.

20- Contreras, A., Guirado, R., Veziroglu, T. (2007) "Design and simulation of the power control system of a plant for the generation of hydrogen via electrolysis, using photovoltaic solar energy", *International Journal of hydrogen energy,* 32, pp. 4635-4640.

21- Paola, A., Fabrizio, Z., Fabio, O. (2011) "Techo-economic optimization of hydrogen production by PV-electrolysis: "RenHydrogen" Simulation program", *International Journal of hydrogen energy*, 36, pp. 1371-1381.

22- Ozsaban, M., Midilli, A., Dincer, I. (2011) "Exergy analysis of a high pressure multistage hydrogen gas storage system", *International Journal of hydrogen energy*, 36, pp. 11440-11450.

23- Akyuz, E., Coskum, C., Oktay, Z., Dincer, I. (2011) "Hydrogen production probability distributions for a PV- electrolyser system", *International journal of hydrogen energy*, 36, PP.11292-11299.

24- Santarelli, M., Macagno, S. (2004) "Hydrogen as an energy carrier in stand-alone applications based on PV and PV-micro-hydro systems", *Energy*, 29, pp.1159-1182.

25- Santarelli, M., Macagno, S. (2004)"A thermoeconomic analysis of a PV-hydrogen system feeding the energy requests of a residential building in an isolated valley of Alps", *Energy conversion and management*, 45, pp. 427-451.

26- Lagorse, J., Simoes, G., Miraoui, A., Costerg, P. (2008) "Energy cost analysis of a solar-hydrogen hybrid energy system for stand-alone applications", *International Journal of hydrogen energy*, 33, pp. 2871-2879.

27- Joshi, A., Dincer, I., Reddy, V. (2010) "Exergetic assessment of solar hydrogen production methods" *International Journal of hydrogen energy*, 35, pp. 4901-4908.

28- Kolb, G., Diver, B., Siegle, N. (2007) "General solar hydrogen power plant", *Journal of solar energy engineering*,129, pp. 179-183.

29- El. Shatter, A., Eskandar, M., El-Hagry, M. (2002) "Hybrid PV/fuel cell system design and simulation", *Renewable energy*, 27, pp. 479-485.

30- Harvey, D. (1996) "Solar-hydrogen electricity generation and global CO_2 emission reduction", *International Journal of hydrogen energy*, 21,(7), pp. 583-595.

31- Park, M., Hanlee, D., Yu, I. (2006) "PSCAD/EMTDC modeling and simulation of solar-powered hydrogen production system", *Renewable energy*, 31, (14), pp. 2342-2355.

32- Eljrushi, G., Veziroglu, T. (1990) "Solar-Hydrogen Energy System for Libya", *International Journal of hydrogen energy*,15, (12), pp. 885-891.

33- Abdullah, M., Asfour, S. , Veziroglu, T. (1999) "Solar-Hydrogen Energy System for Egypt", *International Journal of hydrogen energy*, 24, (6), pp. 505-517.

34- Almogren, S., Viziroglu, T. (2004) "Solar-hydrogen system for Saudi Arabia", *International Journal of hydrogen energy*, 29, pp. 1181-1190.

35- Contreras, A., Carpio, J., Molero, M., Veziroglu, T. (1999) "Solar hydrogen: an energy system for sustainable development in Spain", *International Journal of hydrogen energy*, 24, pp. 1041-1052.

36- Shabani, B., Andrews, J., Watkins, S. (2010) "Energy and cost analysis of a solar-hydrogen combined heat and power system for remote power supply using a computer simulation", *Solar energy*, 84, pp. 144-155.

37- Ganguly, A., Misra, D., Ghosh, S. (2010) "Modeling and analysis of solar photovoltaic-electrolyzer-fuel cell hybrid power system integrated with floriculture greenhouse", *Energy and buildings*, 42, pp. 2036-2043.

38- Lopez, E., Isorna, F., Rosa, F. (2007) "Optimization of a solar hydrogen storage system: Exergetic consideration", *International Journal of hydrogen energy*, 32, pp. 1537-1541.

39- Ulleberg, O., Glöckner, R. (2002) "Hydrogems-hydrogen energy models", *WHEC 2002-14th world hydrogen, conference*, Montreal Canada.

40- Briguglio, N., Ferraro, M., Andalora, L., Antonucci, V. (2008) " New simulation tool helping a feasibility study for renewable hydrogen bus fleet in Messina", *International Journal of hydrogen energy*, 23, pp. 3077-3084.

41- Santarelli, M., Cali, M., Macagno, S. (2004) "Design and analysis of stand-alone hydrogen energy systems with different renewable sources", *International Journal of hydrogen energy*, 29, pp. 1571-1586.

42- Hwang, J., Lai, K., Wu, W., Chang, R. (2009) "Dynamic modeling of a photovoltaic hydrogen fuel cell hybrid system", *International Journal of hydrogen energy*, 34, pp. 9531-9542.

43- Zahedi, A.(2006) "Design, size optimization, performance prediction of solar PV/Hydrogen system supplying electricity for a remote located community", *ISESCO. Science and technology vision*, 2, 1, pp. 5-9.

44- Pedrazzi, S., Zini, G., Tartarini, P. (2010) "Complete modeling and software implementation of a virtual solar hydrogen hybrid system", *Energy conversion and management*, 51, pp. 122-129.

45- Mills, A., Al-Hallaj, S. (2004) "Simulation of hydrogen-based systems using Hybrid2", *International Journal of hydrogen energy*, 29, pp. 991-999.

46- Cetin, E., Yilanci, A., Oner, Y., Colak, M., Kasikci, I., Oziark, K. (2009) "Electrical analysis of a hybrid photovoltaic-hydrogen/fuel cell energy system in Denizli, Turkey", *Energy and buildings*, 41, pp. 975-981.

47- Ahmed, E., El Shenawy, T. (2006) "Optimized photovoltaic system for hydrogen production", *Renewable energy*, 31, pp. 1043-1054.

48- Alam, M., Gao, D. (2007) "Modeling and Analysis of a Wind/PV/Fuel cell Hybrid Power System in HOMER", *Second IEEE conference on Industrial electronics and Applications*, pp.1594-1599.

49- Bilgen, E. (2004) "Domestic hydrogen production using renewable energy", *solar energy*, 77, pp. 47-55.

50- Christopher, K., Dimitrios, R. (2012) "A review on exergy comparison of hydrogen production methods from renewable energy sources", *Energy & environmental sciences*, 5, pp. 6640-6651.

51- Raj, S., Ghosh, P. (2012) "Standalone PV-diesel system vs. PV-H_2 system: An economic analysis", *Energy*, 42, pp. 270-280.

52- Duffie, A., Beckman, A. (1991) "*Solar engineering of thermal processes*", Second edition, John Wiley, New York, USA.

53- Hersch, P., Zweibel, K. (1982) "*Basic photovoltaic principles and methods*", February 1982, published by technical information office, Solar energy institute USA.

54- Muneer, T., Asif, M., Kubie, J. (2003) "Generation and transmission prospects for solar electricity; UK and global markets", *Energy conversion and management*, 44, pp. 35-52.

55- National centre for photovoltaics (NREL), available from: www.nrel.gov/ncpv/.

56- Solar market research and analysis (Solarbuzz), available at: www.solarbuzz.com/facts-and-figures/retal-price-environment/.

57- Hruyshat, E. (2009) "Viability of solar photovoltaics as an electricity generation source for Jordan", *Renewable energy*, 34, pp. 2133-2140.

58- Harder, E., Gibson, J. (2011) "The costs and benefits of large-scale solar photovoltaic production in Abu Dhabi, United Arab Emirates", *Renewable energy*, 36, (2), pp. 789-796.

59- Ramadan, M., Nasseb, A. (2011) "The cost benefit analysis of implementing photovoltaic solar system in the state of Kuwait", *Renewable energy*, 36, pp. 1272-1276.

60- Marafia, H. (2001) "Feasibility study of photovoltaic technology in Qatar" *Renewable energy*, 24, pp. 565-567.

61- EL-Shimy, M. (2009) "Viability analysis of PV power plants in Egypt", *Renewable energy*, 34, pp. 2187-2196.

62- Fuents, M., Nofuentes, G., Aguilera, J., Talavera, D., Castro, M. (2007) "Application and validation of algebraic methods to predict the behaviour of crystalline silicon PV modules in Mediterranean climate", *Solar energy*, 81, pp. 1396-1408.

63- Garsia, M., Balenzategui, L. (2004) "Estimation of photovoltaic module yearly temperature and performance based on Nominal Operation Cell Temperature calculations", *Renewable energy*, 29, pp. 1997-2010.

64- Mattei, M., Notton, G., Cristofari, C., Muselli, M., Poggi, P. (2006) "Calculation of the polycrystalline PV module temperature using a simple method of energy balance", *Renewable energy*, 31, pp. 553-567.

65- Hove, T. (2000) "A method for predicting long-term average performance of photovoltaic systems", *Renewable energy*, 21, pp. 207-229.

66- Kurnik, J., Jankovec, M., Brecl, K., Topic, M. (2011) "Outdoor testing of PV module temperature and performance under different mounting and operational conditions", *Solar energy materials and solar cells*, 95, pp. 373-376.

67- Jones, D., Underwood, P. (2001) "A Thermal Model for photovoltaic systems", *Solar energy*, 70, 4, pp. 349-359.

68- Armstrong, S., Hurley, W. (2010) "A thermal model for photovoltaic panels under varying atmospheric conditions", *Applied thermal engineering*, 30, pp. 1488-1495.

69- Quesda, B., Sanchez, C., Canada, J., Royo, R., Paya, J. (2011) "Experimental results and simulation with TRNSYS of 7.2 kWp grid – connected photovoltaic system", *Applied energy*, 88, (5), pp. 1772-1783.

70- Joshi, A., Dincer, I., Reddy, V. (2009) "Thermodynamic assessment of photovoltaic systems", *Solar energy*, 83, pp. 1139-1149.

71- Eljrushi, G., Zubia, J., (1995) "Photovoltaic Power Plant for the Southern Region Part of Libya", *Applied energy*, 52, pp. 219-227.

72- Chel, A., Tiwari, N. (2011) "A case study of a typical 2.32kWp stand-alone photovoltaic (SAPV) in composite climate of New Delhi (India)", *Applied energy*, 88, pp. 1415-1426.

73- Sarhaddi, F., Farahat, S., Ajam, H., Behzadmehr, A. (2010) "Exergetic performance evaluation of a solar photovoltaic (PV) array", *Australian Journal of basic and applied sciences*, 4, 3, pp. 502-519.

74- Sarhaddi, F., Farahat, S., Ajam, H., Behzadmehr, A. (2010) "Exergy efficiency of a solar photovoltaic array based on exergy destruction", *Journal of power and energy* , 224, (6), pp. 813-825.

75- Skoplaki, E., Playvos, A. (2009) "Operating temperature of photovoltaic modules: A survey of pertinent correlations", *Renewable energy*, 34, pp. 23-29.

76- Cherigui, A., Mahmah, B., Harouadi, F., Belhamel, M., Chader, S., M'Raoui, A. Etievant, C. (2009) "Solar hydrogen energy: The European-Maghreb connection. A new way of excellence for a sustainable energy development", *International Journal of hydrogen energy*, 34, pp. 4934-4940.

77- Rehman, S., Bader. M., AL-Moallem, S. (2007) "Cost of solar energy generated using PV panels", *Renewable and sustainable energy reviews*, 11, pp. 1843-1857.

78- Huld, T., Friesien, G., Skoczek, A., Kenny, R., Sample, T. (2011) "A power rating model for crystalline silicon PV modules", *Solar energy materials & solar cells*, 95, pp. 3359-3369.

79- Tiwari, A., Sodha, M. (2006) "Performance evaluation of Solar PV/T system: An experimental validation", *Solar energy*, 80, pp. 751-759.

80- Cristofari, C., Notton, G., Canaletti, J. (2009) "Thermal behavior of a copolymer PV/Th solar system in low flow rate conditions", *Solar energy*, 83, pp. 1123-1138.

81- Huang, B., Lin, T., Hung, W., Sun, F., (2001) "Performance evaluation of solar photovoltaic/ thermal systems", *Solar energy*, 70, (5), pp. 443-448.

82- Kalogirou, S. (2001) "Use of TRNSYS for modeling and simulation of a hybrid PV-thermal solar system for Cyprus", *Renewable energy*, 23, pp. 247-260.

83- Dubey, S., Tawari, G. (2009) "Analysis of PV/T flat plate water collectors connected in series", *Solar energy*, 83, pp. 1485-1498.

84- Dubey, S., Tiwari, G. (2008) "Thermal modeling of a combined system of photovoltaic thermal (PV/T) solar water heater", *Solar energy*, 82, pp. 602-612.

85- Tiwari, A., Sodha, M. (2006) "Performance of hybrid PV/thermal water/air heating system: A parametric study", *Renewable energy*, 31, pp. 2460-2474.

86- Joshi, A., Tiwari, A., Tiwari, G., Dincer, I., Reddy, B. (2009) "Performance evaluation of a hybrid photovoltaic thermal (PV/T) (glass to glass) system", *International Journal of thermal science*, 48, pp. 154-164.

87- Joshi, A., Tiwari, A. (2007) "Energy and exergy efficiencies of a hybrid photovoltaic-thermal (PV/T) air collector", *Renewable energy*, 32, pp. 2223-2241.

88- Hartmann, N., Glueck, C., Schmidt, F. (2011) "Solar Cooling for small office buildings: Comparison of solar thermal and photovoltaic options for two different European climates", *Renewable energy*, 36, pp. 1329-1338.

89- Abduzadeh, M., Ameri, M. (2009) "Improving the effectiveness of a photovoltaic water pumping system by spraying water over the front of photovoltaic cells", *Renewable Energy*, 34, pp. 91-96.

90- Tiwari, A., Dubey, S., Sandhu, G., Sodha, M., Anwar, S. (2009) " Exergy analysis of integrated photovoltaic thermal solar water heater under constant flow rate and constant collection temperature modes", *Applied energy*, 86, pp. 2592-2597.

91- Sarhaddi, F., Farahat, S., Ajam, H., Behzadmehr, A. (2010) "Exergetic performance assessment of a solar photovoltaic thermal (PV/T) air collector", *Energy and buildings*, 42, pp. 2184-2199.

92- Agrewal, B., Tiwari, G. (2010) "Optimizing the energy exergy of building integrated photovoltaic thermal (BIPVT) systems under cold climate conditions", *Applied energy*, 87, pp. 417-426.

93- Xu, G., Deng, S., Zhang, X., Yang, L., Zhang, Y. (2009) "Simulation of a photovoltaic/thermal heat pump system having a modified collector/evaporator" *Solar energy*, 83, pp. 1967-1976.

94- Chow, T., Fong, K., Pei, G., Ji, J., He, M. (2010) "Potential use of photovoltaic-integrated solar heat pump system in Hong Kong", *Applied thermal engineering*, 30, pp. 1066-1072.

95- Ucar, A., Inalli, M. (2006) "Exergoeconomic analysis and optimization of a solar-assisted heating system for residential buildings", *Building and environment*, 41, pp. 1551-1556.

96- Fang, G., Hu, H., Liu, X. (2010) "Experimental investigation on the photovoltaic-thermal solar heat pump air-conditioning system on water-heating mode", *Experimental Thermal and fluid science*, 34, pp.736-743.

97- Radziemska, E. (2009) "Performance analysis of a photovoltaic-thermal integrated system", International journal of photoenergy, Article ID 732093, 6 pages.

98- Mishra, K., Tiwari, N. (2013) "Energy and exergy analysis of hybrid photovoltaic thermal water collector for constant collection temperature mode", *Solar energy*, 90, pp. 58-67.

99- Rajoria, S., Agrawal, S., Tiwari, N. (2013) "Exergetic and enviroeconomic analysis of novel hybrid PVT array", *Solar energy*, 88, pp. 110-119.

100- Barbir, F., Gomez, T. (1996) "Efficiency and economics of proton exchange membrane (PEM) fuel cells", *International journal of hydrogen energy*, 21, (10), pp. 891-901.

101- EG&G Technical services, Inc (2004) "*Fuel cell handbook, 7th edition*", , U. S. Department of energy, National energy technology laboratory, Wiley-VCH, available from: www.osti.gov/bridge/servlets/purl/834188/834188.pdf.

102-*Fuel cell technologies market report*, June 2011, U. S. Department of energy, available at www.eere.energy.gov/hydrogenfuelcells/pdfs/2010-market-report.pdf.

103- Cook, B. (2001) "*An introduction to fuel cells and hydrogen technology*", Heliocentris, Vancouver,, Canada.

104- Instead, M., Midilli, A., Dincer, I. (2006) "Exergetic performance analysis of a PEM fuel cell", *International journal of energy research*, 30, pp. 307-321.

105- Myer, K. (2006) "*Mechanical engineer's handbook*", 3rd edition, John Wiley&Sons.

106- Rayment, C., Sherwin, S. (2003) " *Introduction to Fuel Cell Technology*", Department of aerospace and mechanical engineering, University of Notre Dame , U.S.A.

107- *Fuel cell technology and validation*, U.S. Department of energy, aviliable at: www.eere.energy.gov/hydrogenfuelcell/fc-challenges.html.

108- Cownden, R., Nahon, M., Rosen, M. (2001) "Exergy analysis of a fuel cell power system for transportation applications", E*xergy, an international journal* 1, (2), pp. 112-121.

109- Haraldsson, K., Wipke, K. (2004) "Evaluating PEM fuel system models", *Journal of power sources*, 126, pp. 88-97.

110- Kazem, A. (2004) "Exergy analysis of a PEM fuel cell at variable operating conditions" , *Energy conversion and management*, 45, pp.1949-1961.

111- Kazem, A. (2005) "Exergoeconomic analysis of a PEM electrolyser at various operating temperatures and pressures", *International journal of energy research*, 29, pp. 539-548.

112- Frangopoulos, C., Nakos, L. (2006) "Development of a model for thermoeconomic design and operation optimization of a PEM fuel cell system", *Energy*, 31, pp.1501-1519.

113- Saidi, M., Ehyaei, M., Abbasi, A. (2005) "Optimization of a combined heat and power PEFC by exergy analysis", *Journal of power sources*, 143, pp. 179-184.

114- Hussain, M., Baschuk, J., Li, X., Dincer, I. (2005) "Thermodynamic analysis of a PEM fuel cell power system", *International journal of thermal sciences*, 44, pp. 903-011.

115- Akkaya, A., Sahin, B., Erdem, H. (2007) "Exergetic performance coefficient analysis of a simple fuel cell system", *International journal of hydrogen energy*, 32, pp. 4600-4609.

116- Mert, S., Dincer, I., Ozcelik, Z. (2007) "Exergoeconomic analysis of a vehicular PEM fuel cell system", *Journal of power sources*, 165, pp. 244-252.

117- Leo, T., Durango, J., Navarro, E. (2010) "Exergy analysis of PEM fuel cells for marine applications", *Energy*, 35, pp.1164-1171.

118- Lagorse, J. , Paire, D. , Miraoui, A. (2008) "Sizing optimization of stand-alone street lightening system powered by a hybrid system using fuel cell, PV and battery", Renewable energy, 34, pp. 683-691.

119- El-shatter, F., Eskander, N., El-Hagry, T. (2002) "Hybrid PV/fuel cell system design and simulation", *Renewable energy*, 27, pp. 479-485.

120- Zoulias, E., Varkoraki, E., Ymberopouls, L., Christodoulu, C. Karagiorgis, G. "A review on water electrolysis", Centre for renewable energy sources (CRES), Europen 5th framework programme, TCJST, 4, 2, pp. 41-71.

121- Rosen, M. (1995) "Energy and exergy analysis of electrolytic hydrogen production", *International journal of hydrogen energy*, 20, (7), pp. 547-553.

122- Ulleberg, O. (2003) "Modeling of advanced alkaline electrolyzers: a system simulation approach", *International journal of hydrogen energy*, 28, pp. 21-33.

123- Kazem, A. (2004) "Exergetic efficiency of a PEM electrolyser at various operation temperature and pressure", *International journal of exergy*, 1, (1), pp. 47-59.

124- Karim, M., Iqbal, M. (2009) "Dynamic modeling and simulation of alkaline type electrolyzers", *IEEE*, pp. 711-715.

125- Ni, M., Leung, M., Leung, D. (2008) "Energy and exergy analysis of hydrogen production by a proton exchange membrane (PEM) electrolyzer plant", *Energy conversion and management*, 49, pp. 2748-2756.

126- Dieguez, P., Ursua, A., Sanchis, P., Sopena, C., Guelbenzu, E., Gandia, L. (2008) "Thermal performance of a commercial alkaline water electrolyzer: Experimental study and mathematical modeling", *International journal of hydrogen energy*, 33, pp. 7338-7354.

127- Balablel, A., Zaky, M. (2011) "Experimental investigation of solar-hydrogen energy system performance", *International journal of hydrogen energy*, 36, pp. 4653-4663.

128- Bannani, F., Sharif, T. Ben-Khalifa, A. (2006) "Estimation of monthly average solar radiation in Libya", *Theoretical and applied climatology*, 83, pp.211-215.

129- *General Meteorological Foundation data*, Libya, Misurata office.

130- *Solar energy centre data*, Libya, Tripoli.

131- *Atmospheric Science Data Centre (ASDC)*, NASA Langley Research Centre, Surface meteorology and solar energy system (Release 6.0), available at: http://eosweb.larc.nasa.gov/cgi-bin/sse/sse.cgi?+s01#s01

132-*Photovoltaic Geographical Information System*(PVGIS), European Commission Joint Research Centre, Institute for Energy and Transport (IET), available at: www.jrc.ec.europa.eu/pvgis/imaps/index.htm

133- *Weather Underground System*, available at: www.wunderground.com.

134- Benghanem, M. (2011) "Optimization of tilt angle for solar panel: case study for Madinah, Saudi Arabia", *Applied energy*, 88, pp. 1427-1433.

135-*North East England Climate office*, Uk Met office available at: www.metoffice.gov.uk/climate/uk/ne/

136- Giglmayr, I. Nixdorf, M., Pogoreutz, M. (2001) "Comparison of software for thermodynamic process calculation", *International journal for electricity and heat generation*, VGB Power Tech. 2, pp. 44-50.

137- Haggstahl, D., Dahlquist, E. (2003) "Evaluation of Prosim and IPSEpro, two heat and mass balance simulation softwares", *The 44th international conference of Scandinavian Simulation Society SIMS2003 on simulation and modeling*, September 18-19, at Malardalen University Vesteras, Sweden.

138-Enginomix LLC, (2010) "*IPSEpro system description*", available at: http://enginomix.net/products/ipsepro-system-description/

139- Kakaras, E., Doukelis, A., Karellas, S. (2004) "Compressor intake-air cooling in gas turbine plants", *Energy*, 29, pp. 2347-2358.

140- Knight, R., Linder, U., Markworth, N., Pertz, E., (2004) "Thermo-economic optimization of whole gas turbine plant (GTPOM)", *Applied thermal engineering*, 24, pp. 1725-1733.

141- Kershman, S., Rheinlander, J., Neumann, T., Goebel, O. (2005) "Hybrid wind/PV and conventional power for desalination in Libya-GECOL's facility for medium and small scale research at Ras Ejder", *Desalination*, 183, pp.1-12.

142- Perz, E., Beergmann, S. (2007) "A simulation environment for the techno-economic performance prediction of water and power cogeneration systems using renewable and fossil energy sources", *Desalination*, 203, pp. 337-345.

143- Masheiti, S. (2011) "*A thermodynamic and economic simulation modeling study of utilizing low-temperature sources to power absorption and organic Rankine cycles*", PhD Thesis, Newcastle university.

144- Sim Tech Simulation Technlogy, 2003. *IPSEpro process simulator manuals: process simulation environment*(PSE).

145- Sim Tech Simulation Technlogy, 2003. *IPSEpro process simulator manuals: Model Development Kit* (MDK).

146- Kotas, J. (1995) "*The exergy method of thermal plant analysis*", Kreger publishing company,Maabar, Florida, USA.

147- Bejan, A. (2002) "Fundamentals of exergy analysis, entropy generation minimization, and the generation of flow architecture", *International journal of energy research*, 26, pp. 545-565.

148- Santarrelli, M. (2004) "Carbon exergy tax: a thermoeconomic method to increase the efficient of exergy resources", *Energy policy*, 32, pp.413-427

149- Bejan, A., Tastasaronis, G., Moran, M. (1996) "*Thermal design and optimization*", John Wiley and Sonc, Inc., Canada.

150- Silveira, J., Tuna, C. (2003) "Thermoeconomic analysis method for optimization of combined heat and power systems. Part I ", *Progress in energy and combustion science*, 29, pp. 479-485.

151- Tastasaronis, G. (2007) "*Application of thermoeconomics to the design and synthesis of energy plants, in exergy, energy systems analysis, and optimization*", Developed under the auspices of the UNISCO, Eolss Publishers, Oxford, UK, [http://www.eolss.net].

152- Abusoglu, A., Kanoglu, M. (2009) " Exergoeconomic analysis and optimization of combined heat and power production: A review", *Renewable and sustainable energy reviews*, 3, pp. 2295-2308.

153- Lopez, R., Agustin, J. (2008) "Multi-objective design of PV-wind-diesel-hydrogen-battery systems", *Renewable energy*, 33, pp. 2559-2572.

154- Mazandarani, A., Mahlia, T., Chong, W., Moghavvemi, M. (2011) "Fuel consumption and emission prediction by Iranian power plants until 2025", *Renewable and sustainable energy reviews*, 15, pp. 1575-1592.

155- "*The cost of generating electricity*", a study carried out and published by PB Power for the Royal Academy of Engineering, March 2004, UK.

156- Ulleberg, O. (1998) "*Stand-Alone power systems for the future: Optimal design, operation & control of solar-hydrogen energy systems*", Ph. D. disseration, Departement of thermal energy and htdropower. Norwegian University of Science and Technology Trandheim.

157- Luque, A., Hegedus, S. (2011) "*Handbook of photovoltaic science and engineering*", Second edition, John Wiley and Sons, Inc., Canada.

158- Joshi, A., Dincer, I., Reddy, B. (2009) "Performance analysis of photovoltaic systems: A review", *Renewable and sustainable energy reviews*, 13, pp. 1884-897.

159- Kanglu, M., Cenegel, Y., Dincer, I., (2012) "*Efficiency evaluation of energy systems*", Springer brief in energy.

160- Makvart, T., (2000) "*Solar electricity*", 2nd edition, John Wiley and Sonc, Inc., Canada..

161- Sartori, E. (2006) "Convection coefficient equations for forced air flow over flat surfaces", *Solar energy*, 80, pp.1063-1071.

162- Loveday, D., Taki, A. (1996) "Convective heat transfer coefficients at plane surface on a full-scale building facade", *International journal of heat and mass transfer*, 39, (8), pp. 1729-1742.

163- Palyvos, J. (2008) "A survey of wind convection coefficient correlations for building envelope energy systems' modelling", *Applied thermal engineering*, 28, pp. 801-808.

164- Energy-Plus Software information Available at http:// www.eere.energy .gov/buildings/ energyplus/

165- McAdams, W. (1954) "Heat *Transmission*", third edition, 490 pages, McGraw Hill, TOKYO, Japan.

166- Herold, K., Radermacher, R., Klein,.A. (1996) "*Absorption Chillers and Heat Pumps*", Florida: CRC Press, Inc.

167- Dincer, I., Rosen, M. (2002) "*Thermal Energy Storage: Systems and Applications*", John Wiley & Sons.

168- Spiegel, C. (2011) "*PEM Fuel Cell Modeling and Simulation Using Matlab*", Academic Press, 2011.

169- Larminie, J., Dicks, A. (2003) "*Fuel Cell Systems Explained*", Second edition, J. Wiley & Sons.

170- Barbir, F. (2012) "*PEM Fuel Cells: Theory and Practice*", Second edition, Academic Press.

171- Photovoltaic module production, a2Peak Power Co. ltd., Taiwan R.O.C., available at: www.a2peak.com.tw.

172- Barker, G., Norton, P. "*Building America system performance test practices: Part1 -photovoltaic systems*", National Renewable Energy Laboratory (NREL), NREL/TP-550-30301, Available from:<http://www.nrel.gov/docs/.

173- Subtask, B., by Ulleberg, O. (2007), *Hydrogen demonstration project evaluation, Final report for IEA (International energy agency), HIA (Hydrogen implementing agreement)*, Task18,

174- Hydrogen generation systems, HySTAT-60 Technical data, Hydrogenics Corporation, Ontario, Avaliable from: www.hydrogenics.com.

175-Brogan, R. J. *et al* (1994). *Selection and costing of heat exchangers, Engineering Scieneces Data Unit (ESDU).* product issue (92013):2008-01,London.

176- Hewitt, G., Pungh, S. (2007) "Approximate design and costing methods for heat exchangers", *Heat transfer engineering*, 28,(2), pp.: 76-86.

177- Kakac, S., Hongtan (2002) "Heat exchangers, selection, rating, and thermal design", Second edition, crc Press, Lcc.

178- Incropera, F., Dewitt, D., (2002) " Introduction to heat transfer", Fourth edition, J. Wiley & Sons.

179- Li, C., Zhu, X., Cao, G., Sui, S., Hu, M. (2009) "Dynamic modeling and sizing optimization of stand-alone photovoltaic power systems using hybrid energy storage technology", *Renewable energy*, 34, pp. 815-826.

180- Andrews, J., Shabani, B., (2012) "Dimensionless analysis of the global techno-economic feasibility of solar-hydrogen systems for constant year-around power supply", *International journal of hydrogen energy*, 37, pp. 6-18.

181- Diaphragm compressor prices, available from: http:// www. alibaba. com/ products /F0/ hydrogen-compressor.

182-Radziemska, E. (2003) "The effect of temperature on power drop in crystalline silicon solar cells", *Renewable energy*, 28, pp:1-12.

APPENDIXES

Appendixes

Appendix A

Solar module Peak on P220-60-240 W_p specification avalible from:

http://www.fortune.com.tw/tw/data/solarpanel/P22060B/Peak%20On%20P220-60%20Black.pdf

Specification	**P220-60**
Nominal power P_m @STC	340 W_p
Nominal voltage V_m @STC	31.49 V
Nominal current I_m @STC	7.62 A
Open circuit V_{oc} @STC	37.72 V
Short circuit I_{SC} @STC	8.10 A
Max. tolerance of P_m	+- 3%
NOCT	47 ˚C +- 2 ˚C
Nominal power P_m @NOCT	173 W_p
Nominal voltage V_m @ NOCT	27.95 V
Nominal current I_m @ NOCT	6.17 A
Open circuit V_{oc} @ NOCT	34.88 V
Short circuit I_{SC} @ NOCT	6.56 A
Module efficiency reduction	- 0.52 % at 200W/m^2
Temperature coeficent of P_m	-0.46 %/ K
Temperature coeficent of V_{oc}	-0.129 %/K
Temperature coeficent of I_{SC}	4.4 m A/K
Module technology	Glass-foil-laminate with aluminium frame.
Module design	High transparent solar glass (tempered), 4 mm Encapsulation / EVA-Solar cees-EVA.
No. and type solar cells	60 Polycrystalline solar cells, 156*156 mm
Dimensions (L*W*H)/Weight	1667*1000*40 mm / 23 kg
Operating temperature	-40 ˚C to + 80˚C
Ambient temperature range	- 40 ˚C to + 45 ˚C
Certificate/Qulification	According to IEC 61215/ IEC 61730
Lifetime	25 years

Appendix B

RE: Fuelcell and Electrolyser price

Marketing [Marketing@ballard.com]

You replied on 04/02/2011 12:31.

Sent: 03 February 2011 21:21

To: Abdulhamid El-sharif

Attachments: SpecSht_DPG_080609.pdf (101 KB)

Dear Mr. El-Sharif,

Thank you for your email and interest in Ballard Power Systems.
I have attached a product specification sheet for our CLEARgen 1MW product. For proprietary reasons, I'm unable to share other technical details.
The electrolyzer is outside of Ballard's scope of supply. You may wish to contact one of the following companies to see if they have a product that meets your requirements:
Proton Energy Systems
Hydrogenics
Teledyne

Kind regards,

Catharine Reid
Sales & Marketing

Ballard Power Systems
T 604.412.3135
Email: catharine.reid@ballard.com

Distributed Generation (PEM fuel cell) - 1MW

Ballard's CLEARgen fuel cell generator is a complete turnkey solution, designed to provide a supply of continuous, zero emission power. The self-contained power modules run on hydrogen fuel; customers range from utilities to chemical companies with available by-product hydrogen.The 1 MW modular units are completely scaleable, enabling tailored solutions to meet each customer's needs. Ballard's fuel cell stacks are at the core of this modular solution. Commercially available today, the fuel cells feature dynamic response, high efficiency, and robust and reliable operation. Various annual service packages are available for the fuel cell generator that include preventative and corrective maintenance, as well as fuel cell stack re-cores to meet the product's 20-year lifetime. The schematic below is a rendering of a 6 MW site, illustrating the scaleable nature of this solution.

Specifications and descriptions in this document were in effect at the time of publication. Ballard Power Systems, Inc. reserves the right to change specifications, product appearance or to discontinue products at any time (07/2010).

Ballard Power Systems, Inc.

9000 Glenlyon Parkway

Burnaby, British Columbia

Canada, V5J 5J8

TEL: (+1) 604.454.0900

FAX: (+1) 604.412.4700

www.ballard.com

Type: PEM (Proton Exchange Membrane) fuel cell generator

PRODUCT SPECIFICATIONS : SPC5103076-0B

Performance: Net Power 1 MW

Voltage efficiency: 48% (± 2%)1

Energy efficiency (without cooling load/HHV): 40% (+-2%)

Output voltage: 200 – 480 V AC2

Output frequency: 50 – 60 Hz

Physical Characterisitcs: Height x width x length 2.9 x 2.4 x 13.7 meters

Weight: <30,000 kg

Fuel: Hydrogen >98%

Fuel consumption: 63 kg/hr (700 m3/hour)

Reliability: Availability >95%

Product Lifetime: >20 years

Available heat: Output heat load 1100 kW4

Stack outlet temperature: <65°C (149°F)

Emissions: Water output < 4 LPM

Noise: <80db @ 1 meter

Pollutants: Zero emissions (no GHG or local air pollutants)

Appendix C

Technical specifications of alkaline alectrolyzer type HySTAT-60, from Hydrogenics company: www.hydrogenics.com.

The core component of the electrolysis skid is the HySTAT™-A bipolar pressurized electrolysis cell stack. The cell stack consists of circular electrolytic cells, each containing two electrodes and an advanced proprietary alkaline inorganic ion-exchange type membrane. The H2 and O2 are generated when current is supplied to the cell stack. The gases are then directed to the gas separator, which is a dual stainless steel pressure vessel and then rinsed in the small pressure vessel located above the gas separator.The equipment included in this section is Zone II compliant and suitable for hydrogen service (SS316L). The Process Part comes as a fully assembled skid that includes equipment such as: Cell stack / Gas separator / Hydrogen gas rinser / Coalescent filters / Heat Exchangers (Plated Shell) for Electrolyte and Gas Cooling / Leak prevention tray with level switch / Hydrogen detector (HTA) / Analyzer panel for hydrogen in oxygen (HTO) / Swagelok® piping / Instrumentation and junction boxes: sensors, transmitters, switches, etc. / Valves / Vent header / Back pressure regulator

Technical specifications (outdoor version)	
Nominal Flow Rate	24 - 60 Nm^3/h
Nominal Pressure	10 bar(g)
Purity	- 99.998% , O2 < 2 ppm - Atm. dew point -75°C
Cell Stacks	4
Specific Power Consumption (full system)	5.2 kWh/Nm3
Specific Power Consumption (electrolyzer only)	4.2 kWh/Nm3
Voltage	400 / 480 / 600 V AC, 3-ph
Frequency	50 / 60 Hz
Max. ambient temperature	40°C
Min. ambient temperature	-20°C
Cooling water	closed loop cooling systems
Dimensions (H x W x D)	2.9*12.2*2.4 m
Weight	18800 kg
Operating temperature	60-80 ˚C
Oxygen pressure	8 bar(g)
Conversion efficiency	+- (80%)
Lifetime	> 20 years (60000 hours)

Appendix D

SHS/IPSEpro MDK equations and configurations

1- PV_Cell PV model

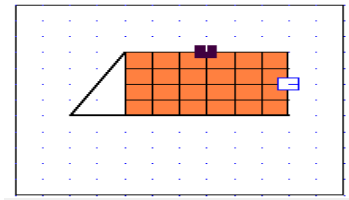

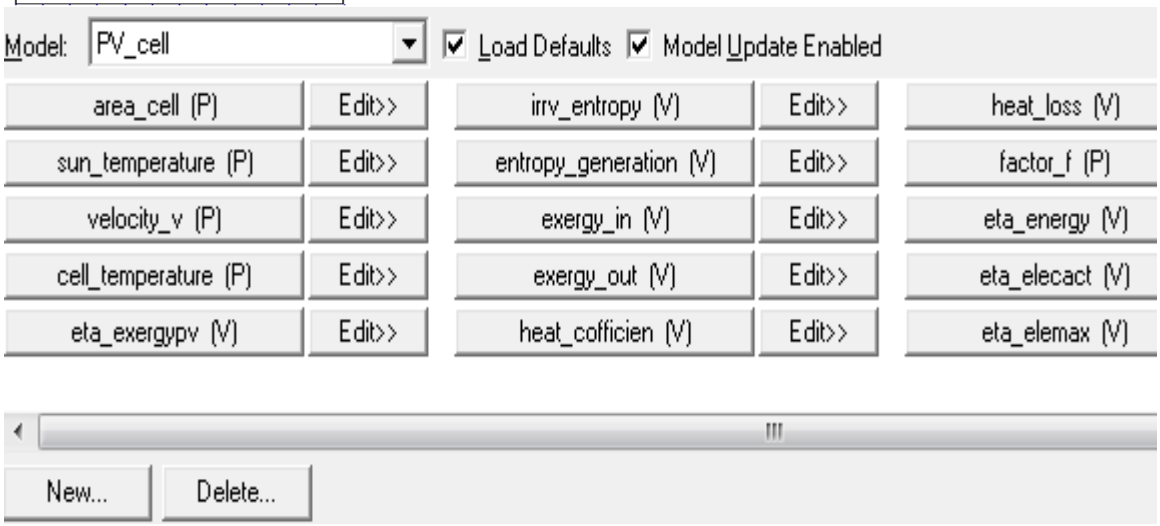

 # PV exergy analysis

fheat_cofficien: heat_cofficien=(5.7+(3.8*velocity_v))/1000;
f2:electricity.power=open_volt*open_current*factor_f*modu_no/1000;
fheat_loss:
heat_loss=(heat_cofficien*area_cell*cell_no*modu_no)*(cell_temperature-ambient.t);
fexergy_in: exergy_in=(heat.sirr_sun*area_cell*cell_no*modu_no)*(1-(ambient.t/sun_temperature));
fexergy_out: exergy_out=electricity.power-((1-(ambient.t/cell_temperature))*heat_loss);
feta_exergy: eta_exergypv= exergy_out/exergy_in;
firrv_entropy: irrv_entropy=(1-eta_exergypv)*exergy_in;
fentropy_generation: entropy_generation=irrv_entropy/ambient.t;
f1:eta_energy=((open_volt*open_current)+heat_loss)/(heat.sirr_sun*area_cell*cell_no*modu_no);
f3:eta_elecact=electricity.power/(heat.sirr_sun*area_cell*cell_no*modu_no);
f4:eta_elemax=(open_volt*open_current)/(heat.sirr_sun*area_cell*cell_no*modu_no);
f5:eta_expvt=(electricity.power+((1-(ambient.t/cell_temperature))*heat_loss))/exergy_in;

2-PV_Cellbab PV model

using constant input heat transfer coefficient parameter

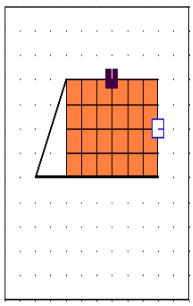

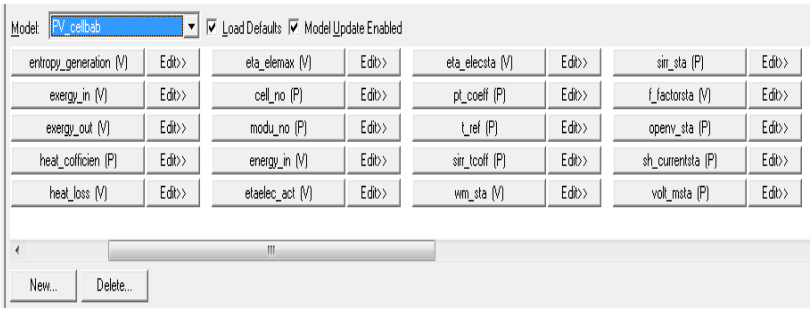

 # PV exergy and thermo-economic analysis

fetaelec_act: etaelec_act=eta_elecsta*(1-(pt_coeff*((cell_temperature)-(t_ref)))+(sirr_tcoff*log(sirr_sta)));
fcell_temperature: (cell_temperature)=(ambient_t)+((((TCNOCT)-(TR))/0.8)*heat.sirr_sun);
feta_electsta:eta_elecsta=wm_sta/(sirr_sta*area_cell*cell_no);
fwm_sta:wm_sta=volt_msta*current_msta/1000;
ff_factorsta: f_factorsta=volt_msta*current_msta/(openv_sta*sh_currentsta);
f2:electricity.power=(etaelec_act*heat.sirr_sun*cell_no*area_cell*modu_no)*ETA_CONV;
fvoc_act: voc_act=openv_sta-(voc_coeff*openv_sta*((cell_temperature)-(t_ref)))+(0.025*ln(heat.sirr_sun/sirr_sta));
fisc_act:
isc_act=(sh_currentsta*(heat.sirr_sun/sirr_sta))*(1+(isc_coeff*((cell_temperature)-(t_ref))));
ff_factoract:
f_factoract=(electricity.power/ETA_CONV)/(voc_act*isc_act*modu_no/1000);
fheat_loss:
heat_loss=heat_cofficien*area_cell*cell_no*modu_no*((cell_temperature)-(ambient_t));
fexergy_out: exergy_out= (electricity.power/ETA_CONV)-(heat_loss*(1-((ambient_t+273)/(cell_temperature+273))));
feta_exergy: eta_exergypv=exergy_out/exergy_in;
firrv_entropy: irrv_entropy=(1-eta_exergypv)*exergy_in;
fentropy_generation: entropy_generation=irrv_entropy/(ambient_t+273);
f4:eta_elemax=(voc_act*isc_act*modu_no/1000)/(ALFATAO*heat.sirr_sun*cell_no*area_cell*modu_no);
fcw: ZT=electricity.cw*electricity.power/1000000;
fZ: ZT=ZCI+COM;
fZCI: ZCI=(ACC*wm_sta*modu_no)/(CF*8760*3600);
fZOM: COM=(CFC*.01*wm_sta*modu_no)/(8760*3600);
fACC: ACC=CFC*CRF;
fCRF: CRF=(ir*((1+ir)^ny))/(((1+ir)^ny)-1);
frk: rk=((1-eta_exergypv)/eta_exergypv)+(ZT/(electricity.cw*electricity.power/1000000));
fk: fk=ZT/(ZT+(electricity.cw*(irrv_entropy/1000000)));

3-PV_Cellba PV model

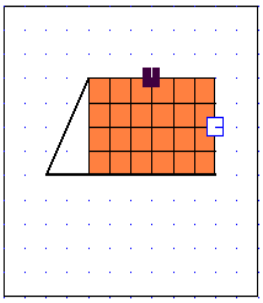

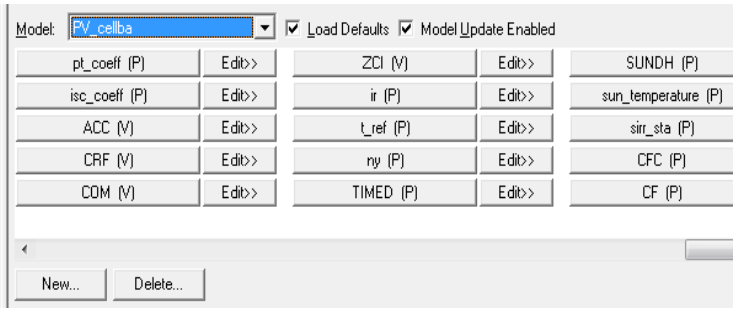

#PV exergy and thermo-economic analysis

fheat_cofficien: heat_cofficien= (5.7+(3.8*velocity_v))/1000;
feta_electsta:eta_elecsta=(wm_sta/(sirr_sta*area_mod))*100;
fwm_sta:wm_sta=volt_msta*current_msta/1000;
ff_factorsta: f_factorsta=volt_msta*current_msta/(openv_sta*sh_currentsta);
fvoc_act: voc_act=openv_sta-(voc_coeff*openv_sta*((cell_temperature)-(t_ref)))+(0.025*ln(heat.sirr_sun/sirr_sta));
fisc_act:
isc_act=(sh_currentsta*(heat.sirr_sun/sirr_sta))*(1+(isc_coeff*((cell_temperature)-(t_ref))));
ff_factoract:
f_factoract=(electricity.power/(ETA_CONV/100))/(voc_act*isc_act*modu_no/1000);
fheat_loss: heat_loss=heat_cofficien*area_mod*modu_no*((cell_temperature)-(ambient_t));
f6:energy_in=((TAOG*ALFAC*BETA)+((1-BETA)*ALFAP*TAOG))*heat.sirr_sun*area_mod*modu_no;
fbeta: BETA= (area_c * cell_no)/area_mod;
fex_loss: ex_loss=(heat_loss*(1-((ambient_t+273.15)/(cell_temperature+273.15))));
fexergy_in: exergy_in=(1-((ambient_t+273.15)/(sun_temperature+273.15)))*(heat.sirr_sun*area_mod*modu_no);
fZ: ZT=ZCI+COM;
fZCI: ZCI=(ACC*wm_sta*modu_no)/((CF/100)*8760*3600);
fZOM: COM=(CFC*(PMOC/100)*wm_sta*modu_no)/(8760*3600);
fACC: ACC=CFC*CRF;
fCRF: CRF=((ir/100)*((1+(ir/100))^ny))/(((1+(ir/100))^ny)-1);
fk: fk=(ZT/(ZT+(electricity.cw*((irrv_entropy+ex_loss)/1000000))))*100;
fCO2_SAVTI: CO2_SAVTI=(electricity.power/1000)* TIMED*CO2_COST*CO2_PF;
fCO2_SAVA: CO2_SAVA=(electricity.power/1000)* 365*SUNDH*CO2_COST*CO2_PF;
fCO2_SAVT: CO2_SAVT= CO2_SAVA*ny;
fCO2_COSkW: CO2_COSkW=(CO2_COST*CO2_PF)/1000;
fPVEL: PVEL=(electricity.cw*3600/1000000)-CO2_COSkW;
fSOCPT: SOCPT=SCF*electricity.power* TIMED;
fASOC: ASOC=SCF*electricity.power*SUNDH*365;
fTSOC:TSOC=ASOC*ny;

fPVELT: PVELT=PVEL-SCF;
fCD:CD=((electricity.cw*((irrv_entropy+ex_loss)/1000000)))*3600 ;

4-PV_Cellbabaa PV model

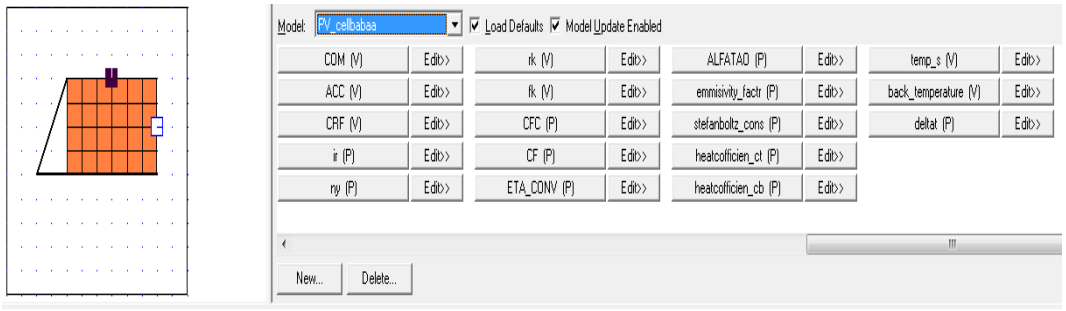

 # PV detailed exergy and thermo-economic analysis

fetaelec_act: etaelec_act=eta_elecsta*(1-(pt_coeff*((cell_temperature)-(t_ref)))+(sirr_tcoff*log(sirr_sta)));
fcell_temperature: (cell_temperature)=(ambient_t)+((((TCNOCT)-(TR))/0.8)*heat.sirr_sun);
feta_electsta:eta_elecsta=wm_sta/(sirr_sta*area_cell*cell_no);
fwm_sta:wm_sta=volt_msta*current_msta/1000;
ff_factorsta: f_factorsta=volt_msta*current_msta/(openv_sta*sh_currentsta);
f2:electricity.power=(etaelec_act*heat.sirr_sun*cell_no*area_cell*modu_no)*ETA_CONV;

fisc_act:
isc_act=(sh_currentsta*(heat.sirr_sun/sirr_sta))*(1+(isc_coeff*((cell_temperature)-(t_ref))));
ff_factoract:
heat_loss=(heatcofficien_ct*area_cell*cell_no*modu_no*((cell_temperature)-(ambient_t)))+(heatcofficien_cb*area_cell*cell_no*modu_no*((back_temperature)-
(ambient_t)))+(stefanboltz_cons*emmisivity_factr*area_cell*cell_no*modu_no*(((cell_temperature)^4)-((temp_s)^4)));
f6:energy_in=(ALFATAO)*heat.sirr_sun*area_cell*cell_no*modu_no;
fexergy_in: exergy_in=(1-((ambient_t+273)/(sun_temperature+273)))*(ALFATAO*heat.sirr_sun*area_cell*cell_no*modu_no);

fback_temperature: back_temperature=cell_temperature-((heat.sirr_sun/sirr_sta)*(deltat));
feta_exergy: eta_exergypv=exergy_out/exergy_in;
ftemp_s: temp_s=ambient_t-6;
firrv_entropy: irrv_entropy=(1-eta_exergypv)*exergy_in;
fentropy_generation: entropy_generation=irrv_entropy/(ambient_t+273);
f4:eta_elemax=(voc_act*isc_act*modu_no/1000)/(ALFATAO*heat.sirr_sun*cell_no*area_cell*modu_no);
fcw: ZT=electricity.cw*electricity.power/1000000;
fZ: ZT=ZCI+COM;
fZCI: ZCI=(ACC*wm_sta*modu_no)/(CF*8760*3600);

fZOM: COM=(CFC*.01*wm_sta*modu_no)/(8760*3600);
fACC: ACC=CFC*CRF;
fCRF: CRF=(ir*((1+ir)^ny))/(((1+ir)^ny)-1);
frk: rk=((1-
eta_exergypv)/eta_exergypv)+(ZT/(electricity.cw*electricity.power/1000000));
fk: fk=ZT/(ZT+(electricity.cw*(irrv_entropy/1000000)));

5-PV_Cellbaa PV/T model

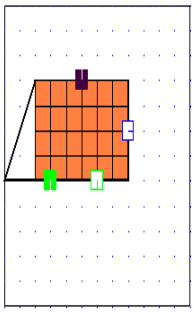

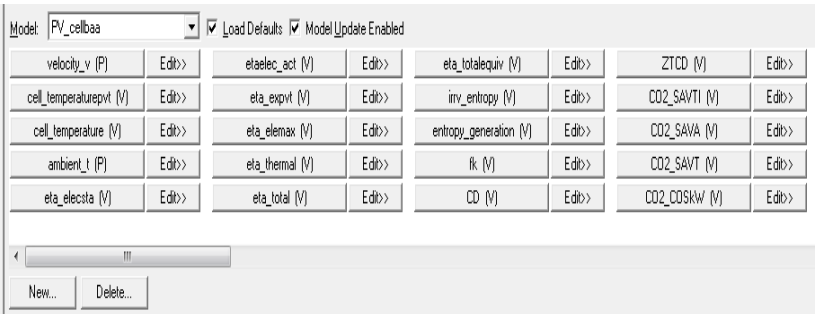

#PV/T thermo-economic analysis

fheat_cofficien: heat_cofficien=(5.67+(3.86*velocity_v))/1000;
fetaelec_act: etaelec_act=((eta_elecsta/100)*(1-(pt_coeff*(cell_temperaturepvt-
t_ref))+(sirr_tcoff*log(heat.sirr_sun))))*100;
fcell_temperature: cell_temperature=(ambient_t)+(((TCNOCT-
TR)/0.8)*heat.sirr_sun);
fcell_temperaturepvt: cell_temperaturepvt=coolingout.t+4;
feta_electsta:eta_elecsta=(wm_sta/(sirr_sta*area_mod))*100;
f2:electricity.power=(TAOG*(etaelec_act/100)*heat.sirr_sun*area_mod*modu_no
)*(ETA_CONV/100);
fvoc_act: voc_act=openv_sta-(voc_coeff*openv_sta*(cell_temperaturepvt-
t_ref))+(0.025*ln(heat.sirr_sun/sirr_sta));
fisc_act:
isc_act=sh_currentsta*(heat.sirr_sun/sirr_sta)*(1+((isc_coeff)*(cell_temperaturep
vt-t_ref)));
ff_factoract:
fheat_loss: heat_loss=heat_cofficien*area_mod*modu_no*(cell_temperaturepvt-
ambient_t);
f6:energy_in=((TAOG*ALFAC*BETA)+((1-
BETA)*ALFAP*TAOG))*heat.sirr_sun*area_mod*modu_no;
fbeta: BETA= (area_c * cell_no)/area_mod;
fexergy_in: exergy_in=(1-
((ambient_t+273.15)/(sun_temperature+273.15)))*(heat.sirr_sun*area_mod*modu
_no);
fex_loss: ex_loss=(heat_loss*(1-
((ambient_t+273.15)/(cell_temperaturepvt+273.15))));
fTout: coolingin.mass=(((energy_in)-
((electricity.power/(ETA_CONV/100))+(heat_loss)))/(Cp_cool*(coolingout.t-
coolingin.t)));
fpres: coolingout.p=coolingin.p-delta_p;
fcool_m: coolingin.mass=coolingout.mass;

f5:eta_expvt=(((electricity.power/(ETA_CONV/100))
+((coolingin.mass*Cp_cool*(coolingout.t-coolingin.t))*(1-
((ambient_t+273.15)/(coolingout.t+273.15)))))/exergy_in)*100;
fcw: electricity.cw=(ZT-(cwa1*
coolingout.mass*coolingout.ex_t/1000000)+(cwa*coolingin.mass*coolingin.ex_t/100
0000))/(electricity.power/1000000);
fZ: ZT=ZCI+COM;
fZCI: ZCI=(ACC*wm_sta*modu_no)/((CF/100)*8760*3600);
fZOM: COM=(CFC*(PMOC/100)*wm_sta*modu_no)/(8760*3600);
fACC: ACC=CFC*CRF;
fCRF: CRF=((ir/100)*((1+(ir/100))^ny))/(((1+(ir/100))^ny)-1);
fk: fk=(ZT/(ZT+(electricity.cw*((irrv_entropy+ex_loss)/1000000))))*100;
fCO2_SAVTI: CO2_SAVTI=(electricity.power/1000)*
TIMED*CO2_COST*CO2_PF;
fCO2_SAVA: CO2_SAVA=(electricity.power/1000)*
365*SUNDH*CO2_COST*CO2_PF;
fCO2_SAVT: CO2_SAVT= CO2_SAVA*ny;
fCO2_COSkW: CO2_COSkW=(CO2_COST*CO2_PF)/1000;
fPVEL: PVEL=(electricity.cw*3600/1000000)-CO2_COSkW;
fSOCPT: SOCPT=SCF*electricity.power* TIMED;
fASOC: ASOC=SCF*electricity.power*SUNDH*365;
fPVELT: PVELT=PVEL-SCF;
fZTCD: ZTCD=((electricity.cw*((irrv_entropy+ex_loss)/1000000)) + ZT)*3600;
fCD:CD=((electricity.cw*((irrv_entropy+ex_loss)/1000000)))*3600 ;

6-PV_Cellbaaa PV/T model

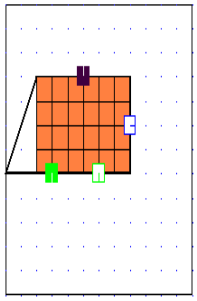

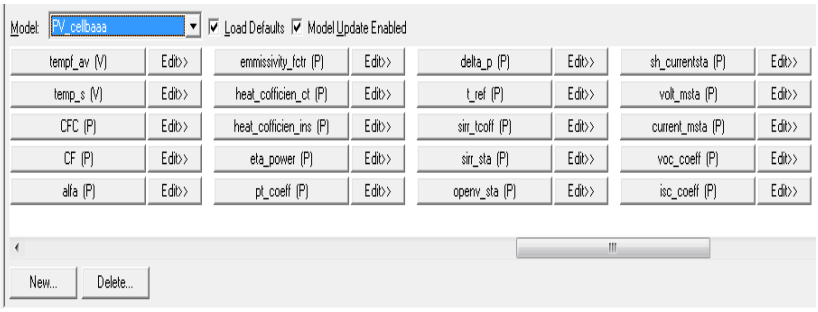

 # PV/T thermo-economic analysis

fetaelec_act: etaelec_act=((eta_elecsta/100)*(1-(pt_coeff*(cell_temperaturepvt-
t_ref))+(sirr_tcoff*log(heat.sirr_sun))))*100;
fcell_temperature: cell_temperature=(ambient_t)+(((TCNOCT-
TR)/0.8)*heat.sirr_sun);
fcell_temperaturepvt: cell_temperaturepvt=coolingout.t+4;
feta_electsta:eta_elecsta=(wm_sta/(sirr_sta*area_mod))*100;
fwm_sta:wm_sta=volt_msta*current_msta/1000;
ff_factorsta: f_factorsta=volt_msta*current_msta/(openv_sta*sh_currentsta);

fisc_act:
isc_act=sh_currentsta*(heat.sirr_sun/sirr_sta)*(1+((isc_coeff)*(cell_temperaturep
vt-t_ref)));

ff_factoract:
f_factoract=(electricity.power/(ETA_CONV/100))/(voc_act*isc_act*modu_no/1000);
fheat_loss:
f6:energy_in=((TAOG*ALFAC*BETA)+((1-BETA)*ALFAP*TAOG))*heat.sirr_sun*area_mod*modu_no;
f8:BETA=(area_cell*cell_no)/area_mod;
fthermal_en: thermal_energy=energy_in-((electricity.power/(ETA_CONV/100))+(heat_loss));
fexergy_in: exergy_in=(1-((ambient_t+273)/(sun_temperature+273)))*(heat.sirr_sun*area_mod*modu_no);
fexergy_out: exergy_out=((electricity.power/(ETA_CONV/100))+((coolingin.mass*Cp_cool*(coolingout.t-coolingin.t))*(1-((ambient_t+273)/(coolingout.t+273)))));
ftempf_av: tempf_av=(coolingin.t+coolingout.t)/2;
ftemp_s: temp_s=ambient_t-6;
firrv_entropy: irrv_entropy=(1-(eta_expvt/100))*exergy_in;
fex_loss: ex_loss=(heat_loss*(1-((ambient_t+273.15)/(cell_temperaturepvt+273.15))));
fentropy_generation: entropy_generation=irrv_entropy/(coolingin.To+273);
f1:eta_thermal=(thermal_energy/(heat.sirr_sun*area_mod*modu_no))*100;
fpres: coolingout.p=coolingin.p-delta_p;
fcool_m: coolingout.mass=coolingin.mass;
f5:eta_expvt=(((electricity.power/(ETA_CONV/100))+((coolingin.mass*Cp_cool*(coolingout.t-coolingin.t))*(1-((ambient_t+273)/(coolingout.t+273)))))/exergy_in)*100;
fcw: electricity.cw=(ZT-((cwa* coolingout.mass*(coolingout.ex_t-coolingin.ex_t))/1000000))/(electricity.power/1000000);
fZ: ZT=ZCI+COM;
fZCI: ZCI=(ACC*wm_sta*modu_no)/((CF/100)*8760*3600);
fZOM: COM=(CFC*(PMOC/100)*wm_sta*modu_no)/(8760*3600);
fACC: ACC=CFC*CRF;
fCRF: CRF=((ir/100)*((1+(ir/100))^ny))/(((1+(ir/100))^ny)-1);
fCO2_SAVTI: CO2_SAVTI=(electricity.power/1000)* TIMED*CO2_COST*CO2_PF;
fCO2_SAVA: CO2_SAVA=(electricity.power/1000)* 365*SUNDH*CO2_COST*CO2_PF;
fCO2_SAVT: CO2_SAVT= CO2_SAVA*ny;
fCO2_COSkW: CO2_COSkW=(CO2_COST*CO2_PF)/1000;
fPVEL: PVEL=(electricity.cw*3600/1000000)-CO2_COSkW;
fSOCPT: SOCPT=SCF*electricity.power* TIMED;
fASOC: ASOC=SCF*electricity.power*SUNDH*365;
fPVELT: PVELT=PVEL-SCF;
fZTCD: ZTCD=((electricity.cw*((irrv_entropy+ex_loss)/1000000)) + ZT)*3600;
fCD:CD=((electricity.cw*((irrv_entropy+ex_loss)/1000000)))*3600;
fk: fk=(ZT/(ZT+(electricity.cw*(irrv_entropy/1000000))))*100;

7-Electrolyzer model

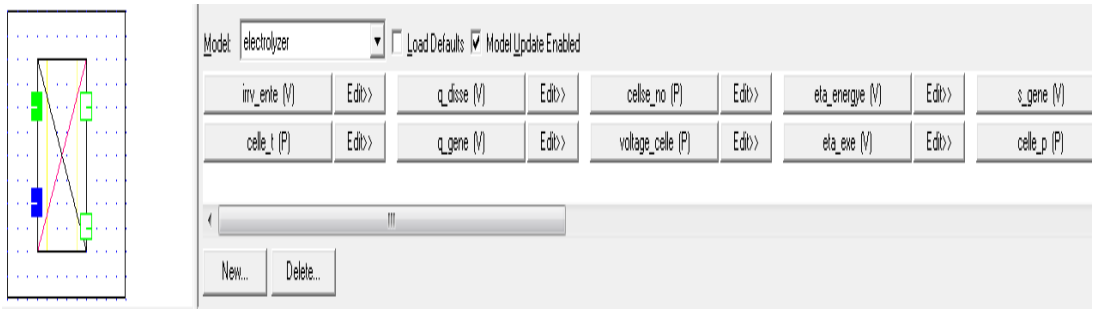

 # Electrolyzer energy and exergy analysis without cooling

fq_gen: q_gene=(voltage_celle-1.481)*((electricty.power-w_acc)/voltage_celle);
fq_diss: q_disse=-q_gene;
fwork_celle:work_celle=(electricty.power-w_acc)/cellse_no;
fwork_net: work_net=electricty.power;
fhyd:hydrogen.mass=(1.05/100000)*((electricty.power-w_acc)/(voltage_celle));
fox:oxygen.mass=(8.29/100000)*((electricty.power-w_acc)/(voltage_celle));
f2:water.mass=(9.34/100000)*((electricty.power-w_acc)/(voltage_celle));
f3:eta_energye=(142000*hydrogen.mass)/work_net;
f4:hydrogen_ext=hydrogen.ex_ph+hydrogen.ex_ch;
f5:hydrogen.ex_ph=14.2091*ambient_t*((celle_t/ambient_t)-1-ln(celle_t/ambient_t))+(4.12418*ambient_t*ln(celle_p/ambient_p));
f6:oxygn_ext=oxygen.ex_ph+oxygen.ex_ch;
f7:oxygen.ex_ph=0.9216*ambient_t*((celle_t/ambient_t)-1-ln(celle_t/ambient_t))+(0.25983*ambient_t*ln(celle_p/ambient_p));
f8:watr_ext=water.ex_ph+water.ex_ch;
f9:water.ex_ph=(water.h-watr_ho)-(ambient_t*(water.s-watr_so));
firrv_ente: irrv_ente=work_net+((1-(ambient_t/celle_t))*q_disse)-(hydrogen.mass*hydrogen_ext)-(oxygen.mass*oxygn_ext)+(water.mass*watr_ext);
fa: eta_exe =1-(irrv_ente/((water.mass*watr_ext)+work_net));
fs_gene: s_gene= irrv_ente/ambient_t;

8-Electrolyzerb model

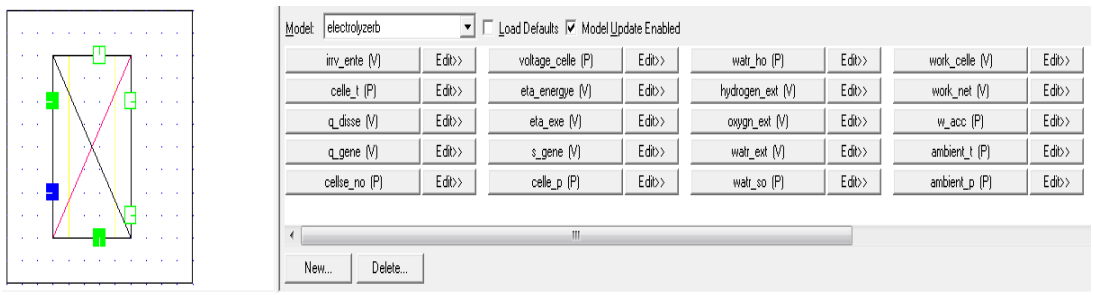

 # Electrolyzer energy and exergy analysis with cooling

fq_gen: q_gene=(voltage_celle-1.481)*((electricty.power-w_acc)/voltage_celle);
fwork:work_celle=(electricty.power-w_acc)/cellse_no;
fwork_net: work_net=electricty.power;
fhyd:hydrogen.mass=(1.05/100000)*((electricty.power-w_acc)/(voltage_celle));
fox:oxygen.mass=(8.29/100000)*((electricty.power-w_acc)/(voltage_celle));
f2:water.mass=(9.34/100000)*((electricty.power-w_acc)/(voltage_celle));
f3:eta_energye=(142000*hydrogen.mass)/work_net;
f4:hydrogen_ext=hydrogen.ex_ph+hydrogen.ex_ch;
f5:hydrogen.ex_ph=14.2091*ambient_t*((celle_t/ambient_t)-1-ln(celle_t/ambient_t))+(4.12418*ambient_t*ln(celle_p/ambient_p));
f6:oxygn_ext=oxygen.ex_ph+oxygen.ex_ch;
f7:oxygen.ex_ph=0.9216*ambient_t*((celle_t/ambient_t)-1-ln(celle_t/ambient_t))+(0.25983*ambient_t*ln(celle_p/ambient_p));
f8:watr_ext=water.ex_ph+water.ex_ch;
f9:water.ex_ph=(water.h-watr_ho)-(ambient_t*(water.s-watr_so));
firrv_ente: -irrv_ente=work_net+((1-(ambient_t/celle_t))*-q_disse)-(hydrogen.mass*hydrogen_ext)-(oxygen.mass*oxygn_ext)+(ext_coolin*coolingin.mass)-(ext_coolout*coolingout.mass)+(water.mass*watr_ext);
feta: eta_exe =1-(irrv_ente/work_net);
fs_gene: s_gene= irrv_ente/ambient_t;
fQ_cool: Q_cool=q_gene-q_disse-Q_stream;
fq_disse: q_disse=0.2*q_gene;
fQ_stream: Q_stream=(oxygen.mass*oxygen.h)+(hydrogen.mass*hydrogen.h);
fTout: coolingout.t=(Q_cool/coolingin.mass*Cp_cool)+coolingin.t;
fMT: LMTD=celle_t-(0.5*(coolingin.t+coolingout.t));
fbalance: coolingin.mass*Cp_cool*(coolingout.t-coolingin.t)=AU_hx*LMTD;
fpres: coolingout.p=coolingin.p-delta_p;
fcool_m: coolingin.mass=coolingout.mass;
fex_phcoolin: coolingin.ex_ph=(coolingin.h-watr_ho)-(ambient_t*(coolingin.s-watr_so));
fex_phcoolout: coolingout.ex_ph=(coolingout.h-watr_ho)-(ambient_t*(coolingout.s-watr_so));
fext_coolin: ext_coolin=coolingin.ex_ph+coolingin.ex_ch;
fext_coolout: ext_coolout=coolingout.ex_ph+coolingout.ex_ch;

9-Electrolyzerba model

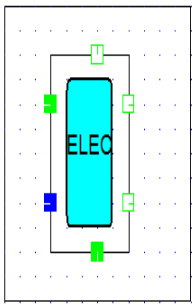

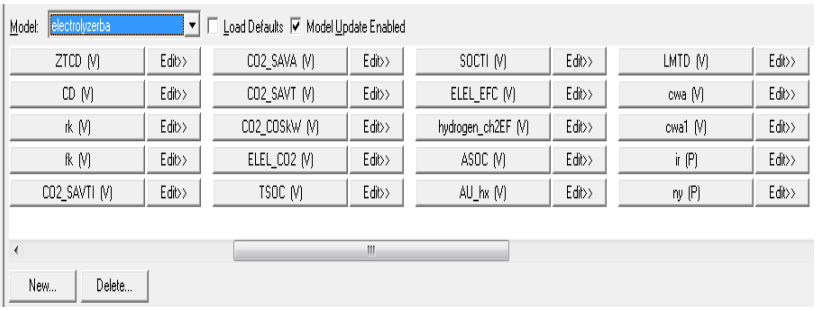

 # Electrolyzerba thermo-economic analysis with cooling and recycling

fq_gen: q_gene=(voltage_celle-1.481)*((electricty.power-w_accs)/voltage_celle);

fwaccs: w_accs=WACCF*electricty.power;
fwork:work_celle=(electricty.power-w_accs)/cellse_no;
fhyd:hydrogen.mass=(ETA_FRA)*(1.05/100000)*((electricty.power-w_accs)/(voltage_celle));
fox:oxygen.mass=(ETA_FRA)*(8.29/100000)*((electricty.power-w_accs)/(voltage_celle));
f2:water.mass=(ETA_FRA)*(9.34/100000)*((electricty.power-w_accs)/(voltage_celle));
oxygen.mass*oxygen.ex_t)+(coolingin.mass*coolingin.ex_t)-(coolingout.mass*coolingout.ex_t)+(RESF*(water.mass*water.ex_t)) ;

fs_gene: s_gene= irrv_ente/(ambient_t+273.15);
fex_loss: ex_loss=((1-((ambient_t+273.15)/(celle_t+273.15)))*q_disse);
fQ_cool: Q_cool=q_gene-q_disse-Q_stream;
fq_disse: q_disse=RHL*q_gene;
fQ_stream: Q_stream=(oxygen.mass*oxygen.h)+(hydrogen.mass*hydrogen.h);
fTout: coolingin.mass=Q_cool/(Cp_cool*(coolingout.t-coolingin.t));
fLMTD: LMTD=(((celle_t-coolingin.t)-(celle_t-coolingout.t))/(ln((celle_t-coolingin.t)/(celle_t-coolingout.t))));
fbalance: coolingin.mass*Cp_cool*(coolingout.t-coolingin.t)=AU_hx*LMTD;
fpres: coolingout.p=coolingin.p-delta_p;
fcool_m: coolingin.mass=coolingout.mass;

fZ: ZT=ZCI+ZOM;
fZCI: ZCI=(ACC*Ws)/((CF/100)*8760*3600);
fZOM: ZOM=(COM*Ws)/(8760*3600);
fACC: ACC=CFC*CRF;
fCRF: CRF=((ir/100)*((1+(ir/100))^ny))/(((1+(ir/100))^ny)-1);
 # The relative cost difference rk analysis assumed that electricity is the main fuel input and hydrogen is the main product
frk: rk=(((1-(eta_exe/100))/(eta_exe/100))+(ZT/(electricty.cw*(hydrogen.ex_t*hydrogen.mass/1000000))))*100;
 # The rk and fk analysis defined the exergy destruction cost as the the cost rate of the additinal fuel that must be supplied to the unit (above the rate needed for the product) to cover the rate of exergy destruction
fk: fk=(ZT/(ZT+(electricty.cw*((irrv_ente+ex_loss)/1000000))))*100;
fZTCD: ZTCD=((electricty.cw*((irrv_ente+ex_loss)/1000000)) + ZT)*3600;
fCD:CD=((electricty.cw*((irrv_ente+ex_loss)/1000000)))*3600 ;
fCO2_SAVTI: CO2_SAVTI=(electricty.power/1000)*TIMED*CO2_COST*CO2_PF;
fCO2_SAVA: CO2_SAVA=(electricty.power/1000)*365*WORH*CO2_COST*CO2_PF;
fCO2_SAVT: CO2_SAVT= CO2_SAVA*ny;
fCO2_COSkW: CO2_COSkW=(CO2_COST*CO2_PF)/1000;
fELEL_CO2: ELEL_CO2=(electricty.cw*3600/1000000)-CO2_COSkW;
fSOCTI: SOCTI=SCF*electricty.power* TIMED;
fASOC: ASOC=SCF*electricty.power*WORH*365;
fTSOC: TSOC=ASOC*ny;
fELEL_EFC: ELEL_EFC=ELEL_CO2 -SCF;
fcwa: cwa=(cwc/coolingin.ex_t)*1000000;
fcwa1: cwa1=(cwh/coolingout.ex_t)*1000000;

fcw2: hydrogen_ch2EF= (ZT- (oxygen.co2 *oxygen.mass*oxygen.ex_t/1000000)+(RESF*cwa1*water.mass*water.ex_t/1000000)+((ELEL_EFC*1000000/3600)*electricty.power/1000000)-((cwa*((coolingout.mass*coolingout.ex_t)-(coolingin.mass*coolingin.ex_t))) /1000000))/(hydrogen.ex_t*hydrogen.mass/1000000);

10-Electrolyzerbaa model

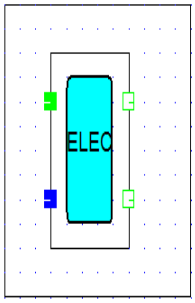

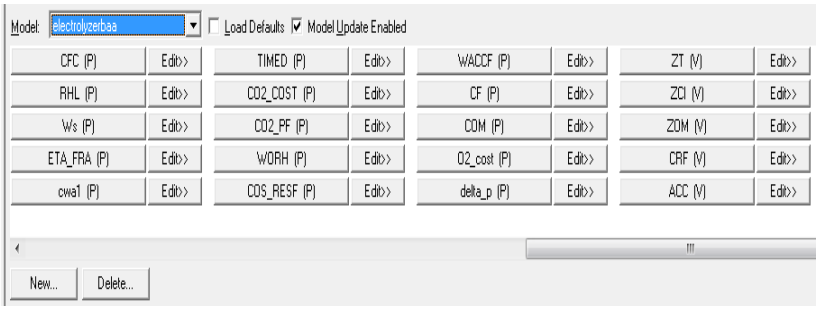

 # Electrolyzer thermo-economic analysis without cooling or recycling

fq_gen: q_gene=(voltage_celle-1.481)*((electricty.power-w_accs)/voltage_celle);
fwaccs: w_accs=WACCF*electricty.power;
fwork:work_celle=(electricty.power-w_accs)/cellse_no;
fhyd:hydrogen.mass=(ETA_FRA)*(1.05/100000)*((electricty.power-w_accs)/(voltage_celle));
fox:oxygen.mass=(ETA_FRA)*(8.29/100000)*((electricty.power-w_accs)/(voltage_celle));
f2:water.mass=(ETA_FRA)*(9.34/100000)*((electricty.power-w_accs)/(voltage_celle));

fs_gene: s_gene= irrv_ente/(ambient_t+273.15);
fex_loss: ex_loss=((1-((ambient_t+273.15)/(celle_t+273.15)))*q_disse);
fq_disse: q_disse=RHL*q_gene;
fco2: oxygen.co2= (O2_cost/oxygen.ex_t)*1000000;
fcw: hydrogen.ch2= (ZT- (oxygen.co2 *oxygen.mass*oxygen.ex_t/1000000)+(cwa1*water.mass*water.ex_t/1000000)+(electricty.cw*electricty.power /1000000))/(hydrogen.ex_t*hydrogen.mass/1000000);
fZ: ZT=ZCI+ZOM;
fZCI: ZCI=(ACC*Ws)/(CF*8760*3600);
fZOM: ZOM=(COM*Ws)/(8760*3600);
fACC: ACC=CFC*CRF;
fCRF: CRF=(ir*((1+ir)^ny))/(((1+ir)^ny)-1);
frk: rk=(((1
fk: fk=(ZT/(ZT+(electricty.cw*((irrv_ente+ex_loss)/1000000))))*100;
fZTCD: ZTCD=((electricty.cw*((irrv_ente+ex_loss)/1000000)) + ZT)*3600;
fCD:CD=((electricty.cw*((irrv_ente+ex_loss)/1000000)))*3600 ;
fCO2_SAVTI: CO2_SAVTI=(electricty.power/1000)* TIMED*CO2_COST*CO2_PF;
fCO2_SAVA: CO2_SAVA=(electricty.power/1000)* 365*WORH*CO2_COST*CO2_PF;
fCO2_SAVT: CO2_SAVT= CO2_SAVA*ny;
fCO2_COSkW: CO2_COSkW=(CO2_COST*CO2_PF)/1000;

fELEL_CO2: ELEL_CO2=(electricty.cw*3600/1000000)-CO2_COSkW;
fELEL_RESTI: ELEL_RESTI=COS_RESF*electricty.power* TIMED;
fELEL_RESA: ELEL_RESA=COS_RESF*electricty.power*WORH*365;
fELEL_REST: ELEL_REST=ELEL_RESA*ny;
fELEL_EFC: ELEL_EFC=ELEL_CO2 -COS_RESF;
fcw2: hydrogen_ch2EF= (ZT- (oxygen.co2 *oxygen.mass*oxygen.ex_t/1000000)+(cwa1*water.mass*water.ex_t/1000000)+((ELEL_EFC*1000000/3600)*electricty .power /1000000))/(hydrogen.ex_t*hydrogen.mass/1000000);

11-fuel_cell3 model

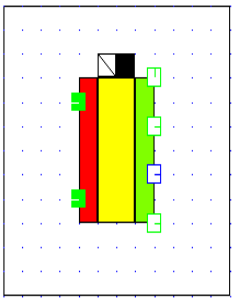

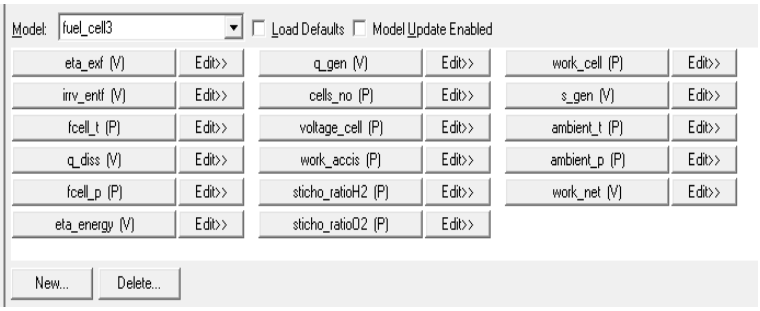

#fuel cell energy and exergy analysis without cooling or recycling system (work cell is a known input parameter and stream exergy equations are integrated in the connection model)

fq_gen: q_gen=(1.481- voltage_cell)*cells_no*work_cell/voltage_cell;
fq_diss: q_diss=0.2*q_gen;
fpower: powerfu.power=(cells_no*work_cell);
fwork_net: work_net=powerfu.power-work_accis;
fhym:hydrogen.mass=(1.05/100000)*sticho_ratioH2*(cells_no*work_cell)/(voltage_cell);
f1:oxygen.mass=(8.29/100000)*sticho_ratioO2*(cells_no*work_cell)/(voltage_cell);
f2:water.mass=(9.34/100000)*(cells_no*work_cell)/(voltage_cell);
f3:eta_energy=(work_net)/(142000*hydrogen.mass);
fs_gen: s_gen=irrv_entf/(ambient_t+273.15);
firrv_entf: irrv_entf=((1-((ambient_t+273)/(fcell_t+273)))*-q_diss)-work_net+(hydrogen.mass*hydrogen.ex_t)+(oxygen.mass*oxygen.ex_t)-(water.mass*water.ex_t)-(hydrogenout.mass*hydrogenout.ex_t)-(oxygenout.mass*oxygenout.ex_t);
fa:eta_exf =work_net/((hydrogen.mass*hydrogen.ex_t)+(oxygen.mass*oxygen.ex_t));
fhymo:hydrogenout.mass=(1.05/100000)*(sticho_ratioH2-1)*(cells_no*work_cell)/(voltage_cell);
foxmo:oxygenout.mass=(8.29/100000)*(sticho_ratioO2-1)*(cells_no*work_cell)/(voltage_cell);

12-fuel_cell3a model

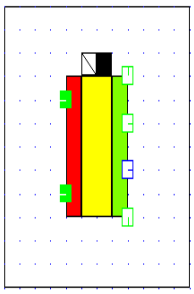

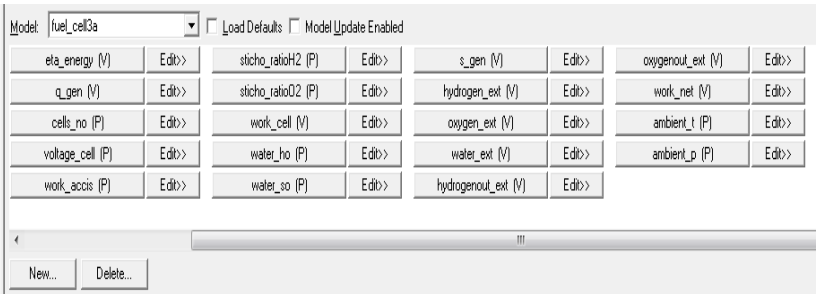

#fuel cell energy and exergy analysis without cooling or recycling (known input hydrogen mass parameter and unknown work cell variable)

fq_gen: q_gen=(1.481- voltage_cell)*powerfu.power/voltage_cell;
fq_diss: q_diss=0.2*q_gen;
fpower:work_net= powerfu.power-work_accis;
fwork_cell:work_cell=powerfu.power/cells_no;
fpo:powerfu.power=(hydrogen.mass*voltage_cell)/((1.05/100000)*sticho_ratioH2);
f2:water.mass=(9.34/100000)*(powerfu.power)/(voltage_cell);
f3:eta_energy=work_net/(148000*hydrogen.mass);
f5:hydrogen.ex_ph=14.2091*(ambient_t+273.15)*(((hydrogen.t+273.15)/(ambient_t+273.15))-1-ln((hydrogen.t+273.15)/(ambient_t+273.15)))+(4.12418*(ambient_t+273.15)*ln(hydrogen.p/ambient_p));
f4:hydrogen_ext=hydrogen.ex_ph+hydrogen.ex_ch;
f7:oxygen.ex_ph=0.9216*ambient_t*(((oxygen.t+273.15)/(ambient_t+273.15))-1-ln((oxygen.t+273.15)/(ambient_t+273.15)))+(0.25983*(ambient_t+273.15)*ln(oxygen.p/ambient_p));
f6:oxygen_ext=oxygen.ex_ph+oxygen.ex_ch;
f9:water.ex_ph=(water.h-water_ho)-((ambient_t+273.15)*(water.s-water_so));
f8:water_ext=water.ex_ph+water.ex_ch;
fs_gen: s_gen=irrv_entf/(ambient_t+273.15);
firrv_entf: irrv_entf=((1-((ambient_t+273.15)/(fcell_t+273.15)))*q_diss)-work_net+(hydrogen.mass*hydrogen_ext)+(oxygen.mass*oxygen_ext)-(water.mass*water_ext)-(hydrogenout.mass*hydrogenout_ext)-(oxygenout.mass*oxygenout_ext);
fa:eta_exf =1-(irrv_entf/((hydrogen.mass*hydrogen_ext)+(oxygen.mass*oxygen_ext)));
fhymo:hydrogenout.mass=(sticho_ratioH2-1)*(hydrogen.mass);
foxmo:oxygenout.mass=(sticho_ratioO2-1)*(oxygen.mass);
fhyoexph:hydrogenout.ex_ph=14.2091*(ambient_t+273.15)*(((hydrogenout.t+273.15)/(ambient_t+273.15))-1-ln((hydrogenout.t+273.15)/(ambient_t+273.15)))+(4.12418*(ambient_t+273.15)*ln(hydrogenout.p/ambient_p));
foxygoph:oxygenout.ex_ph=0.9216*(ambient_t+273.15)*(((oxygenout.t+273.15)/(ambient_t+273.15))-1-ln((oxygenout.t+273.15)/(ambient_t+273.15)))+(0.25983*(ambient_t+273.15)*ln(oxygenout.p/ambient_p));

fhydoext:hydrogenout_ext=hydrogenout.ex_ph+hydrogenout.ex_ch;
foxygext:oxygenout_ext=oxygenout.ex_ph+oxygenout.ex_ch;

13-fuel_cell3b model

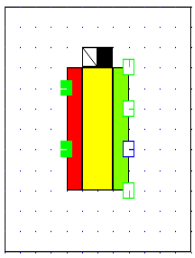

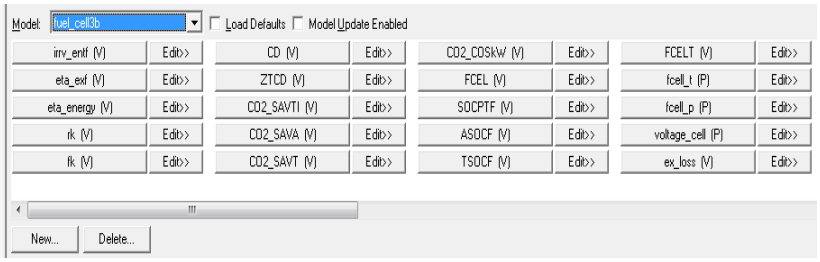

#fuel cell thermo-economic analysis without cooling or recycling

fq_gen: q_gen=(1.481- voltage_cell)*cells_no*work_cell/voltage_cell;
fq_diss: q_diss=RHL*q_gen;
fpower:work_net= (powerfu.power*ETA_CONV)-work_accis;
fwork_cell:work_cell=powerfu.power/cells_no;
fpo:powerfu.power=(hydrogen.mass*voltage_cell)/((1.05/100000)*sticho_ratioH2);
f1:oxygen.mass=(8.29/100000)*sticho_ratioO2*(cells_no*work_cell)/(voltage_cell);
f2:water.mass=(9.34/100000)*(cells_no*work_cell)/(voltage_cell);
f3:eta_energy=((work_net)/(141860*hydrogen.mass))*100;
fs_gen: s_gen=irrv_entf/(ambient_t+273.15);
firrv_entf: irrv_entf=((1-((ambient_t+273.15)/(fcell_t+273.15)))*-q_diss)-work_net+(hydrogen.mass*hydrogen.ex_t)+(oxygen.mass*oxygen.ex_t)-(water.mass*water.ex_t)-(hydrogenout.mass*hydrogenout.ex_t)-(oxygenout.mass*oxygenout.ex_t);
fex_loss: ex_loss=((1
fhymo:hydrogenout.mass=(1.05/100000)*(sticho_ratioH2-1)*(cells_no*work_cell)/(voltage_cell);
foxmo:oxygenout.mass=(8.29/100000)*(sticho_ratioO2-1)*(cells_no*work_cell)/(voltage_cell);
fcw: powerfu.cw=((hydrogen.ch2*hydrogen.ex_t*hydrogen.mass/1000000) +ZT +(oxygen.co2*oxygen.mass*oxygen.ex_t/1000000)-(hydrogenout.ch2*hydrogenout.mass*hydrogenout.ex_t/1000000)-(oxygenout.co2*oxygenout.mass*oxygenout.ex_t/1000000)-(water.mass*water.ex_t*cwa/1000000))/(work_net /1000000);
fZ: ZT=ZCI+ZOM;
fZCI: ZCI=(ACC*Ws)/(CF*8760*3600);
fZOM: ZOM=(COM*Ws)/(8760*3600);
fACC: ACC=CFC*CRF;
fCRF: CRF=(ir*((1+ir)^ny))/(((1+ir)^ny)-1);
frk: rk=(((1-(eta_exf/100))/(eta_exf/100))+(ZT/(hydrogen.ch2*work_net)))*100;
fk: fk=(ZT/(ZT+(hydrogen.ch2*((irrv_entf+ex_loss)/1000000))))*100;
fZTCD: ZTCD=((hydrogen.ch2*((irrv_entf+ex_loss)/1000000)) + ZT)*3600;
fCD:CD=((hydrogen.ch2*((irrv_entf+ex_loss)/1000000)))*3600 ;
fCO2_SAVTI: CO2_SAVTI=(powerfu.power/1000)* TIMED*CO2_COST*CO2_PF;
fCO2_SAVA: CO2_SAVA=(powerfu.power/1000)* 365*WORH*CO2_COST*CO2_PF;
fCO2_SAVT: CO2_SAVT= CO2_SAVA*ny;

fCO2_COSkW: CO2_COSkW=(CO2_COST*CO2_PF)/1000;
fFCEL: FCEL=(powerfu.cw*3600/1000000)-CO2_COSkW;
fSOCPTF: SOCPTF=SCF*powerfu.power* TIMED;
fASOCF: ASOCF=SCF*powerfu.power*WORH*365;
fTSOCF:TSOCF=ASOCF*ny;
fFCELT: FCELT=(FCEL -SCF)*(1000000/3600);

14-fuel_cell3c model

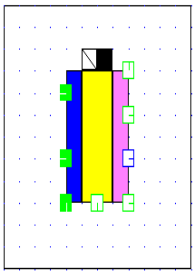

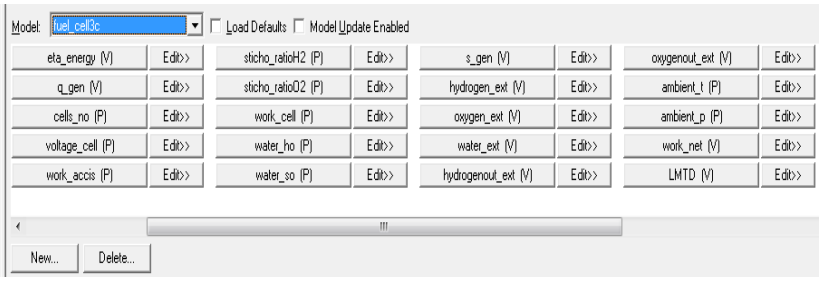

#fuel cell energy and exergy analysis with cooling (stand alone unit)

fq_gen: q_gen=(1.481- voltage_cell)*cells_no*work_cell/voltage_cell;
fq_diss: q_diss=0.2*q_gen;
fpower: powerfu.power=(cells_no*work_cell);
fwork_net: work_net=powerfu.power-work_accis;
fhym:hydrogen.mass=(1.05/100000)*sticho_ratioH2*(cells_no*work_cell)/(voltage_cell);
f1:oxygen.mass=(8.29/100000)*sticho_ratioO2*(cells_no*work_cell)/(voltage_cell);
f2:water.mass=(9.34/100000)*(cells_no*work_cell)/(voltage_cell);
f3:eta_energy=work_net/(141860*hydrogen.mass);
f5:hydrogen.ex_ph=(((14.2091*ambient_t)*((hydrogen.t/ambient_t)-1-ln(hydrogen.t/ambient_t)))+((4.12418*ambient_t)*(ln(hydrogen.p/ambient_p))));
f4:hydrogen_ext=hydrogen.ex_ph+hydrogen.ex_ch;
f7:oxygen.ex_ph=(((0.9216*ambient_t)*((oxygen.t/ambient_t)-1-ln(oxygen.t/ambient_t)))+((0.25983*ambient_t)*(ln(oxygen.p/ambient_p))));
f6:oxygen_ext=oxygen.ex_ph+oxygen.ex_ch;
f9:water.ex_ph=(water.h-water_ho)-(ambient_t*(water.s-water_so));
f8:water_ext=water.ex_ph+water.ex_ch;
fs_gen: s_gen=irrv_entf/ambient_t;
firrv_entf: irrv_entf=((1-(ambient_t/fcell_t))*-q_diss)-work_net+(hydrogen.mass*hydrogen_ext)+(oxygen.mass*oxygen_ext)-(water.mass*water_ext)-(hydrogenout.mass*hydrogenout_ext)-(oxygenout.mass*oxygenout_ext)+(coolingin.mass*ext_coolin)-(coolingout.mass*ext_coolout);
fa:eta_exf =1
foxygoph:oxygenout.ex_ph=0.9216*ambient_t*((oxygenout.t/ambient_t)-1-ln(oxygenout.t/ambient_t))+(0.25983*ambient_t*ln(oxygenout.p/ambient_p));
fhydoext:hydrogenout_ext=hydrogenout.ex_ph+hydrogenout.ex_ch;
foxygext:oxygenout_ext=oxygenout.ex_ph+oxygenout.ex_ch;
fQ_cool: Q_cool=q_gen-q_diss-Q_stream;
fQ_stream: Q_stream=(oxygenout.mass*oxygenout.h)+(hydrogenout.mass*hydrogenout.h)+(water.mass*water.h);
fTout: coolingout.t=(Q_cool/coolingin.mass*Cp_cool)+coolingin.t;

fMT: LMTD=fcell_t-(0.5*(coolingin.t+coolingout.t));
fbalance: coolingin.mass*Cp_cool*(coolingout.t-coolingin.t)=AU_hx*LMTD;
fpres: coolingout.p=coolingin.p-delta_p;
fcool_m: coolingin.mass=coolingout.mass;
fex_phcoolin: coolingin.ex_ph=(coolingin.h-water_ho)-(ambient_t*(coolingin.s-water_so));
fex_phcoolout: coolingout.ex_ph=(coolingout.h-water_ho)-(ambient_t*(coolingout.s-water_so));
fext_coolin: ext_coolin=coolingin.ex_ph+coolingin.ex_ch;
fext_coolout: ext_coolout=coolingout.ex_ph+coolingout.ex_ch;

15-fuel_cell3d model

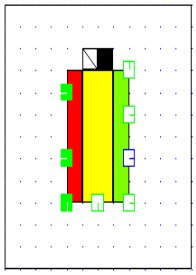

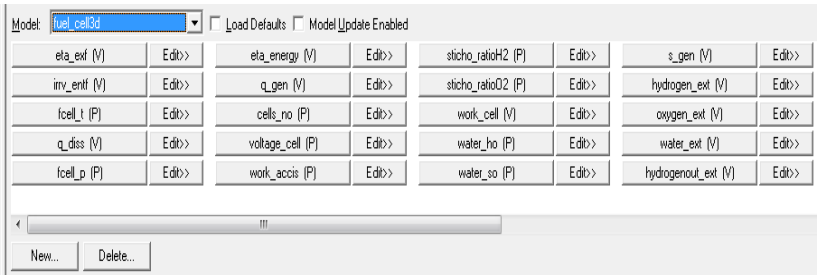

#fuel cell energy and exergy analysis for integrated unit with cooling and recycling system

fq_gen: q_gen=(1.481- voltage_cell)*cells_no*work_cell/voltage_cell;
fq_diss: q_diss=0.2*q_gen;
fpower:work_net= powerfu.power-work_accis;
fwork_cell:work_cell=powerfu.power/cells_no;
fpo:powerfu.power=(hydrogen.mass*voltage_cell)/((1.05/100000)*sticho_ratioH2);
f2:water.mass=(9.34/100000)*(cells_no*work_cell)/(voltage_cell);
f3:eta_energy=work_net/(142000*hydrogen.mass);

f4:hydrogen_ext=hydrogen.ex_ph+hydrogen.ex_ch;

f6:oxygen_ext=oxygen.ex_ph+oxygen.ex_ch;
f9:water.ex_ph=(water.h-water_ho)-(ambient_t*(water.s-water_so));
f8:water_ext=water.ex_ph+water.ex_ch;
fs_gen: s_gen=irrv_entf/ambient_t;
firrv_entf: irrv_entf=((1-(ambient_t/fcell_t))*-q_diss)-work_net+(hydrogen.mass*hydrogen_ext)+(oxygen.mass*oxygen_ext)-(water.mass*water_ext)-(hydrogenout.mass*hydrogenout_ext)-(oxygenout.mass*oxygenout_ext)+(coolingin.mass*ext_coolin)-(coolingout.mass*ext_coolout);
fa:eta_exf =1 hydrogenout.t/ambient_t)-1-ln(hydrogenout.t/ambient_t))+(4.12418*ambient_t*ln(hydrogenout.p/ambient_p));
foxygoph:oxygenout.ex_ph=0.9216*ambient_t*((oxygenout.t/ambient_t)-1-ln(oxygenout.t/ambient_t))+(0.25983*ambient_t*ln(oxygenout.p/ambient_p));
fhydoext:hydrogenout_ext=hydrogenout.ex_ph+hydrogenout.ex_ch;
foxygext:oxygenout_ext=oxygenout.ex_ph+oxygenout.ex_ch;
fQ_cool: Q_cool=q_gen-q_diss-Q_stream;

fQ_stream:
Q_stream=(oxygenout.mass*oxygenout.h)+(hydrogenout.mass*hydrogenout.h)+(water.mass*water.h);
fTout: coolingout.t=(Q_cool/coolingin.mass*Cp_cool)+coolingin.t;
fMT: LMTD=fcell_t-(0.5*(coolingin.t+coolingout.t));
fbalance: coolingin.mass*Cp_cool*(coolingout.t-coolingin.t)=AU_hx*LMTD;
fpres: coolingout.p=coolingin.p-delta_p;
fcool_m: coolingin.mass=coolingout.mass;
fex_phcoolin: coolingin.ex_ph=(coolingin.h-water_ho)-(ambient_t*(coolingin.s-water_so));
fex_phcoolout: coolingout.ex_ph=(coolingout.h-water_ho)-(ambient_t*(coolingout.s-water_so));
fext_coolin: ext_coolin=coolingin.ex_ph+coolingin.ex_ch;
fext_coolout: ext_coolout=coolingout.ex_ph+coolingout.ex_ch;

16-fuel_cell3e model

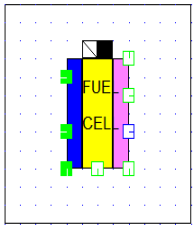

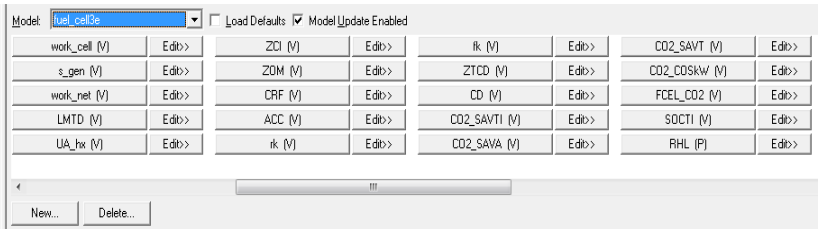

#fuel cell thermo-economic analysis with cooling and recycling system

fq_gen: q_gen=(1.481- voltage_cell)*cells_no*work_cell/voltage_cell;
fq_diss: q_diss=RHL*q_gen;
fpower:work_net= (powerfu.power*(ETA_CONV/100))-wacc_loss;
fwacc_loss: wacc_loss=WACCSF*powerfu.power;
fwork_cell:work_cell=powerfu.power/cells_no;
fpo:powerfu.power=((hydrogen.mass)*voltage_cell)/((1.05/100000)*sticho_ratioH2);
f2:water.mass=(9.34/100000)* (cells_no*work_cell)/(voltage_cell);
f3:eta_energy=((work_net+(Q_cool))/(141860*hydrogen.mass/sticho_ratioH2))*100;
 # exergy analysis of the unit taking in considerations all the streams exergies in and out from the unit
fs_gen: s_gen=irrv_entf/(ambient_t+273.15);
coolingout.mass*coolingout.ex_t)-(water.mass*water.ex_t);
fa:eta_exf =((work_net+((coolingout.mass*coolingout.ex_t)-(coolingin.mass*coolingin.ex_t))+(water.mass*water.ex_t))/(((hydrogen.mass*hydrogen.ex_t)-(hydrogenout.mass*hydrogenout.ex_t))+((oxygen.mass*oxygen.ex_t)-(oxygenout.mass*oxygenout.ex_t))))*100;
fex_loss: ex_loss=((1-((ambient_t+273.15)/(fcell_t+273.15)))*q_diss);
fhymo:hydrogenout.mass=(1.05/100000)*(sticho_ratioH2-1)*(cells_no*work_cell)/(voltage_cell);
foxmo:oxygenout.mass=(8.29/100000)*(sticho_ratioO2-1)*(cells_no*work_cell)/(voltage_cell);
fQ_cool: Q_cool=q_gen-q_diss-Q_stream;

fQ_stream:
Q_stream=(oxygenout.mass*oxygenout.h)+(hydrogenout.mass*hydrogenout.h)+(water.mass*water.h);

fbalance: coolingin.mass*Cp_cool*(coolingout.t-coolingin.t)=UA_hx*LMTD;
fpres: coolingout.p=coolingin.p-delta_p;
fcool_m: coolingin.mass=coolingout.mass;
fcwa: cwa=(cwc/coolingin.ex_t)*1000000;
fcwa1: cwa1=(cwh/ coolingout.ex_t)*1000000;
fcw: powerfu.cw=(((hydrogen.ch2*((hydrogen.mass *hydrogen.ex_t)-(hydrogenout.mass*hydrogenout.ex_t))) /1000000) +ZT-(RECF*water.mass*water.ex_t*cwa1/1000000)-(((cwa1* coolingout.mass*coolingout.ex_t)-(cwa*coolingin.mass*coolingin.ex_t))/1000000)+((oxygen.co2*((oxygen.mass *oxygen.ex_t)-(oxygenout.mass*oxygenout.ex_t))) /1000000))/(work_net /1000000);
fZ: ZT=ZCI+ZOM;
fZCI: ZCI=(ACC*Ws)/((CF/100)*8760*3600);
fZOM: ZOM=(COM*Ws)/(8760*3600);
fACC: ACC=CFC*CRF;
fCRF: CRF=((ir/100)*((1+(ir/100))^ny))/(((1+(ir/100))^ny)-1);
 # The rk and fk analysis defined the exergy destruction cost as the the cost rate of the additinal fuel (consedried hydrogen as the main fuel) that must be supplied to the unit (above the rate needed for the main products defined as the electricity and hot water from cooling system) to cover the rate of exergy destruction
frk: rk=(((1-(eta_exf/100))/(eta_exf/100))+(ZT/((hydrogen.ch2/1000000)*((work_net +((coolingout.mass*coolingout.ex_t)-(coolingin.mass*coolingin.ex_t)))))))*100;
fk: fk=(ZT/(ZT+(hydrogen.ch2*((irrv_entf+ex_loss)/1000000))))*100;
fZTCD: ZTCD=((hydrogen.ch2*((irrv_entf+ex_loss)/1000000)) + ZT)*3600;
fCD:CD=((hydrogen.ch2*((irrv_entf+ex_loss)/1000000)))*3600 ;
fCO2_SAVTI: CO2_SAVTI=(powerfu.power/1000)* TIMED*CO2_COST*CO2_PF;
fCO2_SAVA: CO2_SAVA=(powerfu.power/1000)* 365*WORH*CO2_COST*CO2_PF;
fCO2_SAVT: CO2_SAVT= CO2_SAVA*ny;
fCO2_COSkW: CO2_COSkW=(CO2_COST*CO2_PF)/1000;
fFCEL_CO2: FCEL_CO2=(powerfu.cw*3600/1000000)-CO2_COSkW;
fSOCTI: SOCTI=SCF*powerfu.power* TIMED;
fASOC: ASOC=SCF*powerfu.power*WORH*365;
fTSOC: TSOC=ASOC*ny;
fFCELT: FCELT=(FCEL_CO2 -SCF)*(1000000/3600);

17-htexa model

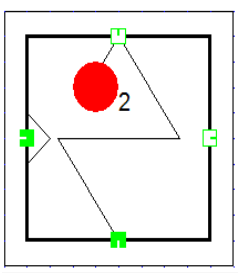

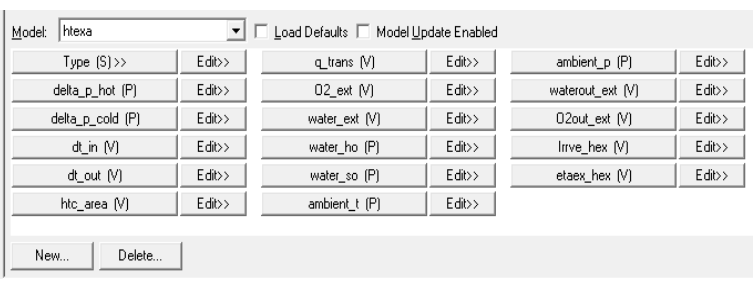

Oxygen heat exchanger energy and exergy analysis

```
# mass balance equations
f1:     feed_cold.mass = drain_cold.mass;
f2:     feed_hot.mass  = drain_hot.mass;

# pressure drops
f3:     feed_cold.p-delta_p_cold = drain_cold.p;
f4:     feed_hot.p-delta_p_hot    = drain_hot.p;

# energy balance
f5:     feed_hot.mass*(feed_hot.h-drain_hot.h) - q_trans = 0.0;
f6:     feed_cold.mass*(feed_cold.h-drain_cold.h) +q_trans = 0.0;

# temperature differences
# They are differently defined for co and counter current heat exchangers.

ifl Type == cocurrent then
        f7_co:  feed_hot.t-dt_in   = feed_cold.t;
        f8_co:  drain_hot.t-dt_out = drain_cold.t;
endifl

ifl Type == counter_current then
        f7_counter:    drain_hot.t-dt_in   = feed_cold.t;
        f8_counter:    feed_hot.t-dt_out = drain_cold.t;
endifl


# logarithmic temperature difference
f9:     if abs(dt_in/dt_out) >=1.2 || abs(dt_out/dt_in) >=1.2 then
                q_trans*ln(dt_in/dt_out)/(dt_in-dt_out) = htc_area;
        else
                q_trans*2.0/(dt_in+dt_out) = htc_area;
fO2_ex_ph:   feed_hot.ex_ph=0.9216*ambient_t*((feed_hot.t/ambient_t)-1-
ln(feed_hot.t/ambient_t))+(0.25983*ambient_t*ln(feed_hot.p/ambient_p));
fwater_ex_ph: feed_cold.ex_ph=(feed_cold.h-water_ho)-(ambient_t*(feed_cold.s-
water_so));

fwaterout_exph: drain_cold.ex_ph=(drain_cold.h-water_ho)-
(ambient_t*(drain_cold.s-water_so));
fwaterext: water_ext=feed_cold.ex_ph+feed_cold.ex_ch;
fO2_ext: O2_ext =feed_hot.ex_ph+feed_hot.ex_ch;
fwateroutext: waterout_ext=drain_cold.ex_ph+drain_cold.ex_ch;
fO2outext:O2out_ext=drain_hot.ex_ph+drain_hot.ex_ch;
fIrrve: Irrve_hex=(feed_hot.mass*(O2_ext-O2out_ext))-
(feed_cold.mass*(waterout_ext-water_ext));
fetaex_hex: etaex_hex=(feed_cold.mass*(waterout_ext-
water_ext))/(feed_hot.mass*(O2_ext-O2out_ext));

# tests
t1:     test (dt_in>0.0)        error "dt_in <= 0.0";
```

t2: test(dt_out>0.0) error "dt_out <= 0.0";
t3: test(q_trans>0.0) error "q_trans <= 0.0";

18-htexaa model

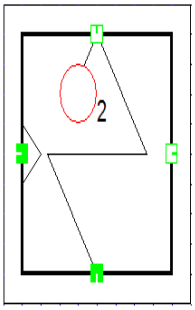

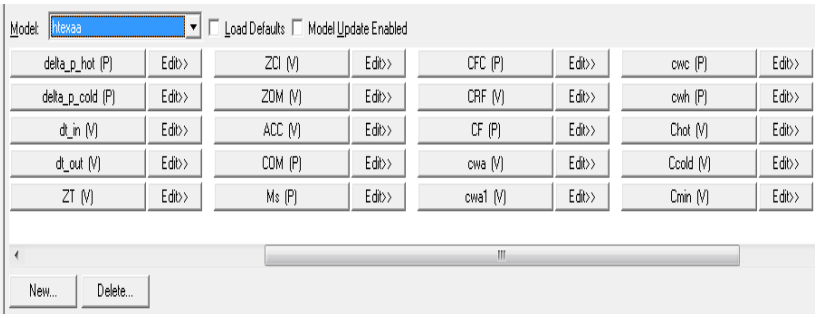

Oxygen heat exchanger thermo-economic analysis

 # mass balance equations
f1: feed_cold.mass = drain_cold.mass;
f2: feed_hot.mass = drain_hot.mass;

 # pressure drops
f3: feed_cold.p-delta_p_cold = drain_cold.p;
f4: feed_hot.p-delta_p_hot = drain_hot.p;

 # energy balance
f5: feed_hot.mass*(feed_hot.h-drain_hot.h) - q_trans = 0.0;
f6: feed_cold.mass*(feed_cold.h-drain_cold.h) +q_trans = 0.0;

 # temperature differences
 # They are differently defined for co and counter current heat exchangers.

ifl Type == cocurrent then
f7_co: feed_hot.t-dt_in = feed_cold.t;
f8_co: drain_hot.t-dt_out = drain_cold.t;
endifl

ifl Type == counter_current then
f7_counter: drain_hot.t-dt_in = feed_cold.t;
f8_counter: feed_hot.t-dt_out = drain_cold.t;
endifl

 # logarithmic temperature difference
f9: if abs(dt_in/dt_out) >=1.2 || abs(dt_out/dt_in) >=1.2 then
q_trans*ln(dt_in/dt_out)/(dt_in-dt_out) = htc_area;
else
q_trans*2.0/(dt_in+dt_out) = htc_area;
fcold: Ccold=feed_cold.mass*4.18;
fchot: Chot=feed_hot.mass*0.9216;

f10: **if Ccold < Chot then**
Ccold=Cmin;

else
Chot=Cmin;

f11: **if Chot < Ccold then**
Ccold=Cmax;
else
Chot=Cmax;

fCR: CR= Cmin/Cmax;
fNTU: NTU=htc_area/Cmin;
fQmax: Qmax= Cmin*(feed_hot.t-feed_cold.t);
fE: Eeffectiv= q_trans/Qmax;
fIrrve: Irrve_hex=(feed_hot.mass*(feed_hot.ex_t-drain_hot.ex_t))-(feed_cold.mass*(drain_cold.ex_t-feed_cold.ex_t));
fetaex_hex: etaex_hex=((feed_cold.mass*(drain_cold.ex_t-feed_cold.ex_t))/(feed_hot.mass*(feed_hot.ex_t-drain_hot.ex_t)))*100;
fcwa: cwa=(cwc/feed_cold.ex_t)*1000000;
/(drain_hot.ex_t*drain_hot.mass/1000000);
fZ: ZT=ZCI+ZOM;
fZCI: ZCI=(ACC*Ms)/(CF*8760*3600);
fZOM: ZOM=(COM*Ms)/(8760*3600);
fACC: ACC=CFC*CRF;
fCRF: CRF=(ir*((1+ir)^ny))/(((1+ir)^ny)-1);

fk: fk=ZT/(ZT+(feed_hot.co2*(Irrve_hex/1000000)))*100;
fZTCD: ZTCD=((feed_hot.co2*(Irrve_hex/1000000)) + ZT)*3600;
fCD:CD=(feed_hot.co2*(Irrve_hex/1000000))*3600 ;

 # tests
t1: **test (dt_in>0.0)** **error "dt_in <= 0.0";**
t2: **test(dt_out>0.0)** **error "dt_out <= 0.0";**
t3: **test(q_trans>0.0)** **error "q_trans <= 0.0";**

19-htex model

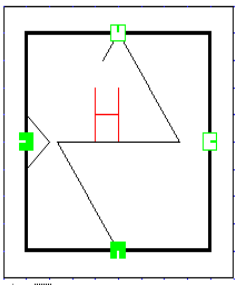

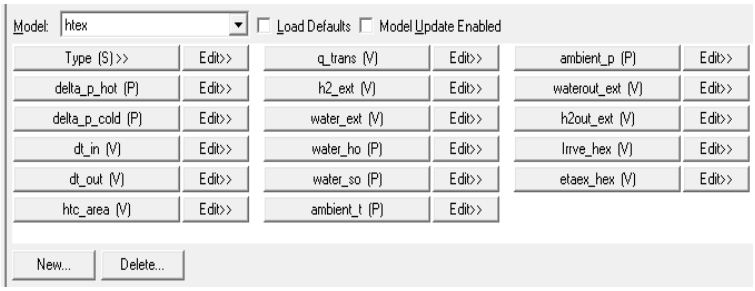

Hydrogen heat exchanger energy and exergy model

```
# mass balance equations
f1:     feed_cold.mass = drain_cold.mass;
f2:     feed_hot.mass  = drain_hot.mass;

# pressure drops
f3:     feed_cold.p-delta_p_cold = drain_cold.p;
f4:     feed_hot.p-delta_p_hot   = drain_hot.p;

# energy balance
f5:     feed_hot.mass*(feed_hot.h-drain_hot.h) - q_trans = 0.0;
f6:     feed_cold.mass*(feed_cold.h-drain_cold.h) +q_trans = 0.0;

# temperature differences
# They are differently defined for co and counter current heat exchangers.

ifl Type == cocurrent then
        f7_co:  feed_hot.t-dt_in   = feed_cold.t;
        f8_co:  drain_hot.t-dt_out = drain_cold.t;
endifl

ifl Type == counter_current then
        f7_counter:    drain_hot.t-dt_in   = feed_cold.t;
        f8_counter:    feed_hot.t-dt_out = drain_cold.t;
endifl



# logarithmic temperature difference
f9:     if abs(dt_in/dt_out) >=1.2 || abs(dt_out/dt_in) >=1.2 then
                q_trans*ln(dt_in/dt_out)/(dt_in-dt_out) = htc_area;
        else
                q_trans*2.0/(dt_in+dt_out) = htc_area;
fh2_ex_ph:   feed_hot.ex_ph=14.2091*ambient_t*((feed_hot.t/ambient_t)-1-
ln(feed_hot.t/ambient_t))+(4.12418*ambient_t*ln(feed_hot.p/ambient_p));
fwater_ex_ph: feed_cold.ex_ph=(feed_cold.h-water_ho)-(ambient_t*(feed_cold.s-
water_so));


fwaterext: water_ext=feed_cold.ex_ph+feed_cold.ex_ch;
fh2_ext: h2_ext =feed_hot.ex_ph+feed_hot.ex_ch;
fwateroutext: waterout_ext=drain_cold.ex_ph+drain_cold.ex_ch;
fh2outext:h2out_ext=drain_hot.ex_ph+drain_hot.ex_ch;
fIrrve: Irrve_hex=(feed_hot.mass*(h2_ext-h2out_ext))-
(feed_cold.mass*(waterout_ext-water_ext));
fetaex_hex: etaex_hex=(feed_cold.mass*(waterout_ext-
water_ext))/(feed_hot.mass*(h2_ext-h2out_ext));

# tests
t1:     test (dt_in>0.0)        error "dt_in <= 0.0";
t2:     test(dt_out>0.0)        error "dt_out <= 0.0";
t3:     test(q_trans>0.0)       error "q_trans <= 0.0";
```

20-htexb model

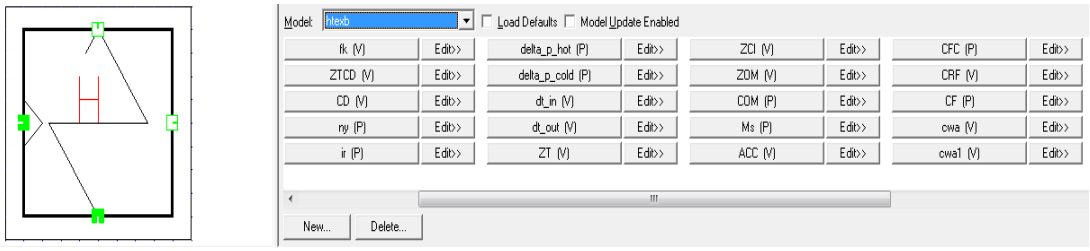

Hydrogen heat exchanger thermo-economic analysis

```
# mass balance equations
f1:     feed_cold.mass = drain_cold.mass;
f2:     feed_hot.mass  = drain_hot.mass;

# pressure drops
f3:     feed_cold.p-delta_p_cold = drain_cold.p;
f4:     feed_hot.p-delta_p_hot   = drain_hot.p;

# energy balance
f5:     feed_hot.mass*(feed_hot.h-drain_hot.h) - q_trans = 0.0;
f6:     feed_cold.mass*(feed_cold.h-drain_cold.h) +q_trans = 0.0;

# temperature differences
# They are differently defined for co and counter current heat exchangers.

ifl Type == cocurrent then
        f7_co:  feed_hot.t-dt_in   = feed_cold.t;
        f8_co:  drain_hot.t-dt_out = drain_cold.t;
endifl

ifl Type == counter_current then
        f7_counter:    drain_hot.t-dt_in   = feed_cold.t;
        f8_counter:    feed_hot.t-dt_out = drain_cold.t;
endifl

# logarithmic temperature difference
f9:     if abs(dt_in/dt_out) >=1.2 || abs(dt_out/dt_in) >=1.2 then
                q_trans*ln(dt_in/dt_out)/(dt_in-dt_out) = htc_area;
        else
                q_trans*2.0/(dt_in+dt_out) = htc_area;
fcold: Ccold=feed_cold.mass*4.18;
fchot: Chot=feed_hot.mass*14.2;

f10:    if Ccold < Chot  then
          Ccold=Cmin;
```

```
            else
              Chot=Cmin;

f11:      if Chot < Ccold  then
              Ccold=Cmax;
            else
              Chot=Cmax;

fCR: CR= Cmin/Cmax;
fNTU: NTU=htc_area/Cmin;
fQmax: Qmax= Cmin*(feed_hot.t-feed_cold.t);

fcwa: cwa=(cwc/feed_cold.ex_t)*1000000;
fcwa1: cwa1=(cwh/ drain_cold.ex_t)*1000000;
fch2: drain_hot.ch2= (-
(cwa1*feed_cold.mass*drain_cold.ex_t/1000000)+(cwa*feed_cold.ex_t*feed_cold.
mass/1000000)+(feed_hot.ch2*feed_hot.ex_t*feed_hot.mass/1000000) +ZT)
/(drain_hot.ex_t*drain_hot.mass/1000000);
fZ: ZT=ZCI+ZOM;
fZCI: ZCI=(ACC*Ms)/(CF*8760*3600);
fZOM: ZOM=(COM*Ms)/(8760*3600);
fACC: ACC=CFC*CRF;
fCRF: CRF=(ir*((1+ir)^ny))/(((1+ir)^ny)-1);

fk: fk=(ZT/(ZT+(feed_hot.ch2*(Irrve_hex/1000000))))*100;
fZTCD: ZTCD=(( feed_hot.ch2*(Irrve_hex/1000000)) + ZT)*3600;
fCD:CD=( feed_hot.ch2*(Irrve_hex/1000000))*3600 ;
# tests
t1:       test (dt_in>0.0)        error "dt_in <= 0.0";
t2:       test(dt_out>0.0)        error "dt_out <= 0.0";
t3:       test(q_trans>0.0)       error "q_trans <= 0.0";
```

21-Compressor model

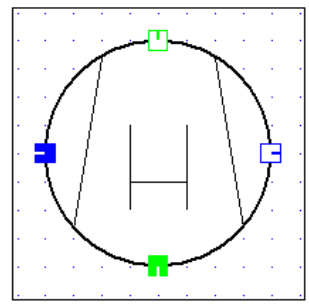

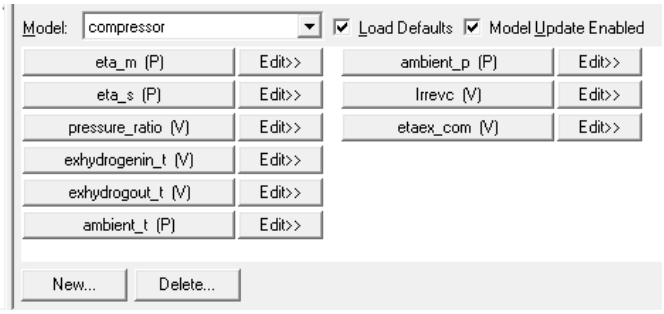

Hydrogen compressor energy and exergy analysis

```
# mass balance
f1:       feed.mass = drain.mass;

f2:       feed.s = drain.Composition.fs(drain.p, feed.h+(drain.h - feed.h)*eta_s);
```

```
@# f2a:        delta_hs = (drain.h - feed.h) *eta_s;
@# f2b:        feed.s = drain.Composition.fs(drain.p, feed.h+delta_hs);

# both sides connected
ifl ref(shaft_in) && ref(shaft_out) then
        f3a:    (feed.h - drain.h)* feed.mass /eta_m + shaft_in.power -
shaft_out.power = 0.0;
endifl

# left side shaft only
ifl ref(shaft_in) && !ref(shaft_out) then
        f3b:    (feed.h - drain.h)* feed.mass / eta_m + shaft_in.power = 0.0;
endifl

# right side shaft only
ifl !ref(shaft_in) && ref(shaft_out) then
        f3c:    (feed.h - drain.h) * feed.mass / eta_m - shaft_out.power = 0.0;
endifl

# pressure ratio

fPressureRatio:       feed.p * pressure_ratio = drain.p;
# exergy analysis

f6: exhydrogenin_t=feed.ex_ph+feed.ex_ch;
f7: exhydrogout_t=drain.ex_ph+drain.ex_ch;
f8: feed.ex_ph=14.2091*ambient_t*((feed.t/ambient_t)-1-
ln(feed.t/ambient_t))+(4.12418*ambient_t*ln(feed.p/ambient_p));
f9: drain.ex_ph=14.2091*ambient_t*((drain.t/ambient_t)-1-
ln(drain.t/ambient_t))+(4.12418*ambient_t*ln(drain.p/ambient_p));
f0: Irrevc=feed.mass*(exhydrogenin_t-exhydrogout_t)+shaft_in.power;
fetaex_com: etaex_com= (feed.mass*(exhydrogout_t-
exhydrogenin_t))/shaft_in.power;


# test conditions
t1:     test((drain.p - feed.p) >= 0.0)       warning "outlet pressure lower than
inlet pressure";
t2:     test ( eta_s >= 0.0)            error "isentropic efficiency < 0.0";
t3:     test ( eta_s <= 1.0)            error "isentropic efficiency >1.0";
t4:     test ( eta_m >= 0.0)            error "mechanical efficiency < 0.0";
t5:     test ( eta_m <= 1.0)            error "mechanical efficiency > 1.0";
```

22-compressora model

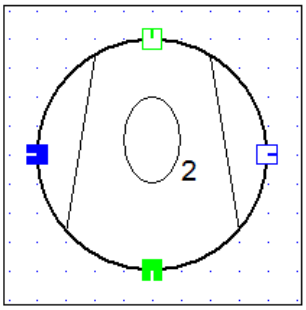

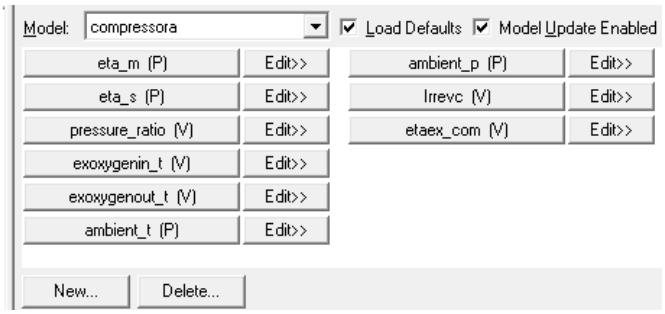

Oxygen compressor energy and exergy analysis
 # mass balance
f1: feed.mass = drain.mass;

f2: feed.s = drain.Composition.fs(drain.p, feed.h+(drain.h - feed.h)*eta_s);

@# f2a: delta_hs = (drain.h - feed.h) *eta_s;
@# f2b: feed.s = drain.Composition.fs(drain.p, feed.h+delta_hs);

 # both sides connected
ifl ref(shaft_in) && ref(shaft_out) then
f3a: (feed.h - drain.h)* feed.mass /eta_m + shaft_in.power - shaft_out.power = 0.0;
endifl

 # left side shaft only
ifl ref(shaft_in) && !ref(shaft_out) then
f3b: (feed.h - drain.h)* feed.mass / eta_m + shaft_in.power = 0.0;
endifl

 # right side shaft only
ifl !ref(shaft_in) && ref(shaft_out) then
f3c: (feed.h - drain.h) * feed.mass / eta_m - shaft_out.power = 0.0;
endifl

 # pressure ratio

fPressureRatio: feed.p * pressure_ratio = drain.p;
 # exergy analysis

f6: exoxygenin_t=feed.ex_ph+feed.ex_ch;
f7: exoxygenout_t=drain.ex_ph+drain.ex_ch;
f8: feed.ex_ph=0.9216*ambient_t*((feed.t/ambient_t)-1-ln(feed.t/ambient_t))+(0.25983*ambient_t*ln(feed.p/ambient_p));
f9: drain.ex_ph=0.9216*ambient_t*((drain.t/ambient_t)-1-ln(drain.t/ambient_t))+(0.25983*ambient_t*ln(drain.p/ambient_p));
f0: Irrevc=feed.mass*(exoxygenin_t-exoxygenout_t)+shaft_in.power;
fetaex_com: etaex_com= feed.mass*(exoxygenout_t-exoxygenin_t)/shaft_in.power;

 # test conditions

t1: test((drain.p - feed.p) >= 0.0) warning "outlet pressure lower than inlet pressure";
t2: test (eta_s >= 0.0) error "isentropic efficiency < 0.0";
t3: test (eta_s <= 1.0) error "isentropic efficiency >1.0";
t4: test (eta_m >= 0.0) error "mechanical efficiency < 0.0";
t5: test (eta_m <= 1.0) error "mechanical efficiency > 1.0";

23-compressoraa model

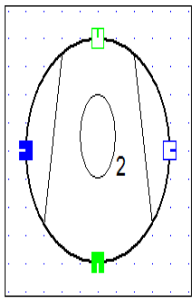

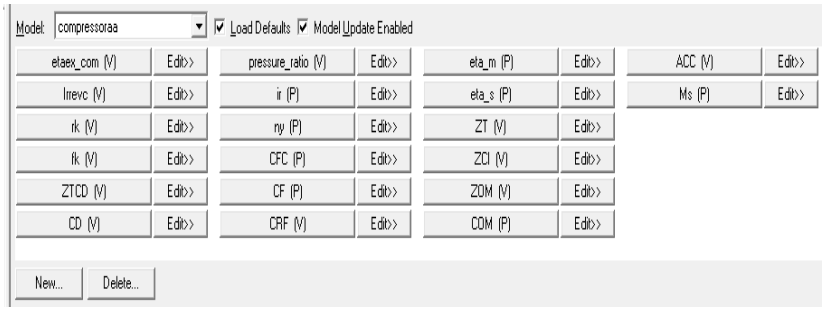

Oyxygen compressor thermo-economic analysis

 # mass balance
f1: feed.mass = drain.mass;

f2: feed.s = drain.Composition.fs(drain.p, feed.h+(drain.h - feed.h)*eta_s);

@# f2a: delta_hs = (drain.h - feed.h) *eta_s;
@# f2b: feed.s = drain.Composition.fs(drain.p, feed.h+delta_hs);

 # both sides connected
ifl ref(shaft_in) && ref(shaft_out) then
f3a: (feed.h - drain.h)* feed.mass /eta_m + shaft_in.power - shaft_out.power = 0.0;
endifl

 # left side shaft only
ifl ref(shaft_in) && !ref(shaft_out) then
f3b: (feed.h - drain.h)* feed.mass / eta_m + shaft_in.power = 0.0;
endifl

 # right side shaft only
ifl !ref(shaft_in) && ref(shaft_out) then
f3c: (feed.h - drain.h) * feed.mass / eta_m - shaft_out.power = 0.0;
endifl

 # pressure ratio

fPressureRatio: feed.p * pressure_ratio = drain.p;
 # exergy analysis consideried the exergy difference between the outlet and the inlet oxygen streams as the product and the electricty is the main fuel

f0: Irrevc=(feed.mass*(feed.ex_t-drain.ex_t))+shaft_in.power;
fetaex_com: etaex_com=((feed.mass*(drain.ex_t-feed.ex_t))/shaft_in.power)*100;
fch2: drain.co2=
(((ZT)+(shaft_in.cw*shaft_in.power/1000000)+(feed.co2*feed.mass*feed.ex_t
/1000000))/ (drain.ex_t*drain.mass/1000000));
fZ: ZT=ZCI+ZOM;
fZCI: ZCI=(ACC*Ms)/(CF*8760*3600);
fZOM: ZOM=(COM*Ms)/(8760*3600);
fACC: ACC=CFC*CRF;
fCRF: CRF=(ir*((1+ir)^ny))/(((1+ir)^ny)-1);
frk: rk=(((1-(etaex_com/100))/(etaex_com/100))+(ZT/(shaft_in.cw*((drain.ex_t-feed.ex_t)*drain.mass/1000000))))*100;
fk: fk=(ZT/(ZT+(shaft_in.cw*(Irrevc/1000000))))*100;
fZTCD: ZTCD=((shaft_in.cw*(Irrevc/1000000)) + ZT)*3600;
fCD:CD=(shaft_in.cw*(Irrevc/1000000))*3600 ;
 # test conditions
t1: test((drain.p - feed.p) >= 0.0) warning "outlet pressure lower than inlet pressure";
t2: test (eta_s >= 0.0) error "isentropic efficiency < 0.0";
t3: test (eta_s <= 1.0) error "isentropic efficiency >1.0";
t4: test (eta_m >= 0.0) error "mechanical efficiency < 0.0";
t5: test (eta_m <= 1.0) error "mechanical efficiency > 1.0";

24-compressorb model

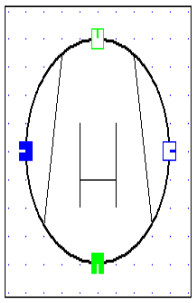

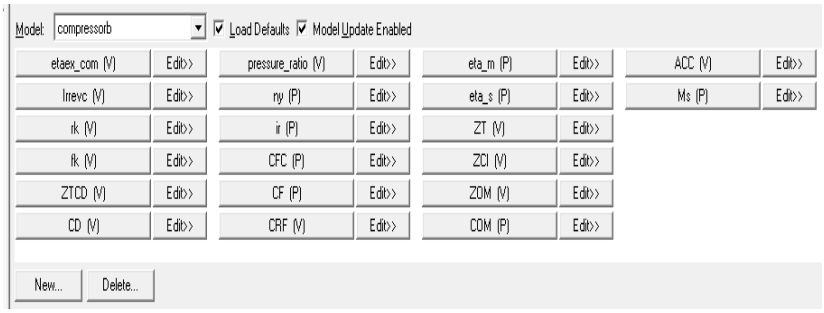

Hydrogen compressor thermo-economic analysis

 # mass balance
f1: feed.mass = drain.mass;

f2: feed.s = drain.Composition.fs(drain.p, feed.h+(drain.h - feed.h)*eta_s);

@# f2a: delta_hs = (drain.h - feed.h) *eta_s;
@# f2b: feed.s = drain.Composition.fs(drain.p, feed.h+delta_hs);

 # both sides connected
ifl ref(shaft_in) && ref(shaft_out) then
f3a: (feed.h - drain.h)* feed.mass /eta_m + shaft_in.power - shaft_out.power = 0.0;
endifl

 # left side shaft only

```
ifl ref(shaft_in) && !ref(shaft_out) then
        f3b:    (feed.h - drain.h)* feed.mass / eta_m + shaft_in.power = 0.0;
endifl

# right side shaft only
ifl !ref(shaft_in) && ref(shaft_out) then
        f3c:    (feed.h - drain.h) * feed.mass / eta_m - shaft_out.power = 0.0;
endifl

# pressure ratio

fPressureRatio:       feed.p * pressure_ratio = drain.p;
# exergy analysis considered the exergy difference between the outlet and the inlet
hydrogen streams as the product and the electricty is the main fuel
f0: Irrevc=(feed.mass*(feed.ex_t-drain.ex_t))+shaft_in.power;
fetaex_com: etaex_com=((feed.mass*(drain.ex_t-feed.ex_t))/shaft_in.power)*100;
fch2: drain.ch2=
(((ZT)+(shaft_in.cw*shaft_in.power/1000000)+(feed.ch2*feed.mass*feed.ex_t
/1000000))/ (drain.ex_t*drain.mass/1000000));
fZ: ZT=ZCI+ZOM;
fZCI: ZCI=(ACC*Ms)/(CF*8760*3600);
fZOM: ZOM=(COM*Ms)/(8760*3600);
fACC: ACC=CFC*CRF;
fCRF: CRF=(ir*((1+ir)^ny))/(((1+ir)^ny)-1);
frk: rk=(((1-(etaex_com/100))/(etaex_com/100))+(ZT/(shaft_in.cw*((drain.ex_t-
feed.ex_t)*drain.mass/1000000))))*100;
fk: fk=(ZT/(ZT+(shaft_in.cw*(Irrevc/1000000))))*100;
fZTCD: ZTCD=((shaft_in.cw*(Irrevc/1000000)) + ZT)*3600;
fCD:CD=((shaft_in.cw*(Irrevc/1000000)))*3600 ;

# test conditions
t1:     test((drain.p - feed.p) >= 0.0)       warning "outlet pressure lower than
inlet pressure";
t2:     test ( eta_s >= 0.0)            error "isentropic efficiency < 0.0";
t3:     test ( eta_s <= 1.0)            error "isentropic efficiency >1.0";
t4:     test ( eta_m >= 0.0)            error "mechanical efficiency < 0.0";
t5:     test ( eta_m <= 1.0)            error "mechanical efficiency > 1.0";
```

25-mixer model

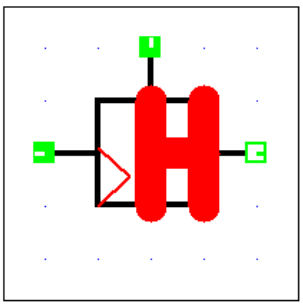

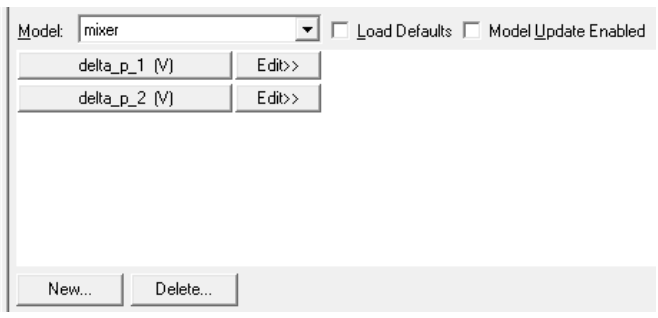

Hydrogen mixer

```
# mass balance
f1:     drain.mass-feed2.mass=feed1.mass;
# energy balance
f2:     feed1.h*feed1.mass+feed2.h*feed2.mass-drain.h*drain.mass = 0.0;
# pressure drop feed_1
f3:     feed1.p-delta_p_1-drain.p = 0.0;
#pressure drop feed_2
f4:     feed2.p-delta_p_2-drain.p = 0.0;
# The equations for the components of the compositions
@# configuration 1
# All composition objects are different
ifl     ref(feed1.Composition) != ref(feed2.Composition)
         && ref(feed1.Composition) != ref(drain.Composition)
         && ref(feed2.Composition) != ref(drain.Composition)
then
        # The mass balance for WATER has been omitted, since it is automatically
satisfied
        fa2:    drain.mass * drain.Composition.AR       = feed1.mass *
feed1.Composition.AR       + feed2.mass * feed2.Composition.AR;
        fa3:    drain.mass * drain.Composition.C2H6     = feed1.mass *
feed1.Composition.C2H6 + feed2.mass * feed2.Composition.C2H6;
        fa4:    drain.mass * drain.Composition.C3H8     = feed1.mass *
feed1.Composition.C3H8     + feed2.mass * feed2.Composition.C3H8;
        fa5:    drain.mass * drain.Composition.CH4      = feed1.mass *
feed1.Composition.CH4      + feed2.mass * feed2.Composition.CH4;
        fa6:    drain.mass * drain.Composition.CO       = feed1.mass *
feed1.Composition.CO       + feed2.mass * feed2.Composition.CO;
        fa7:    drain.mass * drain.Composition.CO2      = feed1.mass *
feed1.Composition.CO2      + feed2.mass * feed2.Composition.CO2;
        fa8:    drain.mass * drain.Composition.H2       = feed1.mass *
feed1.Composition.H2       + feed2.mass * feed2.Composition.H2;
        fa9:    drain.mass * drain.Composition.H2O      = feed1.mass *
feed1.Composition.H2O      + feed2.mass * feed2.Composition.H2O;
        fa10:   drain.mass * drain.Composition.H2S      = feed1.mass *
feed1.Composition.H2S      + feed2.mass * feed2.Composition.H2S;
        fa11:   drain.mass * drain.Composition.N2       = feed1.mass *
feed1.Composition.N2       + feed2.mass * feed2.Composition.N2;
        fa12:   drain.mass * drain.Composition.O2       = feed1.mass *
feed1.Composition.O2       + feed2.mass * feed2.Composition.O2;
        fa13:   drain.mass * drain.Composition.SO2      = feed1.mass *
feed1.Composition.SO2      + feed2.mass * feed2.Composition.SO2;

endifl

@# configuration 2
# both feed streams use the same composition, the drain composition is a different
object.
ifl     ref(feed1.Composition) == ref(feed2.Composition)
        && ref(feed1.Composition) != ref(drain.Composition) then
        # The mass balance for WATER has been omitted, since it is automatically
satisfied
```

```
        fb2:    feed1.Composition.AR        = drain.Composition.AR;
        fb3:    feed1.Composition.C2H6      = drain.Composition.C2H6;
        fb4:    feed1.Composition.C3H8      = drain.Composition.C3H8;
        fb5:    feed1.Composition.CH4       = drain.Composition.CH4;
        fb6:    feed1.Composition.CO        = drain.Composition.CO;
        fb7:    feed1.Composition.CO2       = drain.Composition.CO2;
        fb8:    feed1.Composition.H2        = drain.Composition.H2;
        fb9:    feed1.Composition.H2O       = drain.Composition.H2O;
        fb10:   feed1.Composition.H2S       = drain.Composition.H2S;
        fb11:   feed1.Composition.N2        = drain.Composition.N2;
        fb12:   feed1.Composition.O2        = drain.Composition.O2;
        fb13:   feed1.Composition.SO2       = drain.Composition.SO2;

endifl

@# configuration 3, configuration 4
# feed1 and drain use the same composition, feed2 is different
# or feed2 and drain use the same composition and feed1 is different
ifl     ref(feed1.Composition) != ref(feed2.Composition)
        && (ref(feed1.Composition) == ref(drain.Composition)
        || ref(feed2.Composition) == ref(drain.Composition))
then

        # The mass balance for WATER has been omitted, since it is automatically
satisfied
        fc2:    feed1.Composition.AR        = feed2.Composition.AR;
        fc3:    feed1.Composition.C2H6      = feed2.Composition.C2H6;
        fc4:    feed1.Composition.C3H8      = feed2.Composition.C3H8;
        fc5:    feed1.Composition.CH4       = feed2.Composition.CH4;
        fc6:    feed1.Composition.CO        = feed2.Composition.CO;
        fc7:    feed1.Composition.CO2       = feed2.Composition.CO2;
        fc8:    feed1.Composition.H2        = feed2.Composition.H2;
        fc9:    feed1.Composition.H2O       = feed2.Composition.H2O;
        fc10:   feed1.Composition.H2S       = feed2.Composition.H2S;
        fc11:   feed1.Composition.N2        = feed2.Composition.N2;
        fc12:   feed1.Composition.O2        = feed2.Composition.O2;
        fc13:   feed1.Composition.SO2       = feed2.Composition.SO2;

endifl

@# configuration 5
# If all three streams use the same composition, no additional equations are
required
# test for positive pressure drops
t1:     test (delta_p_1>=0.0)warning "pressure drop delta_p_1 is negative";
t2:     test (delta_p_2>=0.0)warning "pressure drop delta_p_2 is negative";
fch2:   feed1.ch2=drain.ch2;
fch22:  feed2.ch2=drain.ch2;
#test for positive mass flows
t3:     test (feed1.mass >= 0.0)        error "feed1 - mass flow is negative";
t4:     test (feed2.mass >= 0.0)        error "feed2 - mass flow is negative";
```

26-mixera model

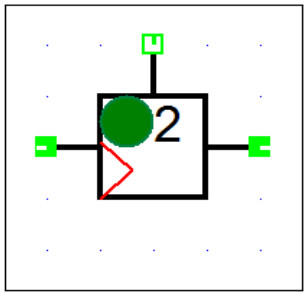

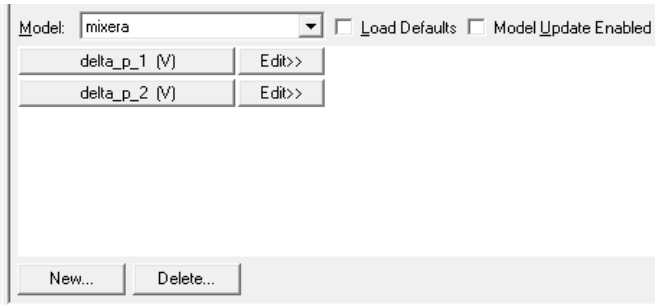

Oxygen mixer

```
# mass balance
f1:     feed1.mass+feed2.mass-drain.mass = 0.0;
# energy balance
f2:     feed1.h*feed1.mass+feed2.h*feed2.mass-drain.h*drain.mass = 0.0;
# pressure drop feed_1
f3:     feed1.p-delta_p_1-drain.p = 0.0;
#pressure drop feed_2
f4:     feed2.p-delta_p_2-drain.p = 0.0;
# The equations for the components of the compositions
@# configuration 1
# All composition objects are different
ifl     ref(feed1.Composition) != ref(feed2.Composition)
         && ref(feed1.Composition) != ref(drain.Composition)
         && ref(feed2.Composition) != ref(drain.Composition)
then
        # The mass balance for WATER has been omitted, since it is automatically
satisfied
        fa2:    drain.mass * drain.Composition.AR       = feed1.mass *
feed1.Composition.AR       + feed2.mass * feed2.Composition.AR;
        fa3:    drain.mass * drain.Composition.C2H6     = feed1.mass *
feed1.Composition.C2H6 + feed2.mass * feed2.Composition.C2H6;
        fa4:    drain.mass * drain.Composition.C3H8     = feed1.mass *
feed1.Composition.C3H8     + feed2.mass * feed2.Composition.C3H8;
        fa5:    drain.mass * drain.Composition.CH4      = feed1.mass *
feed1.Composition.CH4      + feed2.mass * feed2.Composition.CH4;
        fa6:    drain.mass * drain.Composition.CO       = feed1.mass *
feed1.Composition.CO       + feed2.mass * feed2.Composition.CO;
        fa7:    drain.mass * drain.Composition.CO2      = feed1.mass *
feed1.Composition.CO2      + feed2.mass * feed2.Composition.CO2;
        fa8:    drain.mass * drain.Composition.H2       = feed1.mass *
feed1.Composition.H2       + feed2.mass * feed2.Composition.H2;
        fa9:    drain.mass * drain.Composition.H2O      = feed1.mass *
feed1.Composition.H2O      + feed2.mass * feed2.Composition.H2O;
        fa10:   drain.mass * drain.Composition.H2S      = feed1.mass *
feed1.Composition.H2S      + feed2.mass * feed2.Composition.H2S;
        fa11:   drain.mass * drain.Composition.N2       = feed1.mass *
feed1.Composition.N2       + feed2.mass * feed2.Composition.N2;
```

```
        fa12:   drain.mass * drain.Composition.O2       = feed1.mass *
feed1.Composition.O2        + feed2.mass * feed2.Composition.O2;
        fa13:   drain.mass * drain.Composition.SO2      = feed1.mass *
feed1.Composition.SO2       + feed2.mass * feed2.Composition.SO2;

endifl

@# configuration 2
# both feed streams use the same composition, the drain composition is a different
object.
ifl     ref(feed1.Composition) == ref(feed2.Composition)
        && ref(feed1.Composition) != ref(drain.Composition) then

        # The mass balance for WATER has been omitted, since it is automatically
satisfied
        fb2:    feed1.Composition.AR        = drain.Composition.AR;
        fb3:    feed1.Composition.C2H6      = drain.Composition.C2H6;
        fb4:    feed1.Composition.C3H8      = drain.Composition.C3H8;
        fb5:    feed1.Composition.CH4       = drain.Composition.CH4;
        fb6:    feed1.Composition.CO        = drain.Composition.CO;
        fb7:    feed1.Composition.CO2       = drain.Composition.CO2;
        fb8:    feed1.Composition.H2        = drain.Composition.H2;
        fb9:    feed1.Composition.H2O       = drain.Composition.H2O;
        fb10:   feed1.Composition.H2S       = drain.Composition.H2S;
        fb11:   feed1.Composition.N2        = drain.Composition.N2;
        fb12:   feed1.Composition.O2        = drain.Composition.O2;
        fb13:   feed1.Composition.SO2       = drain.Composition.SO2;

endifl

@# configuration 3, configuration 4
# feed1 and drain use the same composition, feed2 is different
# or feed2 and drain use the same composition and feed1 is different
ifl     ref(feed1.Composition) != ref(feed2.Composition)
        && (ref(feed1.Composition) == ref(drain.Composition)
        || ref(feed2.Composition) == ref(drain.Composition))
then
        # The mass balance for WATER has been omitted, since it is automatically
satisfied
        fc2:    feed1.Composition.AR        = feed2.Composition.AR;
        fc3:    feed1.Composition.C2H6      = feed2.Composition.C2H6;
        fc4:    feed1.Composition.C3H8      = feed2.Composition.C3H8;
        fc5:    feed1.Composition.CH4       = feed2.Composition.CH4;
        fc6:    feed1.Composition.CO        = feed2.Composition.CO;
        fc7:    feed1.Composition.CO2       = feed2.Composition.CO2;
        fc8:    feed1.Composition.H2        = feed2.Composition.H2;
        fc9:    feed1.Composition.H2O       = feed2.Composition.H2O;
        fc10:   feed1.Composition.H2S       = feed2.Composition.H2S;
        fc11:   feed1.Composition.N2        = feed2.Composition.N2;
        fc12:   feed1.Composition.O2        = feed2.Composition.O2;
        fc13:   feed1.Composition.SO2       = feed2.Composition.SO2;
endifl
```

@# configuration 5
 # If all three streams use the same composition, no additional equations are required
 # test for positive pressure drops
t1: test (delta_p_1>=0.0)warning "pressure drop delta_p_1 is negative";
t2: test (delta_p_2>=0.0)warning "pressure drop delta_p_2 is negative";
fco2: feed1.co2=drain.co2;
fco22: feed2.co2=drain.co2;
#test for positive mass flows
t3: test (feed1.mass >= 0.0) error "feed1 - mass flow is negative";
t4: test (feed2.mass >= 0.0) error "feed2 - mass flow is negative";

27-splittera model

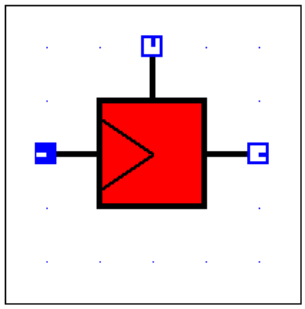

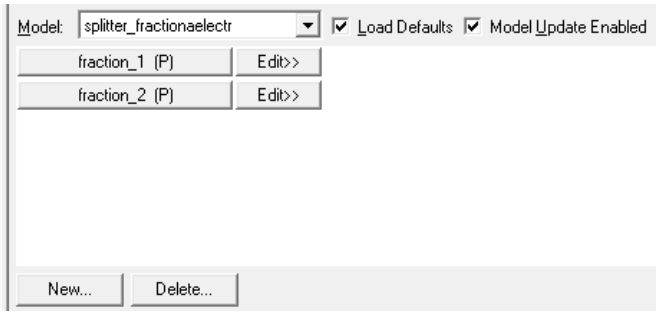

-PV electricity distributor

f1: electricity_pv.power = electricity_elec.power+load.power;
fFraction: electricity_elec.power*fraction_2 = load.power*fraction_1;
fcw: electricity_pv.cw=electricity_elec.cw;
fcw2: load.cw=electricity_pv.cw;

28-splitteraa model

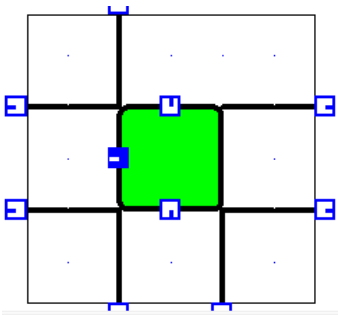

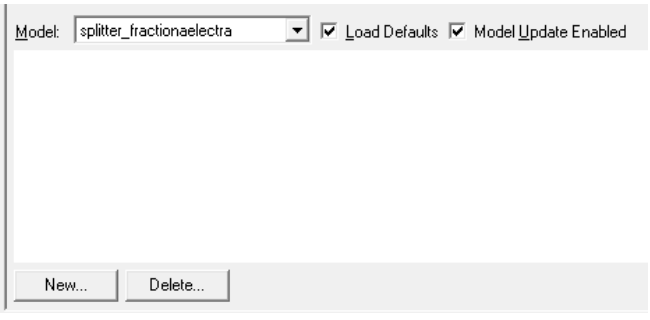

PV electricity distributor nine branches

f1:
elecPVin.power=load1.power+load2.power+load3.power+load4.power+load5.power+load6.power+load7.power+load8.power+load9.power;

fcw1: elecPVin.cw=load1.cw;
fcw2: elecPVin.cw=load2.cw;

fcw3: elecPVin.cw=load3.cw;
fcw4: elecPVin.cw=load4.cw;
fcw5: elecPVin.cw=load5.cw;
fcw6: elecPVin.cw=load6.cw;
fcw7: elecPVin.cw=load7.cw;
fcw8: elecPVin.cw=load8.cw;
fcw9:elecPVin.cw=load9.cw;

29-tankH2 model

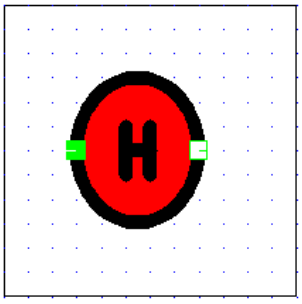

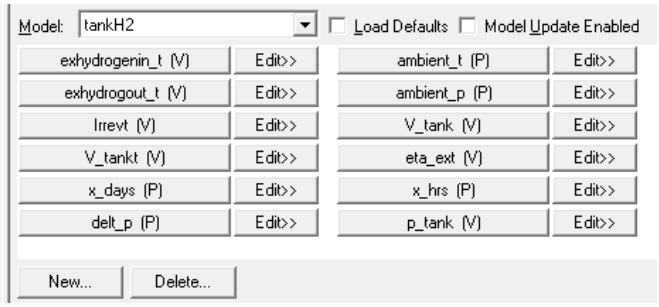

Hydrogen tank exergy analysis

 # compresed hydrogen tank
f1: hydrogen.mass=hydrogenout.mass;
f2: V_tank=hydrogen.v*hydrogen.mass;
f3: exhydrogenin_t=hydrogen.ex_ph+hydrogen.ex_ch;
f4: exhydrogout_t=hydrogenout.ex_ph+hydrogenout.ex_ch;
f6: hydrogenout.ex_ph=14.2091*ambient_t*((hydrogenout.t/ambient_t)-1-ln(hydrogenout.t/ambient_t))+(4.12418*ambient_t*ln(hydrogenout.p/ambient_p));
f7: Irrevt=hydrogen.mass*(exhydrogenin_t-exhydrogout_t);
f8: eta_ext=(exhydrogout_t/exhydrogenin_t);
f9: hydrogenout.p=hydrogen.p-delt_p;
fo: V_tankt=V_tank*x_days*3600*x_hrs;
fp_tank: p_tank=hydrogen.p;

30-tankH2a

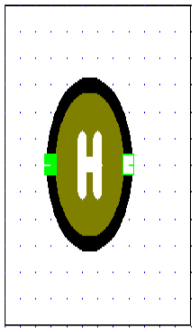

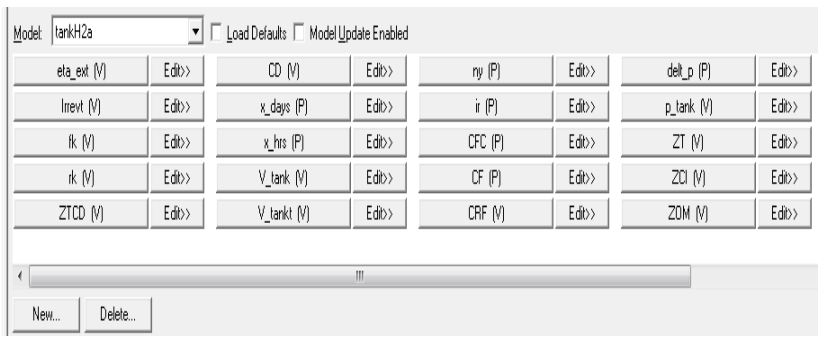

Hydrogen tank thermo-economic analysis

 # compresed hydrogen tank
f1: hydrogen.mass=hydrogenout.mass;
f2: V_tank=hydrogen.v*hydrogen.mass;
f7: Irrevt=hydrogen.mass*(hydrogen.ex_t-hydrogenout.ex_t);
f8: eta_ext=((hydrogenout.ex_t/hydrogen.ex_t))*100;
f9: hydrogenout.p=hydrogen.p-delt_p;
fo: V_tankt=V_tank*x_days*3600*x_hrs;
fp_tank: p_tank=hydrogen.p;
fch2: hydrogenout.ch2=
((hydrogen.ch2*hydrogen.ex_t*hydrogen.mass/1000000)+ZT)
/(hydrogenout.ex_t*hydrogenout.mass/1000000);
fZ: ZT=ZCI+ZOM;
fZCI: ZCI=(ACC*Ms)/(CF*8760*3600);
fZOM: ZOM=(COM*Ms)/(8760*3600);
fACC: ACC=CFC*CRF;
fCRF: CRF=(ir*((1+ir)^ny))/(((1+ir)^ny)-1);
frk:rk=(((1-
(eta_ext/100))/(eta_ext/100))+(ZT/(hydrogen.ch2*(hydrogenout.ex_t*hydrogenout.
mass/1000000))))*100;
fk: fk=(ZT/(ZT+(hydrogen.ch2*(Irrevt/1000000))))*100;
fZTCD: ZTCD=((hydrogen.ch2*(Irrevt/1000000)) + ZT)*3600;
fCD:CD=(hydrogen.ch2*(Irrevt/1000000))*3600 ;

31-tankO2 model

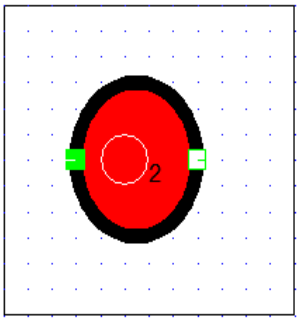

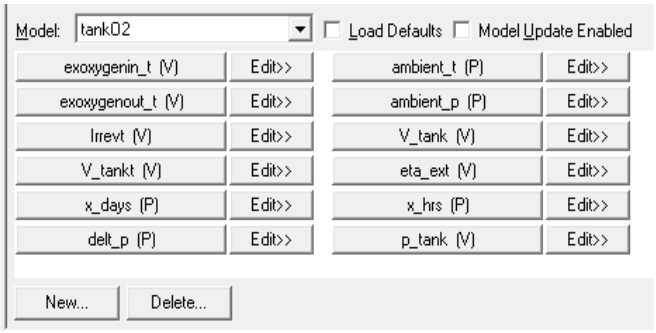

Oxygen tank exergy analysis

 # compresed hydrogen tank
f1: oxygenin.mass=oxygenout.mass;
f2: V_tank=oxygenin.v*oxygenin.mass;
f3: exoxygenin_t=oxygenin.ex_ph+oxygenin.ex_ch;
f4: exoxygenout_t=oxygenout.ex_ph+oxygenout.ex_ch;
f6: oxygenout.ex_ph=0.9216*ambient_t*((oxygenout.t/ambient_t)-1-
ln(oxygenout.t/ambient_t))+(0.25983*ambient_t*ln(oxygenout.p/ambient_p));
f7: Irrevt=oxygenin.mass*(exoxygenin_t-exoxygenout_t);
f8: eta_ext=(exoxygenout_t/exoxygenin_t);
f9: oxygenout.p=oxygenin.p-delt_p;
fo: V_tankt=V_tank*x_days*3600*x_hrs;
fp_tank: p_tank=oxygenin.p;

32-tankO2a model

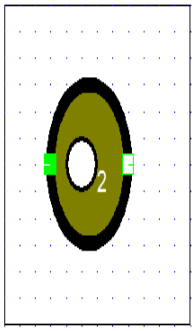

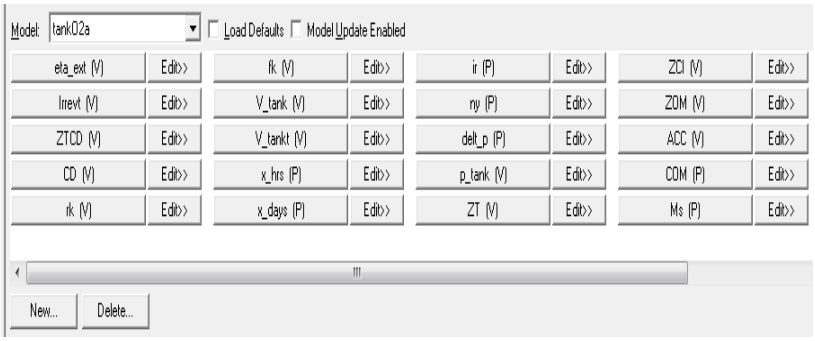

Oxygen tank thermo-economic analysis

 # compresed oxygen tank
f1: oxygenin.mass=oxygenout.mass;
f2: V_tank=oxygenin.v*oxygenin.mass;
f7: Irrevt=oxygenin.mass*(oxygenin.ex_t-oxygenout.ex_t);
f8: eta_ext=((oxygenout.ex_t/oxygenin.ex_t))*100;
f9: oxygenout.p=oxygenin.p-delt_p;
fo: V_tankt=V_tank*x_days*3600*x_hrs;
fp_tank: p_tank=oxygenin.p;
fch2: oxygenout.co2= ((oxygenin.co2*oxygenin.ex_t*oxygenin.mass/1000000)+ZT) /(oxygenout.ex_t*oxygenout.mass/1000000);
fZ: ZT=ZCI+ZOM;
fZCI: ZCI=(ACC*Ms)/(CF*8760*3600);
fZOM: ZOM=(COM*Ms)/(8760*3600);
fACC: ACC=CFC*CRF;
fCRF: CRF=(ir*((1+ir)^ny))/(((1+ir)^ny)-1);
frk: rk=(((1-(eta_ext/100))/(eta_ext/100))+(ZT/(oxygenin.co2*(oxygenout.ex_t*oxygenout.mass/1000000))))*100;
fk: fk=(ZT/(ZT+(oxygenin.co2*(Irrevt/1000000))))*100;
fZTCD: ZTCD=((oxygenin.co2*(Irrevt/1000000)) + ZT)*3600;
fCD:CD=(oxygenin.co2*(Irrevt/1000000))*3600 ;

Appendix E

SM55 Siemens solar module details and specification, Siemens Company, Avalible from: http://www.siemen.co.uk/sm55_sm50.html

Electrical Parameters @STC			**SM55**	
			12V	
Maximum power rating	Pmax	[Watts]	55	
Minimum power rating	Pmin	[Watts]	50	
Rated current	Imp	[Amps]	3.15	
Rated voltage	Vmp	[Volts]	17.4	
Short circuit current	Isc	[Amps]	3.45	
Open circuit voltage	Voc	[Volts]	21.7	
Thermal Parameters				
Nominal operating cell temperature		[°C]	45	
Change of Isc with temperature, α		(+0.04%/K)	+1.2mA/°C	
Change of Voc with temperature, β		(- 0.34%/K)	-0.077 Volts/°C	
Qualification Test Parameters[3]				
Temperature cycling range		[°C]	-40 to +85	
Humidity, freeze, damp heat condition		[% RH]	85	
Maximum system voltage		[Volts]	1000 per ISPRA(EC), 600 per UL 1703	
Wind loading or surface pressure		[N/m^2] (PSF)	2400 (50)	
Maximum distortion		[degrees]	1.2	
Hailstone impact withstand (diameter @ velocity)		[mm @ m/s] (in @ MPH)	25 @ 23 (1.0 @ 52)	
Physical Parameters				
Number of series cells			36	
Length		[mm] (in)	1293 (50.9)	
Width		[mm] (in)	329 (13.0)	
Depth		[mm] (in)	34 (1.3)	
Weight		[kg] (lbs)	5.5 (12.0)	
Warranty				
Power >= 90% of minimum power		[Years]	10	
Power >= 80% of minimum power		[Years]	25	

Appendix F

The figures (F-1 - F-12) representing the results of varying of the SHS components parameters; power, irreversibility, hot water, hydrogen and oxygen mass as well as the cost structure during the summer and winter day for a system installed in Misurata and Newcastle.

1- Misurata Figures

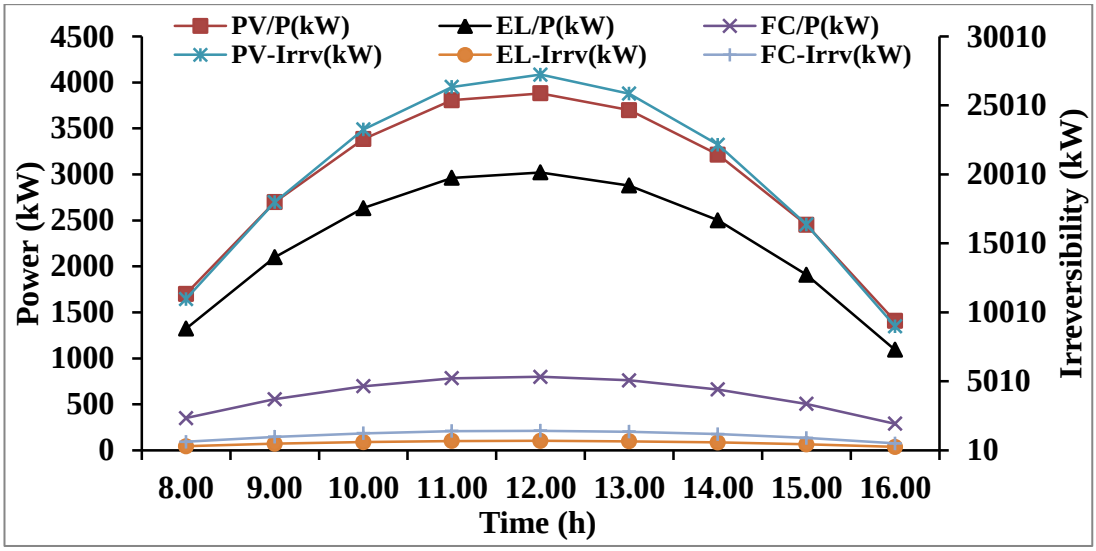

Figure F-1 Varying of the power and irreversibility of SHS components during the daytime of the 15th of January 2011 at Misurata

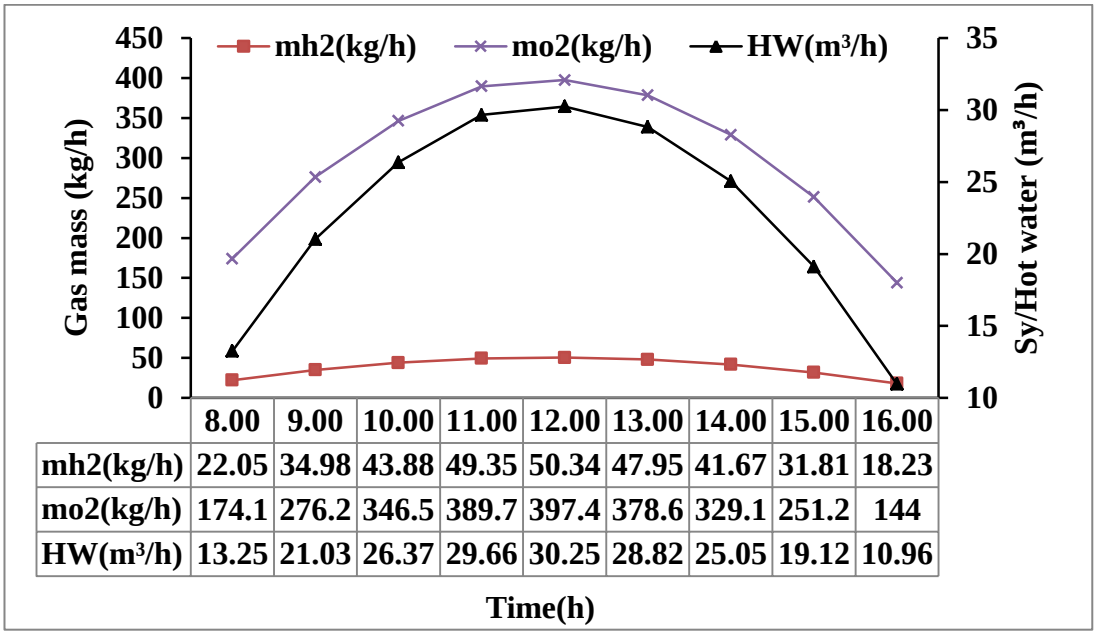

Figure F-2 Varying of gas mass and hot water outputs during the day time of the 15th of January 2011 at Misurata

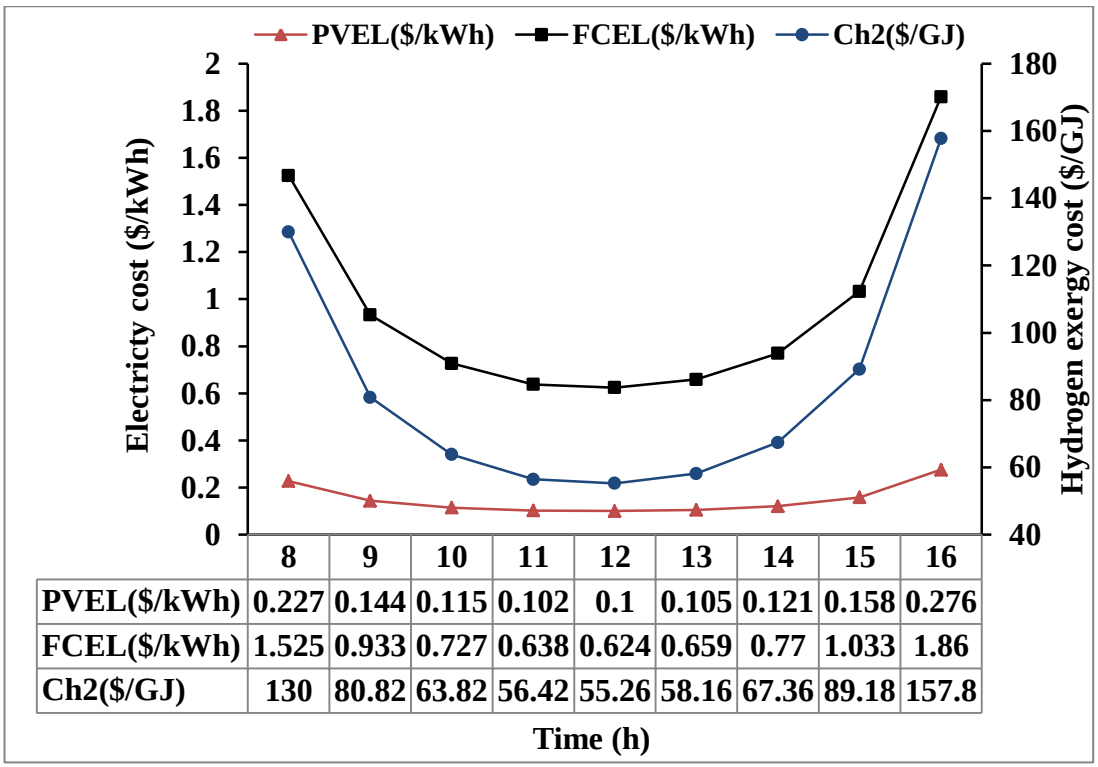

	8	9	10	11	12	13	14	15	16
PVEL($/kWh)	0.227	0.144	0.115	0.102	0.1	0.105	0.121	0.158	0.276
FCEL($/kWh)	1.525	0.933	0.727	0.638	0.624	0.659	0.77	1.033	1.86
Ch2($/GJ)	130	80.82	63.82	56.42	55.26	58.16	67.36	89.18	157.8

Figure F-3 Varying of the PV and FC output electricity and hydrogen cost during the day time of the 15th of January 2011 at Misurata

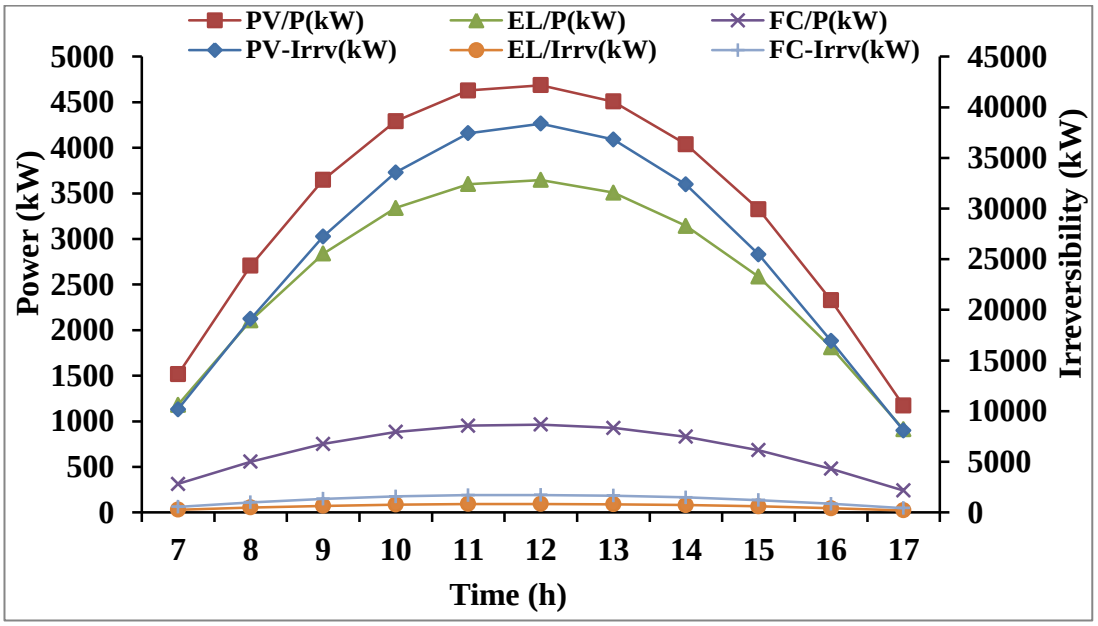

Figure F-4 Varying of the power and irreversibility of SHS components during the daytime of the 15th of August 2010 at Misurata

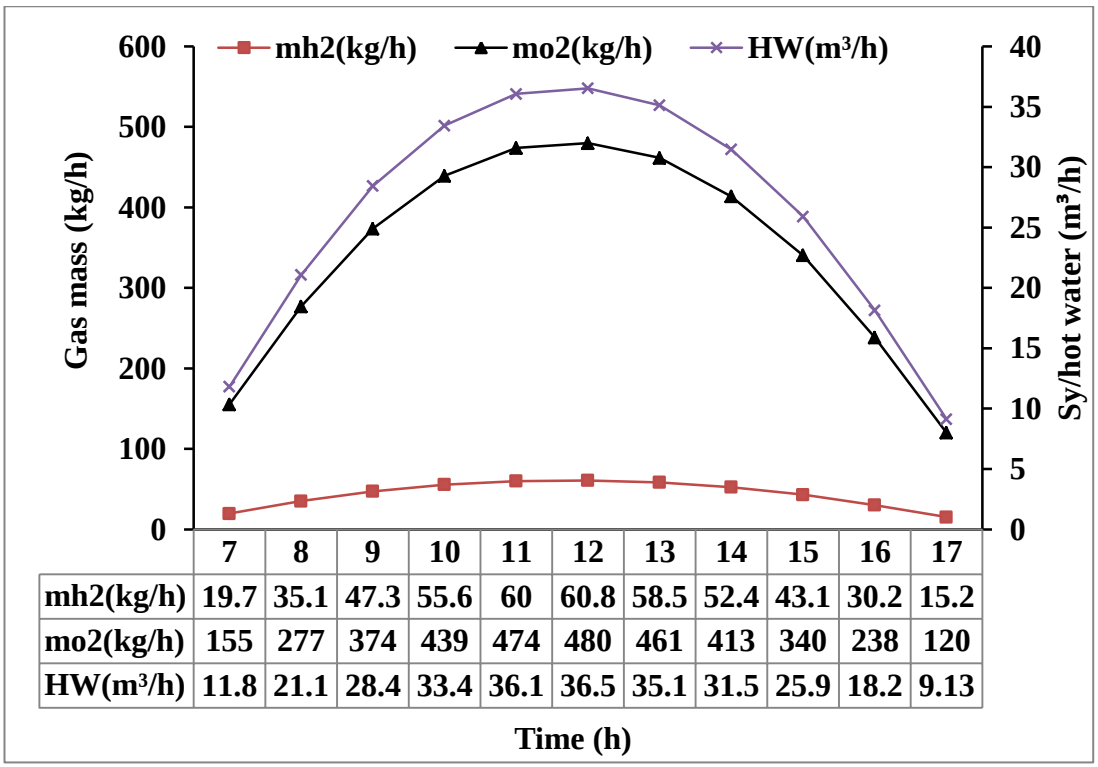

	7	8	9	10	11	12	13	14	15	16	17
mh2(kg/h)	19.7	35.1	47.3	55.6	60	60.8	58.5	52.4	43.1	30.2	15.2
mo2(kg/h)	155	277	374	439	474	480	461	413	340	238	120
HW(m³/h)	11.8	21.1	28.4	33.4	36.1	36.5	35.1	31.5	25.9	18.2	9.13

Figure F-5 Varying of gas mass and hot water outputs during the day time of the 15th of August 2010 at Misurata

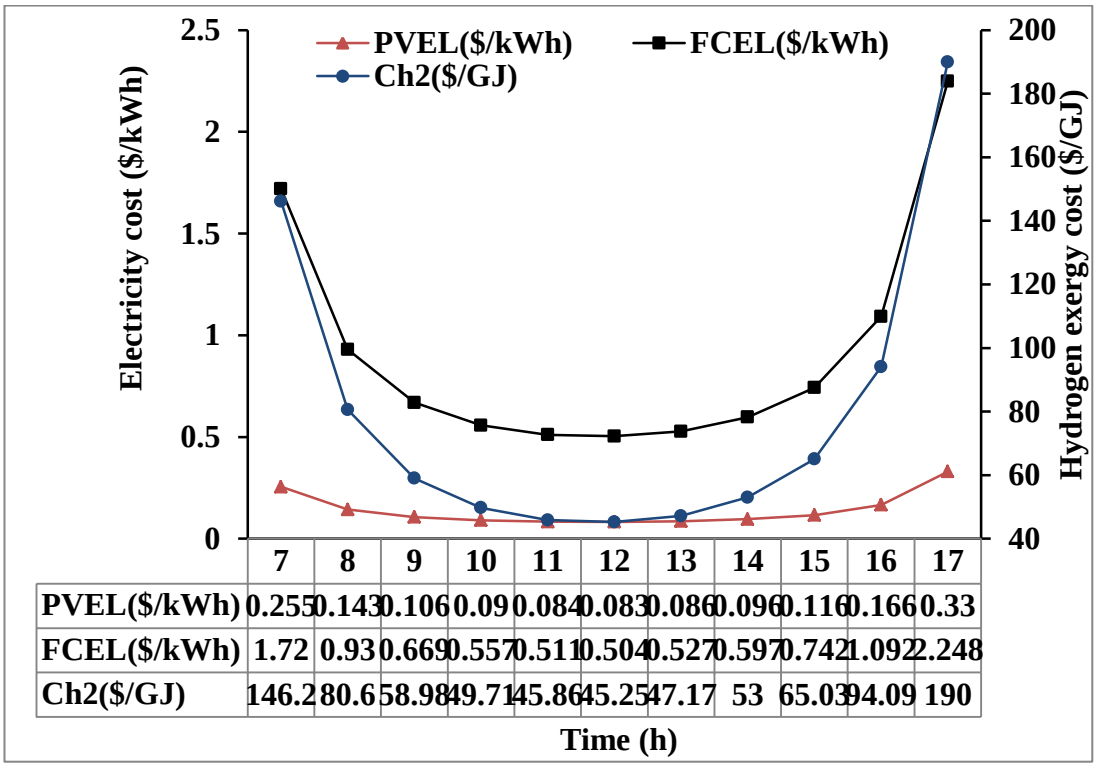

	7	8	9	10	11	12	13	14	15	16	17
PVEL($/kWh)	0.255	0.143	0.106	0.09	0.084	0.083	0.086	0.096	0.116	0.166	0.33
FCEL($/kWh)	1.72	0.93	0.669	0.557	0.511	0.504	0.527	0.597	0.742	1.092	2.248
Ch2($/GJ)	146.2	80.6	58.98	49.71	45.86	45.25	47.17	53	65.03	94.09	190

Figure F-6 Varying of the PV and FC output electricity and hydrogen cost during the day time of the 15th of August 2010 at Misurata

2-Newcastle Figures

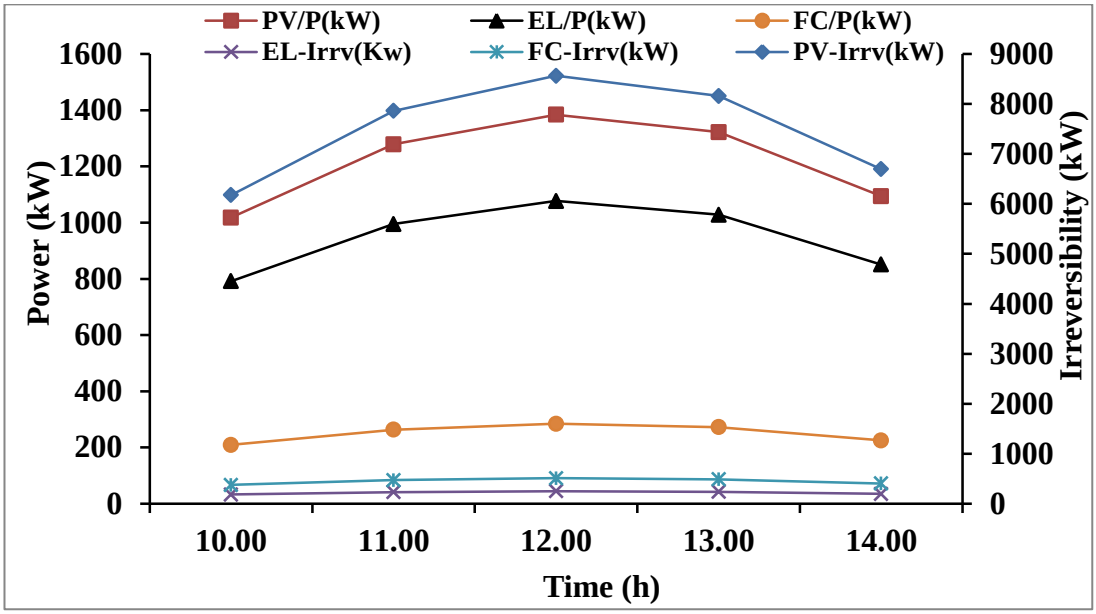

Figure F-7 Varying of the power and irreversibility of SHS components during the daytime of the 15th of January 2011 at Newcastle

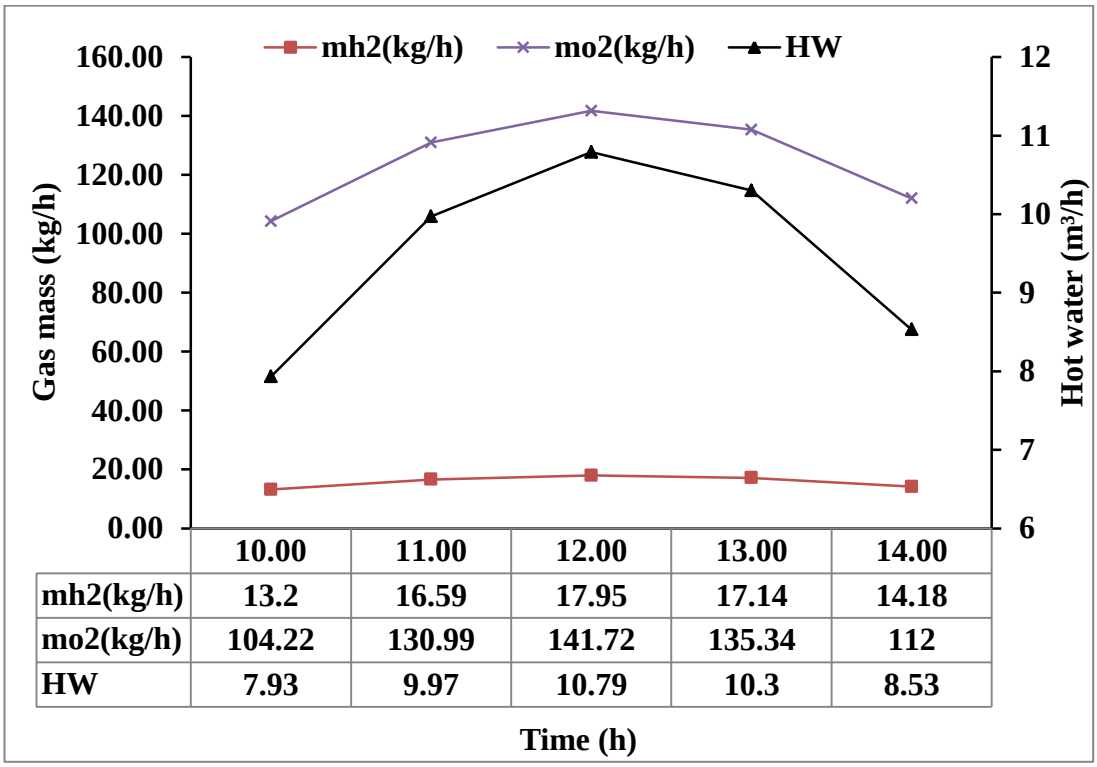

	10.00	11.00	12.00	13.00	14.00
mh2(kg/h)	13.2	16.59	17.95	17.14	14.18
mo2(kg/h)	104.22	130.99	141.72	135.34	112
HW	7.93	9.97	10.79	10.3	8.53

Figure F-8 Varying of gas mass and hot water outputs during the day time of the 15th of January 2011 at Newcastle

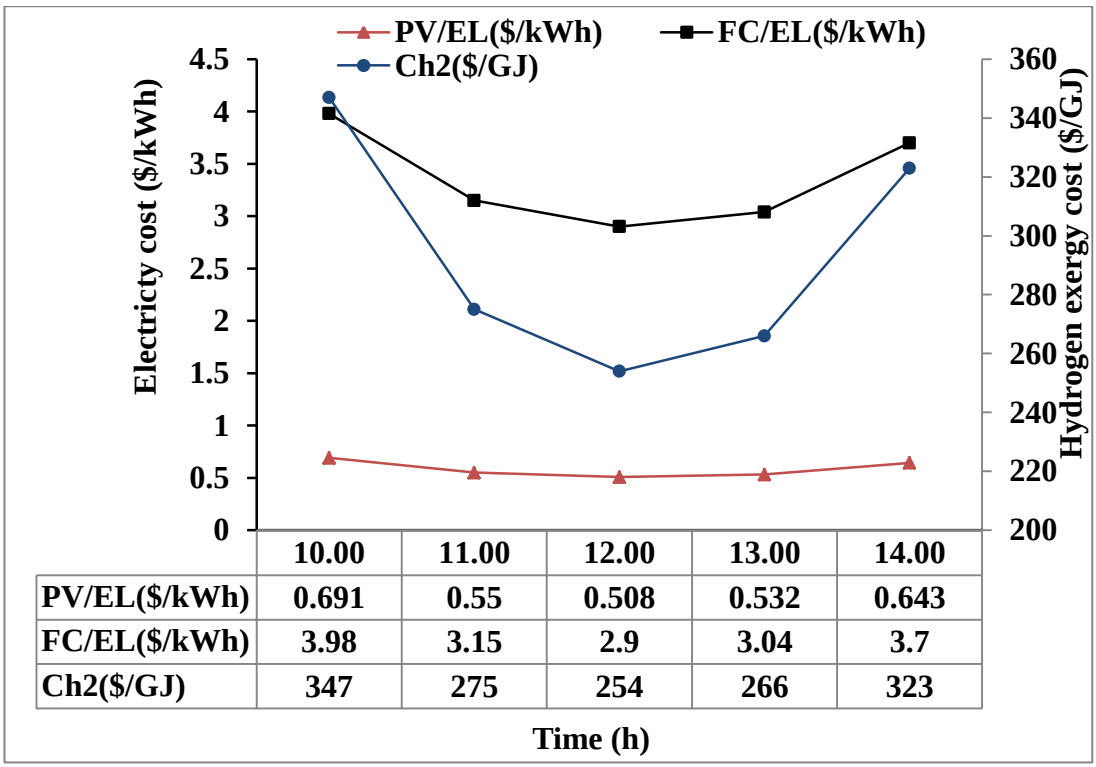

	10.00	11.00	12.00	13.00	14.00
PV/EL($/kWh)	0.691	0.55	0.508	0.532	0.643
FC/EL($/kWh)	3.98	3.15	2.9	3.04	3.7
Ch2($/GJ)	347	275	254	266	323

Time (h)

Figure F-9 Varying of the PV and FC output electricity and hydrogen cost during the day time of the 15th of January 2011 at Newcastle

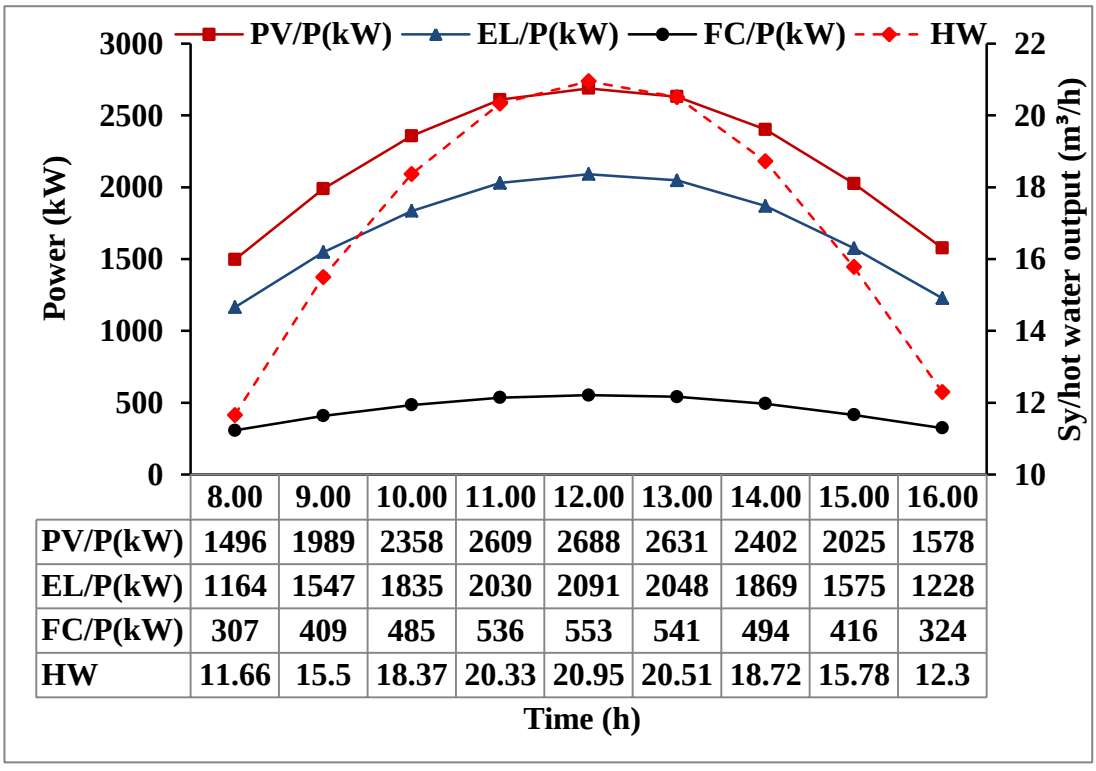

	8.00	9.00	10.00	11.00	12.00	13.00	14.00	15.00	16.00
PV/P(kW)	1496	1989	2358	2609	2688	2631	2402	2025	1578
EL/P(kW)	1164	1547	1835	2030	2091	2048	1869	1575	1228
FC/P(kW)	307	409	485	536	553	541	494	416	324
HW	11.66	15.5	18.37	20.33	20.95	20.51	18.72	15.78	12.3

Time (h)

Figure F-10 Varying of the power and hot water of SHS components during the daytime of the 15th of August 2010 at Newcastle

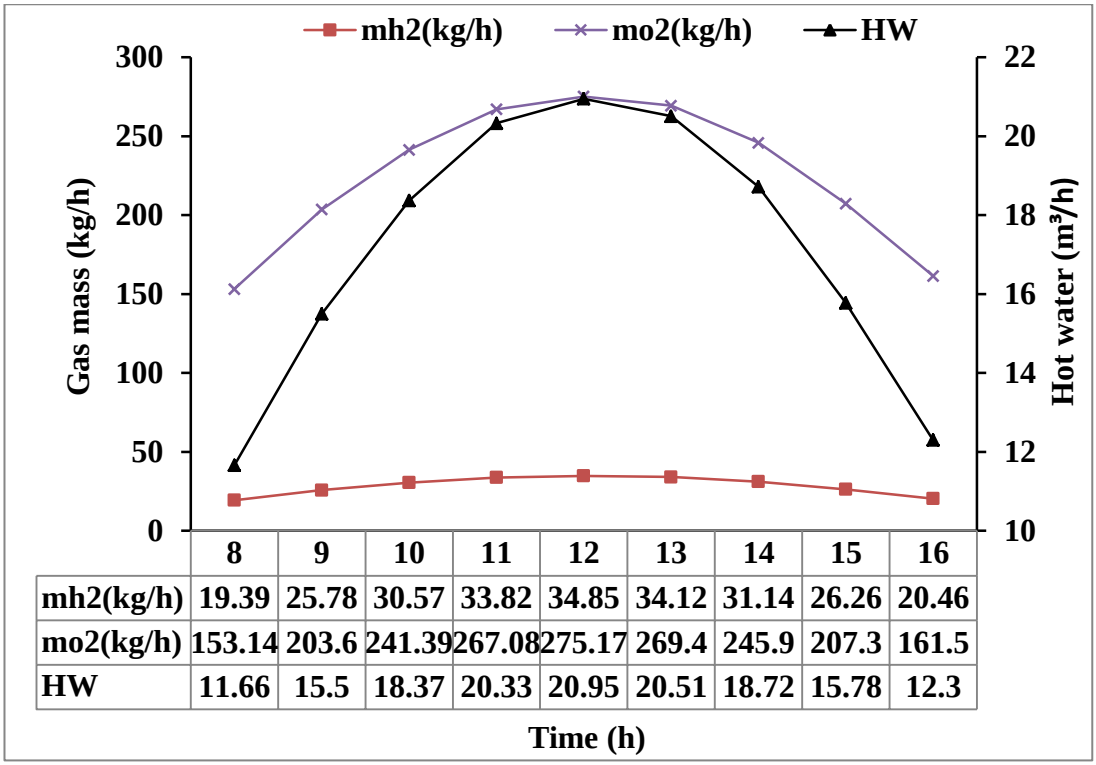

	8	9	10	11	12	13	14	15	16
mh2(kg/h)	19.39	25.78	30.57	33.82	34.85	34.12	31.14	26.26	20.46
mo2(kg/h)	153.14	203.6	241.39	267.08	275.17	269.4	245.9	207.3	161.5
HW	11.66	15.5	18.37	20.33	20.95	20.51	18.72	15.78	12.3

Figure F-11 Varying of gas mass and hot water outputs during the day time of the 15th of August 2010 at Newcastle

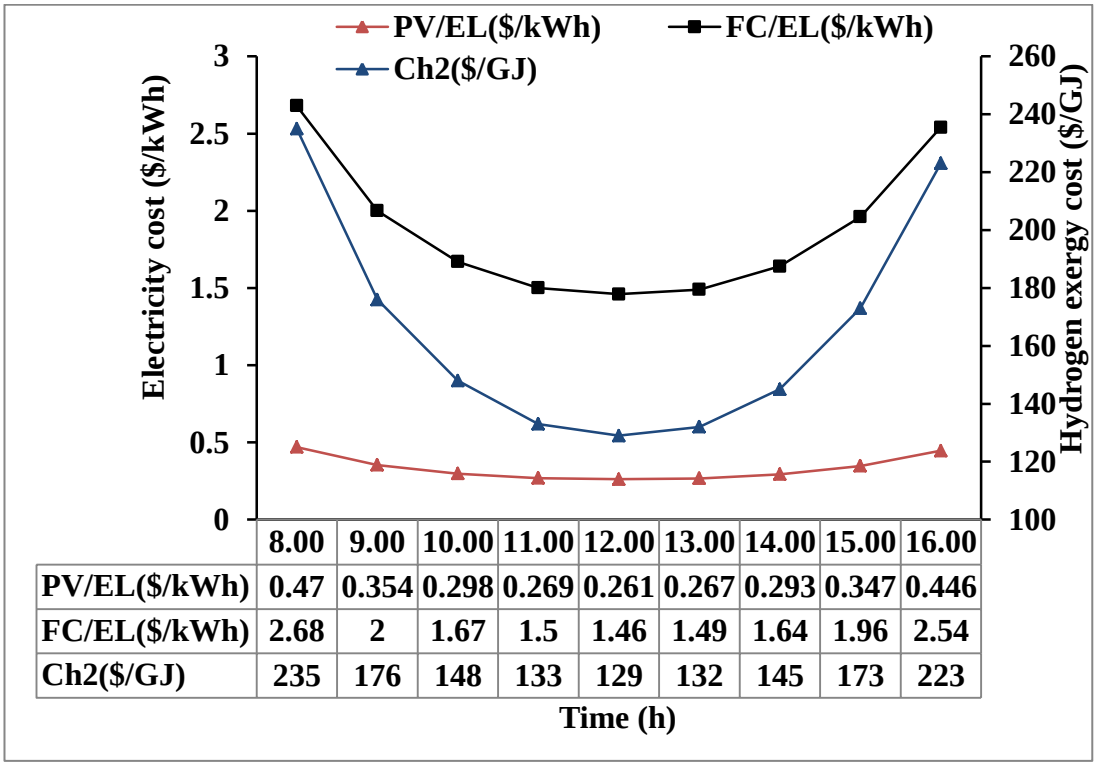

	8.00	9.00	10.00	11.00	12.00	13.00	14.00	15.00	16.00
PV/EL($/kWh)	0.47	0.354	0.298	0.269	0.261	0.267	0.293	0.347	0.446
FC/EL($/kWh)	2.68	2	1.67	1.5	1.46	1.49	1.64	1.96	2.54
Ch2($/GJ)	235	176	148	133	129	132	145	173	223

Figure F-12 Varying of the PV and FC output electricity and hydrogen cost during the day time of the 15th of August 2010 at Newcastle